

Luminescent Materials based on Lanthanide Ions

Gerald Hebbink

2002

Ph.D. thesis
University of Twente



Twente University Press

Also available in print:

<http://www.tup.utwente.nl/catalogue/book/index.jsp?isbn=9036517869>

LUMINESCENT MATERIALS BASED ON LANTHANIDE IONS

The cover shows a detail (in false colors) of etched structures in a thin polymer layer, which is deposited by spincoating on a silicon wafer. The etched polymer (polycarbonate) is doped with an organic neodymium complex.



This research was supported by the Technology Foundation STW, applied science division of NWO and the technology program of the Ministry of Economic Affairs, grant number TST 4447.



Twente University **Press**

Publisher:

Twente University Press, P.O. Box 217, 7500 AE Enschede, the Netherlands

www.tup.utwente.nl

Print: Océ Facility Services, Enschede

© G. A. Hebbink, Enschede, 2002

No part of this work may be reproduced by print, photocopy or any other means without the permission in writing from the publisher.

ISBN 9036517869

LUMINESCENT MATERIALS BASED ON LANTHANIDE IONS
BASIC PROPERTIES AND APPLICATION IN NIR-LEDS AND OPTICAL AMPLIFIERS

PROEFSCHRIFT

ter verkrijging van
de graad van doctor aan de Universiteit Twente,
op gezag van de rector magnificus,
prof. dr. F. A. van Vught,
volgens besluit van het College voor Promoties
in het openbaar te verdedigen
op donderdag 29 augustus 2002 te 13.15 uur.

door

Gerrit Albert Hebbink

geboren op 9 oktober 1973
te Wisch

Dit proefschrift is goedgekeurd door:

Promotor	Prof. dr. ir. D. N. Reinhoudt
Assistent-promotor	Dr. ir. F. C. J. M. van Veggel

Aan mijn ouders

CHAPTER 1

General introduction	1
1.1 General introduction	1
1.2 References	5

CHAPTER 2

Luminescent Ln³⁺ complexes: applications and properties	7
2.1 General introduction	8
2.2 Complexes in polymer waveguide devices: optical amplification	9
2.2.1 Introduction	9
2.2.2 Polymer waveguides and waveguiding	9
2.2.3 Polymers for telecommunication waveguides	11
2.2.4 Polymer-based waveguides doped with lanthanide ion complexes	14
2.3 Near-infrared emitting light-emitting diodes (NIR-LEDs)	15
2.3.1 Electro-luminescence	15
2.3.2 VIS emitting lanthanide(III) ion complexes	17
2.3.3 NIR emitting lanthanide(III) ion complexes	18
2.4 Sensitized NIR Ln ³⁺ emission	20
2.4.1 Introduction	20
2.4.2 Lanthanide luminescence	21
2.4.3 Lanthanide complexes	21
2.4.4 Sensitized emission	24
2.5 Outlook	35
2.6 References	36

CHAPTER 3

Deuterated near-infrared emitting lanthanide(III) complexes	43
3.1 Introduction	44
3.2 Results and discussion	45
3.2.1 Molecular Modeling	45
3.2.2 Synthesis	46
3.2.3 Near-Infrared luminescence	48
3.3 Conclusions	49
3.4 Experimental	49
3.5 References and notes	53

CHAPTER 4

Dyes as sensitizers of near-infrared emitting lanthanide(III) ions	55
4.1 Introduction	56
4.2 Results and discussion	59
4.2.1 Modeling	59
4.2.2 Synthesis	61
4.2.3 Luminescence	62
4.3 Discussion of the energy transfer process	71
4.3.1 Energy transfer	71
4.3.2 Nd ³⁺ sensitization	71
4.3.3 The rate constants of Nd ³⁺ sensitization by fluorescein	72
4.3.4 Er ³⁺ and Yb ³⁺ sensitization	73
4.3.5 Final considerations	74
4.4 Conclusions	74
4.5 Experimental	75
4.6 References and notes	80

CHAPTER 5

Inorganic nanoparticles doped with luminescent lanthanide(III) ions	85
5.1 Introduction	86
5.2 Results and discussion	90
5.2.1 Preparation and characterization of Ln(1)PO ₄ :Ln(2) particles	90
5.2.2 VIS luminescence	91
5.2.3 NIR luminescence	98
5.3 Conclusions	101
5.4 Experimental	102
5.5 References and notes	103
Appendix 5.A	106
Fitting of the luminescence decay curves with an 'onion shell' model	106
5.A.1 Model description	106
5.A.2 Distance dependence of the quenching, the $f_{q,i}$ factor	107
5.A.3 Fitting of LaPO ₄ :Eu	108
5.A.4 Reference	109

CHAPTER 6

Light-emitting diodes doped with lanthanide(III) ion complexes	111
6.1 Introduction	112
6.2 Results and discussion	114

6.2.1 Synthesis	114
6.2.2 Luminescence in solution	115
6.2.3 Electro-chemistry	120
6.2.4 Electro-luminescence	121
6.3 Conclusions	128
6.4 Experimental	128
6.5 References and notes	131

CHAPTER 7

Polymer waveguides doped with lanthanide ions	135
7.1 Introduction	136
7.2 Results and discussion	137
7.2.1 Luminescence of 1.Nd in polymer matrices on quartz substrates.	137
7.2.2 Design of polymer waveguides, their fabrication and characterization	138
7.2.3 Calculation of optical gain in waveguides doped with Nd ³⁺ and Er ³⁺ .	141
7.3 Conclusions	148
7.4 Experimental	148
7.5 References and notes	149
Summary	151
Samenvatting	155
Dankwoord	159
List of publications	161
Curriculum vitae	163

Chapter 1

General introduction

1.1 General introduction

Telecommunication plays an increasingly important role in our society. There are several ways to transport telecommunication signals, like radio signals in wireless applications, electrical signals in copper cables, and laser pulses through glass-fibers. Fiber networks are spanning the earth because of the high transparency of glass fibers in the near-infrared region of the electromagnetic spectrum. However, even the slightest losses will eventually lead to a significant intensity loss over long distances and occasional amplification of the optical signals will thus be necessary.

In order to manipulate optical signals, several components with different functions, like splitters, switches, and (de-)multiplexers are integrated on small substrates ('integrated optics'). The bases for these integrated devices are planar optical waveguides that consist of a high refractive index material embedded in materials with a lower refractive index. Light is guided

through the high refractive index material (the core) as a result of total internal reflection at the interface of the core and the lower refractive index material (cladding). Each manipulation of the light signal may result in intensity losses of the signal and the on-chip integration of optical amplifiers with other components is therefore desired. In many cases, the integrated optics devices are based on organic polymeric materials. These polymers are deposited relatively easily on solid substrates like silicon wafers by spincoating from solution and patterns can be created with standard lithographic techniques.¹ Furthermore, high refractive index contrasts can be achieved with different polymers. A high index contrast gives a strong confinement of the light in the core of the waveguide and relatively strong bends are possible without too large losses.

The most important optical amplifier for long distances is the Er^{3+} -doped fiber amplifier (EDFA).² Er^{3+} has an optical transition in the 1.55 μm telecommunication window and the importance of that window in telecommunication is partly due to this transition.³ Other lanthanide ions that are actually being used in optical amplifiers are Pr^{3+} and Nd^{3+} , which have optical transitions in the 1.33 μm window. With the development of fibers that are transparent in other windows, like 1.4 μm and 1.6 μm , other ions like Ho^{3+} are becoming increasingly important. In integrated optics, it would be convenient to incorporate the lanthanide ions in the devices. A way to do so is to solubilize or disperse the lanthanide ions in organic polymers, which can be achieved with organic complexes. Previously, in our group lanthanide ion complexes^{4,5} have been developed that are based on multidentate ligand like, derived from calix[4]arenes^{6,7} and the *m*-terphenyl moiety.^{8,9} A typical ligand that is based on the *m*-terphenyl is depicted in Figure 1.1.

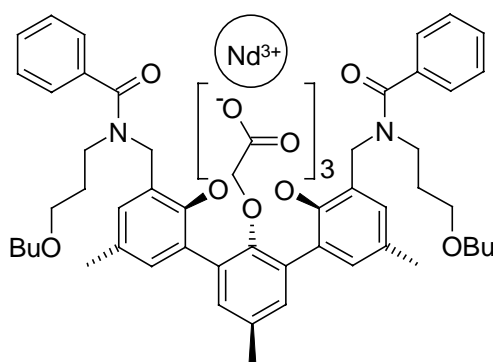


Figure 1.1 A Nd^{3+} complex of a multidentate ligand based on the *m*-terphenyl moiety (the bottom part of the ligand).

Such a preorganized,¹⁰ multidentate ligand forms a stable complex that shields the lanthanide ion from the solvent. Furthermore, these complexes are very well soluble in organic

solvents and in polymers, which makes them attractive for incorporation in the polymer-based optical components.^{11,12}

Optical amplification can not be achieved without providing energy that brings the lanthanide ions in their excited states, a process referred to as pumping. In the EDFAs, which amplify light in the 1.55 μm window, the energy is provided as laser light (optical pumping) at an absorption wavelength of Er^{3+} (0.98 μm or 1.48 μm). This direct pumping of the lanthanide ions is only one way of excitation, and other methods might be used, like for instance indirect excitation via a sensitizer.¹³ The direct and indirect excitation is schematically depicted in Figure 1.2. Upon excitation of the sensitizer, the energy is transferred to the lanthanide ion. For efficient energy transfer the sensitizer needs to be in close proximity of the ion and the energy levels of sensitizer and lanthanide ion should match. In principle, the near-infrared emitting lanthanide ions allow the use of sensitizers that absorb visible light. This sensitization is attractive because it circumvents the low absorption coefficients and the narrow absorption peaks of the lanthanide ions.

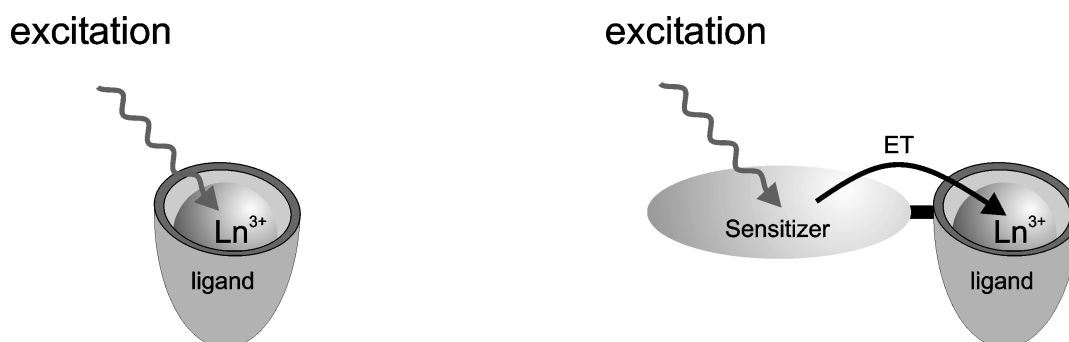


Figure 1.2 Left: direct excitation of a lanthanide ion that is complexed by a ligand. Right: indirect excitation of a lanthanide ion via a sensitizer that is bound to the ligand (ET stands for energy transfer).

The use of sensitizers offers other opportunities for the excitation of the lanthanide ions, for instance via electro-luminescence,¹⁴ where electrical energy is converted directly into excited states on organic molecules. This gives the possibility of electrical pumping of the lanthanide ions.

Two different designs for optical waveguides are depicted in Figure 1.3, one based on optical pumping of the lanthanide ions (directly or indirectly) and one based on electrical pumping of the lanthanide ions. Both designs consist of a channel on a solid substrate in which a laser signal is guided. Optical pumping is achieved by a pump laser that is coupled into the

waveguide. Electrical pumping is achieved by sandwiching the (polymer) waveguide in between two electrodes.

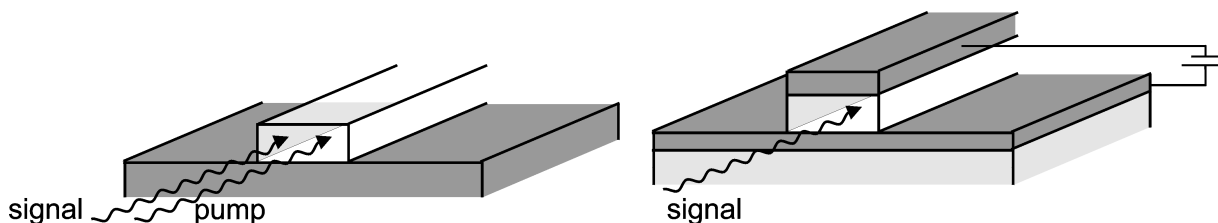


Figure 1.3 Schematic design for optical amplifiers based on polymer waveguide channels on solid substrates. The design on the left utilizes photo-excitation, in the design on the right the polymer waveguide is sandwiched between two electrodes and excited states are generated by the principle of electro-luminescence.

The aim of the work described in this thesis is the development of luminescent lanthanide complexes that can be incorporated in polymer devices, and designed such that non-radiative processes will be suppressed, because these are detrimental for optical amplification. These non-radiative processes depend on ligand and the chemical environment. This means that the ligand should be designed to shield the ion from its surrounding and to avoid quenching groups in the ligand. Furthermore, it is important to design sensitizers for efficient energy transfer to the lanthanide ion, which is necessary for indirect pumping of the ions.

In Chapter 2, the literature concerned with the application and the basic properties of the near-infrared and visible light emitting lanthanide complexes will be reviewed. A number of applications of luminescent lanthanide ions in polymer waveguides and in electro-luminescent devices will be treated. Furthermore, the basic properties of the lanthanide luminescence (radiative and non-radiative properties) and the sensitization properties of lanthanide ions that emit in the near-infrared will be discussed.

In Chapter 3, an approach to obtain more efficient emitting lanthanide ions is described. Lanthanide complexes will be deuterated in order to decrease the number of quenching groups. A significant but not sufficient increase in the luminescent lifetime and quantum yield has been obtained.

In Chapter 4, the photo-excitation of three near-infrared emitting lanthanide ions via a series of sensitizers that absorb visible light is described. This sensitization is studied in detail in order to get more insight in the pathways of the sensitization of the near-infrared emitting ions, and in the parameters that are important for the energy transfer efficiency.

Incorporation of lanthanide ions in inorganic matrices leads to very efficient lanthanide luminescence because of the reduction of quenching processes. The incorporation of luminescent

lanthanide ions in inorganic nanoparticles is described in Chapter 5. These nanoparticles are dispersible in organic solvents, which makes them processable in for instance a polymer matrix. The luminescence of the near-infrared emitting ions like Nd³⁺ and Er³⁺ is enhanced in comparison to the luminescence of these ions in organic complexes.

Chapter 6 deals with the incorporation and luminescence of near-infrared emitting complexes in polymer light-emitting diodes (NIR-LEDs). Nd³⁺ luminescence is observed in devices consisting of semiconducting polymers doped with complexes that are functionalized with sensitizers.

The development of polymer waveguides doped with lanthanide ion complexes is described in the last Chapter of this thesis, Chapter 7. Waveguides are prepared and the luminescence thereof is measured. The feasibility of optical amplification in polymer waveguides with the complexes described in the thesis is investigated with simulations.

1.2 References

- ¹ a) Booth, B. L. *J. Lightw. Techn.* **1989**, 7, 1445; b) Eldada, L.; Shacklette, L. W. *IEEE J. Sel. Top. Quant. Elec.* **2000**, 6, 54-68.
- ² Miniscalco, W. J. *J. Lightw. Techn.* **1991**, 9, 234.
- ³ Polman, A. *Phys. B.* **2001**, 300, 78.
- ⁴ Oude Wolbers, M. P. *Lanthanide ion complexes and their luminescence properties* PhD thesis University of Twente, 1997.
- ⁵ Klink, S. I. *Synthesis and photophysics of light-converting lanthanide complexes* PhD thesis University of Twente, 2000.
- ⁶ Steemers, F. J.; Verboom, W.; Reinhoudt, D. N.; van der Tol, E. B.; Verhoeven, J. W. *J. Am. Chem. Soc.* **1995**, 117, 9408.
- ⁷ Oude Wolbers, M. P.; van Veggel, F. C. J. M.; Peters, F. G. A.; van Beelen, E. S. E.; Hofstraat, J. W.; Geurts, F. A. J.; Reinhoudt, D. N. *Chem. Eur. J.* **1998**, 4, 772.
- ⁸ Oude Wolbers, M. P.; van Veggel, F. C. J. M.; Snellink-Ruël, B. H. M.; Hofstraat, J. W.; Geurts, F. A. J.; Reinhoudt, D. N. *J. Chem. Soc., Perkin Trans. 2* **1998**, 2141.
- ⁹ Klink, S. I.; Hebbink, G. A.; Grave, L. Peters, F. G. A.; van Veggel, F. C. J. M.; Reinhoudt, D. N.; Hofstraat, J. W. *Eur. J. Org. Chem.* **2000**, 1923.
- ¹⁰ Cram, D. J. *Angew. Chem. Int. Ed. Eng.* **1988**, 27, 1009.
- ¹¹ Slooff, L. H.; Polman, A.; Klink, S. I.; Hebbink, G. A.; Grave, L.; van Veggel, F. C. J. M.; Reinhoudt, D. N.; Hofstraat, J. W. *Opt. Mater.* **2000**, 14, 101.

- ¹² Slooff, L. H. *Rare-earth doped polymer waveguides and light-emitting diodes* PhD thesis University of Utrecht, 2000.
- ¹³ Parker, D.; Williams, J. A. *J. Chem. Soc., Dalton Trans.* **1996**, 3613.
- ¹⁴ Friend, R. H.; Gymer, R. W.; Holmes, A. B.; Burroughes, J. H.; Marks, R. N.; Taliani, C.; Bradley, D. D. C.; Dos Santos, D. A.; Bredas, J. L.; Logdlund, M.; Salaneck, W. R. *Nature* **1999**, 397, 121.

Chapter 2

Luminescent Ln³⁺ complexes: applications and properties

In this Chapter, complexes of trivalent near-infrared emitting lanthanide ions are reviewed that have been incorporated in polymer waveguides and in light-emitting diodes. Calculations and the first experiments on polymer waveguides show that optical amplification is possible, although it has not been demonstrated so far at telecommunication wavelengths. In light-emitting diodes near-infrared emission was observed in OLED and PLED devices. Optimization of these devices is an important field of research. The final part of the chapter describes the luminescence and the sensitization of lanthanide ions, mainly focussing on the near-infrared emitting ions. Although a number of sensitizers have been developed, the complete sensitization process of the near-infrared emitting ions is still not fully understood.

2.1 General introduction

Lanthanide ions are ideal in laser applications for many reasons.¹ The ions are very stable under laser action because the luminescence originates from internal transitions of an ion, thus no chemical or physical bonds are involved. Another reason is the long-lived excited state of the ions that facilitate laser action. In addition, by using various ions the whole spectral range from UV to IR is covered almost completely. The luminescence of these ions is reported in several systems from solid phase, e.g. the Nd-YAG laser, to solution. Laser action of Nd³⁺ in solution was already shown in 1966 by Heller *et al.*, who dissolved NdCl₃ in a mixture of SeOCl₂ and SnCl₄ in order to reduce all quenching groups, like the O-H groups of water.² For practical applications, this solvent mixture will not be applicable due to its toxicity, but remarkable luminescence and laser action at 1066 nm was observed. An organic Nd³⁺ complex (neodymium tris(pentafluoropropionate) *o*-phenantroline) showed laser action at 1066 nm in DMSO-*d*₆ solution upon flash excitation of the Nd³⁺ ions,³ however, not so strong as in the SeOCl₂/SnCl₄ mixture. In optical telecommunication, lanthanide ions are of importance because a number of ions have optical transitions at telecommunication wavelengths in the near-infrared (NIR) region.⁴ Therefore, they are employed in optical amplifiers in order to compensate for intensity losses, caused by for instance absorption or scatter in the long fibers. For instance, Er³⁺ has a transition in the 1.55 μm telecommunication window and this ion is doped in the silica fibers, the EDFAs (erbium doped fiber amplifiers).^{5,6} In order to achieve optical amplification the active element (the lanthanide ion) should be excited such that a population inversion is achieved, called pumping. The wavelength of the pump source is determined by the absorption of the lanthanide ion or lanthanide complex. In a population inversion situation, a laser signal that has the same energy as the ion transition stimulates the ions to emit light. These stimulated “photons” have the same direction, phase, and wavelength as the signal, hence the acronym LASER: light amplification via stimulated emission of radiation. In organic complexes, sensitizers can be introduced with broad absorption spectra and in principle, any light source can be used as the pump. An alternative way of pumping could be electro-luminescence where electricity is directly converted to the necessary excited states. Polymers doped with lanthanide ions could be an advantage in the fabrication of amplifiers, because the processing of polymers in waveguides and polymer fibers and polymer light-emitting diodes is relatively easy. In this Chapter, the luminescence of near-infrared emissive lanthanide ions in polymer waveguides and in light-emitting diodes will be described. More in general, properties of the lanthanide

luminescence in organic complexes and sensitization mechanisms will be discussed, with an emphasis on the near-infrared emissive lanthanide ions.

2.2 Complexes in polymer waveguide devices: optical amplification

2.2.1 Introduction

In this paragraph, work published on polymer waveguides doped with lanthanide ions will be described. First, an introduction will be presented to optical waveguiding. Then an overview of polymers will be given that are designed for waveguiding at telecommunication wavelengths in the near-infrared (NIR). Finally, the fabrication and photophysics will be described of polymer waveguides doped with luminescent lanthanide complexes, mainly focussed on near-infrared emissive ions.

2.2.2 Polymer waveguides and waveguiding

Waveguiding is the phenomenon of total internal reflection of a light beam in a material that is embedded in another material with a lower refractive index. Because of this, the light beam is confined and guided through the core of a fiber (see Figure 2.1). A different type of waveguide, but with a similar behavior, is a structure on a solid support, also shown schematically in Figure 2.1. This channel waveguide has a different symmetry, but waveguide characteristics are comparable with that of the (cylindrical) fiber.

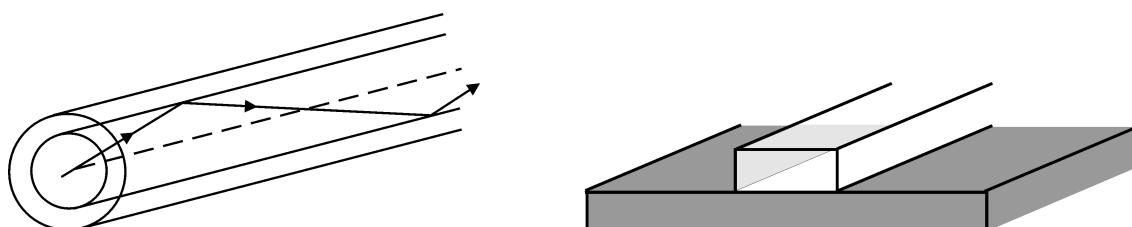


Figure 2.1 Left: schematic picture of a (fiber-)waveguide, consisting of a core material embedded in a cladding material with lower refractive index. Right: schematic picture of a channel waveguide structure on a solid substrate.

In the case of polymers, waveguides on solid support are easily made by spincoating techniques after which channels can be made by standard lithographic techniques. These channels can be embedded in a cladding material by the same spincoating and lithographic techniques. The refractive index of both core and cladding polymers can easily be tuned by using the large variety of available polymers or by chemical modifications of a polymer. In general, the refractive index of polymers varies from 1.25 to 1.85, which makes it possible to create both

high or low refractive index differences by using the same techniques. A high index contrast gives a strong confinement of the light beam in the polymer core and relatively sharp bends are then possible, without too large losses. The latter is of importance for active waveguides in order to design long structures yet on a small area like shown in Figure 2.2.

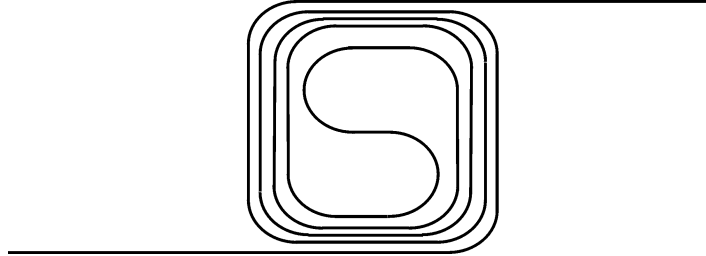


Figure 2.2 Possible waveguide design in order to create a long active path length on a small area.

The electromagnetic radiation is confined in a waveguide core as shown in Figure 2.3 for the first two propagation modes. The horizontal axis represents the distance from the center of the core, with -1 and 1 the positions of the refractive index step (i.e. core/cladding interface). The vertical axis is the intensity of the light. As can be seen, not all intensity of the light is confined in the core of the waveguide, i.e. a substantial part is in the cladding. The intensity of this evanescent field is dependent on the dimensions of the core and on the refractive index contrast. The second guidance mode is shown too, this mode has a node in the waveguide center. The presence of one or more modes is dependent on parameters like the waveguide dimensions, the wavelength of the light, and the refractive index contrast.

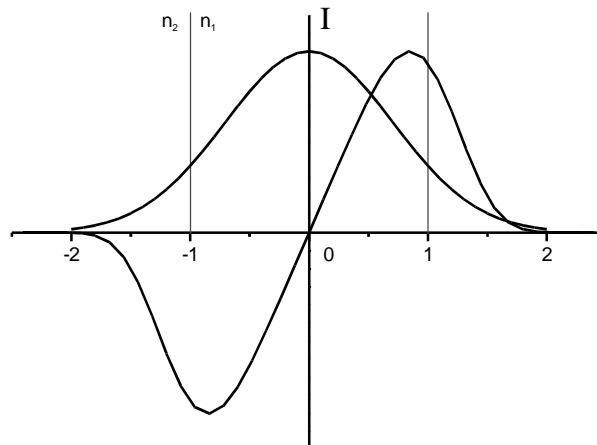


Figure 2.3 The first two optical waveguide modes, the zeroth mode has a Gaussian-like profile, the first mode has a node in the center of the core. The vertical lines at -1 and 1 indicate the interface between core (n_1) and cladding (n_2) of the waveguide.

Single mode waveguiding is desired in many cases, for instance in optical amplification the beams of both pump and signal should be guided in a single mode for maximum overlap and in to minimize signal dispersion. Other options in order to get overlap of pump and signal beams is to design two waveguides in close proximity to each other as is depicted in Figure 2.4. Due to the evanescent field, coupling of one waveguide to the other occurs.⁷

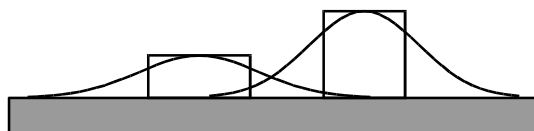


Figure 2.4 Coupled channel waveguides with overlap of the optical modes.

2.2.3 Polymers for telecommunication waveguides

In general, in optical telecommunication light is transmitted at near-infrared wavelengths because of the transparency of silica fibers in this region. Important telecommunication windows are around $1.55 \mu\text{m}$ and $1.33 \mu\text{m}$, but nowadays also the $1.4 \mu\text{m}$ band is becoming available because of the fabrication of fibers with low O-H content.⁸ These O-H groups have a strong absorption in that transmission window caused by the first overtone of the O-H vibration. Optical data-transport through polymers in the near-infrared (NIR) region is limited by the transparency of the materials. Due to the vibrational overtones of O-H and C-H vibrations, relatively strong absorption bands in organic materials are located around $1.1\text{-}1.2 \mu\text{m}$ (second overtone of C-H vibrations), $1.35\text{-}1.45 \mu\text{m}$ (a combination band of C-H stretch and C-H bend vibrations), and above $1.6 \mu\text{m}$ (first overtone C-H vibrations) (see Figure 2.5).

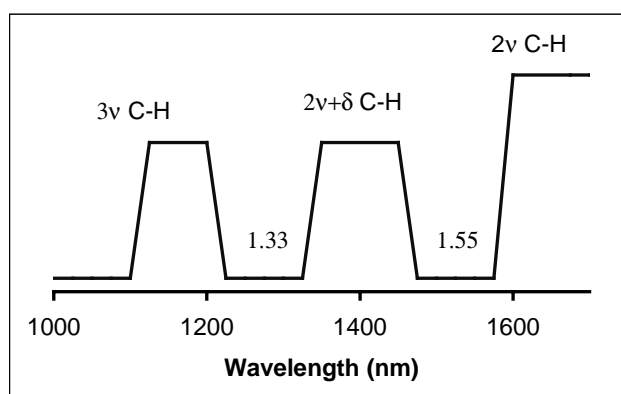


Figure 2.5 Schematic representation of the absorption of polymers in the $1.0\text{-}1.7 \mu\text{m}$ region.

The presence of O-H groups causes an additional absorption around $1.4 \mu\text{m}$, but this can be minimized by the use of polymers without O-H groups and by the exclusion of water from the polymer. Optical windows are located in between these absorption bands at 1.33 and $1.55 \mu\text{m}$

but the absorptions are strong enough at the edges to cause considerable losses. Deuteration and fluorination both decrease these losses. Absorptions are diminished (C-D) or absent (C-F), because the third overtone of C-D is located at 1.5 μm and the third overtone of C-F at 2.6 μm . A number of polymers that have been developed for the use in optical waveguides at telecommunication windows generally contain deuterium and fluorine, like per-deuterated PMMA (**1**, Figure 2.6) and partially fluorinated poly(carbonates).

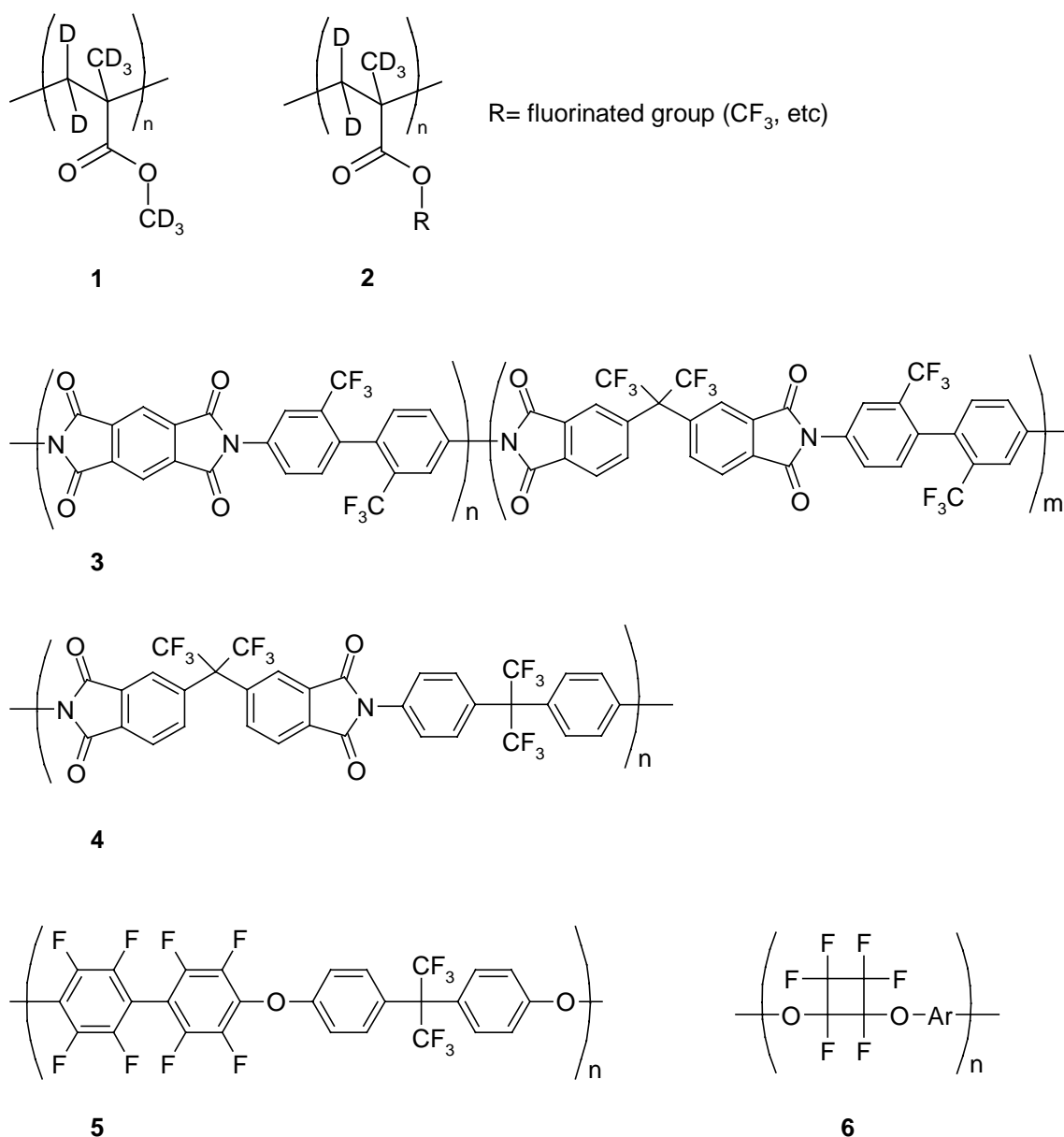


Figure 2.6 Some polymers that have been designed for waveguiding at telecommunication wavelengths in the NIR, **1**: d-PMMA, **2**: d-PFMA, **3**: poly(imide), **4**: poly(imide), **5**: poly(ether), and **6**: fluorinated poly(cyclobutane)

Perdeuterated poly(methyl methacrylate) (*d*-PMMA, **1**) (Figure 2.6) is being used as material in low-loss optical waveguides. These were made with *d*-PMMA as core and partially fluorinated *d*-PFMA (**2**) as the cladding.⁹ The refractive index of PMMA is about 1.49, fully fluorinated PMMA has a much lower value of 1.32. Upon changing the fluorine content their refractive index can be tuned relatively easily. Other halogens like chlorine and bromine are introduced in order to increase the refractive index at high fluorine content, because the index of the core material of a waveguide should not be too low.¹⁰ Halogenation is preferred for the 1.55 μm window, because CD vibrations absorb here (second overtone of the C-D vibration). Deuterated or halogenated polymers are made from the (co-)polymerization of deuterated and halogenated vinylacrylates.¹¹

Poly(imides) have also been reported as a material with low losses in the NIR region^{12,13} and typical structures (**3** and **4**) are shown in Figure 2.6. These types of polymers are made by the condensation of a bisanhydride with a diamine. The fluorine content can be increased or decreased by making copolymers of fluorinated and normal monomers. Advantages of poly(imides) compared to PMMA polymers are the lower water content, the high glass transition temperatures (above 400° C), and the high refractive index. Disadvantages are the low adhesion of these materials to various substrates, but this can be improved by adhesion enhancers (“primers”). The introduction of cross-linkable groups to the main chain improves the polymer properties, especially the long-term adhesion to the substrate and thermal stability. The synthesis of fluorinated poly(ethers) with cross-linkable groups was reported¹⁴ in which the refractive index was controlled by replacing phenyl for methyl groups. Furthermore, deuteration of this material enhances the transparency in the NIR. This material is especially suited for the 1.55 μm region when compared to *d*-PFMA (deuterated polyfluoromethylacrylate). Mickelson *et al.* reported a series of polymers doped with a neodymium complex.¹⁵ The best results were obtained with the Ultradel[®] series of poly(imides) (**4**) and fully fluorinated neodymium chelates. The waveguides were found to be single mode at the telecommunication wavelengths. A material used for a waveguide doped with neodymium chloride is photolime gel. In this material optical gain was measured at 1.06 μm (see below).^{16,17} The photolime gel has a transmission window ranging from 300 nm to 2700 nm, a transmission spectrum illustrated this claim only up to 1100 nm. A range of other polymers has been reported, which in general contain deuterated or fluorinated groups, some examples are the poly(ether) **5** and a perfluorinated cyclobutane ring containing polymer **6** (shown in Figure 2.6).¹⁸

2.2.4 Polymer-based waveguides doped with lanthanide ion complexes

An important issue in telecommunication is the on-chip integration of passive and active components. A convenient way of integration could be the use of polymer-based waveguides, because standard lithography allows for easy patterning. Active waveguides can be derived by doping the polymers with active components like lanthanide(III) ions. Our group reported the fabrication and the luminescence of polymer waveguides doped with a lissamine-functionalized neodymium complex (structure **7**, Figure 2.7).^{19,20,21} The lissamine acts as an antenna-sensitizer for neodymium, which gives the complex a high absorption cross-section ($\sigma_a = 3 \times 10^{-16} \text{ cm}^2$, $\epsilon = 8 \times 10^4 \text{ l mol}^{-1} \text{ cm}^{-1}$ at 580 nm). Waveguides were prepared of a fluorinated poly(carbonate),²² with 3 wt% of the lissamine functionalized Nd^{3+} complex **7**. These exhibited strong Nd^{3+} luminescence, but the lissamine moiety was not stable; at 1 W pumping intensity (515 nm) the lissamine moiety was bleached in 1000 seconds.²⁰ With a coupled waveguide system²³ the high absorption of the pump power can be circumvented, a gain of 1.6 dB was calculated, compared to 0.005 dB for conventional butt coupling, i.e. coupling at the end or beginning of a channel.

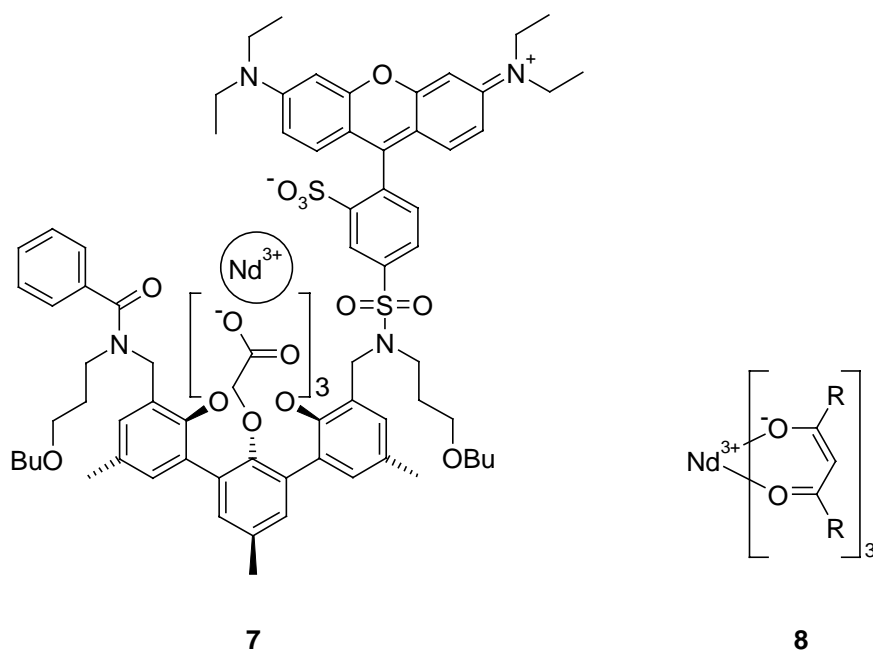


Figure 2.7 Structures of lanthanide complexes, which have been incorporated in polymer waveguides.

Polymer waveguides and polymer fibers have been doped with a number of lanthanide ion complexes: Eu^{3+} ,^{24,25,26,27} Tb^{3+} ,^{24,27} and Sm^{3+} ,^{24,28} which emit in the visible, and Nd^{3+} ,^{29,30,31,32} and Er^{3+} ,^{28,33} as NIR emitting ions. Lanthanide ion salts or complexes with β -diketonates that are commercially available (see Figure 2.7, the Nd^{3+} complex **8**) were used. Although there is relatively much known about polymers doped with visible light-emitting lanthanide complexes,

NIR emissive complexes in polymers are rather rare and are mainly focused on Nd³⁺. Garito *et al.*^{24,28} calculated that an optical gain of 20 dB over 60 cm of a polymer waveguide doped with Sm³⁺ (emission at 645 nm) can be achieved, by doping the polymer with 10²⁰ cm⁻³ Sm³⁺ ions. Chen *et al.* reported optical gain at 1066 nm in neodymium doped waveguide structures.^{34,35,36} They doped gelatin films³⁵ or poly(imide) films³⁴ (Ultradel[®] 9000 series, Amoco Chemicals) with NdCl₃·6H₂O up to 10¹⁹ cm⁻³ Nd³⁺ ions. Doped and undoped poly(imide) layers were spincoated on top of each other to form stacked layers of doped and undoped polymers. This technique was used in order to make thick layers (7 μm) that showed low losses. The Nd³⁺ ions were directly excited at 800 nm with a tunable Ti-sapphire laser as pump source; the output of a 1066 nm Nd-YAG laser was used as a signal beam. A gain of 8 dB at 1066 nm was observed with the Nd³⁺ doped polymer waveguides of 5 cm length. Optical amplification at the 1330 nm telecommunication wavelength in polymer-based waveguides has not been reported so far.

2.3 Near-infrared emitting light-emitting diodes (NIR-LEDs)

2.3.1 Electro-luminescence

In the previous paragraph, polymers doped with lanthanide complexes were discussed. The aim was to achieve optical amplification upon pumping with light, i.e. using photo-luminescence (PL). However, in principle any other method to excite the ions is possible in order to achieve the required excited state. An alternative excitation method is electro-luminescence (EL) where electricity is directly converted into excited states.^{37,38} Furthermore, it is attractive because integration with silicon substrates is possible, which is necessary for integration of devices. In general, two types of light-emitting diodes can be distinguished: organic light-emitting diodes (OLEDs) that are made by vacuum deposition of low molecular weight material on a substrate, and polymer-based light-emitting diodes (PLEDs) that consist of (semiconducting) polymers deposited by techniques such as spincoating. Basic device operation for all LEDs is as follows. A thin layer of semiconducting and fluorescent material is sandwiched between a cathode and an anode (see Figure 2.8), with a typical thickness of the emissive layer of 100 nm. When a bias is applied over the electrodes, holes are injected in the HOMO and electrons in the LUMO of the semiconducting material. Subsequently, the charges are transported through the layer in the direction of the other electrode, driven by the strong electrical field (that is in general larger than 10⁷ V m⁻¹). At some point in the layer, depending on the migration speed of the holes and the electrons, they recombine in an excited state, also called an exciton (which is defined as a bound

hole-electron pair). In an organic dye this exciton is simply an excited state, singlet or triplet, in polymers this pair can be delocalized.

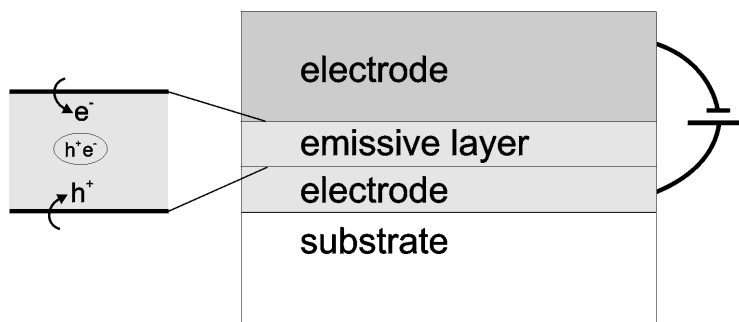


Figure 2.8 Device design: an emissive layer, consisting of a semiconducting material, sandwiched between two electrodes. Generally, the substrate is glass, covered with ITO as a transparent, hole-injecting electrode. Aluminum or another low work-function metal is evaporated on top of the device as electron-injecting counter electrode. Upon migration of the injected charges, recombination yields an excited state.

Nowadays, the emphasis in EL is on organic- and polymer-based materials that cover the whole spectral region (from UV to NIR) and on optimization of the device operation. Due to the spin-statistics both singlet and triplet excited states are formed upon recombination of the charges. Theoretically 75% triplet and 25% singlet excited states are formed, although in PLEDs this ratio is different, closer to 50-50,^{39,40} and ways to utilize these triplet states are investigated. The use of phosphorescent dopings in the devices is a possibility, and a number of applied phosphorescent dopants are depicted in Figure 2.9.^{41,42,43,44}

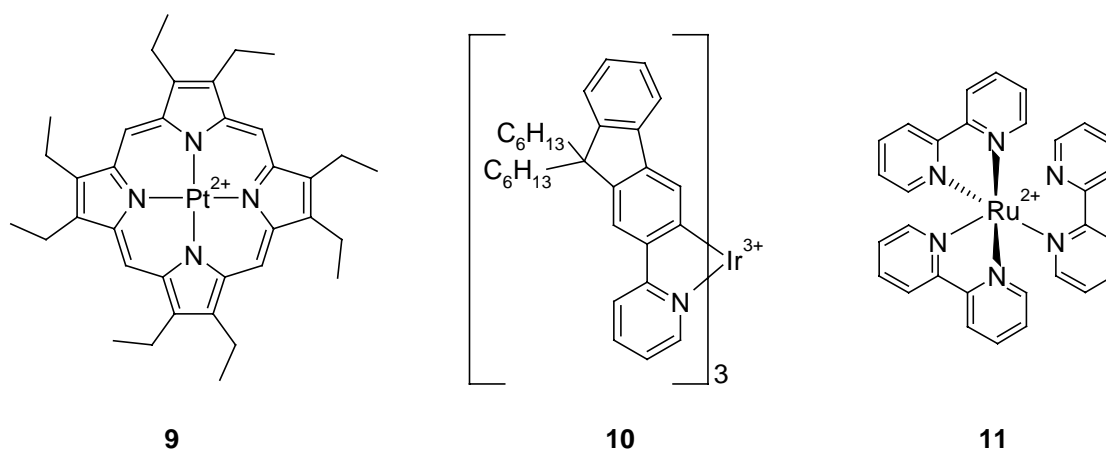


Figure 2.9 Some phosphorescent dopants that were applied in LEDs.

2.3.2 VIS emitting lanthanide(III) ion complexes

Another option to utilize the formed triplet states is to “harvest” them with sensitizer functionalized lanthanide complexes,⁴⁵ because the sensitization of these ions occurs in general via the triplet state of the sensitizer. In fact, a large number of devices based on VIS emitting lanthanide complexes have been made, based on OLEDs with β -diketonate complexes (the complexes **12** and **13**, Figure 2.10).^{46,47}

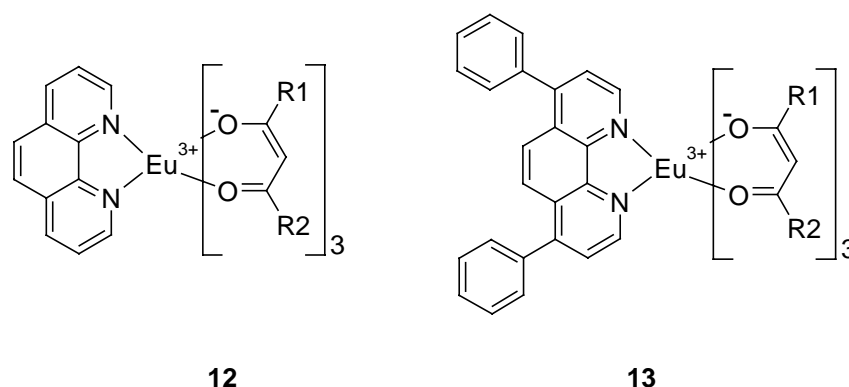


Figure 2.10 Phenanthroline- (**12**) and bathophenanthroline-based (**13**), ternary Eu³⁺ complexes, which are employed in OLED devices.

A quite high efficiency (1-10% external efficiency), good stability, and low turn-on voltages (below 5 V) are obtained with these light-emitting diodes. PLEDs are another class of light-emitting diodes, in which conjugated polymers are doped with lanthanide complexes.^{45,48,49} The processing of polymers in PLED devices is relatively easy, because thin films can be prepared from solution by spincoating.

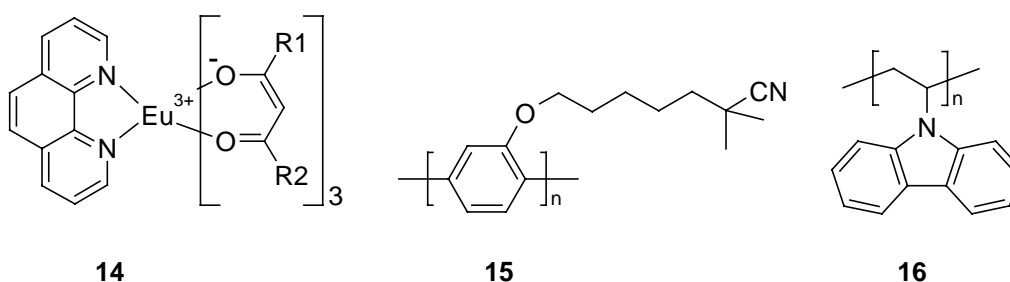


Figure 2.11 Compounds used in the devices by McGehee *et al.*⁴⁵

McGehee *et al.*⁴⁵ reported the EL of europium tris(β -diketonates), **14**, as dopant in the semiconducting polymers CN-PPP, **15**, and PVK, **16**, (Figure 2.11). Blends of several complexes of varying concentrations were made and it was found that a proper choice of energy levels of the ligands for efficient energy transfer and complete quenching of the polymer emission is

necessary. One report⁵⁰ deals with the Eu^{3+} complex **17** in PVK where the Eu^{3+} complex is functionalized with a hole-conducting and an electron-conducting moiety (Figure 2.12). Charge recombination will take place in close proximity to the lanthanide ion, and should lead to efficient lanthanide luminescence, but this was experimentally not proven.

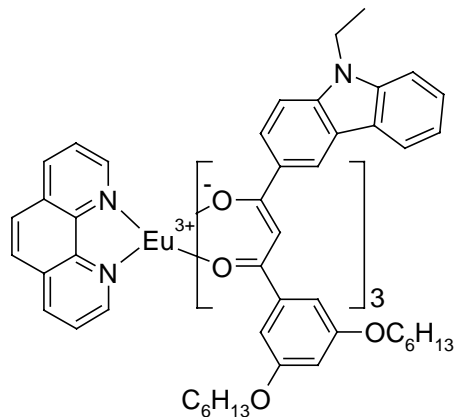
**17**

Figure 2.12 Hole- and electron-transport moiety functionalized Eu^{3+} complex.

2.3.3 NIR emitting lanthanide(III) ion complexes

A number of NIR emissive LEDs have been reported both based on OLED and PLED devices. Gillin and Curry *et al.* reported the production and the photo- and electro-luminescence of OLED devices with ErQ_3 (**18**) or NdQ_3 as the emissive materials (Q is a commonly used abbreviation for the anion of 8-hydroxyquinoline, see Figure 2.13).⁵¹ The complexes, which were vacuum deposited on ITO glass substrates or on silicon wafers, exhibited NIR emission with a maximum at 1536 nm for the ErQ_3 devices with sharper lines than in the photoluminescence experiments. Emission from the ligands (Q) was also observed (in the visible), similar to other Q-based metal complexes like AlQ_3 but with a factor 10^4 lower intensity (AlQ_3 is used in numerous OLED devices as emissive and hole-transport material). Furthermore, Curry *et al.* described the use of silicon as substrate for the OLEDs, where the silicon acts as the hole injection contact. The use of silicon wafers enables direct integration with other silicon-based components.^{51b,d} In most papers, Curry *et al.* refer to Er^{3+} having a long-lived luminescent lifetime, nevertheless, in only one paper the luminescent lifetime is indeed mentioned. They measured a lifetime of about 0.2 ms, but the authors have some reservations about this. It would be the longest lifetimes of Er^{3+} ever measured in organic complexes. In the NdQ_3 based devices they concluded that two isomers of the complex exist, of which one is dominant after the

sublimation step. This conclusion is based on the Stark splitting of the emission around 890 nm, because there are more splitting levels in the starting material than in the sublimated material.

Yanagida *et al.* reported the electro-luminescence of Nd³⁺, Yb³⁺, and Er³⁺, from β -diketonate bathophenanthroline complexes (**20**, Figure 2.13) in OLED devices.⁵² The external efficiencies of the NIR emission are 7×10^{-5} , 3×10^{-4} , and 1×10^{-5} for Nd³⁺-, Yb³⁺-, and Er³⁺-doped devices, respectively. They suggested to use sensitizers with lower excited triplet states in order to enhance the NIR-EL efficiency.

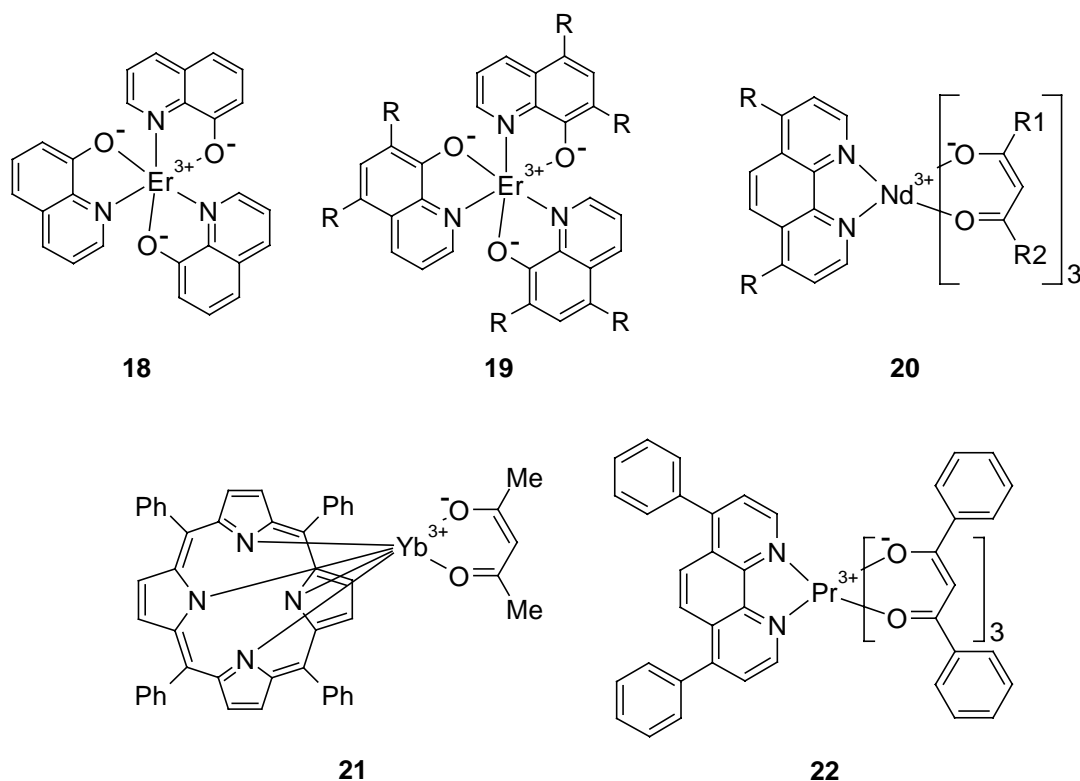


Figure 2.13 NIR emissive Ln³⁺ complexes.

Our group reported the electro-luminescence of the lissamine-functionalized Nd³⁺ complex **7** described above (Figure 2.7). More details are given in Chapter 6 of this thesis. Harrison *et al.* reported the use of porphyrin complexes with Yb³⁺ and Er³⁺ ions (**21**, Figure 2.13) in PLED devices.⁵³ They doped the complex in semiconducting polymers and upon applying a bias, luminescence in the NIR by Yb³⁺ and Er³⁺ was observed. The visible luminescence of the polymer and porphyrin were almost completely quenched and only the NIR emission bands of Yb³⁺ and Er³⁺ were detected. Near-infrared and visible luminescence from a Pr³⁺ β -diketonate complex **22** was reported.⁵⁴ Again, bathophenanthroline was coordinated to the Pr³⁺ tris β -diketonate complex in order to reduce the vapor pressure of the complex. Luminescence in the

NIR at 1000-1100 nm and around 1500 nm was measured at a driving voltage of 12 V. The same complex with Yb^{3+} as the central ion was reported to show electro-luminescence at 980 nm.⁵⁵

2.4 Sensitized NIR Ln^{3+} emission

2.4.1 Introduction

In the previous paragraphs, the terms ‘sensitized emission’ and ‘antenna effect’ are being used. These terms refer to the same phenomenon, i.e. a chromophoric group in a complex is first excited followed by energy transfer to the lanthanide ion, thereby exciting this ion. In this paragraph, the sensitized luminescence of lanthanide ions will be discussed. First, the luminescence of lanthanide complexes will be explained. Subsequently, the sensitization mechanisms of lanthanide ions will be dealt with and finally, lanthanide complexes functionalized with sensitizers will be described, with the focus on the near-infrared emissive lanthanide ions.

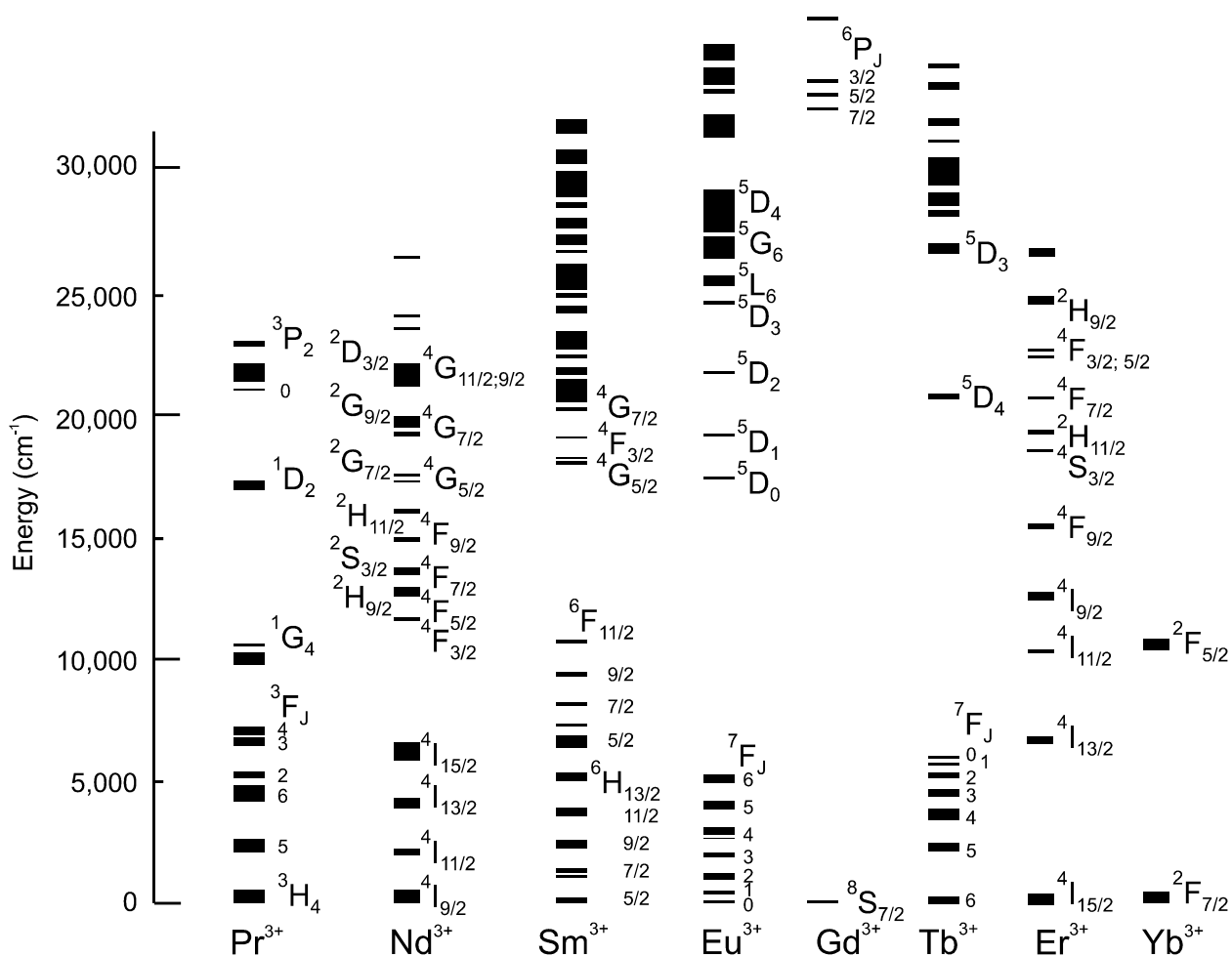


Figure 2.14 Energy level scheme of a number of the lanthanide ions.⁵⁶

2.4.2 Lanthanide luminescence

The energy levels of some of the trivalent lanthanide ions are depicted in Figure 2.14: Nd³⁺, Er³⁺, Yb³⁺, Eu³⁺, Tb³⁺, Sm³⁺, Gd³⁺, and Pr³⁺. These energy levels are denoted as ^(2S+1)Γ_J, where S is the spin multiplicity, Γ the orbital angular momentum, and J the total angular momentum. Transitions within these energy levels are strongly forbidden by the parity selection rules. By ‘stealing’⁵⁷ intensity from allowed transitions (mixing of orbital functions with for instance the 4f-5d transitions) the selection rules are somewhat relaxed and optical absorption transitions of the ions are present but they are relatively weak. Consequently, the reverse process –emission– is also forbidden. This results in long-lived excited states, up to milliseconds. A way to circumvent the low absorption coefficients is to use an antenna. Upon excitation of the antenna, its energy is transferred to the lanthanide ion, which subsequently leads to the lanthanide ion-based emission.

Ermolaev *et al.* reported luminescent lifetimes of a number of lanthanide ions that emit VIS and NIR light in solution.⁵⁸ The luminescence of the NIR emitting ions is strongly quenched by O-H and C-H vibrations. Beeby and Faulkner reported luminescent lifetimes of Nd³⁺ ions in solution, which were found to be in the microsecond region (0.5 μs in CD₃OD and 9.0 μs in DMSO-*d*₆).⁵⁹ They determined quenching constants of O-H and C-H vibrations by measuring the luminescent lifetime in a series of solvents such as water and deuterated water, methanol and deuterated methanol, the latter with varying deuteration grades. Replacing O-H by O-D had a much stronger effect (about ten times) on the lifetime than the replacement of C-H by C-D.⁵⁹

2.4.3 Lanthanide complexes

The ionic radius of the lanthanide ions varies in the series from 1.2 Å for lanthanum to 0.95 Å for lutetium (Figure 2.16). This is a significant difference and the coordination number varies through the series from about 10-11 for lanthanum(III), to 8-9 for lutetium(III). The first complexes reported were based on the β-diketonates.⁶⁰ These negatively charged, bidentate ligands form 3:1 complexes, which are overall neutral. Neutral ligands like phenantroline can be coordinated in addition, because the coordination number of the ions is higher than six. These are of special interest in the fabrication of OLED devices because the ternary complexes with phenantroline or bathophenantroline have a much lower sublimation point that allows easy sublimation of these materials on OLED devices. The lowered sublimation points are caused by distortion of the symmetry in the complexes and vacuum deposition of the complexes is relatively easily achieved.

A large variety of multidentate ligands has been used to complex lanthanide ions. Multidentate ligands have important properties like kinetic and thermodynamic stability and the ability to shield the lanthanide ion from the solvent. Cyclen complexes (Figure 2.15) have extensively been used by the group of Parker.⁶¹

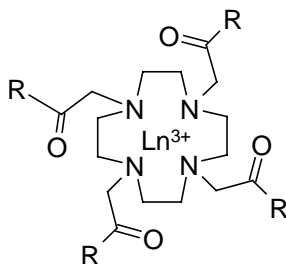


Figure 2.15 Cyclen complex.

These multidentate ligands form strong and stable complexes with lanthanide ions, are water soluble, allow for functionalization with a variety of substituents and sensitizers (see other sections of this Chapter), and have one or two water molecules coordinated to the lanthanide ion, which can be tuned by varying the substituents on the ligand. The number of coordinating water molecules is of importance in magnetic resonance imaging (MRI) where these complexes can be applied as contrast agents.⁶²

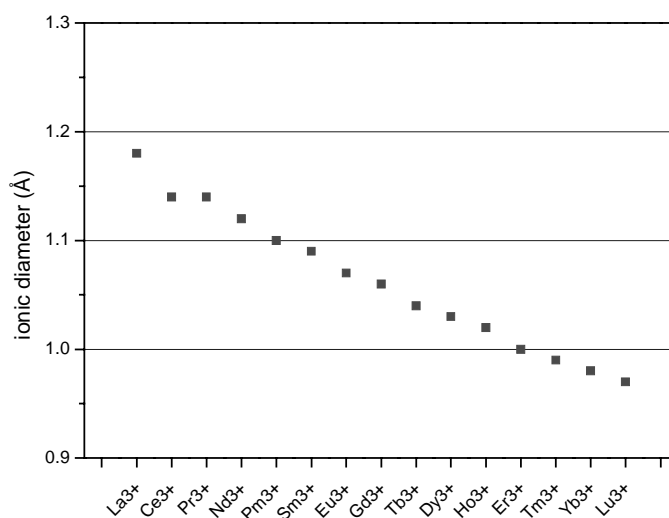


Figure 2.16 Ionic radius of trivalent lanthanide ions with coordination number eight.⁶³

Other multidentate complexes are based on calix[4]arenes⁶⁴ and the *m*-terphenyl moiety (Figure 2.17).^{65,66} These building blocks are easily functionalized with groups like carboxylates, amide, and phosphonic acids, which complex lanthanides. Upon deuteration of the terphenyl-

based ligand **23**, the luminescence of the lanthanide ions was enhanced.^{67,68} Furthermore, it was shown that upon changing the cyclic systems of **23** and **24** to a less rigid open system in **25** the solubility was enhanced. This knowledge led to the development of terphenyl-based ligands with amide side chains (**26-28**). These amides enhance the complexation and give complexes that are highly soluble. Upon changing the amide substituents from acetyl (**26**) to benzoyl (**27**) and from an amide to a sulfonamide (**28**) no significant changes were found in the Eu³⁺ emission and in the NIR emission of Nd³⁺, Er³⁺, and Yb³⁺. This renders the *m*-terphenyl moiety very useful in various applications.

Other complexes used are EDTA,⁶⁹ DTPA,⁷⁰ and crown ethers.⁷¹ The kinetic stability and the shielding towards the solvent of these complexes are in general lower than that of the above treated preorganized multidentate ligands like **26**.

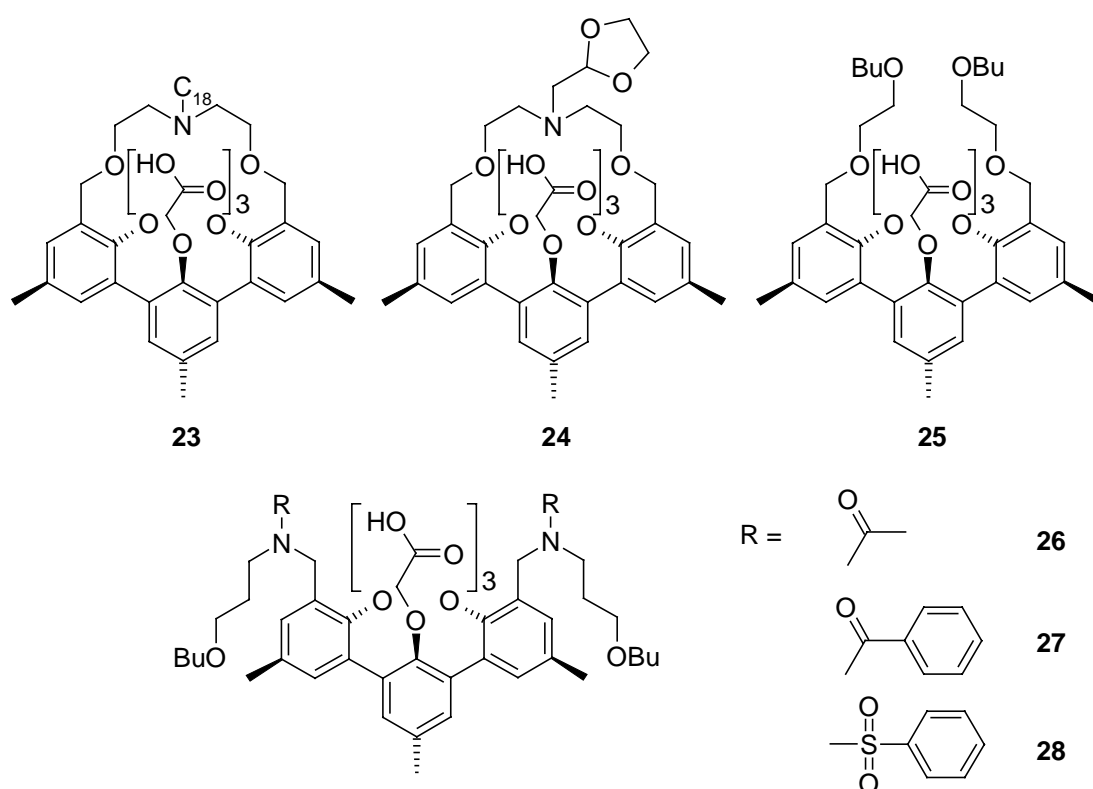


Figure 2.17 *m*-Terphenyl-based lanthanide complexes.^{65,66}

Yanagida and Hasegawa *et al.* described the “remarkable” NIR luminescence of deuterated and fluorinated β -diketonate complexes.^{72,73} Their strategy is to decrease the number of hydrogen atoms in the ligands as much as possible. They synthesized fluorinated and deuterated (at the α -position) β -diketonates **29** (Figure 2.18) with long fluorinated tails, which shield the

ions from solvents. The highest luminescent lifetime of **29** was 6.3 μs in $\text{DMSO-}d_6$ solution (with a quantum yield of 1.1 %).

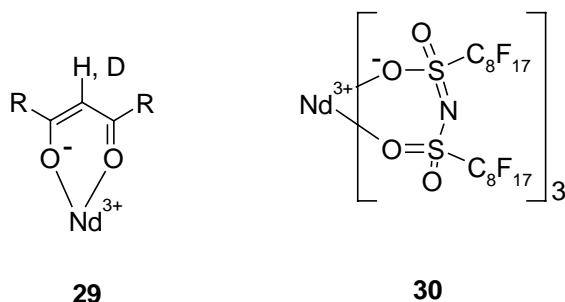


Figure 2.18 Fluorinated complex by Yanagida et al.⁷⁴

More recently,⁷⁴ they reported the perfluorinated sulfonylaminato Nd^{3+} complex **30**, which has no hydrogen or deuterium at all. The luminescent lifetime in acetone is 12.0 μs , and in deuterated acetone 13.0 μs . The luminescent quantum yield is about 3%, the highest ever reported in a hydrogen containing organic solvent. The small difference in lifetime in methanol and in deuterated methanol proves that the chelate shields the ion from the solvent very efficiently.

Other complexes are fullerenes like C_{82} or C_{84} , doped with lanthanide ions.⁷⁵ The formation of doped fullerenes was monitored with UV spectroscopy, as the doped fullerenes have a different absorption spectrum than the undoped ones. The emissive level of Er^{3+} is below the excited levels of the fullerenes, which minimizes energy losses via non-radiative processes. For all lines of the Ar^+ ion laser, luminescence at 1536 nm was observed, indicative of Er^{3+} emission sensitized by the fullerenes.

2.4.4 Sensitized emission

Energy transfer

Sensitizers are being used to excite the lanthanide ions via an energy transfer from the sensitizer (or antenna) to the lanthanide ion. This energy transfer is schematically depicted in a Jablonski diagram in Figure 2.19. Upon absorption of light the sensitizer is excited to the singlet excited state. This state can transfer its energy to the lanthanide ion (singlet energy transfer, ET_S), can convert to the triplet state (intersystem crossing, ISC), or can decay to the ground state (by fluorescence or non-radiatively). From the triplet state energy is transferred to the lanthanide ion (ET_T) or the triplet state decays to the ground state. In general, energy is transferred via the triplet state because the intersystem crossing is enhanced by the nearby, paramagnetic lanthanide

ions, and because energy transfer via the singlet state is not fast enough to compete with the fluorescence or the intersystem crossing.

Energy transfer can proceed via dipolar or multipolar interactions between sensitizer and acceptor (lanthanide ion), a Förster mechanism of transfer,⁷⁶ or via an exchange mechanism, the Dexter mechanism of transfer.⁷⁷ The main difference between these two types of energy transfer is that in the Dexter mechanism orbital overlap is needed, whereas in the Förster mechanism the transfer is through space and is strongly dependent on the spectral overlap of the emission spectrum of the donor and the absorption spectrum of the acceptor. The distance dependence of the Dexter mechanism is exponentially, in the Förster mechanism this is to the power -6. In the Dexter mechanism, the spectral overlap is independent of the oscillator strength of the transitions (emission and absorption spectra are normalized such that the areas of the spectra are unity). Energy transfer by the Dexter mechanism is only efficient at very small distances (<10 Å), whereas Förster energy transfer has been reported to occur over much longer distances.⁷⁸

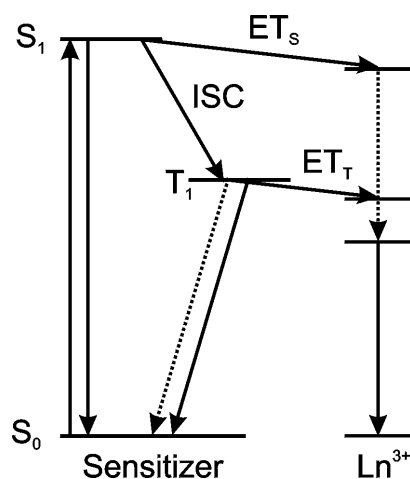


Figure 2.19 Jablonski diagram for sensitized emission of lanthanide ions by a sensitizer.

Malta *et al.* performed theoretical calculations on the sensitization of Eu³⁺, Yb³⁺, and Sm³⁺ by sensitizers.^{79,80} They derived formulas for dipolar and multipolar energy transfer (Förster type) and for an exchange mechanism (Dexter type). For energy transfer from an excited singlet or triplet state to the ^(2S+1)Γ_J levels of lanthanide ions the selection rules for energy transfer are:

$|\Delta J| = 0, 1$ ($J = J' = 0$ excluded) for a Dexter mechanism or

$|\Delta J| = 2, 4, 6$ for a Förster mechanism.

Accepting levels of the lanthanide ions were selected according to three criteria: (i) the energy gap between donor (sensitizer singlet or triplet state) and acceptor (lanthanide ion levels) should not be too large, (ii) the selection rules outlined above, and (iii) significant matrix elements of the orbital overlap. The latter were calculated from the molecular orbital wave

functions given by molecular modeling simulations. Theoretical values were calculated for rate constants and quantum yields of the sensitized europium emission and these were confirmed by experimental data. Important in the cases they calculated is that all possible pathways for energy transfer are considered. However, energy transfer from the triplet state is the most dominant mechanism. These calculations justify the presumptions generally made that energy transfer proceeds solely via triplet states of the sensitizers. These theoretical calculations were recently also performed on the Yb^{3+} and Sm^{3+} complexes of ligand **31**, Figure 2.20.

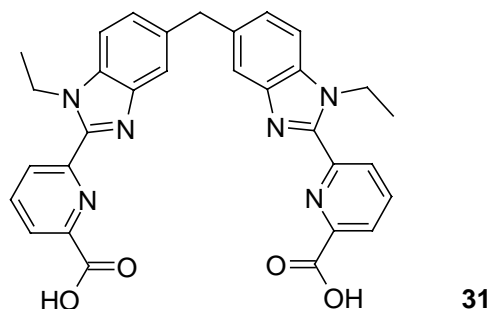


Figure 2.20 Ligand that forms triple helicates with two lanthanide(III) ions.

As an illustration of the selection rules, the results of the calculations of the energy transfer from **31** to Sm^{3+} are presented in Table 2.1. From these rate constants, theoretical quantum efficiencies were calculated and these correspond very well with the observed quantum efficiencies for energy transfer and Sm^{3+} luminescence.

Table 2.1 Calculated energy transfer rates from **31** to Sm^{3+} .⁸⁰

donor ^a	acceptor	ΔJ^b	E (cm ⁻¹)	k_{ET} (s ⁻¹)	k_{BT} (s ⁻¹) ^c
T	⁴ G _{5/2} ⁽¹⁾	0	17,900	8.4×10 ⁹	2.7×10 ⁸
T	⁴ I _{9/2}	2	20,500	4.7×10 ⁶	601
S	⁴ H _{9/2}	2	29,000	6.0×10 ⁵	1.2×10 ³
S	⁴ H _{13/2}	4	29,800	1.4×10 ⁵	1.3×10 ⁴
S	⁴ G _{9/2}	2	30,100	1.5×10 ⁶	5.9×10 ⁵
S	⁴ G _{5/2} ⁽²⁾	0	30,323	1.8×10 ⁸	1.3×10 ⁸

a Triplet energy level: 18,620 cm⁻¹, singlet energy level: 30,300 cm⁻¹.

b ΔJ for the transition from the groundstate ⁶H_{5/2} to the reported excited state.

c Energy back transfer: from excited lanthanide ion to sensitizer.

From Table 2.1 it is clear that the energy transfer to excited states in which a transition $\Delta J = 0$, is involved are the fastest. This is the case because Dexter energy transfer at short distances to the lanthanide ions is much faster from both the singlet and the triplet excited state. The fact that in general there is no energy transfer from the singlet state is due to the rapid deactivation of the singlet state to the ground state or to the triplet state.

Our group reported a lanthanide ion complex that is functionalized with a triphenylene antenna (**32**.Ln, Figure 2.21).⁸¹ Upon excitation of the triphenylene visible luminescence of Eu³⁺ and Tb³⁺ was observed in methanol. The number of coordinated solvent molecules was calculated according to the formula by Horrocks and Parker⁸² from the luminescent lifetime in methanol and deuterated methanol and it was found that one methanol is coordinating to the lanthanide ion. Sensitized NIR emission was also observed from Nd³⁺, Er³⁺, and Yb³⁺. The energy transfer takes place completely via the triplet state of the sensitizer, which is confirmed by transient absorption measurements. The energy transfer rate is the fastest in the complexes of the ions that emit in the visible: $8.0 \times 10^7 \text{ s}^{-1}$ (**32**.Eu³⁺) and $1.0 \times 10^7 \text{ s}^{-1}$ (**32**.Tb³⁺) complexes. The transfer rate in the NIR emissive complexes is $1.3 \times 10^7 \text{ s}^{-1}$ (**32**.Nd³⁺), $3.8 \times 10^6 \text{ s}^{-1}$ (**32**.Er³⁺), and $4.9 \times 10^6 \text{ s}^{-1}$ (**32**.Yb³⁺) complex.

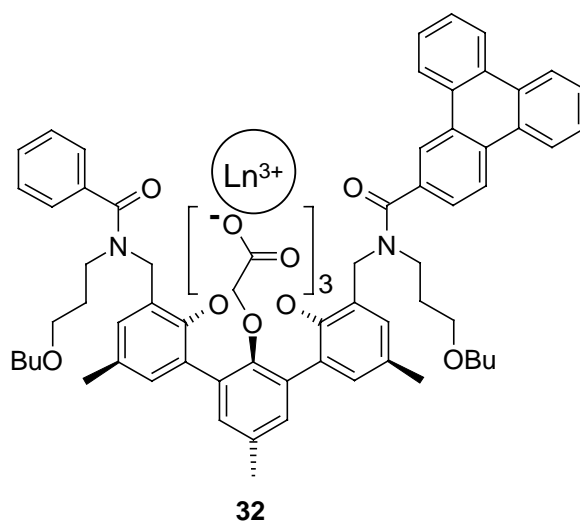


Figure 2.21 Triphenylene-functionalized lanthanide complex.

In some cases, the sensitization of Yb³⁺ and Eu³⁺ proceeds via an alternative, charge transfer mechanism, because these ions are relatively easily reduced to Ln²⁺ by a photon-induced electron transfer. The driving force for such a mechanism can be estimated with Eq. 2.1.⁸³

$$\Delta G = E_{\text{sens}^{\bullet+}/\text{sens}} - E_{\text{sens}^*} - E_{\text{Ln}^{3+}/\text{Ln}^{2+}} \quad \text{Eq. 2.1}$$

In Eq. 2.1, the driving force ΔG is determined by the oxidation potential of the sensitizer ($E_{\text{sens}^{\bullet+}/\text{sens}}$), the excited state energy of the sensitizer (E_{sens^*}), and the reduction potential of the lanthanide ion ($E_{\text{Ln}^{3+}/\text{Ln}^{2+}}$). Reduction of organic Eu^{3+} complexes does not lead to sensitization because the charge transfer state is too low in energy to be able to deactivate the the $^5\text{D}_J$ excited levels of Eu^{3+} . The reduction of Yb^{3+} may lead to emission in the NIR region, because the excited level of Yb^{3+} is much lower in energy and deactivation of the charge transfer state leads to an excited Yb^{3+} ion.

Another important phenomenon in the sensitization of lanthanide ions is energy back transfer from the excited lanthanide ion to the sensitizer. This happens in cases where the donating sensitizer level is (too) close to the accepting lanthanide ion level, which makes thermally activated energy back transfer possible. In the cases of Eu^{3+} and Tb^{3+} this has been measured by Mukkala *et al.*⁸⁴ who showed that the triplet state of a sensitizer should at least be $1,200\text{ cm}^{-1}$ higher in energy than the accepting levels of Tb^{3+} and Eu^{3+} . So far, this has not been shown for the NIR emissive lanthanide ion complexes (see Chapter 4 of this thesis).

UV absorbing sensitizers

Given the fact that in Eu^{3+} the $^5\text{D}_1$ level at $19,000\text{ cm}^{-1}$ is the receiving level and that the triplet state of the sensitizer should be $1,000\text{-}2,000\text{ cm}^{-1}$ above this level, it follows that the singlet and absorbing state of the sensitizer should be in the order of $25,000\text{ cm}^{-1}$, which is the UV region.

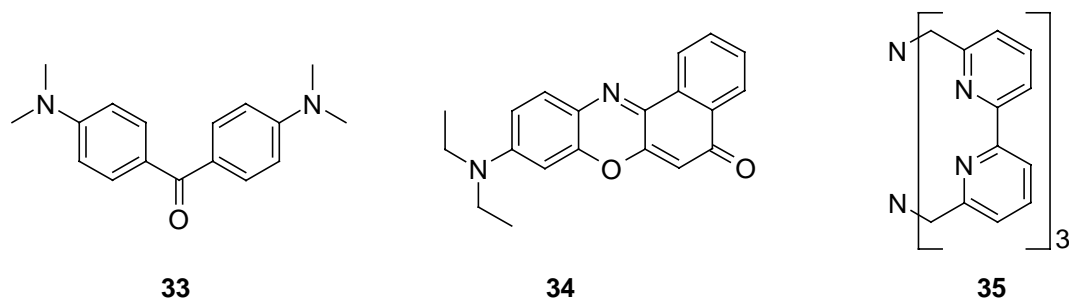


Figure 2.22 Michler's Ketone (**33**), Nile Red (**34**), and the Lehn cryptand (**35**).

β -Diketonate complexes form strong 3:1 complexes and have absorption bands, which can be tuned easily by changing substituents on the chelate. Furthermore, due to high intersystem crossing efficiencies and a short distance between sensitizer and ion, the sensitization of the lanthanide luminescence is quite efficient. In neutral 1:3 complexes, the coordination number on the lanthanide ion is six. This means that the coordination of the lanthanide ions is unsaturated

and additional ligands can be incorporated. This was already discussed in the preparation of OLED devices where phenanthroline-like ligands were used to increase the volatility of the emitters. Werts^{85,86} used β -diketonate ligands in order to make ternary complexes (Eu-FOD and Nd-FOD) with additional sensitizers like Michler's Ketone (**33**) and Nile Red (**34**, Figure 2.22). Upon complexation of the carbonyl moiety in these two sensitizers to a lanthanide ion, a bathochromic shift was observed. Due to this shift, Michler's Ketone enables visible light sensitization of Eu³⁺.

In our group, ternary complexes were made that are based on the terphenyl-⁸⁷ and calix[4]arene complexes⁸⁸ of Nd³⁺, Yb³⁺, and Er³⁺, and β -diketonates. The terphenyl complexes leave room for additional ligands and β -diketonates were good candidates, as they enhanced the luminescent properties by better shielding of the ternary complex from the quenching solvent. Upon coordination sensitization by the β -diketonates was observed. NIR luminescence from Pr³⁺, sensitized by β -diketonates, was also reported.⁸⁹ Kazakov *et al.* reported one of the few cases of sensitized luminescence in organic Pr³⁺ complexes.⁸⁹ They showed that the Pr³⁺ luminescence spectrum is dependent on the triplet state of the β -diketonates, because the receiving level can be either the ³P₀ or the ¹D₂ level (Figure 2.14), leading to different emission spectra. In the case of TTA (trifluorothienoyl β -diketone) and BTFA (trifluorobenzoylacetone) the triplet state is lower than the ³P₀ level and energy is only transferred to the ¹D₂ level, whereas the other β -diketonates transfers the energy also to the ³P₀ level. In the emission spectrum, the luminescence from the ³P₀ level was only observed in the case of the latter β -diketonates. NIR emission was observed from the ¹D₂ level at 850 nm (¹D₂→³F₂) and at 1050 nm (¹D₂→³F₄).

Some other UV absorbing chromophores are phenanthridine,⁹⁰ bipyridine (e.g. in the Lehn cryptand **35**⁹¹), and terpyridine.⁹² The luminescent lifetimes of the Nd³⁺ and Yb³⁺ complexes of the Lehn cryptand were reported to be 5.2 μ s for Yb³⁺ in D₂O and 0.3 μ s for Nd³⁺ in D₂O.⁹¹ Based on the number of coordinated water molecules (q) to lanthanide ions in other complexes (EDTA complexes, $q = 2$) the number of coordinating water molecules on Nd³⁺ and Yb³⁺ were calculated for the cryptand from the luminescent lifetimes in H₂O and D₂O. The Yb³⁺ complex gave a value of $q = 1.5$, close to the number of the Eu³⁺ and the Tb³⁺ complexes, the Nd³⁺ complex gave a number of about 0.5, but the authors question this number. This value could not be determined accurately because of the low intensity of Nd³⁺ luminescence. The phenanthridine chromophore and related chromophores are sensitizers used by the group of Parker for the sensitization of Eu³⁺ because of the sensitivity of these chromophores to properties like pH and pO₂.⁹³ A number of lanthanide complexes made by Parker *et al.* are based on sulfonamide

complexes.^{94,95,96} These can be deprotonated and a response of the lanthanide ion luminescence can easily be detected. Furthermore, a number of complexes were made that contain a chromophore in the chelate structure like calix[4]arenes and the *m*-terphenyl moiety.⁶⁷ Upon UV excitation of the *m*-terphenyl moiety, luminescence was observed of a whole series of lanthanide ions (**23**.Sm³⁺, **23**.Tb³⁺, **23**.Dy³⁺, **23**.Pr³⁺, **23**.Nd³⁺, **23**.Er³⁺, and **23**.Yb³⁺).⁶⁵

Fluorescent dyes as sensitizer

The great advantage of the use of VIS absorbing antennas for the NIR luminescence is that there is a broad availability of inexpensive excitation sources (e.g. lamps, diode lasers), normal glass can be used for substrate handling instead of quartz, and there is less energy dissipation in the sensitization process. One of the first papers that reported visible absorbing and fluorescent dyes as sensitizers for Nd³⁺ and Yb³⁺ describe the use of triphenylmethane derivatives such as xylenol orange (**36**, Figure 2.23).⁹⁷ There, the best sensitization properties were reported for the dyes that contain a sulfonic acid moiety, of which **36** was the best. The complexing carboxylates form a strong complex between dye and the lanthanide ions in solution.

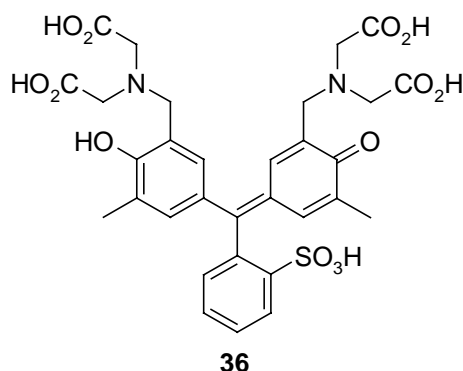


Figure 2.23 Xylenol orange.

Klink *et al.* reported the dyes lissamine and Texas red as Nd³⁺ sensitizers (**39-40**, Figure 2.24). Despite the strong inherent fluorescence (>90%) of these dyes, upon complexation of Nd³⁺ the fluorescence was quenched and Nd³⁺ emission sensitized by these dyes was observed.⁹⁸ This emission is due to either enhanced intersystem crossing by the nearby heavy and paramagnetic lanthanide ions, or by singlet energy transfer. Sensitization of Nd³⁺ was also reported by dansyl or coumaryl that are excited with UV light. Upon complexation of Nd³⁺, the fluorescence was strongly reduced in these fluorophores, and Nd³⁺ emission was observed. Dansyl was reported as sensitizer of Nd³⁺ luminescence in a dendrimer, terminated with dansyl moieties. The authors suggest an energy transfer mechanism via the singlet state.⁹⁹ Their argument is mainly based on

the fact that dansyl does not show phosphorescence, which is, however, not completely true because under harsh conditions dansyl phosphorescence was observed.¹⁰⁰ These conditions involved are a concentrated thallium nitrate solution (intersystem crossing perturber) in the presence of sodium sulfite as deoxygenator.

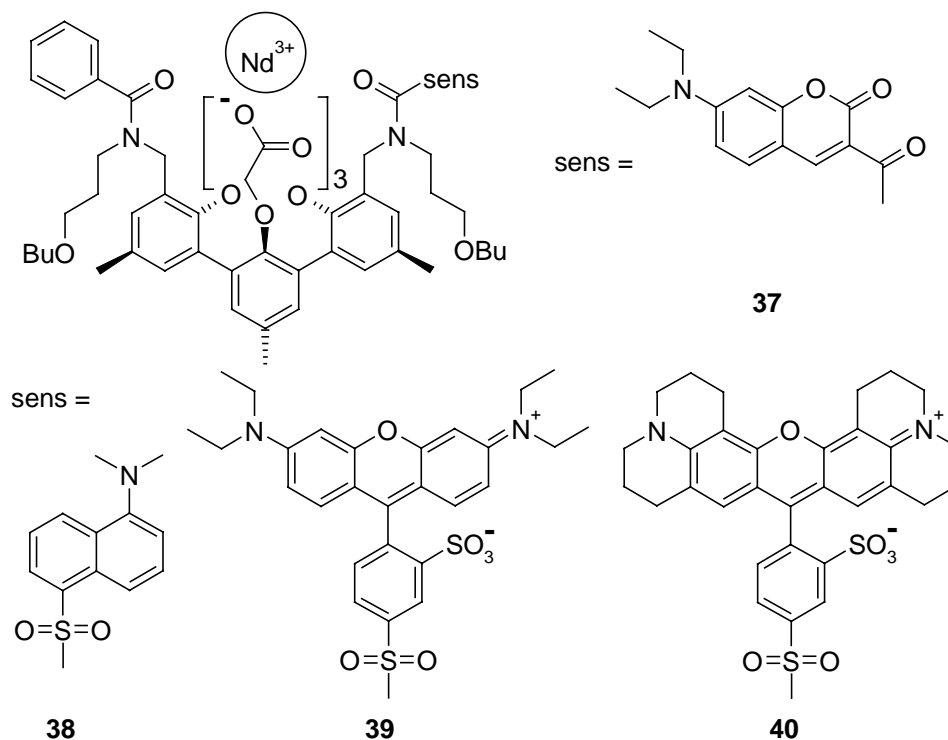


Figure 2.24 Dye-functionalized lanthanide complexes based on the *m*-terphenyl building block, **37**: coumaryl, **38**: dansyl, **39**: lissamine, **40**: Texas Red.

Fluorescein

One of the most important dyes in biology is fluorescein, which is used as green fluorescent probe in various applications. The great advantage of fluorescein is the absorption maximum around 488 nm, which makes it suitable for excitation with an Argon laser. Eosin and erythrosin are structurally similar dyes. However, they possess heavy atoms (bromine in eosin and iodine in erythrosin) which results in lower fluorescence quantum yields because of enhanced intersystem crossing to the triplet state of the dye. Werts *et al.* coupled DTPA ligands to fluorescein and eosin and made NIR emissive lanthanide complexes.⁷⁰ They observed the sensitized emission of Nd³⁺, and Yb³⁺ in H₂O and for Nd³⁺, Yb³⁺, and Er³⁺ in D₂O solution. They found that eosin is more efficient as a sensitizer than fluorescein, due to the enhanced intersystem crossing by the bromine atoms in eosin. Furthermore, they found that the energy transfer is rather slow, especially for Yb³⁺, because the sensitized emission is strongly oxygen

dependent. Oxygen quenches the triplet state of the dyes and this competes with the energy transfer to the lanthanide ions.

The sensitization of Nd^{3+} , Er^{3+} , and Yb^{3+} by fluorexon, **41** has been reported, a dye similar to fluorescein (Figure 2.25).¹⁰¹ This compound forms 1:1 complexes with lanthanide ions and the fluorescence is strongly reduced, mainly due to enhanced intersystem crossing and NIR emission from Nd^{3+} , Er^{3+} , and Yb^{3+} . Deoxygenation of the solutions did not enhance the sensitized luminescence, which shows that energy transfer to the lanthanide ions is fast. A near-infrared luminescent label was made, based on the Yb^{3+} ion and a fluorexon derivative (**42**, Figure 2.25).¹⁰² The isothiocyanate function in this compound makes reaction with amine functionalities in biological compounds possible, e.g. on avidine. The great advantage of using this complex as label is that visible light can be used as excitation source, and that the long-lived Yb^{3+} -luminescence (microseconds) allows distinguishing this light from the auto-fluorescence (nanoseconds) of biological systems. Calix[4]arenes have been functionalized with fluorescein and NIR luminescence, sensitized by the fluorescein moiety was observed of Nd^{3+} and Er^{3+} .⁶⁴

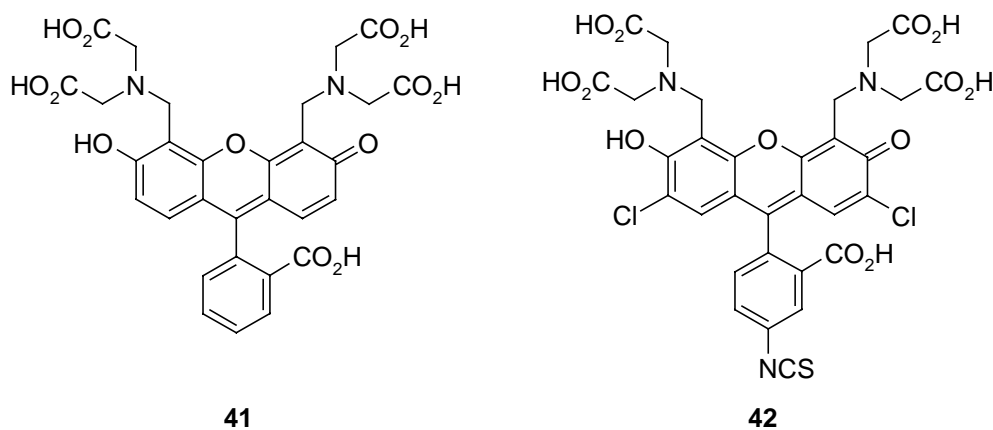


Figure 2.25 Fluorexon (**41**) and a fluorexon derivative with a coupling moiety (isothiocyanate) (**42**).

Porphyrins

Other classes of lanthanide complexing compounds are porphyrins (**43**), phthalocyanines (**44**), and texaphyrins (**45**, Figure 2.26).¹⁰³ The first two compounds can form double-decker complexes with the lanthanide ion sandwiched in between two porphyrins. In other complexes the lanthanide ion is complexed by one ring and the coordination on the ion is completed with β -diketonates (e.g. complex **22** in Figure 2.13). The ring of texaphyrins (**45**) is somewhat larger and can accommodate a lanthanide ion in the center. NIR emission, sensitized by texaphyrins was not reported, probably because the primary use of these complexes is in photodynamic

phototherapy and as MRI contrast agent. It is already known that the heavy and paramagnetic lanthanide ions deactivate the singlet excited state of texaphyrins, but recently an extensive study showed that the decrease in fluorescence can be related to the magnetic moment of the complexed ion.¹⁰³ Yb³⁺ luminescence in porphyrin complexes was already reported in 1976.¹⁰⁴ It was found that the singlet emission is quenched due to enhanced intersystem crossing, intramolecular energy transfer from the singlet excited state to the lanthanide ion, or by intramolecular charge-transfer from the π -system of the porphyrin to the ion. This charge transfer mechanism was observed in the Eu³⁺ and Yb³⁺ complexes, but this only lead to emission of Yb³⁺.¹⁰⁵ Strong deactivation of the fluorescence was also observed for Sm³⁺ complexes.¹⁰⁶

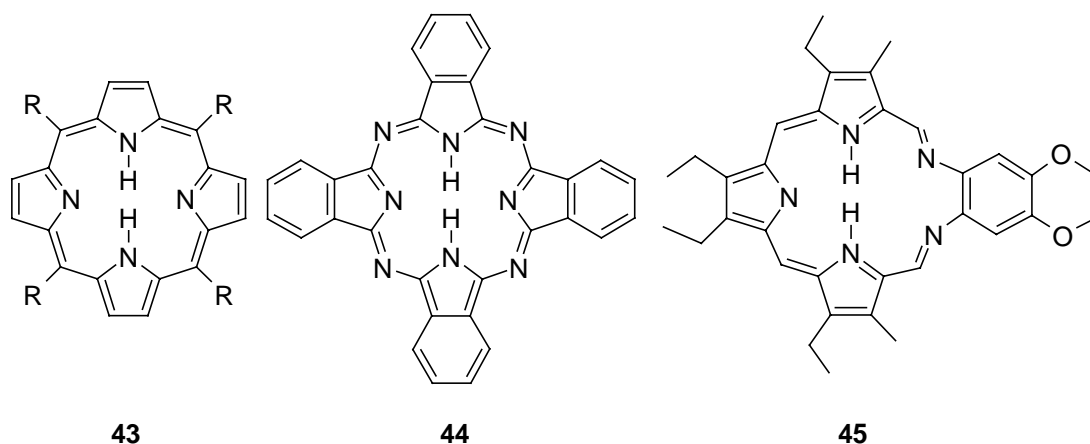


Figure 2.26 From left to right: porphyrin (**43**), phthalocyanine (**44**), and texaphyrine (**45**).

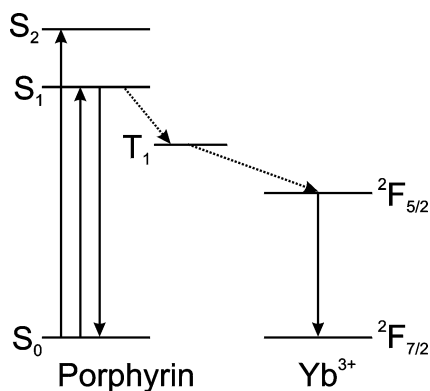


Figure 2.27 Jablonski diagram for the sensitization of Yb³⁺ by a porphyrin.

Recently,^{107,108} porphyrin sensitized Yb³⁺ emission (Figure 2.27) was measured at various temperatures. At low temperature the high-energy side bands of the 975 nm emission of Yb³⁺ had disappeared. This behavior is ascribed to the thermal population of higher energy levels in the crystal field split ²F_{5/2} excited Yb³⁺ level. Yb³⁺ luminescence was enhanced when the porphyrin ring was functionalized with four crown-ether rings.¹⁰⁹ Due to the formation of

sandwich type complexes of alkali metal ions by the crown-ether rings, the ion was shielded more efficiently from the solvent.

Inorganic transition-metal complexes

A complex where the lanthanide ion is not in the core of a porphyrin was reported by Beeby *et al.*¹¹⁰ They showed the Yb³⁺ sensitized emission from a DOTA complex functionalized with a porphyrin with a palladium center (**46**). Klink *et al.* reported a new class of sensitizers of NIR Nd³⁺ and Yb³⁺ luminescence, the transition metal complexes ruthenium tris(bipyridine) **47** and ferrocene **48**.¹¹¹ These complexes were covalently coupled to a lanthanide ion complex (see Figure 2.17 and Figure 2.24). The sensitized emission by ferrocene and the ruthenium complex was proven by the excitation spectra. The ³MLCT (Metal to Ligand Charge Transfer) level of Ru(bpy)₃ is the donating energy level, because the rise-time of the lanthanide luminescence corresponded with the decay of the ³MLCT emission. Sensitization by ferrocene is faster in the case of Yb³⁺ as acceptor, probably with energy transfer via the triplet state, although a singlet state pathway could not be ruled out.

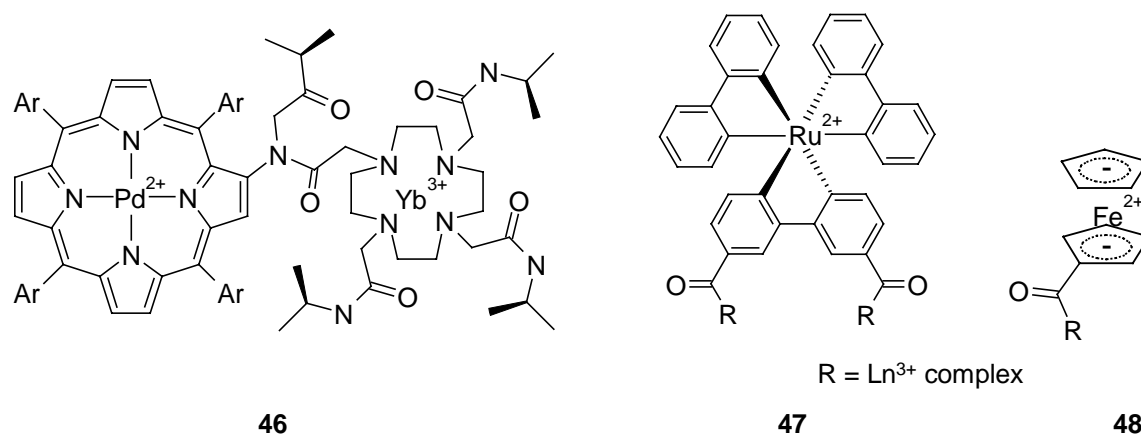


Figure 2.28 Transition-metal based lanthanide ion sensitizers.

Inorganic sensitizers

Some examples of sensitization of lanthanide ions by inorganic antennas will be discussed here. Doping of inorganic materials was achieved by ion implanting or wet chemical synthesis of powders. An important doping contains both Yb³⁺ and Er³⁺ in which Yb³⁺ is the sensitizer of Er³⁺ luminescence. The sensitization of Nd³⁺ by Cr³⁺ in an YAlO₃ crystal was reported in which Cr³⁺ ion pairs transfer energy to the Nd³⁺ single ion acceptor.¹¹² Laser action of Nd³⁺ in YAG (Yttrium Aluminum Garnet) doped with Cr³⁺ and Nd³⁺ is reported in which the Cr³⁺ ion centers were pumped.¹¹³ Re⁴⁺ and Mo³⁺ were reported as sensitizers of Tm³⁺ luminescence.¹¹⁴ Polman *et*

al. reported silicon nanocrystals as sensitizer for Er³⁺ luminescence.¹¹⁵ First silicon oxide was bombarded with silicon and after annealing at 1100 °C nanoparticles were formed with a bandgap of about 1.1 eV. Subsequently, Er³⁺ ions were implanted and upon excitation of the silicon nanocrystals, Er³⁺ luminescence was observed. Redispersible erbium doped silicon dots were made, by passivating the surface of doped Si particles with silane groups.¹¹⁶ Er³⁺ emission at 1536 nm was observed, however, this was obtained by exciting Er³⁺ directly at 488 nm and not via the excitation of Si. Recently, Bol *et al.* re-synthesized doped II-VI semiconductor nanocrystals (such as CdS or CdSe), following several literature procedures,¹¹⁷ but they did not observe Eu³⁺ sensitized luminescence by the semiconductor particles.

In conclusion, the sensitization of lanthanide ions by inorganic semiconductor particles is still not fully understood and this is an active area of research, because these particles combine stable sensitizers with lanthanide emission.

2.5 Outlook

The aim of this Chapter was to give an overview of waveguiding and light-emitting diodes with near-infrared emitting lanthanide ions. In order to design complexes with optimal properties a good understanding of the basic properties of the lanthanide ion complexes is necessary.

Although there are numerous reports that deal with the application of the visible emitting lanthanide ion complexes in polymers and in light-emitting diodes, the use of near-infrared emitting ions in such applications is still limited. Optical amplification with organic NIR emitting complexes is possible, but it has never been shown to the best of our knowledge at telecommunication wavelengths. Doping of light-emitting diodes in OLED devices was shown with neat lanthanide complexes that were sublimed onto substrates. Doping of polymer light-emitting diodes resulted in near-infrared emission, but the energy transfer processes still need to be further investigated in order to optimize the luminescence. A number of near-infrared emitting lanthanide complexes for sensitized emission have been investigated. However, many questions remain, like the pathway of energy transfer and optimization of the luminescence efficiency of the NIR emissive lanthanide ions is still needed. In this thesis, basic properties of lanthanide ion complexes are investigated and these complexes are applied in light-emitting devices and in polymer waveguides.

2.6 References

- 1 Reisfeld, R.; Jørgensen, C. K. *Lasers and excited states of rare earths* Springer, Berlin, 1977.
- 2 a) Heller, A. *Appl. Phys. Lett.* **1966**, *9*, 106; b) Lempicki, A.; Heller, A. *Appl. Phys. Lett.* **1966**, *9*, 108.
- 3 Heller, A. *J. Am. Chem. Soc.* **1967**, *89*, 167.
- 4 Weber, J. K. R.; Felten, J. J.; Cho, B.; Nordine, P. C. *Nature* **1998**, *395*, 769.
- 5 Miniscalco, W. J. *J. Lightw. Techn.* **1991**, *9*, 234.
- 6 Polman, A. *Proc. SPIE-Int. Soc. Opt. Eng.* **2000**, *3942*, 2.
- 7 Slooff, L. H.; Kik, P. G.; Tip, A.; Polman, A. *J. Lightw. Techn.* **2001**, *19*, 1740.
- 8 Lucent Technologies, AllWave™ fibers, see <http://www.lucent.com>.
- 9 a) Yoshimura, R.; Kikita, M.; Tomura, S.; Imamura, S. *J. Lightw. Techn.* **1998**, *16*, 1030; b) Hida, Y.; Onose, K.; Imamura, S. *Appl. Optics* **1997**, *36*, 6828; Hida, Y.; c) Imamura, S. *Jpn. J. Appl. Phys.* **1995**, *34*, 6416; d) Watanabe, T.; Ooba, N.; Hida, Y.; Hikita, M. *Appl. Phys. Lett.* **1998**, *72*, 1533; e) Yoshimura, R.; Hikita, M.; Tomaru, S.; Imamura, S. *Electr. Lett.* **1997**, *33*, 1240; f) Hida, Y.; Ooba, N.; Yoshimura, R.; Watanabe, T.; Hikita, M.; Kurihara, T. *Electr. Lett.* **1997**, *33*, 627.
- 10 Knoche, Th.; Müller, L.; Klein, R.; Neyer, A. *Electr. Lett.* **1996**, *32*, 1284.
- 11 Commercially available *d*-PMMA: ABCR GmbH & Co, Germany, price: \$906/g; Cambridge Isotope Laboratories; C/D/N Isotopes Inc.
- 12 Matsuura, T.; Kobayashi, J.; Ando, S.; Maruno, T.; Sasaki, S.; Yamamoto, F. *Appl. Optics* **1999**, *38*, 966.
- 13 Ando, S.; Matsuura, T.; Sasaki, S. *ChemTech* **1994**, 20.
- 14 Lee, H. -J.; Lee, M. -H.; Oh, M. -C.; Ahn, J. -H.; Han, S. G. *J. Pol. Sc. A* **1999**, *37*, 2355.
- 15 Lin, S.; Feuerstein, R. J.; Mickelson, A. R. *J. Appl. Phys.* **1996**, *79*, 2868.
- 16 An, D.; Yue, Z.; Chen, R. T. *Appl. Phys. Lett.* **1998**, *72*, 2806.
- 17 Chen, R. T.; Lee, M.; Natarajan, S.; Lin, C.; Ho, Z. Z.; Robinson, D. *IEEE Phot. Tech. Lett.* **1993**, *5*, 1328.
- 18 Shah, H.; Hoeglund, A.; Radler, M.; Langhoff, C.; Smith, D. W. Jr. *Pol. Prep.* **1999**, *40*, 1293.
- 19 Slooff, L. H.; Polman, A.; Klink, S. I.; Hebbink, G. A.; Grave, L.; van Veggel, F. C. J. M.; Reinhoudt, D. N.; Hofstraat, J. W. *Opt. Mater.* **2000**, *14*, 101.
- 20 Slooff, L. H.; Polman, A.; Klink, S. I.; Grave, L.; van Veggel, F. C. J. M.; Hofstraat, J. W. *J. Opt. Soc. Am. B* **2001**, *18*, 1690.
- 21 Slooff, L. H.; van Blaaderen, A.; Polman, A.; Hebbink, G. A.; Klink, S. I.; van Veggel, F. C. J. M.; Reinhoudt, D. N.; Hofstraat, J. W. *J. Appl. Phys.* **2002**, *91*, 3955.
- 22 Woudenberg, R. H.; Boonstra, T. A. *Polymers comprising a fluorinated carbonate moiety*, International Patent, deposited September 3, 1998, #WO 9838237.
- 23 Slooff, L. H.; Kik, P. G.; Tip, A.; Polman, A. *J. Lightw. Techn.* **2001**, *19*, 1740.

- 24 Gao, R.; Koeppen, C.; Zheng, G.; Garito, A. F. *Appl. Optics* **1998**, *37*, 7100.
- 25 Kobayashi, T.; Nakatsuka, S.; Iwafuji, T.; Kuriki, K. Imai, N.; Nakamoto, T.; Claude, C. D.; Sasaki, K.; Koike, Y.; Okamoto, Y. *Appl. Phys. Lett.* **1997**, *71*, 2421.
- 26 Pagnot, T.; Audebert, P.; Tribillon, G. *Chem. Phys. Lett.* **2000**, *322*, 572.
- 27 Gameiro, C. G.; da Silva Jr., E. F.; Alves Jr., S.; de Sá, G. F.; Santa-Cruz, P. A. *J. All. Comp.* **2001**, *323-324*, 820.
- 28 Koeppen, C.; Yamada, S.; Jiang, G.; Garito, A. F.; Dalton, L. R. *J. Opt. Soc. Am. B* **1997**, 155.
- 29 Lin, S.; Feuerstein, R. J.; Mickelson, A. R. *J. Appl. Phys.* **1996**, *79*, 2868.
- 30 Hasegawa, Y. Sogabe, K.; Wada, Y.; Kitamura, T.; Nakashima, N.; Yanagida, S. *Chem. Lett.* **1999**, 35.
- 31 Xu, X.; Ming, H.; Zhang, Q. *Opt. Commun.* **2001**, *199*, 369.
- 32 Kuriki, K.; Kobayashi, T.; Imai, N.; Tamura, T.; Nishihara, S.; Tagay, A.; Koike, Y.; Okamoto, Y. *IEEE Photonic Technol. Lett.* **2000**, *12*, 989.
- 33 Sosa Fonseca, R.; Flores, M.; Rodriguez, R. T.; Hernández, J.; Munoz, A. F. *J. Lumin.* **2001**, *93*, 327.
- 34 Karve, G.; Bihari, B.; Chen, R. T. *Appl. Phys. Lett.* **2000**, *77*, 1253.
- 35 An, D.; Yue, Z.; Chen, R. T.; *Appl. Phys. Lett.* **1998**, *72*, 2806.
- 36 Chen, R. T.; Lee, M.; Natarajan, S.; Lin, C.; Ho, Z. Z.; Robinson, D. *IEEE Photonic Technol. Lett.* **1993**, *5*, 1328.
- 37 Friend, R. H.; Gymer, R. W.; Holmes, A. B.; Burroughes, J. H.; Marks, R. N.; Taliani, C.; Bradley, D. D. C.; Dos Santos, D. A.; Bredas, J. L.; Logdlund, M.; Salaneck, W. R. *Nature* **1999**, *397*, 121.
- 38 Forrest, S. *M.R.S. Bull.* **2001**, *26*, 108.
- 39 Cao, Y.; Parker, I. D.; Yu, G.; Zhang, C.; Heeger, A. J. *Nature* **1999**, *397*, 414.
- 40 Wohlgenannt, M.; Tandon, K.; Mazumdar, S.; Ramasesha, S.; Vardeny, Z. V. *Nature* **2001**, *409*, 494.
- 41 Baldo, M. A.; O'Brien, D. F.; You, Y.; Shoustikov, A.; Sibley, S.; Thompson, M. E.; Forrest, S. R. *Nature* **1998**, *395*, 151.
- 42 Cleave, V.; Yahioglu, G.; Le Barny, P.; Friend, R. H.; Tessler, N. *Adv. Mater.* **1999**, *11*, 285.
- 43 Gong, X.; Robinson, M. R.; Ostrowski, J. C.; Moses, D.; Bazan, G. C.; Heeger, A. J. *Adv. Mater.* **2002**, *14*, 581.
- 44 Gao, F. G.; Bard, A. J. *J. Am. Chem. Soc.* **2000**, *122*, 7426.
- 45 McGehee, M. D.; Bergstedt, T.; Zhang, C.; Saab, A. P. O'Regan, M. B.; Bazan, G. C.; Srdanov, V. I.; Heeger, A. J. *Adv. Mater.* **1999**, *11*, 1349.
- 46 Adachi, C.; Baldo, M. A.; Forrest, S. R. *J. Appl. Phys.* **2000**, *87*, 8049.
- 47 Hong, Z.; Liang, C.; Li, R.; Li, W.; Zhao, D.; Fan, D.; Wang, D.; Chu, B.; Zang, F.; Hong, L. -S.; Lee, S. T. *Adv. Mater.* **2001**, *13*, 1241.
- 48 Kido, J.; Nagai, K. *J. Alloys Compounds* **1993**, *192*, 30.

- 49 Edwards, A.; Claupe, C.; Sokolik, I.; Chu, T.Y.; Okamoto, Y.; Dorsinville, R. *J. Appl. Phys.* **1997**, 82, 1841.
- 50 Robinson, M. R.; O'Regan, M. B.; Bazan, G. C. *Chem. Commun.* **2000**, 1645.
- 51 a) Gillin, W. P.; Curry, R. L. *Appl. Phys. Lett.* **1999**, 74, 798; b) Curry, R. J.; Gillin, W. P. *Appl. Phys. Lett.* **1999**, 75, 1380; c) Curry, R. J.; Gillin, W. P. *J. Appl. Phys.* **2000**, 88, 781; d) Curry, R. J.; Gillin, W. P. *Synth. Metals* **2000**, 111-112, 35; e) Curry, R. J.; Gillin, W. P.; Knights, A. P.; Gwilliam, R. *Appl. Phys. Lett.* **2000**, 77, 2271; f) Khreis, O. M.; Curry, R. J.; Somerton, M.; Gillin, W. P. *J. Appl. Phys.* **2000**, 88, 777; g) Curry, R. L.; Gillin, W. P.; Knights, A. P.; Gwilliam, R. *Opt. Mater.* **2001**, 17, 161.
- 52 a) Kawamura, Y.; Wada, Y.; Hasegawa, Y.; Iwamuro, M.; Kitamura, T.; Yanagida, Y. *Appl. Phys. Lett.* **1999**, 74, 3245; b) Kawamura, Y.; Wada, Y.; Iwamuro, M.; Kitamura, T.; Yanagida, S. *Chem. Lett.* **2000**, 280; c) Kawamura, Y.; Wada, Y.; Yanagida, S. *Jpn. J. Appl. Phys.* **2001**, 40, 350.
- 53 Harrison, B. S.; Foley, T. J.; Bouguettaya, M.; Boncella, J. M.; Reynolds, J. R.; Schanze, K. S.; Shim, J.; Holloway, P. H.; Padmanaban, G.; Ramakrishnan, S. *Appl. Phys. Lett.* **2001**, 79, 3770.
- 54 Hong Z.; Liang, C.; Li, R.; Zang, F.; Fan, D.; Li, W.; Hung, L. S.; Lee, S. T. *Appl. Phys. Lett.* **2001**, 79, 1942.
- 55 Hong Z. R.; Liang, C. J.; Li, R. G.; Zhao, D.; Fan, D.; Li, W. L. *Thin Solid Films* **2001**, 391, 122.
- 56 Carnall, W. T.; Goodman, G. L.; Rajnak, K.; Rana, R. S. *J. Phys. Chem.* **1989**, 90, 3443.
- 57 Blasse, G.; Grabmaier, B. C. *Luminescent Materials*, Springer, Berlin, 1994.
- 58 Ermolaev, V. L.; Sveshnikov, E. B. *Russ. Chem. Rev.* **1994**, 63, 905.
- 59 Beeby A.; Faulkner, S. *Chem. Phys. Lett.* **1997**, 266, 116.
- 60 Melby, L. R.; Rose, N. J.; Abramson, E.; Caris, J. C. *J. Am. Chem. Soc.* **1964**, 86, 5125.
- 61 Parker, D. *Coord. Chem. Rev.* **2000**, 205, 106.
- 62 Peters, J. A.; Huskens, J.; Raber, D. *J. Prog. Nucl. Mag. Res. Sp.* **1996**, 28, 283.
- 63 D. R. Lide (ed.) *Handbook of chemistry and physics*, 76th edition, CRC press, New York, 1996.
- 64 Oude Wolbers, M. P.; van Veggel, F. C. J. M.; Peters, F. G. A.; van Beelen, E. S. E.; Hofstraat, J. W.; Geurts, F. A. J.; Reinhoudt, D. N. *Chem. Eur. J.* **1998**, 4, 772.
- 65 Oude Wolbers, M. P.; van Veggel, F. C. J. M.; Hofstraat, J. W.; Geurts, F. A. J.; Reinhoudt, D. N. *J. Chem. Soc., Perkin Trans. 2* **1997**, 2275.
- 66 Klink, S. I.; Hebbink, G. A.; Grave, L.; Peters, F. G. A.; van Veggel, F. C. J. M.; Reinhoudt, D. N.; Hofstraat, J. W. *Eur. J. Org. Chem.* **2000**, 1923.
- 67 Oude Wolbers, M. P.; van Veggel, F. C. J. M.; Snellink-Ruël, B. H. M.; Hofstraat, J. W.; Geurts, F. A. J.; Reinhoudt, D. N. *J. Am. Chem. Soc.* **1997**, 119, 138.
- 68 Oude Wolbers, M. P.; van Veggel, F. C. J. M.; Snellink-Ruël, B. H. M.; Hofstraat, J. W.; Geurts, F. A. J.; Reinhoudt, D. N. *J. Chem. Soc., Perkin Trans. 2* **1998**, 2141.
- 69 Michels, J. J.; Huskens, J.; Reinhoudt, D. N. *J. Am. Chem. Soc.* **2002**, 124, 2056.

- 70 Werts, M. H. V.; Hofstraat, J. W.; Geurts, G. A. J.; Verhoeven, J. W. *Chem. Phys. Lett.* **1997**, 276, 196.
- 71 Liu, Y.; Han, B. H.; Chen, Y. T. *Coord. Chem. Rev.* **2000**, 200, 53.
- 72 a) Hasegawa, Y.; Murakoshi, K.; Wada, Y.; Yanagida, S.; Kim, J.-H.; Nakashima, N.; Yamanaka, T. *Chem. Phys. Lett.* **1996**, 248, 8; b) Hasegawa, Y.; Murakoshi, K.; Wada, Y.; Kim, J.-H.; Nakashima, N.; Yamanaka, T.; Yanagida, S. *Chem. Phys. Lett.* **1996**, 260, 173; c) Hasegawa, Y.; Kimura, Y.; Murakoshi, K.; Wada, Y.; Kim, J.-H.; Nakashima, N.; Yamanaka, T.; Yanagida, S. *J. Phys. Chem.* **1996**, 100, 10201; d) Iwamuro, M.; Hasegawa, Y.; Wada, Y.; Murakoshi, K.; Kitamura, T.; Nakashima, N.; Yamanaka, T.; Yanagida, S. *Chem. Lett.* **1997**, 1067; e) Hasegawa, Y.; Iwamuro, M.; Murakoshi, K.; Wada, Y.; Arakawa, R.; Yamanaka, T.; Nakashima, N.; Yanagida, S. *Bull. Chem. Soc. Jpn.* **1998**, 71, 2573; f) Iwamuro, M.; Wada, Y.; Kitamura, T.; Nakashima, N.; Yanagida, S. *Phys. Chem. Chem. Phys.* **2000**, 2, 2291; g) Yanagida, S.; Hasegawa, Y.; Wada, Y. *J. Lumin.* **2000**, 87-89, 995.
- 73 Yanagida, S.; Hasegawa, Y.; Murakoshi, K.; Wada, Y.; Nakashima, N.; Yamanada, T. *Coord. Chem. Rev.* **1998**, 171, 461.
- 74 Hasegawa, Y.; Ohkubo, T.; Sogabe, K.; Kwamura, Y.; Wada, Y.; Nakashima, N.; Yanagida, S. *Angew. Chem. Int. Ed.* **2000**, 39, 357.
- 75 a) Hoffmann, K. R.; DeLapp, K.; Andrews, H. *J. Lumin.* **1995**, 66-67, 244; b) Xiaoya, D.; Geng, L.; Lascola, R.; Wright, J. C. *J. Lumin.* **1997**, 72-74, 553.
- 76 Förster, T. *Discuss. Faraday Soc.* **1959**, 27, 7.
- 77 Dexter, D. L. *J. Chem. Phys.* **1953**, 21, 836.
- 78 Horrocks, W. DeW.; Rhee, M. -J.; Snyder, A. P.; Sudnick, D. R. *J. Am. Chem. Soc.* **1980**, 102, 3650.
- 79 de Sá, G. F.; Malta, O. L.; de Mello Donegá, C.; Simas, A. M.; Longo, R. L.; Santa-Cruz, P. A.; da Silva, E. F. *Coord. Chem. Rev.* **2000**, 196, 165.
- 80 Gonçalves e Silva, F. R.; Malta, O. L.; Reinhard, C.; Güdel, H. -U.; Piguet, C.; Moser, J. E.; Bünzli, J. -C. G. *J. Phys. Chem. A* **2002**, 106, 1670.
- 81 a) Klink, S. I.; Grave, L.; Reinhoudt, D. N.; van Veggel, F. C. J. M.; Werts, M. H. V.; Geurts, F. A. J.; Hofstraat, J. W. *J. Phys. Chem. A* **2000**, 104, 5457; b) Klink, S. I.; Hebbink, G. A.; Grave, L.; van Veggel, F. C. J. M.; Reinhoudt, D. N.; Slooff, L. H.; Polman, A.; Hofstraat, J. W. *J. Appl. Phys.* **1999**, 86, 1181.
- 82 a) Kropp, J. L.; Windsor, M. W. *J. Chem. Phys.* **1965**, 42, 1599; b) Horrocks, W. DeW.; Sudnick, D. R. *Acc. Chem. Res.* **1981**, 14, 384; c) Holz, R. C.; Chang, C. A.; Horrocks, W. DeW. *Inorg. Chem.* **1991**, 30, 3270; d) Beeby, A.; Clarkson, J. M.; Dickins, R. S.; Faulkner, S.; Parker, D.; Royle, L.; de Sousa, A. S.; Williams, J. A. G.; Woods, M. *J. Chem. Soc., Perkin Trans. 2* **1999**, 493.

- 83 Horrocks, W. DeW.; Bolender, J. P.; Smith, W. D.; Supkowski, R. M. *J. Am. Chem. Soc.* **1997**, *119*, 5972.
- 84 a) Sato, S.; Wada, M. *Bull. Chem. Soc. Jpn.* **1970**, *43*, 1955; b) Latva, M.; takalo, H.; Mikkala, V. M.; Matachescu, C.; Rodriguez-Ubis, J. C.; Kankare, J. *J. Lumin.* **1997**, *75*, 149.
- 85 Werts, M. H. V.; Duin, M. A.; Hofstraat, J. W.; Verhoeven, J. W. *Chem. Commun.* **1999**, 799.
- 86 Werts, M. H. V. *Luminescent lanthanide complexes* PhD thesis University of Amsterdam, 2000.
- 87 Klink, S. I.; Hebbink, G. A.; Oude Alink, P. G. B.; Grave, L.; van Veggel, F. C. J. M.; Werts, M. H. V. *J. Phys. Chem. A* **2002**, *106*, 3681.
- 88 Hebbink, G. A.; Klink, S. I.; Oude Alink, P. G. B.; van Veggel, F. C. J. M. *Inorg. Chim. Acta* **2001**, *317*, 114.
- 89 Voloshin, A. I.; Shavaleev, N. M.; Kazakov, V. P. *J. Lumin.* **2001**, *93*, 199.
- 90 a) Maupin, C. L.; Parker, D.; Williams, J. A. G.; Riehl, J. P. *J. Am. Chem. Soc.* **1998**, *120*, 10563; b) Maupin, C. L.; Dickins, R. S.; Govenock, G.; Mathieu, C. E.; Parker, D.; Williams, J. A. G.; Riehl, J. P. *J. Phys. Chem. A* **2000**, *104*, 6709.
- 91 Faulkner, S.; Beeby, A.; Carrié, M. –C.; Dadabhoy, A.; Kenwright, A. M.; Sammes, P. G. *Inorg. Chem. Commun.* **2001**, *4*, 187.
- 92 Hasegawa, M.; Nakao, A.; Masui, M.; Tamura, T.; Suzuki, D.; Linert, W.; Fukuda, Y.; Hoshi, T. *Chem. Phys.* **2001**, *269*, 323.
- 93 a) Parker, D.; Senanayake, K.; Williams, J. A. G. *J. Chem. Soc., Perkin Trans. 2* **1998**, 2129; b) Gunnlaugsson, T.; Mac Dónaill, D. A.; Parker, D. *J. Am. Chem. Soc.* **2001**, *123*, 12866; c) Parker, D. *Coord. Chem. Rev.* **2000**, *205*, 109.
- 94 Lowe, M. P.; Parker, D.; Reany, O.; Aime, S.; Botta, M.; Castellano, G.; Gianolio, E.; Pagliarin, R. *J. Am. Chem. Soc.* **2001**, *123*, 7601.
- 95 Lowe, M. P.; Parker, D. *Inorg. Chim. Acta* **2001**, *317*, 163.
- 96 Aoki, S.; Hawatani, H.; Goto, T.; Kimura, E.; Shiro, M. *J. Am. Chem. Soc.* **2001**, *123*, 1123.
- 97 Meshkova, S. B.; Rusakova, N. V.; Bolshoi, D. V. *Acta Chim. Hung.* **1992**, *129*, 317.
- 98 Klink, S. I.; Oude Alink, P.; Grave, L.; Peters, F. G. A.; Hofstraat, J. W.; Geurts, F. A. J.; van Veggel, F. C. J. M. *J. Chem. Soc., Perkin Trans. 2* **2001**, 363.
- 99 Vögtle, F.; Gorka, M.; Vicinelli, V.; Ceroni, P.; Maestri, M.; Balzani, V. *Chem. Phys. Chem.* **2001**, *769*.
- 100 a) L. Li, Y. Chem, Y. Zhao, A. Tong, *Anal. Chim. Acta* **1997**, *341*, 241; b) L. Li, Y. Zhao, Y. Wu, A. Tong, *Talanta* **1998**, *46*, 1147.
- 101 Werts, M. H. V.; Verhoeven, J. W.; Hofstraat, J. W. *J. Chem. Soc., Perkin Trans. 2* **2000**, 433.
- 102 Werts, M. H. V.; Woudenberg, R. H.; Emmerink, P. G.; van Gassel, R.; Hofstraat, J. W.; Verhoeven, J. W. *Angew. Chem. Int. Ed.* **2000**, *39*, 4542.
- 103 Guldi, D. M.; Mody, T. D.; Gerasimchuk, N. N.; Magda, D.; Sessler, J. L. *J. Am. Chem. Soc.* *122*, 8289.

- ¹⁰⁴ Gouterman, M.; Schumaker, C. D.; Srivastave, T. S.; Yonetani, T. *Chem. Phys. Lett.* **1976**, *40*, 456.
- ¹⁰⁵ Tsvirko, M. P.; Steelmakh, G. F.; Pyatosin, V. E.; Solovyov, K. N.; Kachura, T. F. *Chem. Phys. Lett.* **1980**, *73*, 80.
- ¹⁰⁶ Tsvirko, M. P.; Steelmakh, G. F.; Pyatosin, V. E.; Solovyov, K. N.; Kachura, T. F.; Piskarskas, A. S.; Gadonas, R. A. *Chem. Phys.* **1986**, 467.
- ¹⁰⁷ Asano-Someda, M.; Kaizu, Y. *J. Photochem. Photobiol. A* **2001**, *139*, 161.
- ¹⁰⁸ a) Meng J. X.; Li, K. F.; Yuan, J.; Zhang, L. L.; Wong, W. K.; Cheah, K. W. *Chem. Phys. Lett.* **2000**, 332, 313; b) Wong, W. K.; Hou, A. X.; Guo, J. P.; He, H. S.; Zhang, L. L.; Wong, W. Y.; Li, K. F.; Cheah, K. W.; Xue, F.; Mak, T. C. W. *J. Chem. Soc., Dalton Trans.* **2001**, 3092.
- ¹⁰⁹ Korovin, Y. U.; Zhilina, Z.; Rusakova, N.; Kuz'min, V.; Vodzinsky, S.; Ishkov, Yu. *J. Porph. Phthal.* **2001**, *5*, 481.
- ¹¹⁰ Beeby, A.; Dickins, R. S.; FitzGerald, S.; Govenlock, L. J.; Maupin, C. L.; Parker, D.; Riehl, J. P.; Siligardi, G.; Williams, J. A. G. *Chem. Commun.* **2000**, 1183.
- ¹¹¹ Klink, S. I.; Keizer, H.; van Veggel, F. C. J. M. *Angew. Chem. Int. Ed.* **2000**, *39*, 4319.
- ¹¹² Mahpoud, S.; Chamiel, N.; Weiss, A. M.; Rosenbluh, M.; Herman, A.; Shoham, A.; Lipavsky, B.; Rotman, S. R. *Opt. Mater.* **1999**, *13*, 55.
- ¹¹³ Dong J.; Deng, P. Z.; Zhang, Y. H.; Liu, Y. P.; Xu, J.; Chen, W. *Microw. Opt. Techn. Lett.* **2000**, *26*, 124.
- ¹¹⁴ Kirk, A. D.; Furer, N.; Gudel, H. U. *J. Lumin.* **1996**, *68*, 77.
- ¹¹⁵ Kik, P. G.; Polman, A. *J. Appl. Phys.* **2001**, *91*, 534.
- ¹¹⁶ Ji, J. M.; Chen, Y. D.; Senter, R. A.; Coffer, J. L. *Chem. Mater.* **2001**, *13*, 4783.
- ¹¹⁷ Bol, A. A.; van Beek, R.; Meijerink, A. *Chem. Mater.* **2002**, *14*, 1121.

Chapter 3

*Deuterated near-infrared emitting lanthanide(III) complexes**

*The luminescence of lanthanide(III) ions emitting in the near-infrared region is ideally suited for telecommunication applications and a number of applications have been developed. However, in organic matrices molecular vibrations like C-H and O-H stretching modes quench the lanthanide excited state. Replacing them by less quenching groups enhances the luminescence lifetime and therefore also the luminescence quantum yield. In this Chapter, a synthesis route was developed to deuterate all C-H groups that contribute to the quenching in an organic lanthanide complex. The luminescence was measured of three near-infrared emitting lanthanide ions Nd^{3+} , Er^{3+} , and Yb^{3+} . The maximum effect achieved upon deuteration is a factor 2-3, but lifetimes remain in the microsecond region (**1.Nd**: 5.5 μs , **1.Yb**: 52.3 μs , and **1.Er**: 5.4 μs).*

* The work described in this Chapter was published: Hebbink, G. A.; Reinhoudt, D. N.; van Veggel, F. C. J. M.; *Eur. J. Org. Chem.* **2001**, 4101-4106.

3.1 Introduction

Lanthanide ions attract a great deal of interest,¹ because their luminescence properties are useful in a variety of applications like optical amplification for telecommunication, light-emitting diodes,² and fluoro-immuno assays.³ The luminescence of the lanthanide ions stems from intra 4f-transitions, which are in principal forbidden transitions resulting in relatively long-lived excited states. This makes them suited for laser applications. Erbium ions are actually used as the active component in optical amplification in Erbium Doped Fiber Amplifiers (EDFAs)⁴ in telecommunication devices. Compared to inorganic materials polymer-based materials could have advantages in devices because fabrication and integration of polymer waveguide based optical components, like splitters, switches, and multiplexers, is relatively easy with standard lithographic techniques. For incorporation of lanthanide ions in organic materials, they must be made soluble in the organic polymer matrix by encapsulating them in organic polydentate ligands. Besides solubilizing the ions, the polydentate ligand shields them from luminescence quenching moieties in the matrix.⁵ For europium and terbium ions, with emissions in the visible region of the spectrum, the quenching by oscillating groups such as O-H groups has been studied extensively.⁶ Ligands that shield effectively from the solvent have been synthesized, and the remaining quenching is mainly due to C-H groups within the ligand itself.⁷ For the near-infrared emitting lanthanide ions the quenching by the ligands is even more strongly reflected in their quantum yields in organic media.^{8,9} Even with effective shielding of the ion from the solvent the lifetimes remain low compared to lifetimes in inorganic materials.¹⁰ A strategy to increase the quantum yield of the lanthanide ions is to eliminate the C-H oscillators in close proximity of the lanthanide ion by introduction of deuterium or fluorine instead of hydrogen.^{7,11} The C-D and C-F bonds oscillate at lower energy and quenching of the lanthanide excited state is reduced.

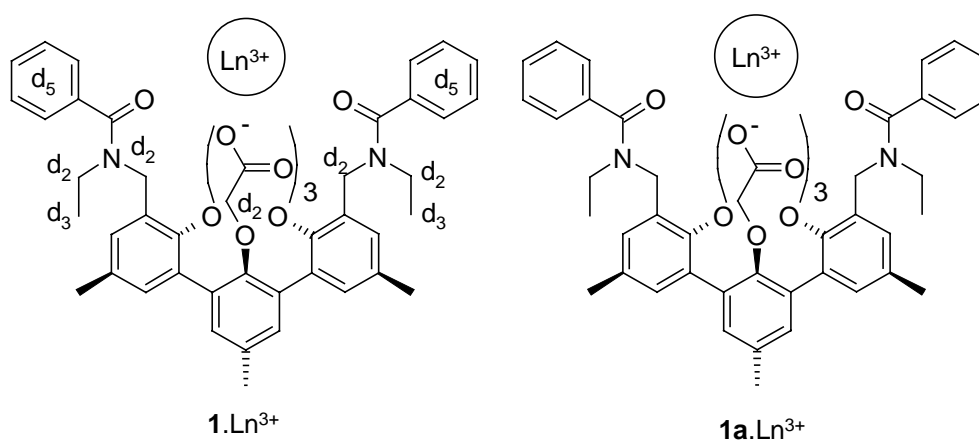


Figure 3.1 Terphenyl-based lanthanide complexes.

Our strategy is to fully deuterate all C-H groups that contribute to quenching in a lanthanide ligand.¹² The complex (**1**.Ln and **1a**.Ln, Figure 3.1) has advantages in terms of solubility, shielding of the ion to solvent molecules, and easy functionalization with chromophores and dyes.^{8,12,13,14}

3.2 Results and discussion

3.2.1 Molecular Modeling

The quenching rate is strongly distance dependent ($1/r^6$). C-H groups about 6 Å and further from the lanthanide ion will not quench significantly and thus do not have to be deuterated.¹⁵ Average distances between hydrogens and the lanthanide ion were determined from molecular dynamics simulations in a box of OPLS methanol (Figure 3.2).^{16,17} In the simulation Eu^{3+} was taken as representative for the NIR emitting ions.¹⁸

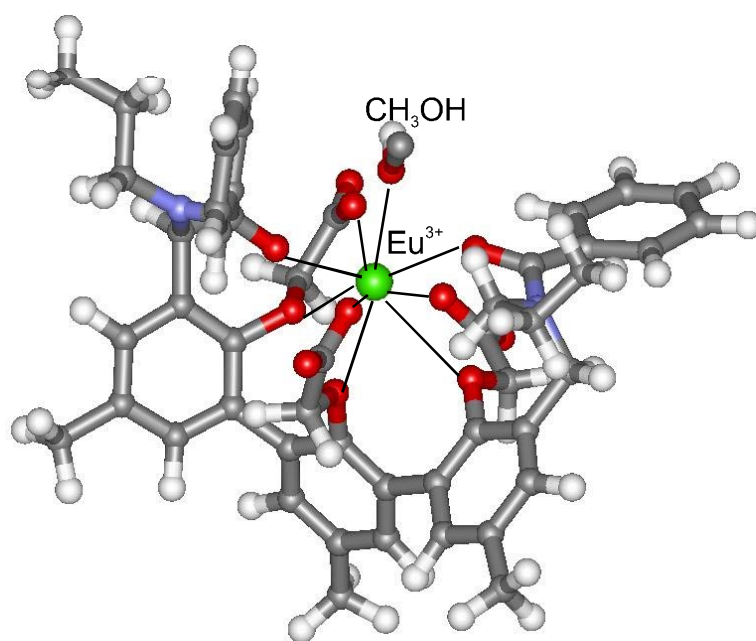


Figure 3.2 Snapshot of **1**.Eu in OPLS methanol. One CH_3OH molecule is coordinated in the first coordination sphere of the lanthanide ion. Instead of ethyl groups, propyl groups were used in the modeling. This has no effect on the complexation behavior of the complexes. For further details see Ref. 16.

In Table 3.1 the average distances between the lanthanide ion and the hydrogens derived from the MD simulation are represented. It is clear from the results that the hydrogens of the *m*-terphenyl moiety are relatively far away from the lanthanide ion compared to the other

hydrogens and will not significantly contribute to the luminescence quenching. All the other groups will have to be deuterated to reduce the quenching.

Table 3.1 Distances of C-H groups to Eu^{3+} (in Å) derived from the molecular modeling study.^a

$\text{ArH}^{\text{terph, i}}$	$\text{ArH}^{\text{terph, o}}$	ArCH_3	ArCH_2N	$\text{CH}^{\text{tail, 1, b}}$	$\text{CH}^{\text{tail, 2, b}}$	$\text{ArH}^{\text{Bz, 1, b}}$	$\text{ArH}^{\text{Bz, 2, b}}$	CH_2CO_2
6.3±0.1	6.4±0.1	8.2±0.3	5.3±0.1	3.8±0.4	6.2±0.1	4.8±0.3	4.0±0.2	4.3±0.2
6.2±0.1	6.6±0.2	7.9±0.2	3.8±0.2	4.4±0.4	6.4±0.1	6.8±0.3	6.4±0.2	4.3±0.1
	6.3±0.1	8.0±0.2	5.1±0.2	6.1±0.4 ^c	6.7±0.6 ^c	7.7±0.2	8.0±0.2	4.3±0.1
	6.3±0.1		5.8±0.1			7.1±0.2	7.9±0.1	3.8±0.2
						5.3±0.3	6.1±0.1	4.2±0.1
								3.7±0.1

a The different hydrogen positions in the ligand are denoted as follows: terphenyl aromatic hydrogens ($\text{ArH}^{\text{terph}}$, with 'i' as the inner ring and 'o' for the outer rings), terphenyl CH_3 hydrogens ($\text{ArCH}^{\text{terph}}$), benzylic hydrogens (ArCH_2N), aliphatic hydrogens on the amine tail (CH^{tail}), aromatic hydrogens of the benzoyl groups (ArH^{Bz}), and hydrogens on the acetic acid arms (OCH_2CO_2). Different values in one column represent different hydrogens on this position.

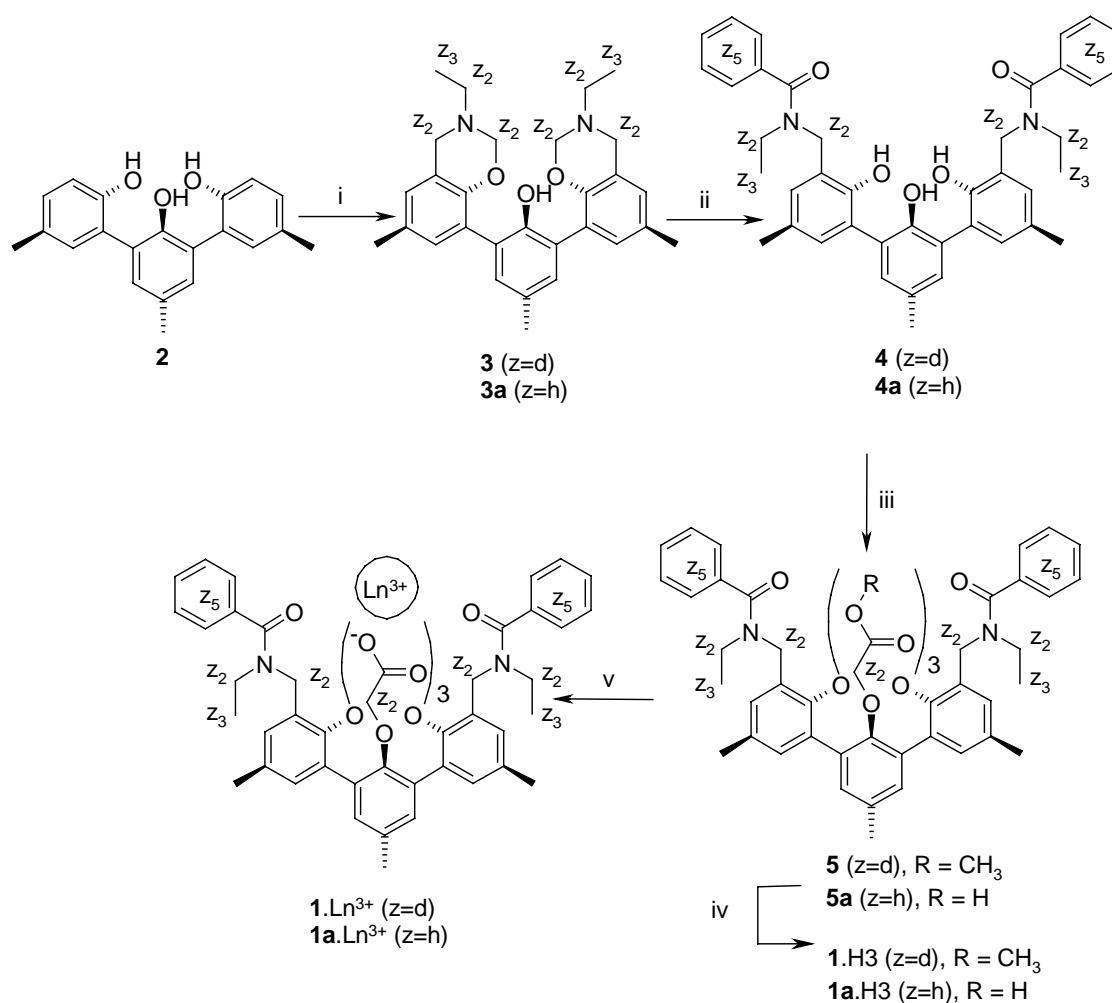
b Due to the unsymmetry in the complex, the different ethyl and benzoyl groups have different distances to the Ln^{3+} ion.

c This value is for all hydrogens at the β -position.

3.2.2 Synthesis

A new synthesis route has been designed to produce deuterated lanthanide complexes that allow the use of commercially available deuterated reagents. The key step in this route is the Mannich reaction¹⁹ of an amine, formaldehyde, and a phenol. The synthesis route is depicted in Scheme 3.1. The same procedure was used to prepare deuterated (**1.Ln**) and non-deuterated (**1a.Ln**) lanthanide complexes. The benzoxazine **3** was prepared by refluxing a solution of the building block **2**,²⁰ deuterated ethylamine, and an excess of formaldehyde in a mixture of 1,4-dioxane and water. The benzoxazine was converted into the amine by refluxing the yellow solid in ethanol with a few drops of concentrated hydrochloric acid. After the amidation with perdeuterated benzoyl chloride in dichloromethane with triethylamine, the crude product was refluxed with potassium carbonate in a mixture of water and methanol to hydrolyze the esters of the phenol groups and excess benzoyl chloride. Subsequently, bisamide **4** was alkylated with three equivalents of deuterated methyl bromoacetate in acetonitrile in the presence of potassium carbonate under reflux for three hours. The methyl esters were hydrolyzed by refluxing terphenyl **5** in water-methanol in the presence of potassium carbonate. Deuteration for all intermediates was confirmed by comparing spectroscopic data, i.e. NMR and FT-IR, with these data derived

from the non-deuterated analogues. In ^{13}C NMR spectra (^1H decoupled, ^2H coupled) the deuterated carbons show up as multiplets caused by coupling with the ^2H nuclei. The FT-IR spectra exhibit peaks corresponding to the C-D vibrations between $2200\text{-}2000\text{ cm}^{-1}$.²¹ After hydrolysis of the ester groups in **5** the lanthanide complexes were easily obtained by reacting the lanthanide nitrate salts ($\text{Nd}(\text{NO}_3)_3 \cdot 5\text{H}_2\text{O}$, $\text{Er}(\text{NO}_3)_3 \cdot 6\text{H}_2\text{O}$, and $\text{Yb}(\text{NO}_3)_3 \cdot 6\text{H}_2\text{O}$) in the presence of triethylamine in methanol.



Scheme 3.1 i: D_2CO , $\text{Et-d}_5\text{-NH}_3\text{Cl}$, NaOAc , 1,4-dioxane/ D_2O , reflux, 70%; ii: aqueous HCl , CH_3OD , reflux; $\text{Bz-d}_5\text{-Cl}$, Et_3N , CH_2Cl_2 ; K_2CO_3 , $\text{CH}_3\text{OD}/\text{D}_2\text{O}$, reflux, 56%; iii: Methyl bromoacetate- d_2 , K_2CO_3 , CH_3CN , reflux, 78%; iv: K_2CO_3 , $\text{CH}_3\text{OD}/\text{D}_2\text{O}$, reflux, 96%; v: $\text{Ln}(\text{NO}_3)_3 \cdot x\text{H}_2\text{O}$, Et_3N , CH_3OD , quantitative.

Complex formation was confirmed by mass spectrometry, which showed the parent mass peak with the correct isotope pattern for the corresponding lanthanide ion. In the infrared spectra an absorption at 1600 cm^{-1} for the carboxylates is present. The complexes are soluble in most common solvents like chloroform, dichloromethane, and DMSO.

3.2.3 Near-Infrared luminescence

The metal-centered luminescence of the NIR emitting lanthanide ions was measured by exciting the ions indirectly *via* the *m*-terphenyl chromophore.⁸ Figure 3.3 shows the excitation and emission spectra of the Yb³⁺, Nd³⁺, and Er³⁺ complexes measured in DMSO-*d*₆. The excitation spectra closely resemble the absorption spectra (maximum around 300 nm) proving the sensitized emission in which the *m*-terphenyl moiety acts as the sensitizer.

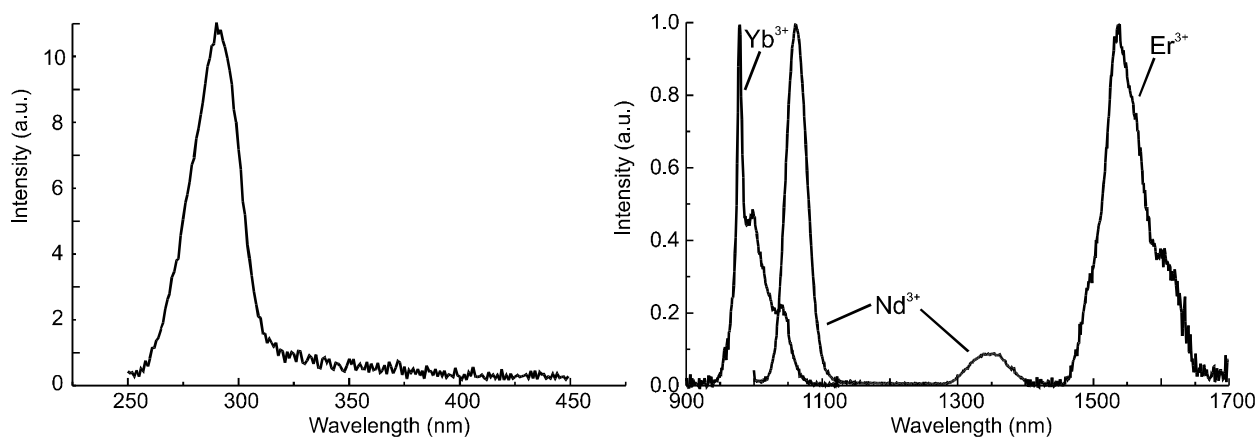


Figure 3.3 Excitation spectrum (left) of 1.Nd, measured by measuring the emission at 1060 nm; and the (normalised) emission spectra (right) of 1.Yb, 1.Nd, and 1.Er by exciting at 300 nm, all measured in DMSO-*d*₆ solution.

The emission spectra clearly show the typical emission characteristics originating from the 4f-4f transitions of Nd³⁺ (880 (⁴F_{3/2} → ⁴I_{9/2}, not shown²²), 1064 (⁴F_{3/2} → ⁴I_{11/2}), 1330 nm (⁴F_{3/2} → ⁴I_{13/2})), Yb³⁺ (980 nm (²F_{5/2} → ²F_{7/2})), and Er³⁺ (1550 nm (⁴I_{13/2} → ⁴I_{15/2})). Lifetime measurements were performed by exciting the ions *via* the *m*-terphenyl moiety with a pulsed nitrogen laser operating at 337 nm and by collecting the decay curves at the appropriate wavelength; 1060 nm for Nd³⁺, 980 nm for Yb³⁺, and 1550 nm for Er³⁺. All the decay curves could be fitted with a single exponential curve and the results of the fitting are summarized in Table 3.2, together with lifetimes obtained from the non-deuterated complexes. For comparison, lifetimes in the absence of quenchers were calculated from the absorption spectra or taken from literature.¹⁴ The lifetimes and the intrinsic luminescent quantum yields of the ions were increased with a factor of 2-3 compared with these parameters of the non-deuterated compounds. Quantum yields, calculated by dividing the observed lifetime by the radiative lifetime τ_0 , were increased with the same factor ($\phi_{1.Nd} = 0.02$, $\phi_{1.Er} = 0.0004$, $\phi_{1.Yb} = 0.03$). Towards our ultimate goal this is an important achievement as longer lifetimes are beneficial in the optical amplification process.

However, the lifetimes are still much lower compared to inorganic systems¹⁰ and from this and from other reports^{7,8,11,23} we conclude that in organic complexes lifetimes will remain in the microsecond region.

Table 3.2 Luminescent lifetimes of lanthanide ion complexes in DMSO-*d*₆ solution.

	τ (μ s); Ln ³⁺ =Nd ³⁺	τ (μ s); Ln ³⁺ =Er ³⁺	τ (μ s); Ln ³⁺ =Yb ³⁺
1.Ln	5.5	5.4	52.3
1a.Ln	2.5	3.3	19.0
τ_0^a	250	14 \times 10 ³	2 \times 10 ³

a Calculated radiative lifetime, according reference 14.

3.3 Conclusions

A new synthesis route has been developed to decrease the number of C-H quenchers in *m*-terphenyl-based lanthanide ion complexes. Complexes were made and the photophysical properties of these deuterated complexes were measured. The lanthanide ions were excited in the UV region via the *m*-terphenyl moiety and emitted the corresponding near-infrared light. The luminescence lifetimes of the deuterated compounds were increased with a factor 2-3 compared to the non-deuterated analogues. The luminescence lifetimes of the near-infrared emitting lanthanide ions in organic complexes remain in the microsecond region.

3.4 Experimental

General

Melting points were determined with a Reichert melting point apparatus and are uncorrected. Mass spectra were recorded on a Finnigan MAT 90 spectrometer using *m*-NBA (nitrobenzyl alcohol) or Magic Bullet (MB)²⁴ as a matrix. IR spectra were recorded with a Perkin Elmer Spectrum BX FT-IR System using KBr pellets as matrix. Elemental analyses were performed on a Carlo Erba EA 1106 apparatus. ¹H NMR and ¹³C NMR spectra were recorded with Varian-300 or Varian-400 spectrometers with CDCl₃ as the solvent unless stated otherwise, using residual CHCl₃ (δ = 7.26 ppm) and CDCl₃ (δ = 77.0 ppm) as the internal standards, respectively. In the assignments of the protons the 'o' and 'i' superscripts stand for the protons on the *m*-terphenyl moiety on the outer and inner phenolic rings, respectively. Multiplets in the ¹³C spectrum were unresolved and assigned with an 'm'. Deuterated reagents, 20% formalin-*d*₂ solution in D₂O, ethyl-*d*₅-amine hydrochloric acid, benzoyl-*d*₅-chloride, and methyl bromoacetate-*d*₂, were purchased from Isotec Inc. Deuterated solvents, D₂O, CH₃OD, CD₃OD, were purchased from Merck and all other

chemicals were purchased from Aldrich. All chemicals were used as received without further purification. CH₂Cl₂, CHCl₃, and hexane were distilled from CaCl₂, ethyl acetate was distilled from K₂CO₃, Et₃N was distilled in vacuo and stored over KOH. 1,4-dioxane and acetonitrile were of analytical grade and were dried over molecular sieves (4 Å) prior to use. Preparative column chromatography separations were performed using Merck silica gel (particle size 0.040-0.063 mm, 230-400 mesh) or Merck LiChroprep RP-18 (particle size 0.025-0.040 mm).

Compound 3

A solution of 0.5 g (1.56 mmol) *m*-terphenyl²⁰ in 10 ml dioxane was added to a solution of 1.23 g (7.8 mmol) deuterated formalin (20% solution D₂CO in D₂O), 0.32 g (3.7 mmol), deuterated ethylamine.HCl salt, and 0.32 g (3.9 mmol) sodium acetate in 25 ml 1,4-dioxane. Subsequently, 5 ml D₂O was added to dissolve all the salts and the solution was refluxed for three hours. After cooling down to room temperature and evaporation of the solvents 100 ml dichloromethane was added and the solution was washed twice with water and once with brine. The organic layer was dried over Na₂SO₄ and after filtration of the salts the solution was concentrated to dryness under vacuum. The crude product was purified with reversed phase (RP18) column chromatography with methanol as the eluent. A yellow solid was obtained, yield 0.52 g, 70%, m.p. 79-82 °C. ¹H NMR (CDCl₃): δ 7.11 (s, 2 H, ArHⁱ), 7.05 (d, *J* = 3.0 Hz, 2 H, ArH^o), 6.82 (d, *J* = 3.0 Hz, 2 H, ArH^o), 6.42 (s, 1 H, OH), 2.38 (s, 3 H, ArCH₃ⁱ), 2.32 (s, 6 H, ArCH₃^o); ¹³C NMR (CDCl₃): δ 149.0, 148.7, 131.3-126.6, 119.6, 81.9 (m), 66.9, 49.0 (m), 44.3 (m), 20.5, 12.3 (m); MS (FAB, NBA): *m/z* 476.5 [(M+H)⁺, calcd for C₂₉H₁₆N₂O₃D₁₈: 476.4]; IR (KBr): 2222, 2149, 2126, 2075 cm⁻¹ (C-D); C₂₉H₁₆N₂O₃D₁₈.1.5H₂O: calcd C 69.15, H 7.40, N 5.56; found C 68.97, H 6.95, N 5.18.

Compound 3a

The undeuterated compound was synthesized analogously to the deuterated compounds. With the difference that 37% formalin solution in H₂O containing 25% methanol was used, reflux overnight, and purification using silica gel with ethyl acetate as eluent.²⁵ Yield: 0.32 g, 45%, m.p. 81-82 °C. ¹H NMR (CDCl₃): δ 7.05 (s, 2 H, ArHⁱ), 6.98 (d, *J* = 3.0 Hz, 2 H, ArH^o), 6.75 (d, *J* = 3.0 Hz, 2 H, ArH^o), 6.36 (s, 1 H, OH), 4.83 (s, 4 H, ArCH₂N), 3.94 (s, 4 H, NCH₂O), 2.77 (q, *J* = 6.7 Hz, 4 H, NCH₂CH₃), 2.28 (s, 3 H, ArCH₃ⁱ), 2.25 (s, 6 H, ArCH₃^o), 1.05 (t, *J* = 7.3 Hz, 6 H, N-CH₂-CH₃); ¹³C NMR (CDCl₃): δ 149.4, 149.0, 130.5-119.8, 82.3, 49.5, 47.3, 20.3, 12.8; MS (FAB, NBA): *m/z* 459.3 [(M+H)⁺, calcd for C₂₉H₃₅N₂O₃: 459.3], C₂₉H₃₄N₂O₃.1H₂O calcd C 73.08, H 7.61, N 5.88; found C 73.17, H 7.50, N 5.68.

Compound 4

A solution of 0.2 g (0.44 mmol) of **3** in ethanol with a few drops of concentrated HCl was refluxed for 1 hour. After evaporation to dryness the remaining white solid was dissolved in 50 ml dichloromethane and 0.26 ml (1.78 mmol) Et₃N and subsequent 0.13 ml (1.11 mmol) benzoyl-*d*₅-chloride were added and the solution was stirred overnight. The solution was diluted to 100 ml with dichloromethane and washed twice with 1 N HCl and once with brine. After drying over MgSO₄ and filtration of the salts, the

dichloromethane was removed under vacuum. The crude product was dissolved in a mixture of methanol-*d*/D₂O (1:1) with 0.17 g (1.2 mmol) K₂CO₃ and refluxed for 1 hour. The mixture was extracted three times with dichloromethane and the combined organic layers were washed twice with 1 N HCl and once with brine. After drying over MgSO₄, filtration, and removal of dichloromethane the product was purified by column chromatography with ethyl acetate/hexane (40:60) as eluent. Yield: 0.16 g, 56 %, m.p. 100-101 °C. ¹H NMR (CD₃OD): δ 7.18-6.92 (m, 6H, ArH), 2.35 (m, 9 H, ArCH₃); ¹³C NMR (CD₃OD): δ 175.0, 174.4, 151.7, 151.4, 150.1, 137.9, 137.1, 137.0, 133.3-124.8, 44.1, 40.7, 33.2, 30.8, 30.6, 24.3, 23.8, 20.8, 18.5, 14.5; MS (FAB, NBA): *m/z* 667.5 [(M+H)⁺, calcd for C₄₁H₁₉N₂O₅D₂₄: 667.9]; IR (KBr): 2272, 2227, 2148, 2118, 2070 (C-D); 1587 (C=O) cm⁻¹, C₄₁H₁₈N₂O₅D₂₄: calcd C 73.83, H 6.35, N 4.20, found C 73.43, H 6.12, N 3.57.

Compound 4a

This compound was synthesized as **4** but non-deuterated reagents were used. Yield: 0.17 g, 62%, m.p. 99-101 °C. ¹H NMR (CD₃OD): δ 7.50-7.40 (m, 10H, ArH^{benzoyl}), 7.18-6.92 (m, 6H, ArH), 4.72 (s, 4H, ArCH₂N), 3.46-3.40 (m, 4H, NCH₂CH₃), 2.37-2.33 (m, 9 H, ArCH₃), 1.40-1.36 (m, 6H, NCH₂CH₃); ¹³C NMR (CD₃OD): δ 172.9, 172.3, 167.9, 149.6, 149.3, 148.0, 135.9, 135.2, 131.2-125.6, 123.5, 122.8, 43.2, 42.8, 39.4, 18.8, 12.0, 10.7; MS (FAB, NBA): *m/z* 643.3 [(M+H)⁺, calcd for C₄₁H₄₃N₂O₅: 643.8]. C₄₁H₄₂N₂O₅: calcd C 76.61, H 6.59, N 4.36, found C 76.38, H 6.54, N 4.60.

Compound 5

A mixture of 0.36 g (0.54 mmol) bisamide **4**, 0.16 ml (1.7 mmol) methyl bromoacetate-*d*₂, and 0.3 g (2.2 mmol) K₂CO₃ in 50 ml acetonitrile was refluxed for 3 hours. After cooling down, the salts were removed by filtration and the acetonitrile was removed under vacuum. After addition of 100 ml dichloromethane the mixture was washed twice with 1 N HCl followed by washing with water. The organic layer was dried over MgSO₄, filtered to remove the salts, and concentrated to dryness. The crude product was purified by column chromatography using ethyl acetate/hexane (1:1) as the eluent. Yield: 0.37 g, 78 %, m.p. 58-61 °C. ¹H NMR (CDCl₃): δ 7.20-7.15 (m, 2H, ArH), 7.15-7.10 (m, 4H, ArH), 3.70-3.65 (m, 3H, OMe), 3.63-3.58 (m, 3H, OMe), 3.42-3.38 (m, 3H, OMe), 2.39 (s, 9H, ArCH₃); ¹³C NMR (CDCl₃): δ 171.8, 169.0, 168.6, 152.2, 151.3, 136.5-125.5, 68.5 (m), 51.5, 51.1, 42.3-39.0 (m), 20.8, 20.5; MS (FAB, NBA): *m/z* 889.3 [(M+H)⁺, calcd. for C₅₀H₂₅N₂O₁₁D₃₀: 889.6]; IR (KBr): 2270, 2226, 2149, 2116, 2100, 2072 (C-D), 1761 (C=O^{ester}), 1630 (C=O^{amide}) cm⁻¹.

Compound 5a

This product was synthesized analogously to **5**, with the exception that un-deuterated methyl bromoacetate was used. Yield: 0.22 g, 81%, m.p. 57-59 °C. ¹H NMR (CDCl₃): δ 7.56-7.40 (m, 8 H, ArH^{benzoyl}), 7.40-7.35 (m, 2 H, ArH^{benzoyl}), 7.20-7.15 (m, 2H, ArHⁱ), 7.14-7.04 (m, 4H, ArH^o), 4.98 (s, 2H, ArCH₂N), 4.84 (s, 2H, ArCH₂N), 4.28 (s, 2H, OCH₂CO₂), 4.18 (s, 2H, OCH₂CO₂), 4.03 (s, 2H, OCH₂CO₂), 3.67 (s, 3H, OCH₃), 3.56 (s, 3H, OCH₃), 3.48 (s, 3H, OCH₃), 3.42-3.38 (m, 2H, NCH₂CH₃), 3.34-3.30 (m, 2H, NCH₂CH₃), 2.40-2.36 (m, 9H, ArCH₃), 1.32-1.30 (m, 3H, NCH₂CH₃), 1.20-1.16 (m,

3H, NCH₂CH₃); ¹³C NMR (CDCl₃): δ 171.8, 169.0, 168.6, 152.2, 151.3, 136.5-125.5, 69.5, 68.5, 68.0, 51.5, 51.1, 46.8, 42.5, 41.7, 40.0, 20.8, 20.5, 13.8, 12.0; MS (FAB, NBA): *m/z* 859.3 [(M+H)⁺, calcd for C₅₀H₅₅N₂O₁₁: 859.4]; IR (KBr): 1762 (C=O^{ester}), 1632 (C=O^{amide}) cm⁻¹, C₅₀H₅₅N₂O₁₁: calcd C 69.91, H 6.34, N 3.26, found C 69.52, H 6.14, N 3.12.

Compound 1.H₃

Trimethyl ester **5**, 0.20 g (0.23 mmol), was refluxed for 1 hour with 0.12 g (0.90 mmol) K₂CO₃ in 50 ml of a mixture of D₂O and MeOD. After cooling down to room temperature 100 ml of dichloromethane and 100 ml of 1 N HCl solution were added. The organic layer was separated and washed twice with 100 ml 1 N HCl, once with 100 ml water and dried over MgSO₄, filtered, and concentrated to dryness. Yield: 0.18 g, 96 %, m.p. 121-123 °C. ¹H NMR (CD₃OD): δ 7.18-7.09 (m, 2H, ArH), 7.08-7.02 (m, 2H, ArH), 6.98-6.92 (m, 2H, ArH), 2.22 (s, 9H, ArCH₃); ¹³C NMR (CD₃OD): δ 174.3, 172.8, 153.5, 152.0, 137.5-127.1, 69.8 (m), 30.7, 30.4, 28.4, 23.7, 20.9, 20.8, 14.4; MS (FAB, NBA): *m/z* 869.9 [(M+Na)⁺, calcd for C₄₇H₁₈N₂O₁₁D₃₀Na: 869.5]; IR (KBr): 2228, 2149, 2098 (C-D), 1749 (C=O^{acid}), 1627 (C=O^{amide}) cm⁻¹, C₄₇H₁₈N₂O₁₁D₃₀.1H₂O: calcd C 65.25, H 5.83, N 3.24, found C 65.42, H 6.34, N 2.79.

Compound 1a.H₃

The hydrolysis was carried out in the same way as for **1.H₃**, with the exception that non-deuterated solvents were used. Yield: 0.15 g, 97%, m.p. 120-123 °C. ¹H NMR (CD₃OD): δ 7.43 (s, 6H, ArH), 7.40 (s, 4H, ArH), 7.20 (s, 2H, ArH), 7.17 (s, 2H, ArH), 7.05 (s, 2H, ArH), 4.95 (s, 2H, ArH₂N), 4.68 (s, 2H, ArCH₂N), 4.22 (s, 2H, OCH₂CO₂), 4.10 (s, 2H, OCH₂CO₂), 3.93 (s, 2H, OCH₂CO₂), 3.62-3.57 (m, 2H, NCH₂CH₃), 3.25-3.20 (m, 2H, NCH₂CH₃), 2.38 (s, 9H, ArCH₃), 1.25-1.20 (m, 3H, NCH₂CH₃), 1.06-1.02 (m, 3H, NCH₂CH₃); ¹³C NMR (CD₃OD): δ 172.4, 170.4, 151.7, 137.8-125.4, 68.8, 68.5, 68.4, 42.8, 41.0, 39.8, 19.0, 12.1, 10.7; MS (FAB, NBA): *m/z* 839.4 [(M+Na)⁺, calcd for C₄₇H₄₈N₂O₁₁Na: 839.3]; IR (KBr): 1756 (C=O^{acid}), 1633 (C=O^{amide}) cm⁻¹, C₄₇H₄₈N₂O₁₁.1H₂O calcd C 67.61, H 6.04, N 3.36, found C 67.74, H 5.97, N 3.40.

Procedure for the preparation of the lanthanide complexes (1.Ln and 1a.Ln)

To a 0.02 M solution of ligand (**1.H₃** and **1a.H₃**) in methanol with 4 equivalents of Et₃N a solution of 1.3 equivalents Ln(NO₃)₃.xH₂O, where x = 5 or 6 depending on the lanthanide ion, were added. After 1 hour the methanol was removed under vacuum and the residue was dissolved in chloroform and washed three times with water. The organic solutions were dried over MgSO₄, filtered, and evaporated to dryness.²⁶

1.Nd m.p. > 300 °C (decomp.); MS (FAB, MB): *m/z* 988.3 [(M+H)⁺, calcd for C₄₇H₁₅N₂O₁₁D₃₀Nd: 988.3]; IR (KBr): 2270, 2227, 2118, 2072 (C-D), 1622 (C=O^{amide}), 1599 (C=O^{carboxylate}) cm⁻¹.

1.Er m.p. > 300 °C (decomp.); MS (FAB, MB): *m/z* 1012.5 [(M+H)⁺, calcd for C₄₇H₁₅N₂O₁₁D₃₀Er: 1011.3]; IR (KBr): 2270, 2228, 2104, 2072 (C-D), 1634 (C=O^{amide}), 1594 (C=O^{carboxylate}) cm⁻¹.

1.Yb m.p. > 300 °C (decomp.); MS (FAB, MB): *m/z* 1018.5 [(M+H)⁺, calcd for C₄₇H₁₅N₂O₁₁D₃₀Yb: 1017.4]; IR (KBr): 2229, 2155, 2109 (C-D), 1635 (C=O^{amide}), 1600 (C=O^{carboxylate}) cm⁻¹.

1a.Nd m.p. > 300 °C (decomp.); MS (FAB, MB): m/z 958.2 [(M+H)⁺, calcd for C₄₇H₄₅N₂O₁₁Nd: 958.1]; IR (KBr): 1628 (C=O^{amide}), 1598 (C=O^{carboxylate}) cm⁻¹.

1a.Er m.p. > 300 °C (decomp.); MS (FAB, MB): m/z 981.2 [(M+H)⁺, calcd for C₄₇H₄₅N₂O₁₁Er: 981.1]; IR (KBr): 1630 (C=O^{amide}), 1600 (C=O^{carboxylate}) cm⁻¹.

1a.Yb m.p. > 300 °C (decomp.); MS (FAB, MB): m/z 987.5 [(M+H)⁺, calcd for C₄₇H₄₅N₂O₁₁Yb: 986.9]; IR (KBr): 1629 (C=O^{amide}), 1601 (C=O^{carboxylate}) cm⁻¹.

Photophysical

NIR emission and excitation spectra were recorded on a Photon Technology International (PTI) Alphascan spectrofluorimeter. Emitted light was collected by a North Coast liquid nitrogen cooled germanium detector under an angle of 90° with optically chopped (40 Hz) excitation light. Lifetime measurements in the NIR were performed on an Edinburgh Analytical Instruments LP900 system by exciting the samples with a pulsed nitrogen laser operating at 337 nm. Decay curves were measured by collecting the emitted light with a liquid nitrogen cooled Ge detector by a single photon counting technique. Deconvolution of the curves was performed using the response of the instrument to a fast dye (IR 140 in methanol, fluorescence lifetime below 1 ns, much shorter than the instrument response). Deconvolution and fitting was performed with commercial software, installed on the instrument computer system (Edinburgh Instruments).

3.5 References and notes

- ¹ Hofstraat, J. W.; Oude Wolbers, M. P.; van Veggel, F. C. J. M.; Reinhoudt, D. N.; Werts, M. H. V.; Verhoeven, J. W. *J. Fluoresc.* **1998**, *8*, 301.
- ² McGehee, M. D.; Bergstedt, T.; Zhang, C.; Saab, A. P.; O'Regan, M. B.; Bazan, G. C.; Srdanov, V.; I. Heeger, A. J. *Adv. Mater.* **1999**, *11*, 1349.
- ³ a) Steemers, F. J.; Verboom, W.; Reinhoudt, D. N.; van der Tol, E. B.; Verhoeven, J. W. *J. Am. Chem. Soc.* **1995**, *117*, 9408; b) Werts, M. H. V.; Woudenberg, R. H.; Emmerink, P. G.; van Gassel, R.; Hofstraat, J. W.; Verhoeven, J. W. *Angew. Chem. Int. Ed.* **2000**, *39*, 4542.
- ⁴ Miniscalco, W. J. *J. Lightwave Tech.* **1991**, *9*, 234.
- ⁵ Slooff, L. H.; Polman, A.; Oude Wolbers, M. P.; van Veggel, F. C. J. M.; Reinhoudt, D. N.; Hofstraat, J. W. *J. Appl. Phys.* **1998**, *83*, 497.
- ⁶ a) Horrocks, W. De W.; Sudnick, D. R. *Acc. Chem. Res.* **1981**, *14*, 384; b) Beeby, A.; Clarkson, I. M.; Dickins, R. S.; Faulkner, S.; Parker, D.; Royle, L.; De Sousa, A. S.; Williams, J. A. G.; Woods, M. J. *Chem. Soc., Perkin Trans. 2* **1999**, 493.
- ⁷ a) Oude Wolbers, M. P.; van Veggel, F. C. J. M.; Hofstraat, J. W.; Geurts, F. A. J.; Reinhoudt, D. N. *J. Chem. Soc., Perkin Trans. 2* **1997**, 2275; b) Oude Wolbers, M. P.; van Veggel, F. C. J. M.; Snellink-Ruël, B. H. M.; Hofstraat, J. W.; Geurts, F. A. J.; Reinhoudt, D. N. *J. Am. Chem. Soc.*

- 1997, 119, 138; c) Oude Wolbers, M. P.; van Veggel, F. C. J. M.; Snellink-Ruël, B. H. M.; Hofstraat, J. W.; Geurts, F. A. J.; Reinhoudt, D. N. *J. Chem. Soc., Perkin Trans. 2* **1998**, 2141.
- 8 Oude Wolbers, M. P.; van Veggel, F. C. J. M.; Peters, F. G. A.; van Beelen, E. S. E.; Hofstraat, J. W.; Geurts, F. A. J.; Reinhoudt, D. N. *Chem., Eur. J.* **1998**, 4, 772.
- 9 Klink, S. I.; Hebbink, G. A.; Grave, L.; Peters, F. G. A.; van Veggel, F. C. J. M.; Reinhoudt, D. N.; Hofstraat, J. W. *Eur. J. Org. Chem.* **2000**, 10, 1923.
- 10 Slooff, L. H.; de Dood, M. J. H.; van Blaaderen, A.; Polman, A. *Appl. Phys. Lett.* **2000**, 76, 3682.
- 11 Hasegawa, Y.; Ohkubo, T.; Sogabe, K.; Kawamura, Y.; Wada, Y.; Nakashima, N.; Yanagida, S. *Angew. Chem. Int. Ed.* **2000**, 39, 357.
- 12 Slooff, L. H.; Polman, A.; Klink, S. I.; Hebbink, G. A.; Grave, L.; van Veggel, F. C. J. M.; Reinhoudt, D. N.; Hofstraat, J. W. *Opt. Mat.* **2000**, 14, 101.
- 13 Klink, S. I.; Keizer, H.; van Veggel, F. C. J. M. *Angew. Chem. Int. Ed.* **2000**, 39, 4319.
- 14 Klink, S. I.; Hebbink, G. A.; Grave, L.; van Veggel, F. C. J. M.; Reinhoudt, D. N.; Slooff, L. H.; Polman, A.; Hofstraat, J. W. *J. Appl. Phys.* **1999**, 86, 1181.
- 15 The quenching of C-H at 8 Å is only 1.5% of that at 4 Å.
- 16 van Veggel, F. C. J. M.; Oude Wolbers, M. P.; Reinhoudt, D. N. *J. Phys. Chem.* **1998**, 102, 3060.
- 17 OPLS: Optimized Potentials for Liquid Simulations; Jorgensen, W. L. *J. Phys. Chem.* **1986**, 90, 1276.
- 18 van Veggel, F. C. J. M.; Reinhoudt, D. N. *Chem. Eur. J.* **1999**, 5, 90.
- 19 Tramontini, M.; Angiolini, L. *Tetrahedron* **1990**, 46, 1791, and references cited therein.
- 20 Koenig, K. E.; Lein, G. M.; Stuckler, P.; Kaneda, T.; Cram D. J. *J. Am. Chem. Soc.* **1979**, 101, 3553.
- 21 Hesse, M.; Meier H.; Zeeh, B. *Spektroskopische Methoden in der Organischen Chemie*, 4th edition, Georg Thieme Verlag, Stuttgart-New York, 1991.
- 22 This is a Nd³⁺ transition from the same excited level as the 1060 and 1330 nm emissions, and therefore present in the emission spectrum but this transition could not be detected with the detector used.
- 23 a) Ermolaev, V. L.; Sveshnikova, E. B. *Russ. Chem. Rev.* **1994**, 63, 905, and references cited therein; b) Haas, Y.; Stein, G. *J. Phys. Chem.* **1971**, 75, 3668; c) Kropp, J. L.; Windsor, M. W. *J. Chem. Phys.* **1965**, 42, 1599; d) Takalo, H.; Hänninen, E.; Kankare, J. *Helv. Chim. Acta* **1993**, 76, 877; e) Hemmilä, I.; Mikkala, V.-M.; Takalo, H. *J. Fluoresc.* **1995**, 5, 159.
- 24 MB is a mixture of dithioerythritol and dithiothreitol, 1:5 (by wt.).
- 25 Because this reaction is very sensitive to the conditions used, the different quality formaldehyde caused that some alterations in the procedure were needed.
- 26 No reliable elemental analyses could be obtained from the lanthanide ion complexes. This was already mentioned in reference 7.

Chapter 4

Dyes as sensitizers of near-infrared emitting lanthanide(III) ions

Near-infrared emissive lanthanide complexes were synthesized with covalently attached sensitizers that absorb visible light, i.e. fluorescein, eosin, and erythrosin. It was expected that an intrinsic high intersystem crossing would be beneficial in the sensitization process, because energy transfer occurs through the triplet state of sensitizers. However, due to the enhanced intersystem crossing of the sensitizers by the nearby heavy and paramagnetic lanthanide ions, these intrinsic differences were largely diminished. It was even found that fluorescein acts as a more efficient sensitizer for the NIR emission of Nd^{3+} , Er^{3+} , and Yb^{3+} than eosin and erythrosin. The $^4\text{F}_{9/2}$ level of Nd^{3+} was determined as the receiving level of energy from the donating triplet state of the sensitizers.

4.1 Introduction

Sensitized lanthanide ion emission attracts a large interest,¹ because it is an efficient way to circumvent the low absorption coefficients of these ions.² The main interest of this research has been focused on the visible (VIS) emission of europium and terbium,^{3,4} which can be sensitized with UV absorbing sensitizers. Only in recent years, the interest has shifted to the near-infrared (NIR) emissive ions, like neodymium, ytterbium, and erbium.^{5,6,7,8,9,10,11} The use of the NIR emissive ions has a number of advantages compared to the VIS emitting ions. For instance, the emission in the NIR is ideally applicable to biology,¹² because biological tissue is relatively transparent to NIR light, and to telecommunication where the ions act as active material in optical amplifiers of the NIR signals.¹³ Furthermore, sensitizers that absorb in the visible region can be used here to sensitize the NIR emitting lanthanide ions.¹⁴ This gives the advantages of cheap excitation sources like diode lasers and the possibility to use glass instead of quartz for substrate handling in biological tests. The sensitization of these ions is still not fully understood and the search for the ‘perfect’ sensitizer-lanthanide complex combination is an ongoing process.

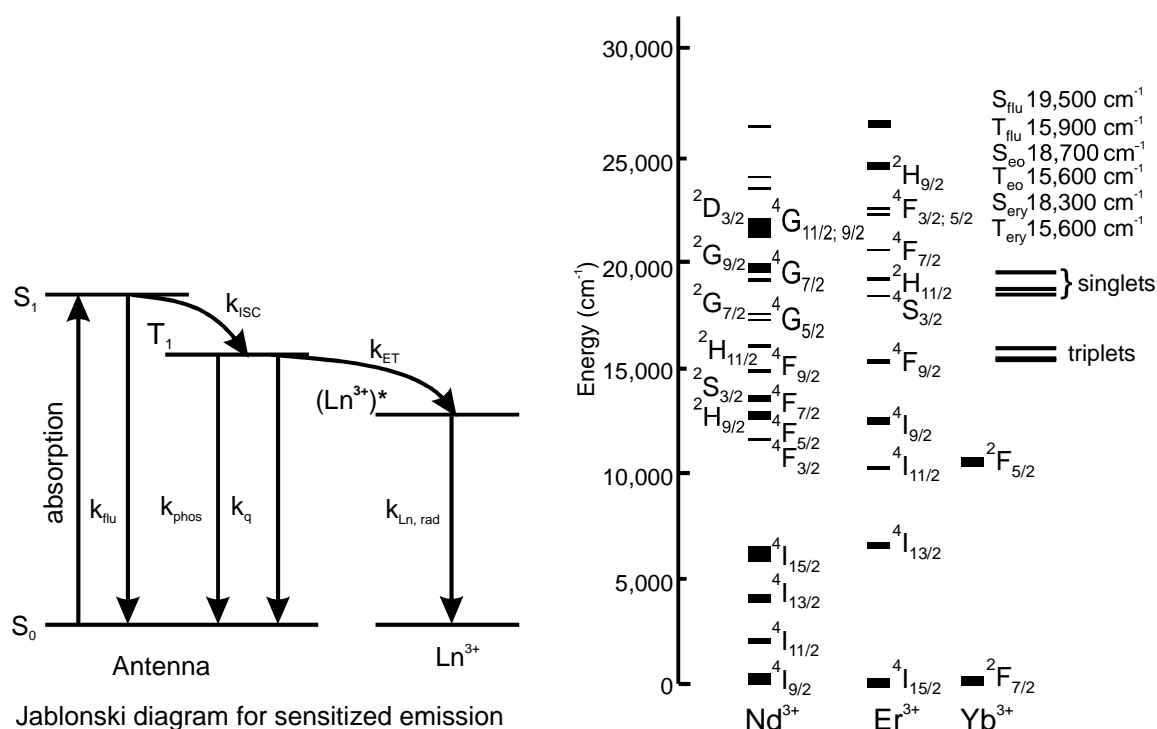


Figure 4.1 Left: simplified Jablonski diagram for sensitized emission, k_{flu} : rate of fluorescence, k_{ISC} : intersystem crossing rate, k_{phos} : phosphorescence rate, k_q : triplet quenching rate, k_{ET} : energy transfer rate, and $k_{Ln,rad}$: radiative decay rate. Right: diagram with the energy levels²³ of Yb^{3+} , Nd^{3+} and Er^{3+} together with the singlet and triplet state energies of the three dyes (in methanol, this work⁵¹), ‘flu’ stands for fluorescein, ‘eo’ for eosin, and ‘ery’ for erythrosin.

The luminescence of the lanthanide ions originates from transitions within the partially filled 4f orbitals, which are in principle spin-forbidden.¹⁵ Lanthanide ions with completely filled (Lu^{3+}) or unfilled (Y^{3+} and La^{3+}) 4f orbitals do not possess any luminescence. The luminescence of the other ions ranges from the UV to the NIR. Characteristics of this luminescence are the line-like emissions, low absorption coefficients, and high luminescent lifetimes, up to milliseconds. The energy levels of the emission are hardly affected by the environment of the ions, as the filled 5s and 5p orbitals shield the electrons in the 4f levels; in other words, the effect of the ligand field is very small.

A simplified Jablonski diagram for the sensitized emission of lanthanide ions is depicted in Figure 4.1. After excitation of the antenna and subsequent intersystem crossing, the energy is transferred to the lanthanide ion. In general, it is accepted that this sensitization occurs from the triplet state via a Dexter mechanism,² although energy transfer from the singlet state can not be ruled out completely.^{16,17} Taking the sensitization via the triplet state, the overall quantum yield of sensitized lanthanide ion emission (ϕ_{SE}) is determined by three individual steps: the intersystem crossing quantum yield (ϕ_{ISC}), the energy transfer efficiency (η_{ET}), and the lanthanide ion quantum yield (ϕ_{Ln}), Eq. 4.1.¹⁸

$$\phi_{\text{SE}} = \phi_{\text{ISC}} \times \eta_{\text{ET}} \times \phi_{\text{Ln}} \quad \text{Eq. 4.1}$$

In the sensitization of europium it was found that the gap between sensitizer triplet state and the energy accepting state of Eu^{3+} has to be about 1000-2000 cm^{-1} to avoid possible energy back transfer.^{19,20} This limits the sensitization to UV or violet light.^{21,22} When this rule is applied to the NIR emitting lanthanide ions, it can be seen that there is in principle no limitation in the use of sensitizers that absorb in the visible. The lower limit in the triplet state energy, which still gives sensitized emission, will of course depend on the individual lanthanide ion (see Figure 4.1 for the energy levels of Yb^{3+} , Nd^{3+} , and Er^{3+}).²³

A number of NIR emitting lanthanide ion complexes have been reported that have visible light absorbing antennas.²⁴ Some examples of these sensitizers that absorb in the visible region of the electromagnetic spectrum are fluorescein,^{25,26} lissamine,²⁷ porphyrins,^{28,29} ferrocene,³⁰ and ruthenium complexes.³⁰ However, the energy transfer pathways are still not fully understood for the sensitization of the NIR emitting lanthanide ions by these sensitizers.

For efficient lanthanide emission, complexes should have a high absorption coefficient, a high intersystem crossing quantum yield, an efficient energy transfer, and an efficient lanthanide

luminescence. The absorption coefficient is not a real problem as many organic dyes and chromophores absorb strongly. Ideally, the intersystem crossing quantum yield of a sensitizer should be 100%. The intersystem crossing is enhanced by the introduction of heavy atoms like bromine or iodine in the dye system. The energy transfer is mainly determined by the distance between sensitizer and lanthanide ion and by the normalized spectral overlap between the sensitizer and the ion (*vide infra*).³¹

In this Chapter, the sensitization properties of NIR emitting lanthanide ions by a series of dyes based on the xanthene moiety that are structurally very similar is reported. Complexes were made of ligands functionalized with fluorescein, eosin, or erythrosin (Figure 4.2).

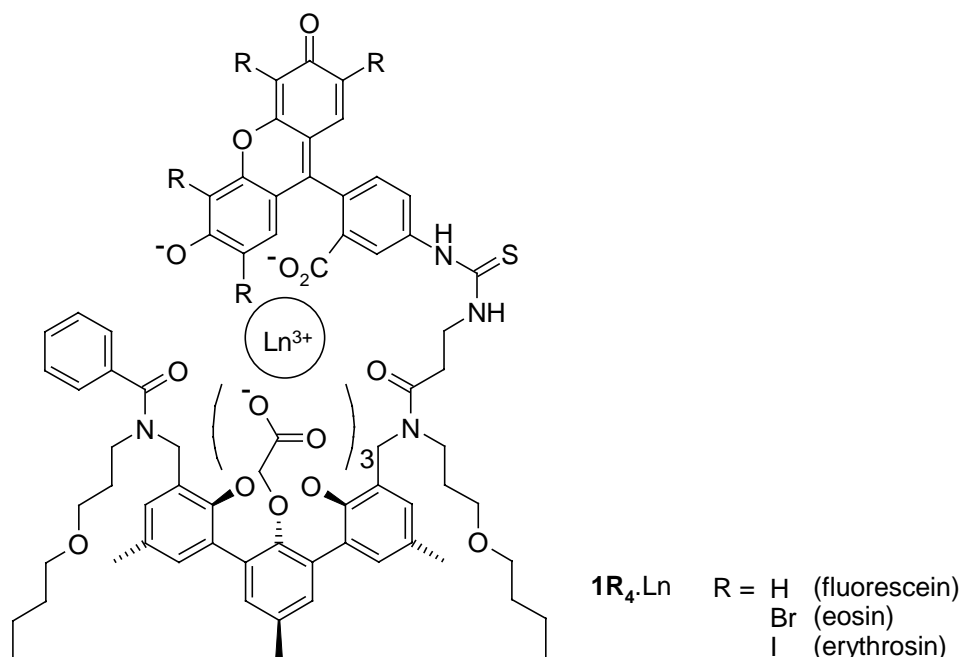


Figure 4.2 *m*-Terphenyl complexes functionalized with fluorescein, eosin, and erythrosin.

The major difference in these dyes is the intrinsic intersystem crossing (ISC) quantum yield.³² This difference is the result of the presence of heavy atoms in the dyes: bromine in eosin, and iodine in erythrosin. This results in ISC quantum yields in water of 2% for fluorescein, 18% for eosin, and 82% for erythrosin. Furthermore, efficient energy transfer can be achieved by reducing the distance between the sensitizer and the lanthanide ion by exploiting the carboxylate group of these dyes. Because the complexes used are structurally similar, conclusions can be drawn on the effect of this inherent ISC on the sensitization properties. So far, no systematic studies have been done on the NIR emitting complexes with a series of related sensitizers. From

Eq. 4.1, it would be expected that the higher the intrinsic ISC is, the better the sensitization efficiency is.

This Chapter is structured as follows. First, the design of the complexes is discussed with the aid of molecular modeling simulations, followed by their synthesis. Subsequently, the luminescent properties in the NIR and the VIS region of these complexes are presented. Finally, this luminescence and the energy transfer mechanism from sensitizer to ion will be discussed together with the efficiency of sensitization by three sensitizers.

4.2 Results and discussion

4.2.1 Modeling

One of the advantages of this terphenyl moiety is the possibility to functionalize the building block, without altering the complexing moiety. An example of the structure of a terphenyl-based complex (Bz.Ln), without a sensitizer, is depicted in Figure 4.3. These complexes serve as model or reference compounds.

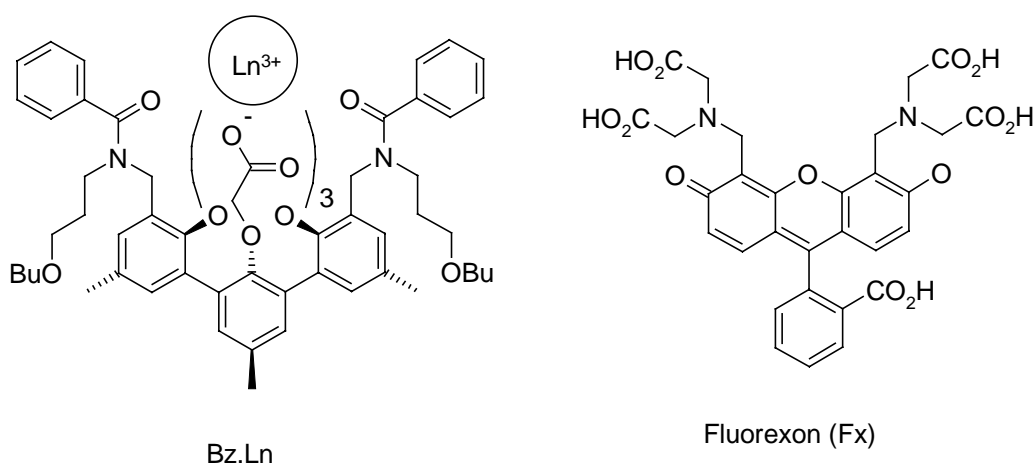


Figure 4.3 The molecular structures of Bz.Ln³³ (left) and fluorexon (Fx)³⁵ (right).

We have used the terphenyl moiety previously as building block for lanthanide complexes, functionalized with sensitizers.^{5,27,30,33} In these reports it was emphasized that these complexes have eight coordinating groups, leaving room for a ninth ligand on the lanthanide ion. In most cases this place was occupied by the solvent, in other cases this place was occupied by a sensitizer, creating ternary complexes.³⁴ This “free” site is used here to bring the xanthene moiety of the antennas in close proximity of the lanthanide ion via coordination of its carboxylate group. A β -alanine spacer connected via an isothiocyanate moiety enables the free carboxylate of the dye to coordinate to the lanthanide ion in the ligand as was confirmed by

molecular dynamics simulations for 1000 ps (see Figure 4.4) in OPLS methanol.^{35,36} In this snapshot the xanthene unit is at the top of the Figure and the terphenyl moiety is at the bottom. The lanthanide ion is complexed by four carboxylates, two amides, and three ether oxygens leaving no room for any solvent.

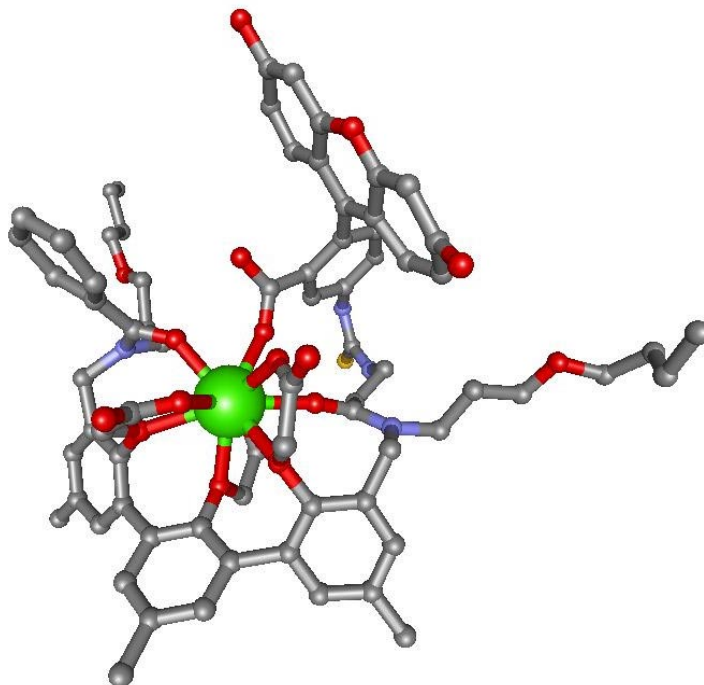
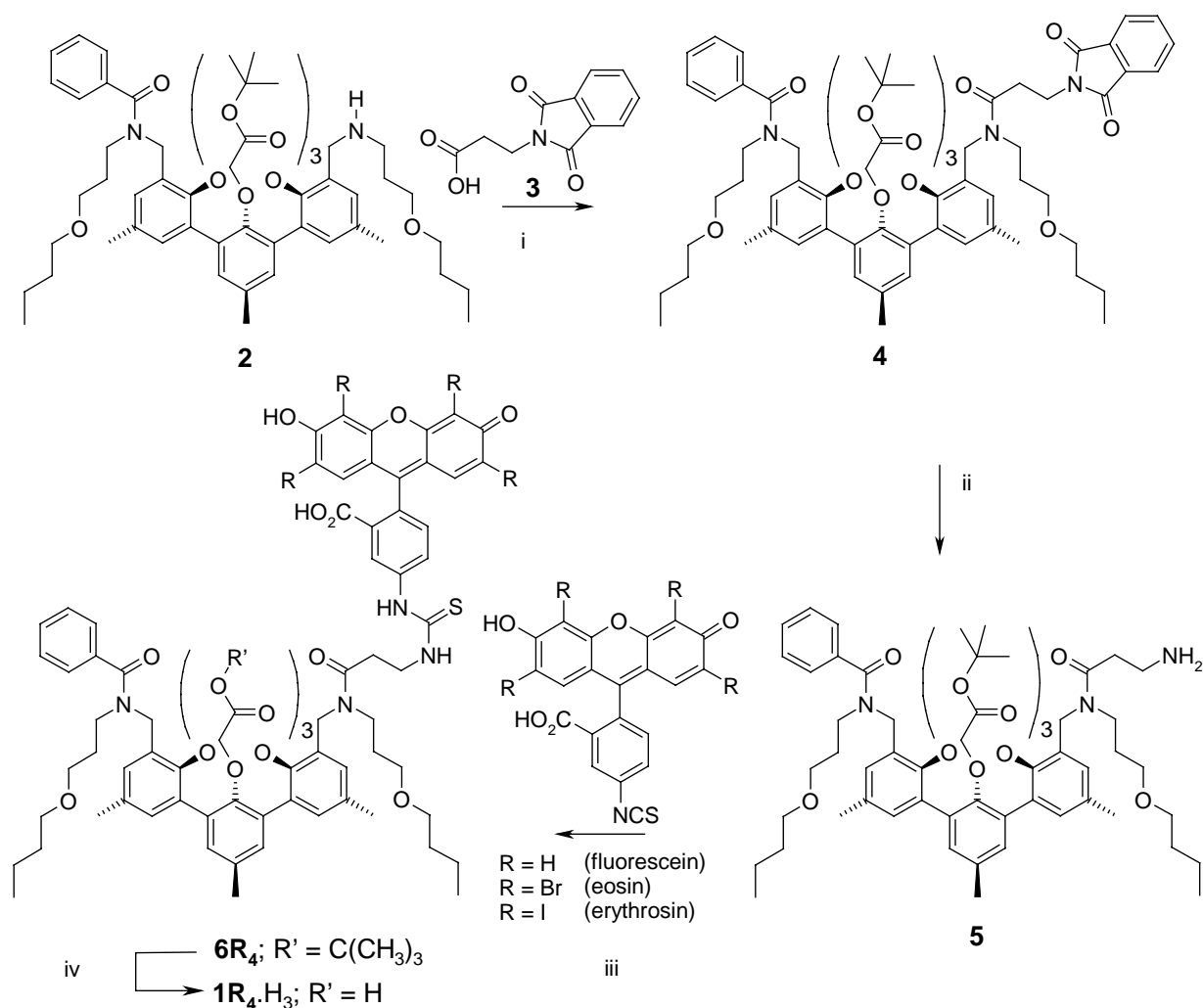


Figure 4.4 Snapshot of **1H₄.Eu**, derived from a molecular dynamics simulation in OPLS³⁶ methanol. Hydrogens are omitted for clarity. See text for more details.

The average distance between the lanthanide ion and the xanthene unit³⁷ was determined from periodically saved sets of coordinates during the simulations. The distances found were $6.1 \pm 0.2 \text{ \AA}$ for **1H₄.Ln** and $6.2 \pm 0.1 \text{ \AA}$ for **1I₄.Ln**, which is much smaller than the distance of about 10 \AA in similar complexes with a dye moiety attached via a rigid spacer.³⁸ The larger iodine atoms in **1I₄.Ln** do not influence the distance between sensitizer and ion. Furthermore, in **1I₄.Ln** in about half of the snapshots a methanol was found to be in relative close proximity of the ion, $2.7 \pm 0.2 \text{ \AA}$, which is the distance between lanthanide(III) ion and the methanol oxygen. This distance is too large for direct binding in the first coordination sphere of the lanthanide(III) ion, but may act as a second sphere quencher.^{39,40} The β -alanine spacer thus enables the carboxylate of the xanthene dyes to coordinate to the lanthanide ion in the complex. Doing so, the distance between sensitizer and ion is decreased and no space is left for solvents to coordinate directly to the ion.

4.2.2 Synthesis

The synthesis of the complexes was carried out as depicted in Scheme 4.1 with monoamine **2** as the starting material.⁶² β -Alanine was protected as the phthalimide **3** by heating the amino acid with phthalic anhydride, yielding **3** in almost quantitative yield. By refluxing **3** in oxalylic chloride the acid function was converted into the acid chloride, which was subsequently reacted with monoamine **2** to yield the bisamide **4**.⁶²



Scheme 4.1 i: 1) $C_2O_2Cl_2$, room temperature; 2) TEA, CH_2Cl_2 , room temperature, yield: 62%; ii: $N_2H_4 \cdot H_2O$, EtOH, reflux, yield: 99%; iii: TEA, CH_2Cl_2 , dye isothiocyanate, room temperature, yield: 60%; iv: TFA, room temperature, yield: quantitative.

After purification, the formation of **4** was confirmed by mass spectrometry, where a peak corresponding to **4** was found and by the 1H NMR spectrum, where no signals corresponding to protons next to an amine moiety or a carboxylic acid were present, but only signals corresponding to the amides. Furthermore, four strong peaks are found in the IR spectrum in the carbonyl region around 1700 cm^{-1} , 1753 cm^{-1} for the esters, 1644 cm^{-1} for the amides, and 1717

cm^{-1} for the phthalimide. The deprotection of the phthalimide moiety in **4** was carried out in ethanol with hydrazine monohydrate under reflux conditions. The reaction was quantitative and the ^1H NMR and IR spectra confirmed complete removal of the phthalimide. The isothiocyanate functionalized dyes were coupled to this amine **5** by stirring overnight a mixture in CH_2Cl_2 with a slight excess of dye. Purification was carried out by size separation chromatography (Sephadex) in order to remove the salts (TEA salts) and the excess of unreacted dye, and by thin layer chromatography. Typical yields of the dye functionalized compounds **6R₄** (R = H, Br, or I) are in the order of 60% of the strongly colored products (absorption coefficients in the range of 77,000 - 84,000 $\text{l}\times\text{mol}^{-1}\times\text{cm}^{-1}$ at the maximum between 500-550 nm in methanol solution). The fluorescein (**6H₄**) and eosin (**6Br₄**) compounds are highly fluorescent in solution, whereas the erythrosin compound (**6I₄**) exhibits much less fluorescence. The *tert*-butyl ester compounds (**6R₄**) were converted to the triacids **1R₄.H₃** by mild hydrolyses in pure TFA. Complete hydrolysis was confirmed by ^1H NMR spectroscopy and by mass spectrometry. In the IR spectra, the resonance around 1730 cm^{-1} for the carboxylic acid is present. The purity of the compounds was checked with TLC with 15% methanol in CH_2Cl_2 as the eluent. Single spots were found with an r_F of about 0.4. The lanthanide(III) ion complexes **1R₄.Ln** were made in methanol by deprotonation of the ligand with five equivalents TEA and subsequent addition of one equivalent of lanthanide(III) nitrate salt. Complete deprotonation of the complexes, which consist of three carboxylate moieties on the terphenyl, the carboxylate on the xanthene moiety, and the phenol group on the xanthene moiety, was confirmed by UV spectroscopy, where the absorption of the dianion form of the dyes was found.³² Complexes were made of the nitrate salts of Nd^{3+} , Yb^{3+} , and Er^{3+} , which exhibit sensitized NIR emission, and of Eu^{3+} and Gd^{3+} , which were used in addition to determine the deactivation of the singlet excited state of the dyes. The mass spectrometry (ESI-TOF) data of the complexes are summarized in Table 4.4 (in the experimental section). The found molecular masses and the isotope patterns, correspond excellently with the calculated spectra.

4.2.3 Luminescence

In this section, the luminescence of the sensitizer-functionalized complexes will be described. This is done according to the simplified Jablonski diagram in Figure 4.1 starting with the NIR luminescence of the lanthanide ions and then the fluorescence and the phosphorescence in the visible region of the sensitizer. Finally, the energy transfer efficiency and the energy transfer rates will be discussed. The reported luminescent properties are the emission and

excitation spectra, quantum yields, lifetimes, and the rates of the various transitions. The luminescence properties of Bz.Ln (Figure 4.3)⁶² are reported in Table 4.2, in order to have a comparison. The emission in the visible region is also reported of the Gd³⁺ and Eu³⁺ complexes. These complexes (**1R₄**.Gd and **1R₄**.Eu) are a good model for the sensitizer fluorescence and phosphorescence as these ions have similar sizes as the emissive ions, and they are paramagnetic as well. However, they cannot accept energy, because the lowest excited states are too high in energy to be populated by the dyes (32,200 cm⁻¹ for Gd³⁺ and 17,300 cm⁻¹ for Eu³⁺).

4.2.3.1 NIR luminescence

Spectra of the Nd³⁺, Yb³⁺, Er³⁺ complexes

In the emission spectra (Figure 4.5), the typical emission lines for Nd³⁺ at 890 (⁴F_{3/2}→⁴I_{9/2}), 1064 (⁴F_{3/2}→⁴I_{11/2}), and 1330 nm (⁴F_{3/2}→⁴I_{13/2}),⁴¹ for Er³⁺ at 1536 nm (⁴I_{13/2}→⁴I_{15/2}), and for Yb³⁺ at 980 nm (²F_{5/2}→²I_{7/2}) are present. The emission of the **1H₄**.Ln complexes is shown here as representative for the emission of the other complexes (**1Br₄**.Ln, **1I₄**.Ln).

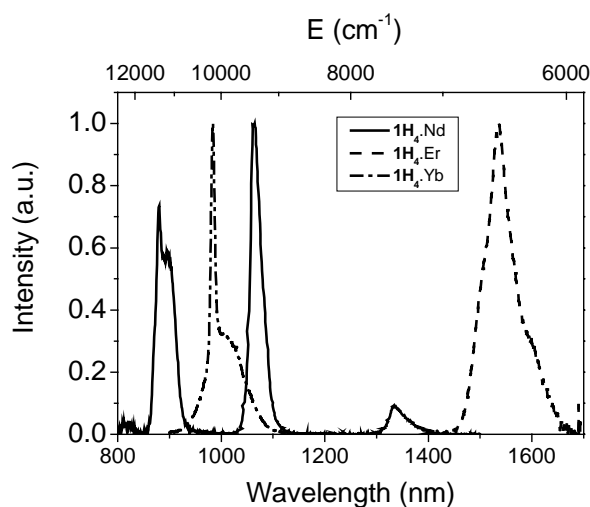


Figure 4.5 NIR emission spectra of **1H₄**.Nd, **1H₄**.Yb, and **1H₄**.Er in CH₃OD (Nd³⁺ and Yb³⁺) and in CD₃OD (Er³⁺) solution.

The absorption and excitation spectra of the Nd³⁺ complexes are shown in Figure 4.6 as representative for all absorption and excitation spectra.

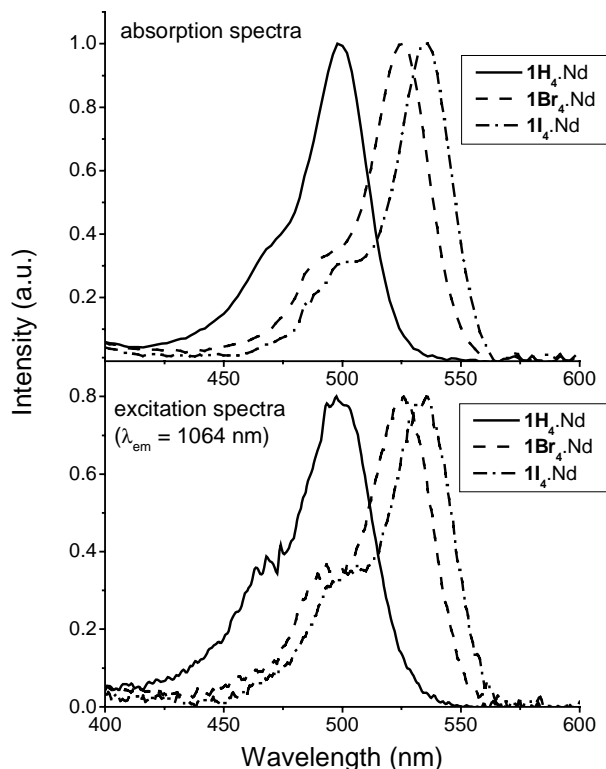


Figure 4.6 (Normalised) absorption (top) and excitation spectra (bottom) of $1\mathbf{H}_4.\text{Nd}$, $1\mathbf{Br}_4.\text{Nd}$, and $1\mathbf{I}_4.\text{Nd}$ in CD_3OD solution. The excitation spectra were collected by measuring the emission at 1066 nm.

The absorption maxima of these dyes are 505 nm for fluorescein, 535 nm for eosin, and 545 nm for erythrosin (measured in methanol solution), which are red shifted by about 5-10 nm compared to the absorption maxima of these dyes in water.²⁶ The resemblance of the excitation spectra to the absorption spectra proves the sensitized emission by the dyes.

Overall Quantum yield (ϕ_{SE})

Quantum yields of sensitized emission in deuterated methanol (ϕ_{SE}) were determined by using Fx.Nd and Fx.Yb (Figure 4.3)⁶⁴ as a standard for the Nd^{3+} and Yb^{3+} emission, respectively, and they are tabulated in Table 4.1. The luminescence $1\mathbf{R}_4.\text{Er}$ was only measured relative to $1\mathbf{H}_4.\text{Er}$ due to the very low intensities of the signals, which prevented accurate quantum yield measurements. The relative quantum yields ($\phi_{\text{SE, rel}}$) show that for all three lanthanide ions the quantum yields are somewhat lower than that for Fx.Ln .

Table 4.1 The NIR emission sensitization properties $1R_4Ln$ (with $R = H, Br, \text{ and } I$ and $Ln^{3+} = Yb^{3+}, Nd^{3+}, \text{ and } Er^{3+}$).^a

Complex	$\phi_{SE, rel}^b$	ϕ_{SE}^c	τ (μs)	τ (μs) ^d	ϕ_{Ln}^e	$(\phi_{ISC} \times \eta_{ET})^f$
1H₄.Yb	0.52	2.3×10^{-3}	11.1	9.8	5.5×10^{-3}	0.4
1Br₄.Yb	0.32	1.4×10^{-3}	11.2	11.6	5.6×10^{-3}	0.3
1I₄.Yb	0.37	1.7×10^{-3}	11.5	10.2	5.8×10^{-3}	0.3
1H₄.Nd	0.78	3.0×10^{-4}	0.41	0.24	1.6×10^{-3}	0.2
1Br₄.Nd	0.37	1.4×10^{-4}	0.41	0.36	1.6×10^{-3}	0.1
1I₄.Nd	0.31	1.2×10^{-4}	0.37	0.25	1.5×10^{-3}	0.1
1H₄.Er	1.00 ^g	- ^h	0.91	nd	6.5×10^{-5}	-
1Br₄.Er	0.51 ^g	- ^h	nd ^h	nd	-	-
1I₄.Er	0.43 ^g	- ^h	nd ^h	nd	-	-

a Properties determined in deuterated methanol, at $\sim 10^{-6}$ M, aerated solution, 22 °C, unless stated otherwise.

b Relative quantum yield, with $\phi_{Fx, Ln} = 1.0$; error (from triplos): ± 0.05 .

c Absolute quantum yield, calculated from absolute quantum yield of Fx.Ln: $\phi_{SE} = \phi_{SE, rel} \times \phi_{Fx, Ln}$ with $\phi_{Fx, Yb} = 4.5 \times 10^{-3}$; $\phi_{Fx, Nd} = 3.8 \times 10^{-4}$.⁶⁴

d Luminescent lifetime of the lanthanide(III) ions in normal methanol.

e Calculated from $\phi_{Ln} = \tau / \tau_{rad}$, where τ_{rad} is the pure radiative lifetime of Ln ($\tau_{rad, Nd} = 0.25$ ms, $\tau_{rad, Yb} = 2.0$ ms, $\tau_{rad, Er} = 14$ ms).^{5,6} It should be noted that τ_{rad} are estimates.

f Efficiency of the sensitization process: $(\phi_{ISC} \times \eta_{ET}) = \phi_{SE} / \phi_{Ln}$. However, the ligand field of the three complexes are virtually the same, which means that the relative values of $(\phi_{ISC} \times \eta_{ET})$ will be unaffected.

g Relative quantum yield, $\phi_{rel}(1H_4.Er)$ is set to 1.

h No standard available.

A striking observation is that the complexes with fluorescein as the sensitizer have the highest quantum yields. At first glance this is in contrast with the fact that fluorescein has the lowest intrinsic intersystem crossing quantum yield, the reason for this is presented in the discussion section. Despite the deuterated solvent, the ϕ_{SE} are rather low, which is mainly caused by vibrational modes within the complex itself. These modes quench the excited state of the lanthanide(III) ions and this is commonly observed in organic complexes of these NIR emitting ions. In fact, the highest quantum yield reported for Nd^{3+} in organic solution is only 0.03, measured in a completely fluorinated ligand and in a perdeuterated solvent.⁷

Quantum yield of NIR lanthanide(III) emission (ϕ_{Ln})

The quantum yields of lanthanide emission were calculated from the ratio of the measured lifetimes and the radiative lifetimes of the ions. Luminescent lifetimes of the lanthanide(III) ion complexes in the NIR were determined in normal and deuterated methanol and these are also reported in Table 4.1. For comparison, the luminescent lifetimes of Bz.Ln ($Ln^{3+} = Yb^{3+}, Nd^{3+}, Er^{3+}$, Figure 4.3), which lacks an additional antenna, are reported in Table 4.2.⁶² The lifetimes of the ytterbium complexes **1H₄**.Yb, **1Br₄**.Yb, and **1I₄**.Yb are about 11 μ s in both deuterated methanol and normal methanol. A rate constant of quenching by the solvent of these complexes ($k_{q, solv} = 1/\tau_{CH_3OH} - 1/\tau_{CD_3OD}$) is $\leq 3 \times 10^4 \text{ s}^{-1}$, whereas the quenching by the solvent in Bz.Yb is $\leq 3 \times 10^5 \text{ s}^{-1}$. This means that the ligand and coordinating sensitizer shield the ion very well from the solvent. The lifetimes of the **1R₄**.Nd complexes are comparable to each other, about 0.4 μ s in deuterated methanol and about 0.3 μ s in methanol. From this weak solvent effect, it is concluded that no solvent is coordinating to the ion. The quenching rate by the solvent for **1R₄**.Nd is $\leq 1 \times 10^6 \text{ s}^{-1}$, caused by the quenching of solvent vibrations in the second coordination sphere. In comparison, the quenching of Bz.Nd, with first sphere solvent molecules, is $\leq 2.3 \times 10^6 \text{ s}^{-1}$.

Table 4.2 Lanthanide luminescent lifetimes of Bz.Ln (Figure 4.3),⁶² in μ s.

Ln^{3+}	CH ₃ OH	CD ₃ OD	$k_{q, solv.}^a$
Yb ³⁺	2.47	10.9	$3.1 \times 10^5 \text{ s}^{-1}$
Nd ³⁺	0.27	0.73	$2.3 \times 10^6 \text{ s}^{-1}$
Er ³⁺	nd	1.53	-

a Determined according to $k_{q, solv} = 1/\tau_{CD_3OD} - 1/\tau_{CH_3OH}$.

The gap between the lowest excited state and the highest ground state of Yb³⁺ ($\sim 10,200 \text{ cm}^{-1}$) is much larger than the gap in Nd³⁺ ($\sim 5,000 \text{ cm}^{-1}$), which makes Yb³⁺ less sensitive to high energy vibrations of the organic environment than Nd³⁺.^{42,43} Furthermore, second-sphere coordination solvents can be more important in the Nd³⁺ complexes, because Nd³⁺ is a larger ion than Yb³⁺ allowing more space for second sphere quenchers. The lifetime of **1H₄**.Er in deuterated methanol is about 0.9 μ s, which is comparable with the Er³⁺ lifetimes in other reports.^{26,62,33,44} The lifetimes of the other complexes could not be determined, due to the low intensity of the collected traces. From these measured lifetimes and the radiative lifetimes of the ions, the quantum yields of lanthanide emission were determined. The radiative lifetimes were

taken from literature,^{13,45} where they were calculated to be $2 \times 10^3 \mu\text{s}$ for Yb^{3+} , and $14 \times 10^3 \mu\text{s}$ for Er^{3+} . The radiative lifetime for Nd^{3+} was estimated to be $250 \mu\text{s}$.⁴⁶ From this it follows that Yb^{3+} has the largest intrinsic quantum yield (5.5×10^{-3}), then Nd^{3+} (1.6×10^{-3}), and Er^{3+} the lowest (6.5×10^{-5}). This significantly lower quantum yield of Er^{3+} was observed previously in organic complexes, and is caused by the efficient quenching by C-H vibrations of the long-lived excited state of erbium⁴⁷ and probably also by inefficient sensitization (*vide infra*).

The efficiency of sensitization (as the product of intersystem crossing and energy transfer) is calculated from $\phi_{\text{SE}}/\phi_{\text{Ln}}$ (Table 4.1). The efficiency of Yb^{3+} sensitization is higher than the efficiency of Nd^{3+} sensitization. Furthermore, fluorescein is a more efficient sensitizer for Nd^{3+} and for Yb^{3+} luminescence than eosin and erythrosin, despite the lower intrinsic intersystem crossing quantum yield of fluorescein. Although the efficiencies for energy transfer could not be calculated for the Er^{3+} complexes, it is clear from the relative quantum yields ($\phi_{\text{SE,rel}}$) that also here fluorescein is a better sensitizer for erbium luminescence than the other two sensitizers.

4.2.3.2 VIS luminescence

Fluorescence and phosphorescence spectra

The excitation, fluorescence, and phosphorescence spectra of **1H₄Gd**, **1Br₄Gd**, and **1I₄Gd** are depicted in Figure 4.7. The excitation spectra of the three dyes are similar to the absorption spectra (shown in Figure 4.7). The maxima of the fluorescence are around 510 nm (**1H₄Gd**), 540 nm (**1Br₄Gd**), and 550 nm (**1I₄Gd**), red shifted by about 10-15 nm (200-400 cm^{-1}) compared to the spectra in water.^{26,48} The fluorescence spectra of all the other complexes **1R₄Ln** and of **6R₄** have the same shape as the **1R₄Gd³⁺** spectra, but they vary in intensities. This shows that the ions do not effect the transitions energetically. Fluorescence lifetimes were determined and are 4.3 ns for **6H₄**, 2.5 ns for **6Br₄**, and 0.4 ns for **6I₄**. The fluorescent lifetimes of the complexes **1R₄Ln** were all shorter than the detector response, i.e. faster than 0.3 ns. Applying the approximation that this is completely due to the enhancement of the intersystem crossing it follows that $k_{\text{ISC}} \approx 1/\tau_{\text{flu,complex}} - 1/\tau_{\text{flu,ligand}}$, thus $k_{\text{ISC}} \geq 3 \times 10^9 \text{ s}^{-1}$. The phosphorescence of **1R₄Gd³⁺** was detected at 77 K in an ethanol-methanol glass, with a delay between excitation and emission.⁴⁹ The peak of the phosphorescence is located at 640 nm for **1H₄Gd** and at 660 for **1Br₄Gd** and **1I₄Gd**, which is also red shifted by about 10-15 nm compared to the phosphorescence of the dyes in water. The lifetimes of the phosphorescence of the **1R₄Gd** complexes at 77 K were determined to be 1.6 ms for **1H₄Gd**, 2.0 ms for **1Br₄Gd**, and 1.5 ms for **1I₄Gd**. Of all the other complexes, phosphorescence was only observed for **1R₄Eu³⁺**. The Gd^{3+}

and the Eu^{3+} complexes exhibit phosphorescence, because there are no energy levels of these ions that can accept energy from the triplet states of the dyes. The absence of phosphorescence in the other complexes is due to energy transfer from the triplet states to the Nd^{3+} , Yb^{3+} , and Er^{3+} ions.

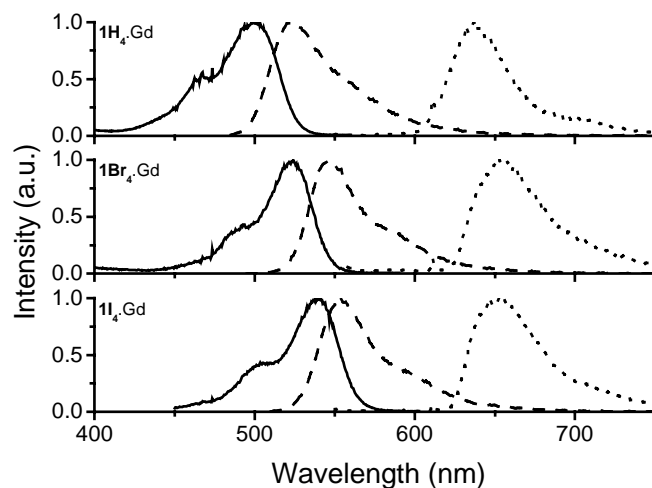


Figure 4.7 Excitation (solid), fluorescence (dashed, in CH_3OH), and phosphorescence (dotted) spectra of $1\mathbf{R}_4.\text{Gd}$. The phosphorescence was measured at 77K in MeOH/EtOH (1:4) glass with a delay between excitation and emission to distinguish it from fluorescence.

Quantum yield of dye fluorescence

Fluorescence quantum yields of the sensitizers were determined for the NIR emitting lanthanide complexes and $6\mathbf{R}_4$ and they are presented in Table 4.3. These *tert*-butyl protected compounds were used as representative of the inherent dye fluorescence. The fluorescence of fluorescein is reduced from about 85% in $6\mathbf{H}_4$ to 1-5% in the complexes. The same behavior is found for the eosin ($6\mathbf{Br}_4$) and erythrosin ($6\mathbf{I}_4$) compounds, albeit to a smaller extent. The decrease in fluorescence upon complexation are from 76% in $6\mathbf{Br}_4$ to 2.6% in $1\mathbf{Br}_4.\text{Nd}$, 30% in $1\mathbf{Br}_4.\text{Yb}$, and 20% in $1\mathbf{Br}_4.\text{Er}$ and from 8.4% in $6\mathbf{I}_4$ to 7.4% in $1\mathbf{I}_4.\text{Yb}$, 1.2% in $1\mathbf{I}_4.\text{Nd}$, and 5.6% in $1\mathbf{I}_4.\text{Er}$. The decrease in the fluorescence of the dyes is due to the enhancement in intersystem crossing, caused by the nearby paramagnetic lanthanide ions.^{5,27,50} This conclusion is further corroborated by the fact that the dye fluorescence is reduced to the same extent in the Gd^{3+} and the Eu^{3+} complex and because of the presence of phosphorescence in these complexes. The Gd^{3+} and Eu^{3+} ions cannot accept energy from both the singlet and triplet excited states of the dyes, because the lowest excited states of the lanthanide ions are too high in energy. The small

differences in the fluorescence quantum yields with varying lanthanide ion can be explained by variation in atomic weight and magnetic moment of the ions.^{50,51} Although the fluorescence in the **1R₄**.Nd complexes is quenched almost completely, the **1H₄**.Yb and **1H₄**.Er complexes are quenched more strongly than **1Br₄**.Yb, **1Br₄**.Er, **1I₄**.Yb, and **1I₄**.Er. This difference is of importance in the sensitization efficiency as discussed below.

Table 4.3 Fluorescence quantum yields of the lanthanide complexes (in %).^a

R	6R₄	1R₄ .Gd	1R₄ .Yb	1R₄ .Nd	1R₄ .Er	1R₄ .Eu
H	83	8.8	6.8	0.3	2.6	1.4
Br	76	33	30	2.6	20	23
I	8.4	6.3	7.4	1.2	5.6	4.3

a The fluorescence quantum yields were determined in methanol with Ru(bpy)₃ in deoxygenated water as a standard.

Energy transfer

In order to get insight in the lifetime of the triplet state, a triplet quencher was added to the solutions, i.e. ferrocene, which resulted in quenching of the lanthanide ion luminescence. This quenching was plotted in a Stern-Volmer plot (not shown) and a triplet lifetime of 10⁸ s⁻¹ was found.

Temperature-dependent measurements were performed on **1H₄**.Nd and **1Br₄**.Nd to determine the presence of a possible thermally activated energy-back transfer process. In the **1H₄**.Nd complex, the luminescence *decreased* about 40% going from 0° C to 50° C. The **1Br₄**.Nd also showed a *decrease* in intensity as well, about 20% going from 15° C to 45° C. The slope in a plot of ln(I₀/I) versus 1/T is the energy gap (ΔE/k) between the donor state (from Nd³⁺) and the acceptor state (the triplet state of the dyes) because I₀/I ~ k_{BT} = Ae^(-ΔE/kT) with I₀/I the reciprocal of the normalized luminescence intensity, k_{BT} the back transfer rate, A a constant, ΔE the energy gap (in J), k the Boltzmann constant, and T the absolute temperature.⁵² The slopes (Figure 4.8) correspond to an energy gap of 700 cm⁻¹ in the **1H₄**.Nd complex and 400 cm⁻¹ in the **1Br₄**.Nd complex. This difference between the two complexes (i.e. 300 cm⁻¹) is about the same as the difference in the position of the phosphorescence maxima, which shows that the main accepting level of Nd³⁺ is the same for both complexes. The absolute rate of the back-transfer (k_{BT}) at 50° C must be of the same order of magnitude as the energy transfer rate from the dye to the lanthanide ion (k_{BT} ~ k_{ET}), because there is a relative strong effect. Furthermore, it must be

competitive with the internal conversion to the emissive excited state of Nd^{3+} (${}^4\text{F}_{3/2}$), because if one of the processes was dominating no energy back-transfer should be observed ($k_{\text{BT}} \ll k_{\text{ic}}$, where k_{ic} is the internal conversion rate) or no Nd^{3+} luminescence ($k_{\text{BT}} \gg k_{\text{ic}}$). In organic complexes, no information on the internal conversion rate is available. In inorganic matrices luminescence from higher excited states to the ground state of Nd^{3+} was detected, and it was found that these emissive rates vary between 10 ns to the picosecond region,⁵³ which supports the estimate of the lower limit for energy transfer in this work ($k_{\text{ic}} \sim k_{\text{BT}} \sim k_{\text{ET}}$). A plot of the natural logarithm of the energy-transfer efficiencies (at 20° C, $\phi_{\text{ISC}} \times \eta_{\text{ET}}$, Table 4.1 ($\phi_{\text{ISC}} \approx 1$)) versus the energy gap⁵⁴ gives a lower estimate of the energy gap to prevent energy back-transfer. This lower limit of the energy gap is about $1,300 \text{ cm}^{-1}$, a value comparable to that found in Eu^{3+} and Tb^{3+} complexes.²⁰

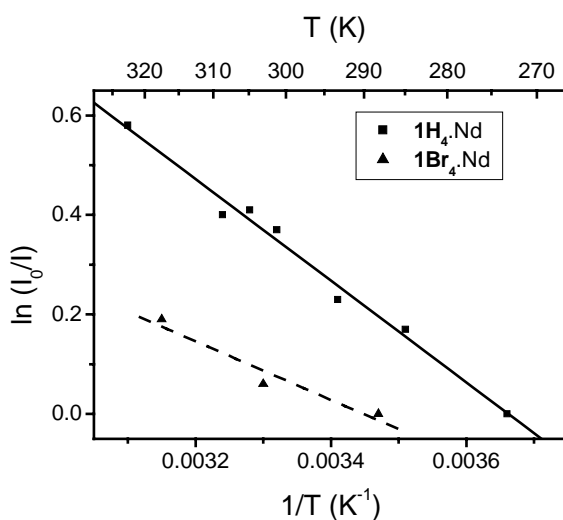


Figure 4.8 Plot of $\ln(I_0/I)$ versus $(1/T)$ of the NIR luminescence of $1\text{H}_4.\text{Nd}$ and $1\text{Br}_4.\text{Nd}$, with I the integrated emission intensity of the ${}^4\text{F}_{3/2} \rightarrow {}^4\text{I}_{11/2}$ transition around 1066 nm and excitation at 505 nm ($1\text{H}_4.\text{Nd}$) or 530 nm ($1\text{Br}_4.\text{Nd}$) in CD_3OD .

The efficiencies of energy transfer to Er^{3+} were not determined because of the low intensity of the signals. The low intensity observed is due to the efficient quenching of Er^{3+} by the organic environment (as discussed above) and to inefficient energy transfer as well, which will be treated in the discussion of the energy transfer processes below. Fluorescein acts as a better sensitizer for the Yb^{3+} luminescence than eosin and erythrosin. This is due to the stronger decrease in fluorescein fluorescence compared to that in eosin and erythrosin (see Table 4.3).

4.3 Discussion of the energy transfer process

4.3.1 Energy transfer

The most remarkable observation in the luminescence is that fluorescein acts as a better sensitizer for the NIR luminescence than eosin and erythrosin, despite the lower intrinsic ISC of fluorescein. One of the reasons is that the intersystem crossing of the dyes is greatly enhanced upon complexation of a heavy and paramagnetic lanthanide ion. Due to this enhancement, the phosphorescent properties of the three sensitizers are about the same: the same fluorescence quenching (k_{ISC}) and phosphorescence lifetimes (k_{phos}) in the three Gd^{3+} complexes.

The acceptor levels of the ions are important in determining the energy transfer mechanisms from dye to lanthanide ion. A choice of potential accepting levels can be made based on the energy difference between donor (sensitizer) and acceptor level (Ln^{3+}), which should not be too large for sufficient spectral overlap,²⁰ and on the selection rules for energy transfer. Malta *et al.* performed theoretical analysis of Eu^{3+} and Sm^{3+} luminescence.^{2,55} The selection rules for energy transfer from sensitizer to the $Ln^{3+} (2S+1)\Gamma_J 4f$ levels are $|\Delta J| = 2, 4, 6$ for the dipolar and multipolar energy transfer (Förster type) and $|\Delta J| = 0, 1$ (but forbidden for $J = J' = 0$) for the electron exchange mechanism (Dexter type). It should be noted that these rules are (somewhat) relaxed by mixing or ‘stealing’ from allowed transitions (e.g. 4f-5d transitions).⁵⁶ In this work, energy transfer takes place from the triplet excited state, because the singlet state of the dyes are depopulated very fast to the triplet state and the Dexter type of transfer is in general the dominant mechanism.^{2,55}

4.3.2 Nd^{3+} sensitization

Applying these considerations to fluorescein, eosin, and erythrosin and Nd^{3+} , the levels that are expected to accept energy are the ${}^4F_{7/2}$ (at $13,400\text{ cm}^{-1}$) and ${}^4F_{9/2}$ (at $15,000\text{ cm}^{-1}$) for all three dyes (Figure 4.1).⁵⁷ In combination with the information obtained from the temperature-dependent measurements, it is concluded that the ${}^4F_{9/2}$ state is the main channel for energy transfer. The unlikeness of the ${}^4F_{7/2}$ level as acceptor level can be illustrated with a calculation of the spectral overlap of the Nd^{3+} absorption and the phosphorescence spectra of the sensitizers (Figure 4.9). The spectral overlap (J) of the dye phosphorescence and the absorption of Nd^{3+} (see Figure 4.9) of the ${}^4F_{7/2}$ and the ${}^4F_{9/2}$ is calculated according to $J = \int \epsilon(\lambda)F(\lambda)d\lambda$,³¹ with the absorption of each accepting transition ($\int \epsilon(\lambda)d\lambda$) and the phosphorescence ($\int F(\lambda)d\lambda$) normalized to 1. This calculation shows that the spectral overlap of the dyes is about 10 times higher with the ${}^4F_{9/2}$ transition than the spectral overlap with the ${}^4F_{7/2}$ transition. It should be noted that for

both transitions (${}^4F_{9/2}$ and ${}^4F_{7/2}$) the spectral overlap with fluorescein is a factor 2 smaller than with eosin and erythrosin. However, the energy back-transfer is more efficient in the case of eosin and erythrosin because of the smaller energy gap between the triplet state and the Nd^{3+} excited state than in the case of the fluorescein Nd^{3+} complex. Thus, the main energy accepting level of Nd^{3+} from the triplet states of fluorescein, eosin, and erythrosin is the ${}^4F_{9/2}$ level. For efficient sensitization it was calculated that the triplet state of the sensitizer should at least be $1,300\text{ cm}^{-1}$ above this receiving level.

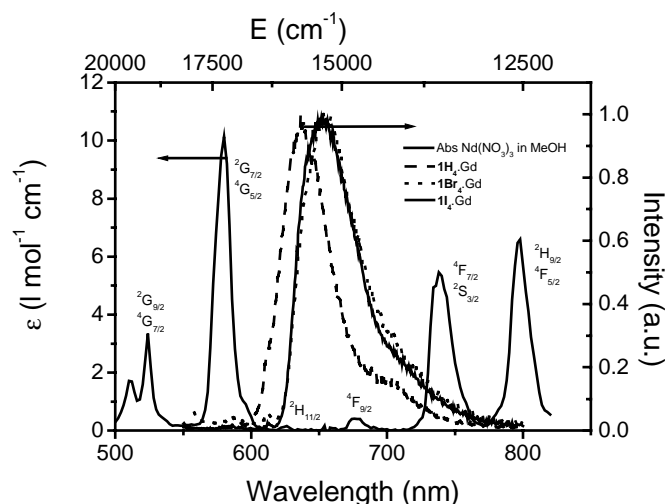


Figure 4.9 The phosphorescence spectra of $1\mathbf{R}_4\text{Gd}$ at 77 K in a MeOH/EtOH (1:4) glass and part of the absorption spectrum of a 0.2 M $\text{Nd}(\text{NO}_3)_3$ solution in MeOH.

4.3.3 The rate constants of Nd^{3+} sensitization by fluorescein

All rate constants and efficiencies of the sensitization of Nd^{3+} by fluorescein (in the $1\mathbf{H}_4\text{Nd}$ complex) are summarized in the Jablonski diagram in Figure 4.10. After excitation, the singlet level is depopulated very fast to the triplet state. From this triplet state, the energy is transferred to the ${}^4F_{9/2}$ level of Nd^{3+} . This level deactivates non-radiatively to the emissive ${}^4F_{3/2}$ level (internal conversion) or by energy-back transfer to the fluorescein triplet state. From the ${}^4F_{3/2}$ level, the neodymium luminescence is observed at 890, 1066, and 1330 nm.

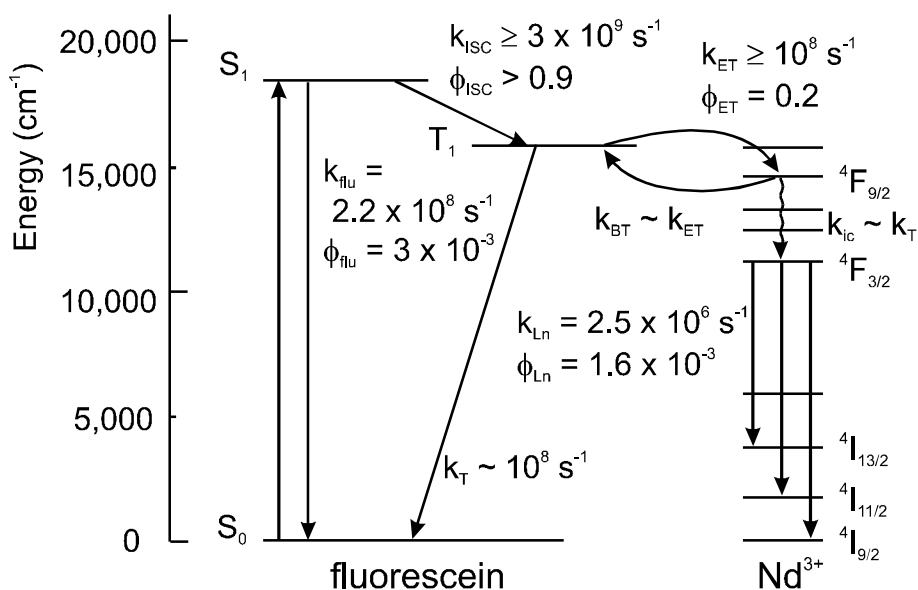


Figure 4.10 Jablonski diagram of the sensitization of Nd^{3+} by fluorescein ($1\text{H}_4\text{Nd}$), with the rate constants and efficiencies of the various transitions.

4.3.4 Er^{3+} and Yb^{3+} sensitization

Applying the same selection rules to the sensitization of Er^{3+} , only one level can be assigned that allows for excitation via an exchange mechanism, i.e. the $^4\text{I}_{13/2}$ at $6,500\text{ cm}^{-1}$. This implies that the energy gap between the triplets of the sensitizers and the accepting level is very large, which would result in a very small k_{ET} . Additional pathways, due to relaxation of the selection rules may be the reason for sensitization of this ion. An additional pathway in the case of fluorescein sensitization may be one of the reasons of the more efficient sensitization of Er^{3+} by fluorescein. The $^4\text{F}_{9/2}$ level of Er^{3+} (at $15,500\text{ cm}^{-1}$) could be an additional pathway in the fluorescein complex. Moreover, the decrease in fluorescence of fluorescein is stronger than in the eosin and erythrosin fluorescence deactivation (Table 4.3), which is a second reason for the higher sensitization efficiency by fluorescein.

For Yb^{3+} , fluorescein is found to be a more efficient sensitizer as well. The difference in sensitization of fluorescein compared to the other dyes is somewhat smaller than in the Nd^{3+} and Er^{3+} complexes. The fluorescence of eosin and erythrosin is less quenched than the fluorescence of fluorescein in $1\text{R}_4\text{Yb}$ (Table 4.3). The receiving energy level of Yb^{3+} can only be the $^2\text{F}_{5/2}$ at $10,200\text{ cm}^{-1}$, as this is the only excited state of this ion. A Dexter type mechanism to this level is allowed by the selection rules, because $|\Delta J| = 1$. The energy gap between the triplet states of the sensitizers and this receiving level is about $4,000\text{ cm}^{-1}$, a gap that is not too large for energy transfer but is too large for energy back transfer. A photon-induced electron transfer⁵⁸ might be a pathway in the sensitization process, because Yb^{3+} is easily reduced to Yb^{2+} . However, this is not

likely here because there is no different quenching effect on the fluorescence of the dyes in the Yb^{3+} complexes compared to other complexes (see above under fluorescence quantum yields and Table 4.3). Furthermore, the calculated driving force for charge transfer, according to Rehm and Weller,⁵⁹ is very small: -0.18 eV for transfer from the singlet excited state of fluorescein.⁶⁰ An additional argument is that in the Eu^{3+} complex, which is reduced more easily than Yb^{3+} ,⁶¹ phosphorescence is observed. This leads to the conclusion that in the current work the sensitization of Yb^{3+} occurs by a Dexter mechanism from the triplet excited state of the dyes.

4.3.5 Final considerations

In the work by Werts *et al.*²⁶ eosin was found a better sensitizer for the NIR emissive lanthanide ions than fluorescein. However, they also found a strong molecular oxygen effect on the sensitization of the NIR emitting ions, which is indicative for slow energy transfer. This oxygen effect was not found for the $\mathbf{1R}_4\text{Ln}$ complexes. The slow energy transfer means that the distance between dye and ion is much larger than in the current complexes. The implication is that the ISC is not enhanced as strongly as in the current work. Therefore, the sensitization efficiency ($\phi_{\text{ISC}} \times \eta_{\text{ET}}$) in Werts' work²⁶ is determined by both the intrinsic ISC quantum yields of the dyes and the energy transfer (ϕ_{ISC} and η_{ET}), whereas the transfer in the $\mathbf{1R}_4\text{Ln}$ complexes is determined entirely by the energy-transfer (η_{ET}). This leads to overall quantum yields determined by energy transfer mechanisms and not by the intrinsic intersystem crossing quantum yield. In the $\mathbf{1R}_4\text{Nd}$ complexes it was found that the energy gap between the triplet states of the sensitizers and the accepting state of Nd^{3+} was too small. For efficient energy-transfer, a gap of at least $1,300\text{ cm}^{-1}$ is necessary.

4.4 Conclusions

NIR emitting lanthanide complexes were designed and synthesized that bring the sensitizer in close proximity to the ion and that shield the ion completely from the solvent. The sensitizers coupled to lanthanide complexes are fluorescein, eosin, and erythrosin, which enable visible light (green) sensitization of the NIR lanthanide emission. The fluorescence of the sensitizers was strongly reduced, due to the enhancement in intersystem crossing by the nearby paramagnetic lanthanide ions. The sensitization of the NIR emitting ions is solely determined by the energy transfer step, because of the enhanced intersystem crossing quantum yields. Surprisingly, the efficiency of sensitization was found the highest for the fluorescein complexes $\mathbf{1H}_4\text{Ln}$. In the $\mathbf{1R}_4\text{Nd}$ complexes it was found that the main channel for energy transfer is the $^4\text{F}_{9/2}$ Nd^{3+} level.

Fluorescein is a more efficient sensitizers than eosin or erythrosin, because of the larger gap between the triplet of fluorescein with this receiving Nd^{3+} level which leads to less energy back transfer. An energy gap of at least $1,300\text{ cm}^{-1}$ is necessary to prevent energy back transfer. In the Yb^{3+} complexes, the more efficient excitation is most likely due to the less efficient enhancement of the intersystem crossing of eosin and erythrosin. The reason of the more efficient sensitization by fluorescein in the Er^{3+} complexes is that an additional level of Er^{3+} is probably capable of accepting energy from fluorescein but not from eosin or erythrosin. As long as these sensitizers, and especially fluorescein, are in close proximity ($< 6\text{ \AA}$) of the energy accepting ions, the energy transfer is determined by the energy levels involved.

4.5 Experimental

General

Ethanol, methanol, acetone, and toluene were purchased from Merck (*pro analysis* quality) and used as received. Dichloromethane and hexane were freshly distilled from CaCl_2 , ethyl acetate was distilled from K_2CO_3 . These solvents were stored over molecular sieves (4 \AA , Merck). Deuterated solvents, d_4 -methanol, d_1 -chloroform, and d_6 -dimethylsulfoxide were purchased from Merck. Trifluoroacetic acid (TFA), triethylamine (TEA), phthalic anhydride, oxalylic chloride, and hydrazine monohydrate were purchased from Aldrich. The monoamine **2** was synthesized as published previously.⁶² Purifications were carried out with silica gel 60 (Merck, size 0.040-0.063 mm, 230-400 mesh), Sephadex LH20 (Sigma, size 0.025-0.100 mm), or by preparative thin layer chromatography (silica gel 60, Merck). The lanthanide(III) nitrate salts were the penta- or hexahydrate forms, from Aldrich or Acros, 99.999% purity and more, used as received. Fluorescein, eosin, and erythrosin isothiocyanates were purchased from Molecular Probes, Leiden, the Netherlands, and were used as received. Melting points were determined with a Reichert melting point apparatus and are uncorrected. Mass spectra were recorded on a Finnigan MAT 90 spectrometer using *m*-NBA (nitrobenzyl alcohol) or Magic Bullet (MB, which is a mixture of dithioerythritol and dithiothreitol, 1:5 (by wt.)) as a matrix. The prepared lanthanide complexes were injected as methanol solution in a Micromass Electrospray ionization Time-of-Flight (ESI-TOF) mass spectrometer. IR spectra were recorded with a Perkin Elmer Spectrum BX FT-IR System using KBr pellets as matrix. Elemental analyses were performed on a Carlo Erba EA 1106 apparatus. ^1H NMR and ^{13}C NMR spectra were recorded with a Varian INOVA (300 MHz) or a Varian Unity 400 WB spectrometer with CDCl_3 or CD_3OD as solvents. Residual CHCl_3 ($\delta_{1\text{H}} = 7.26\text{ ppm}$) and CDCl_3 ($\delta_{13\text{C}} = 77.0\text{ ppm}$) or CHD_2OD ($\delta_{1\text{H}} = 3.30\text{ ppm}$) and CD_3OD ($\delta_{13\text{C}} = 49.0\text{ ppm}$) were used as the internal standards, respectively. In the assignment of the proton NMR the superscripts ‘phth’ for phthalimide protons, ‘terph’ for protons on the terphenyl moiety, ‘sens’ for protons belonging to the sensitizer groups (the dyes), and ‘tail’ for protons on both the butoxy propoxy moieties and the β -alanine moiety were used.

Compound 3: 10.0 g (0.11 mol) of β -alanine was heated with 16.6 g (0.11 mol) of phthalic anhydride at 150 °C for 1 hr with an open flask to evaporate the formed water. After cooling down, the remaining solid was stirred in water, and the formed powder was collected by filtration. Yield: 22.5 g, 93%, Mp: 148-151 °C. ^1H NMR (CDCl_3): δ 9.08 (s, 1H, CO_2H), 7.89-7.86 (m, 2H, ArH^{phth}), 7.76-7.73 (m, 2H, ArH^{phth}), 4.02 (t, $J = 7.1$ Hz, 2H, $\text{NCH}_2\text{CH}_2\text{CO}_2$), 2.82 (t, $J = 7.1$ Hz, 2H, $\text{NCH}_2\text{CH}_2\text{CO}_2$). ^{13}C NMR (CDCl_3): δ 175.9, 167.5, 133.6, 131.4, 122.9, 32.9, 32.0. MS (FAB, NBA): m/z 220.1 $[(\text{M}+\text{H})^+]$, calcd for $\text{C}_{11}\text{H}_{10}\text{NO}_4$: 220.0]. IR (KBr): ν 1769.4 ($\text{C}=\text{O}^{\text{acid}}$), 1721.0 ($\text{C}=\text{O}^{\text{phth}}$), 1706.8 ($\text{C}=\text{O}^{\text{phth}}$), 1690.8 ($\text{C}=\text{O}^{\text{phth}}$) cm^{-1} . Anal. Calcd. for $\text{C}_{11}\text{H}_9\text{NO}_4$: C, 60.28; H, 4.14; N, 6.39. Found: C, 60.21; H, 4.05; N, 6.38.

Compound 4: Compound **3** was first converted into the acid chloride by stirring 0.28 g (1.3 mmol) of the acid with 10 ml of oxalyl chloride at room temperature for one hour. After removal of the excess of the oxalyl chloride under vacuum, the acid chloride was dissolved in 20 ml CH_2Cl_2 and added to a solution of 0.68 g (0.64 mmol) monoamine **2** and 0.13 g (1.3 mmol) TEA in 100 ml CH_2Cl_2 . After stirring for one night under argon atmosphere, the solution was diluted with CH_2Cl_2 , washed twice with 1 N HCl, once with water, dried over MgSO_4 . After removal of the salts the organic solvent was evaporated under vacuo. The crude product was purified by column chromatography with silica as the stationary state and hexane/EtOAc 1:1 as the eluent. Yield: 0.5 g (62%) of an off-white solid, Mp 47-49 °C. ^1H NMR (CDCl_3): δ 7.89-7.81 (m, 2H, ArH^{phth}), 7.75-7.68 (m, 2H, ArH^{phth}), 7.47-7.35 (m, 5H, ArH), 7.14-6.83 (m, 6H, $\text{ArH}^{\text{terph}}$), 5.02-4.77 (m, 4H, ArCH_2N), 4.17-3.89 (m, 6H, $\text{ArOCH}_2\text{CO}_2$), 3.68-3.22 (m, 12H, $\text{CH}_2^{\text{tail}}$), 2.96-2.82 (m, 2H, $\text{CH}_2^{\text{tail}}$), 2.34 (s, 6H, ArCH_3), 2.29 (s, 3H, ArCH_3), 2.07-1.87 (m, 2H, $\text{CH}_2^{\text{tail}}$), 1.63-1.47 (m, 2H $\text{CH}_2^{\text{tail}}$), 1.45-1.21 (m, 36H, $\text{C}(\text{CH}_3)_3$, $\text{CH}_2^{\text{tail}}$), 0.94-0.77 (m, 6H, $\text{CH}_3^{\text{tail}}$). ^{13}C NMR (CDCl_3): δ 169.7, 168.3, 167.8, 165.5, 165.4, 164.5, 149.8, 148.8, 131.2-120.5 (m, ArC), 79.0, 78.4, 68.2, 68.1, 67.8, 68.1, 67.7, 67.2, 67.1, 66.0, 64.8, 44.6, 41.7, 41.4, 39.8, 32.1, 31.9, 29.2, 28.9, 28.8, 26.0, 25.4, 25.4 25.3, 25.2, 18.4, 18.3, 18.0, 16.7, 11.3, 11.2. MS (FAB, NBA): m/z 1254.9 $[(\text{M}+\text{H})^+]$, calcd for $\text{C}_{73}\text{H}_{96}\text{N}_3\text{O}_{15}$: 1254.7]; 1276.9 $[(\text{M}+\text{Na})^+]$, calcd for $\text{C}_{73}\text{H}_{95}\text{N}_3\text{O}_{15}\text{Na}$: 1276.7]. IR (KBr): ν 1753.0 ($\text{C}=\text{O}^{\text{ester}}$), 1717.9 ($\text{C}=\text{O}^{\text{phth}}$), 1640.2 ($\text{C}=\text{O}^{\text{amide}}$) cm^{-1} . Anal. Calcd. for $\text{C}_{73}\text{H}_{95}\text{N}_3\text{O}_{15}$: C, 69.89; H, 7.63; N, 3.35. Found: C, 69.67; H, 7.73; N, 3.34.

Compound 5: Compound **4** was converted into the amine **5** by refluxing 0.40 g (0.32 mmol) **4** with 40 equivalents (0.64 ml) hydrazine monohydrate in 50 ml ethanol for 1 hour under argon atmosphere. After cooling down to room temperature and removal of the ethanol under vacuo, the residue was dissolved in 100 ml of CH_2Cl_2 and was washed twice with 1 N KOH and once with water. After drying over MgSO_4 the solvent was removed under vacuo. The amine **5** was obtained in quantitative yield (0.36 g, 99%) as a colorless oil and was immediately used in the following reaction. ^1H NMR (CDCl_3): δ 7.48-7.35 (m, 5H, ArH), 7.19-6.83 (m, 6H, $\text{ArH}^{\text{terph}}$), 5.03-4.78 (m, 4H, ArCH_2N), 4.16-3.93 (m, 6H, $\text{ArOCH}_2\text{CO}_2$), 3.66-3.38 (m, 12H, $\text{CH}_2^{\text{tail}}$), 3.27-3.22 (m, 4H, $\text{CH}_2^{\text{tail}}$), 3.12-2.98 (m, 2H, $\text{CH}_2^{\text{tail}}$), 2.68-2.50 (m, 4H, $\text{CH}_2^{\text{tail}}$), 2.35-2.29 (m, 9H, ArCH_3), 2.06-1.87 (m, 2H, $\text{CH}_2^{\text{tail}}$), 1.62-1.51 (m, 4H, $\text{CH}_2^{\text{tail}}$), 1.41-1.25 (m, 29H, $\text{C}(\text{CH}_3)_3$, $\text{CH}_2^{\text{tail}}$), 0.96-0.87 (m, 6H, $\text{CH}_3^{\text{tail}}$). ^{13}C NMR (CDCl_3): δ 172.3, 171.7, 167.7, 167.5, 167.4,

166.7, 166.6, 151.8, 151.3, 150.8, 136.2-125.7, 81.1, 81.0, 80.9, 80.4, 70.2, 70.1, 69.9, 69.7, 69.2, 68.0, 67.1, 66.9, 52.9, 47.9, 46.5, 45.8, 43.8, 43.5, 42.6, 42.0, 41.8, 37.8, 36.0, 35.4, 31.2, 28.1, 27.5, 27.3, 27.0, 20.4, 20.1, 18.7, 13.4. IR (KBr): ν 1754.9 (C=O^{ester}), 1644.4 (C=O^{amide}) cm⁻¹. MS (FAB, NBA): m/z 1124.9 [(M+H)⁺, calcd for C₆₅H₉₄N₃O₁₃: 1124.7].

General procedure for the coupling of the isothiocyanate functionalised dyes to 5: Amine **5** was dissolved in CH₂Cl₂, together with 5 eq. TEA. To this solution, a solution of the dye (1.1 eq) was added. The mixture was left stirring overnight under argon atmosphere and exclusion of light. The solution was diluted and washed with 5% KHSO₄ solution and once with water. The solvents were removed under vacuo after filtration. First the salts and excess of dye was removed by column chromatography with sephadex LH20 and MeOH/ CH₂Cl₂ as eluent. Further purification was performed with preparative TLC with 15% MeOH in CH₂Cl₂ as eluent.

Compound 6H₄: This reaction was performed according the general procedure for the coupling of the dyes with 50 mg (0.044 mmol) amine **5** and 21 mg (0.052 mmol) fluorescein isothiocyanate. Yield: 41 mg (60%) of a yellow ($\epsilon_{498 \text{ nm}}$ (MeOH) = 90,900 l×mol⁻¹×cm⁻¹) solid, Mp: 139-141 °C. ¹H NMR (CD₃OD): δ 8.07 (s, 1H, ArH^{sens}), 7.78-7.69 (m, 1H, ArH^{sens}), 7.45-7.42 (m, 5H, ArH), 7.19-7.01 (m, 6H, ArH), 6.94 (s, 1H, ArH^{sens}), 6.84-6.81 (m, 2H, ArH^{sens}), 6.67-6.66 (m, 2H, ArH^{sens}), 6.58-6.54 (m, 2H, ArH^{sens}), 4.95-4.57 (m, 4H, ArCH₂N), 4.18-3.83 (m, 6H, ArOCH₂CO₂), 3.65-3.20 (m, 14H, CH₂^{tail}), 2.95-2.88 (m, 2H, CH₂^{tail}), 2.34-2.27 (m, 9H, ArCH₃), 1.94-1.81 (m, 4H, CH₂^{tail}), 1.59-1.45 (m, 4H, CH₂^{tail}), 1.45-1.21 (m, 31H, C(CH₃)₃, CH₂^{tail}), 0.93-0.82 (m, 6H, CH₃^{tail}). ¹³C NMR (CD₃OD): δ 180.5, 174.3, 172.6, 172.4, 172.2, 171.2, 169.6, 168.0, 167.6, 153.7, 151.4, 140.1, 135.8, 133.3-125.5, 119.5, 114.2, 110.9, 101.7, 81.3, 69.9, 69.7, 69.5, 69.4, 69.2, 68.9, 68.8, 68.6, 68.0, 67.9, 66.7, 42.2, 39.7, 31.0, 27.7, 27.6, 27.0, 26.4, 12.4. MS (FAB, NBA): m/z 1513.9 [(M+H)⁺, calcd for C₈₆H₁₀₅N₄O₁₈S: 1513.7], 1535.9 [(M+Na)⁺, calcd for C₈₆H₁₀₄N₄O₁₈SNa: 1535.7]. IR (KBr): ν 1749.9 (C=O^{ester}), 1615.0 (C=O^{amide}) cm⁻¹.

Compound 6Br₄: The general procedure was applied to synthesize this compound with 360 mg (0.32 mmol) amine, 340 mg (0.48 mmol) eosin isothiocyanate, and 160 mg (1.6 mmol) TEA in 50 ml CH₂Cl₂. Yield: 410 mg (70%) of a strongly red colored ($\epsilon_{525 \text{ nm}}$ (MeOH) = 82,000 l×mol⁻¹×cm⁻¹) solid. Mp: 190-193°C. ¹H NMR (CD₃OD): δ 8.29 (s, 2H, ArH^{sens}), 7.96 (d, J = 8.0 Hz, 1H, ArH^{sens}), 7.86 (d, J = 8.0 Hz, 1H, ArH^{sens}), 7.43-6.94 (m, 12H, ArH, ArH^{sens}), 4.90-4.72 (m, 4H, ArCH₂N), 4.18-3.87 (m, 6H, ArOCH₂CO₂), 3.54-3.35 (m, 8H, CH₂^{tail}), 3.30-3.19 (m, 4H, CH₂^{tail}), 3.00-2.85 (m, 4H, CH₂^{tail}), 2.33-2.28 (m, 9H, ArCH₃), 1.92-1.78 (m, 4H, CH₂^{tail}), 1.55-1.47 (m, 2H, CH₂^{tail}), 1.39-1.22 (m, 29H, C(CH₃)₃, CH₂^{tail}), 0.91-0.80 (m, 6H, CH₃^{tail}). ¹³C NMR (CD₃OD): δ 180.4, 175.8, 172.4, 168.2, 167.6, 161.3, 153.0, 151.3, 150.4, 140.5, 135.7, 133.6-125.7, 117.3, 111.4, 99.2, 96.8, 81.5, 69.9, 69.8, 69.5, 67.6, 66.7, 42.2, 39.7, 31.0, 27.8, 27.0, 26.6, 26.5, 19.1, 19.0, 18.5, 12.5, 12.4. MS (FAB, NBA): m/z 1825.4 [(M+H)⁺, calcd for C₈₆H₁₀₁⁷⁹Br₄N₄O₁₈S: 1825.4]. IR (KBr): ν 1733.2 (C=O^{ester}), 1620.2 (C=O^{amide}) cm⁻¹.

Compound 6I₄: The standard procedure for the coupling of isothiocyanates and amines was carried out with 42 mg (4.2×10⁻⁵ mol) amine, 25 mg (2.8×10⁻⁵ mol) erythrosin isothiocyanate and 20 μ l TEA in 25

ml of CH_2Cl_2 . Yield: 45 mg (63%) of a red ($\epsilon_{532 \text{ nm}}(\text{MeOH}) = 55,000 \text{ l}\times\text{mol}^{-1}\times\text{cm}^{-1}$) solid, Mp: 176-178 °C. ^1H NMR (CD_3OD): δ 8.28 (s, 2H, ArH^{sens}), 8.00 (d, $J = 8.4$ Hz, 1H, ArH^{sens}), 7.80 (s, 1H, ArH^{sens}), 7.60-6.90 (m, 12H, ArH , ArH^{sens}), 4.90-4.78 (m, 4H, ArCH_2N), 4.20-3.82 (m, 6H, $\text{ArOCH}_2\text{CO}_2$), 3.61-3.05 (m, 12H, $\text{CH}_2^{\text{tail}}$), 3.00-2.80 (m, 4H, $\text{CH}_2^{\text{tail}}$), 2.40-2.23 (m, 9H, ArCH_3), 1.96-1.78 (m, 4H, $\text{CH}_2^{\text{tail}}$), 1.65-1.47 (m, 2H, $\text{CH}_2^{\text{tail}}$), 1.40-1.16 (m, 29H, $\text{C}(\text{CH}_3)_3$, $\text{CH}_2^{\text{tail}}$), 0.95-0.75 (m, 6H, $\text{CH}_3^{\text{tail}}$). ^{13}C NMR (CD_3OD): δ 171.8, 167.4, 166.8, 156.8, 150.5, 148.7, 136.9, 136.5, 135.0, 133.0-125.0 (m, ArC), 112.8, 112.4, 112.3, 80.8, 80.6, 80.4, 80.2, 73.3, 73.1, 69.3, 69.1, 68.9, 68.7, 68.5, 68.2, 67.9, 66.9, 66.8, 66.0, 30.4, 30.3, 30.2, 28.1, 27.8, 27.0, 26.9, 21.1, 18.4, 18.3, 17.8, 17.7, 11.8, 11.7. MS (FAB, NBA): m/z 2040.4 $[(\text{M}+\text{Na})^+]$, calcd for $\text{C}_{86}\text{H}_{100}\text{N}_4\text{O}_{18}\text{Si}_4\text{Na}$: 2039.3]. IR (KBr): ν 1756.6 ($\text{C}=\text{O}^{\text{ester}}$), 1633.7 ($\text{C}=\text{O}^{\text{amide}}$) cm^{-1} .

General procedure of the hydrolysis of the *tert*-butyl The dye functionalised terphenyl **6R₄** was dissolved in 15 ml of dry TFA and stirred under Ar atmosphere for 1 hr. After removal of the TFA by repeated azeotropic distillation with three times 25 ml toluene the tricarboxylic acid **1R₄.H₃** was purified with preparative thin layer chromatography and obtained in high yield.

Compound 1H₄.H₃: According to the general procedure for the deprotection of the *tert*-butyl ester with 90 mg **6H₄**. Yield: 85% of a yellow/orange solid ($\epsilon_{496 \text{ nm}}(\text{MeOH}) = 77,300 \text{ l}\times\text{mol}^{-1}\times\text{cm}^{-1}$), Mp: 122-125 °C. This compound showed only one single spot, $r_F = 0.35$, on TLC (silica gel) with 15% methanol in CH_2Cl_2 as the eluent. ^1H NMR (CD_3OD): δ 8.11-8.04 (m, 1H, ArH^{sens}), 7.68-7.62 (m, 1H, ArH^{sens}), 7.39-7.30 (m, 5H, ArH), 7.19-6.85 (m, 7H, ArH , ArH^{sens}), 6.61-6.58 (m, 4H, ArH^{sens}), 6.47-6.42 (m, 2H, ArH^{sens}), 4.95-4.57 (m, 4H, ArCH_2N), 4.18-3.83 (m, 6H, $\text{ArOCH}_2\text{CO}_2$), 3.55-3.15 (m, 14H, $\text{CH}_2^{\text{tail}}$), 2.85-2.75 (m, 2H, $\text{CH}_2^{\text{tail}}$), 2.34-2.27 (m, 9H, ArCH_3), 1.94-1.60 (m, 4H, $\text{CH}_2^{\text{tail}}$), 1.51-1.40 (m, 4H, $\text{CH}_2^{\text{tail}}$), 1.31-1.11 (m, 4H, $\text{CH}_2^{\text{tail}}$), 0.93-0.82 (m, 6H, $\text{CH}_3^{\text{tail}}$). ^{13}C NMR (CD_3OD): δ 180.5, 174.7, 172.0, 172.2, 163.8, 163.0, 162.2, 153.7, 142.2, 137.9, 135.5, 133.1-127.8, 115.0, 103.6, 71.9, 71.8, 71.0, 70.9, 70.7, 70.5, 70.3, 69.7, 69.5, 68.8, 68.6, 33.1, 31.7, 29.7, 28.4, 28.0, 27.9, 27.7, 21.1, 20.8, 20.6, 14.4. MS (FAB, NBA): m/z 1370.5 $[(\text{M}+\text{Na})^+]$, calcd for $\text{C}_{74}\text{H}_{80}\text{N}_4\text{O}_{18}\text{S}$: 1370.5]. IR (KBr): ν 1732.8 ($\text{C}=\text{O}^{\text{acid}}$), 1615.2 ($\text{C}=\text{O}^{\text{amide}}$) cm^{-1} .

Compound 1Br₄.H₃: This compound was made according to the general procedure for the deprotection of the *tert*-butyl ester with 120 mg **6Br₄**. Yield: 82% of a red solid ($\epsilon_{522 \text{ nm}}(\text{MeOH}) = 88,800 \text{ l}\times\text{mol}^{-1}\times\text{cm}^{-1}$), Mp: 127-129 °C. Purity was checked with TLC (silica gel, 15% methanol in CH_2Cl_2 as eluent): only one spot was found, $r_F = 0.4$. ^1H NMR (CD_3OD): δ 8.35-8.25 (m, 2H, ArH^{sens}), 7.85-7.78 (m, 2H, ArH^{sens}), 7.41-7.35 (m, 5H, ArH), 7.23-6.90 (m, 7H, ArH , ArH^{sens}), 4.85-4.60 (m, 4H, ArCH_2N), 4.15-3.83 (m, 6H, $\text{ArOCH}_2\text{CO}_2$), 3.60-3.10 (m, 14H, $\text{CH}_2^{\text{tail}}$), 2.85-2.75 (m, 2H, $\text{CH}_2^{\text{tail}}$), 2.40-2.25 (m, 9H, ArCH_3), 2.01-1.75 (m, 4H, $\text{CH}_2^{\text{tail}}$), 1.57-1.11 (m, 8H, $\text{CH}_2^{\text{tail}}$), 0.90-0.78 (m, 6H, $\text{CH}_3^{\text{tail}}$). ^{13}C NMR (CD_3OD): δ 184.9, 176.9, 176.2, 175.5, 175.0, 174.8, 171.8, 155.5, 155.4, 155.2, 154.4, 154.2, 153.8, 140.1, 138.2, 135.2-130.1, 117.1, 103.6, 74.3, 74.2, 74.0, 73.4, 73.0, 72.8, 72.6, 72.0, 71.1, 47.9, 47.5, 47.2, 46.9, 46.8, 44.1, 43.9, 35.4, 35.6, 33.2, 32.1, 31.4, 31.0, 30.4, 23.5, 23.3, 22.8, 16.8, 11.7. MS (FAB, NBA): m/z 1683.2 $[(\text{M}+\text{Na})^+]$, calcd for $\text{C}_{74}\text{H}_{76}^{79}\text{Br}_4\text{N}_4\text{O}_{18}\text{S}_1\text{Na}$: 1684.1]. IR (KBr): ν 1733.1 ($\text{C}=\text{O}^{\text{acid}}$), 1615.6 ($\text{C}=\text{O}^{\text{amide}}$) cm^{-1} .

Compound 1I₄.H₃: Made according the general procedure for the deprotection of the *tert*-butylesters with 55 mg **6I₄**, yielding 35 mg (67%) of a red solid ($\epsilon_{530\text{ nm}}$ (MeOH) = 94,300 l×mol⁻¹×cm⁻¹, mp: 133-136 °C). The purity of this compound was checked with TLC (silicagel, 15% MeOH in CH₂Cl₂): only one spot, r_F = 0.4. ¹H NMR (CD₃OD): δ 8.30-8.20 (m, 2H, ArH^{sens}), 7.80-7.75 (m, 2H, ArH^{sens}), 7.44-6.85 (m, 12H, ArH, ArH^{sens}), 4.85-4.62 (m, 4H, ArCH₂N), 4.21-3.78 (m, 6H, ArOCH₂CO₂), 3.68-3.20 (m, 14H, CH₂^{tail}), 2.85-2.75 (m, 2H, CH₂^{tail}), 2.30-2.18 (m, 9H, ArCH₃), 1.95-1.05 (m, 12H, CH₂^{tail}), 0.85-0.78 (m, 6H, CH₂^{tail}). ¹³C NMR (CD₃OD): δ = 175.2, 174.7, 171.0, 152.4, 152.2, 144.8, 144.6, 140.1, 137.8-125.4, 118.2, 76.5, 76.2, 72.9, 72.7, 72.5, 72.3, 71.9, 71.5, 71.1, 68.8, 68.4, 44.5, 43.6, 33.4, 32.5, 32.2, 30.4, 30.1, 29.8, 29.5, 23.5, 20.8, 20.6, 20.1, 19.9, 16.8, 12.4, 9.5, 8.2. MS (FAB, NBA): m/z 1871.6 [(M+Na)⁺, calcd for C₇₄H₇₆I₄N₄O₁₈S₁Na: 1872.1]. IR (KBr): ν 1733.4 (C=O^{acid}), 1602.3 (C=O^{amide}) cm⁻¹.

Table 4.4 Mass spectrometry data of the **1R₄.Ln** complexes.

Complex	ESI-TOF ^a (m/z)	Calc (m/z)	Fragment	Formula
1H₄.Nd	1486.4	1486.4	(M+H) ⁺	C ₇₄ H ₇₈ N ₄ O ₁₈ SNd
1H₄.Yb	1515.6	1515.4	(M+H) ⁺	C ₇₄ H ₇₈ N ₄ O ₁₈ SYb
1H₄.Er	1510.5	1510.4	(M+H) ⁺	C ₇₄ H ₇₈ N ₄ O ₁₈ SEr
1H₄.Gd	1500.4	1500.4	(M+H) ⁺	C ₇₄ H ₇₈ N ₄ O ₁₈ SGd
1H₄.Eu	1495.2	1495.5	(M+H) ⁺	C ₇₄ H ₇₈ N ₄ O ₁₈ SEu
1Br₄.Nd	1800.1	1801.1	(M+H) ⁺	C ₇₄ H ₇₄ Br ₄ N ₄ O ₁₈ SNd
1Br₄.Yb	1832.3	1832.1	(M+H) ⁺	C ₇₄ H ₇₄ Br ₄ N ₄ O ₁₈ SYb
1Br₄.Er	1826.3	1826.1	(M+H) ⁺	C ₇₄ H ₇₄ Br ₄ N ₄ O ₁₈ SEr
1Br₄.Gd	1816.7	1816.1	(M+H) ⁺	C ₇₄ H ₇₄ Br ₄ N ₄ O ₁₈ SGd
1Br₄.Eu	1811.7	1811.1	(M+H) ⁺	C ₇₄ H ₇₄ Br ₄ N ₄ O ₁₈ SEu
1I₄.Nd	1988.8	1989.0	(M+H) ⁺	C ₇₄ H ₇₄ I ₄ N ₄ O ₁₈ SNd
1I₄.Yb	2018.1	2020.0	(M+H) ⁺	C ₇₄ H ₇₄ I ₄ N ₄ O ₁₈ SYb
1I₄.Er	2014.1	2014.0	(M+H) ⁺	C ₇₄ H ₇₄ I ₄ N ₄ O ₁₈ SEr
1I₄.Gd	2005.5	2005.4	(M+H) ⁺	C ₇₄ H ₇₄ I ₄ N ₄ O ₁₈ SGd
1I₄.Eu	2000.4	2000.0	(M+H) ⁺	C ₇₄ H ₇₄ I ₄ N ₄ O ₁₈ SEu

a Electron Spray Ionization, Time-of-Flight.

General procedure for the synthesis of the lanthanide(III) complexes. The complexes were made in situ, by dissolving one equivalent of free ligand **1R₄.H₃** in methanol. Subsequently, five equivalents of TEA and one equivalent of the appropriate lanthanide(III) nitrate salt were added. See Table 4.4 for details on the characterization of the complexes.

Luminescence:

All measurements, except temperature-dependent measurements, were performed at room temperature or at 77 K, cooled by liquid nitrogen. The temperature dependent measurements were performed in a temperature-controlled cell varying between 0 and 50°C. Absorption spectra were recorded on a HP8452A diode array spectrometer. Emission spectra in the visible and the NIR and decay traces in the visible were measured on an Edinburgh Analytical Instruments FL/FS 900 fluorimeter, equipped with a 450 W Xe lamp as steady state excitation source and nano- and micro-flashlamps for time-resolved experiments. The excitation light was fed to a monochromator (single grating, 1800 lines/mm) and focused on a square quartz cuvette (1.00×1.00 cm²) containing the sample. The emitted visible light was fed to a second monochromator (1800 lines/mm grating) and collected on a Hamamatsu R955 photomultiplier tube. Near-infrared light was fed to the same monochromator, but equipped with a 600 lines/mm grating, and was collected after optical chopping (89 Hz) by an Edinburgh Analytical Instruments liquid nitrogen-cooled ultra-sensitive germanium detector using standard lock-in techniques. All excitation and emission spectra were corrected for the instrumental spectral response. Lifetimes in the nanosecond regime were fitted exponentially with Edinburgh software, implemented on the instrument software, with deconvolution of the decay traces for the instrumental response. This instrumental response was measured on a highly scattering and non-fluorescent sample (Ludox). Lifetimes in the NIR were measured on an Edinburgh Analytical Instruments LP900 system, with a pulsed N₂ laser as the excitation source (0.5 ns pulse of a LTB MSG 400 nitrogen laser, operating at 337.1 nm at 10 Hz, pulse energy: 20 μJ). The emitted signal was collected with a Northcoast liquid nitrogen-cooled germanium detector. The decay traces were averaged by an oscilloscope (Tektronix) and fed to a computer. Fitting of the lifetimes in the microsecond region was performed with Edinburgh Analytical Instruments LP900 software, with deconvolution of the traces using the instrument response measured with IR140 (Aldrich) in methanol ($\tau < 1$ ns, much faster than the detector response, which is about 200 ns). Measurements were performed on solutions with absorption below 0.3 and for quantum yield determinations absorption below 0.15. For quantum yield determinations in the visible region Ru(bpy)₃Cl₂ (Aldrich) in deoxygenated water ($\phi = 0.042$) was used as a standard.⁶³ In the NIR, fluorexon (Molecular Probes, Leiden, The Netherlands) complexes were used (Fx.Ln, see Figure 4.3) as standard.⁶⁴

4.6 References and notes

- ¹ For a review see: Parker, D.; Williams, J. A. G. *J. Chem. Soc., Dalton Trans.* **1996**, 3613.
- ² De Sa, G. F.; Malta, O. L.; de Mello Donega, C.; Simas, A. M.; Longo, R. L.; Santa-Cruz, P. A.; da Silva Jr., E. F. *Coord. Chem. Rev.* **2000**, *196*, 165.
- ³ Steemers, F. J.; Verboom, W.; Reinhoudt, D. N.; van der Tol, E. B.; Verhoeven, J. W. *J. Am. Chem. Soc.* **1995**, *117*, 9408.

- 4 Hemmilä, I. K. *Applications of Fluorescence in Immunoassays*, Wiley and Sons, New York, 1991.
- 5 Klink, S. I.; Grave, L.; Reinhoudt, D. N.; van Veggel, F. C. J. M.; Werts, M. H. V.; Geurts, F. A. J.; Hofstraat, J. W. *J. Phys. Chem. A* **2000**, *104*, 5457.
- 6 Klink, S. I.; Hebbink, G. A.; Grave, L.; van Veggel, F. C. J. M.; Reinhoudt, D. N.; Slooff, L. H.; Polman, A.; Hofstraat, J. W. *J. Appl. Phys.* **1999**, *86*, 1181.
- 7 Hasegawa, Y.; Ohkubo, T.; Sogabe, K.; Kawamura, Y.; Wada, Y.; Nakashima, N.; Yanagida, S. *Angew. Chem. Int. Ed.* **2000**, *39*, 357.
- 8 Beeby, A.; Faulkner, S. *Chem. Phys. Lett.* **1997**, *266*, 116.
- 9 Maupin, C. L.; Dickins, R. S.; Govenlock, L. G.; Mathieu, C. E.; Parker, D.; Williams, J. A. G.; Riehl, J. P. *J. Phys. Chem. A* **2000**, *104*, 6709.
- 10 Voloshin, A. I.; Shavaleev, N. M.; Kazakov, V. P. *J. Luminesc.* **2001**, *93*, 115.
- 11 Slooff, L. H.; Polman, A.; Oude Wolbers, M. P.; van Veggel, F. C. J. M.; Reinhoudt, D. N.; Hofstraat, J. W. *J. Appl. Phys.* **1998**, *83*, 497.
- 12 Werts, M. H. V.; Woudenberg, R. H.; Emmerink, P. G.; van Gassel, R.; Hofstraat, J. W.; Verhoeven, J. W. *Angew. Chem. Int. Ed.* **2000**, *39*, 4542.
- 13 Miniscalco, W. J. *J. Lightwave Tech.* **1991**, *9*, 234.
- 14 For an early paper see: Meshkova, S. B.; Rusakova, N. V.; Bolshoi, D. V. *Acta Chim. Hung.* **1992**, *129*, 317.
- 15 Gschneidner, K. A.; Eyring, L. R. *Handbook on the Physics and Chemistry of Rare Earths*, North Holland Publishing Company, Amsterdam, 1979.
- 16 Lowe, M. P.; Parker, D. *Inorg. Chim. Acta* **2001**, *317*, 163.
- 17 Vögtle, F.; Gorka, M.; Vicinelli, V.; Ceroni, P.; Maestri, M.; Balzani, V. *Chem. Phys. Chem.* **2001**, *769*.
- 18 Sabbatini, N.; Guardigli, M.; Lehn, J. –M. *Coord. Chem. Rev.* **1993**, *123*, 201.
- 19 Sato, S.; Wada, M. *Bull. Chem. Soc. Jpn.* **1970**, *43*, 1955.
- 20 Latva, M.; Takalo, H.; Mukkala, V. M.; Matachescu, C.; Rodriguez-Ubis, J. C.; Kankare, J. *J. Luminesc.* **1997**, *75*, 149.
- 21 Werts, M. H. V.; Duin, M. A.; Hofstraat, J. W.; Verhoeven, J. W. *Chem. Commun.* **1999**, 799.
- 22 Dadabhoy, A.; Faulkner, S.; Sammes, P. G. *J. Chem. Soc. Perkin Trans. 2* **2000**, 2359.
- 23 Stein, G.; Würzberg, E. *J. Phys. Chem.* **1975**, *62*, 208.
- 24 Korovin, Y.; Rusakova, N. *Rev. Inorg. Chem.* **2001**, *21*, 299.
- 25 Oude Wolbers, M. P.; van Veggel, F. C. J. M.; Peters, F. G. A.; van Beelen, E. S. E.; Hofstraat, J. W.; Geurts, F. A. J.; Reinhoudt, D. N. *Chem. Eur. J.* **1998**, *4*, 772.
- 26 Werts, M. H. V.; Hofstraat, J. W.; Geurts, F. A. J.; Verhoeven, J. W. *Chem. Phys. Lett.* **1997**, *276*, 196.
- 27 Klink, S. I.; Oude Alink, P.; Grave, L.; Peters, F. G. A.; Hofstraat, J. W.; Geurts, F. A. J.; van Veggel, F. C. J. M. *J. Chem. Soc., Perkin Trans. 2* **2001**, 363.

- 28 Wong, W. K.; Hou, A.; Guo, J.; He, H.; Zhang, L.; Wong, W. Y.; Li, K. F.; Cheah, K. W.; Xue, F.; Mak, T. C. W. *J. Chem. Soc., Dalton Trans.* **2001**, 3092.
- 29 Beeby, A.; Dickins, R. S.; FitzGerald, S.; Govenlock, L. J.; Maupin, C. L.; Parker, D.; Riehl, J. P.; Siligardi, G.; Williams, J. A. G. *Chem. Commun.* **2000**, 1183.
- 30 Klink, S. I.; Keizer, H.; van Veggel, F. C. J. M. *Angew. Chem. Int. Ed.* **2000**, 39, 4319.
- 31 Dexter, D. L. *J. Chem. Phys.* **1953**, 21, 836.
- 32 Murov, S. L.; Carmichael, I.; Hug, G. L. *Handbook of photochemistry*, 2nd edition, Marcel Dekker, New York, 1993.
- 33 Hebbink, G. A.; Reinhoudt, D. N.; van Veggel, F. C. J. M. *Eur. J. Org. Chem.* **2001**, 4101.
- 34 a) Klink, S. I.; Hebbink, G. A.; Oude Alink, P. G. B.; Grave, L.; van Veggel, F. C. J. M.; Werts, M. H. V. *J. Phys. Chem. A* **2002**, in press; b) Hebbink, G. A.; Klink, S. I.; Oude Alink, P. G. B.; van Veggel, F. C. J. M. *Inorg. Chim. Acta* **2001**, 317, 114.
- 35 For the procedure see: van Veggel, F. C. J. M.; Oude Wolbers, M. P.; Reinhoudt, D. N. *J. Phys. Chem. A* **1998**, 102, 3060; for the Lennard Jones parameters for the lanthanide ions: van Veggel, F. C. J. M.; Reinhoudt, D. N. *Chem. Eur. J.* **1999**, 5, 90.
- 36 Jorgensen, W. L. *J. Phys. Chem.* **1986**, 90, 1276 (OPLS stands for Optimized Potentials for Liquid Simulations).
- 37 The central carbon atom of the xanthene unit, at the para position to the oxygen in the central ring, was taken as a measure of the distance.
- 38 Slooff, L. H.; Polman, A.; Klink, S. I.; Hebbink, G. A.; Grave, L.; van Veggel, F. C. J. M.; Reinhoudt, D. N.; Hofstraat, J. W. *Opt. Mater.* **2000**, 14, 101; Slooff, L. H.; Polman, A.; Hebbink, G. A.; van Veggel, F. C. J. M.; Reinhoudt, D. N.; Cacialli, F.; Friend, R. H. *Appl. Phys. Lett.* **2001**, 78, 2122.
- 39 Horrocks, W. DeW.; Sudnick, D. R. *Acc. Chem. Res.* **1981**, 14, 384.
- 40 Beeby, A.; Clarkson, I. M.; Dickins, R. S.; Faulkner, S.; Parker, D.; Royle, L.; de Sousa, A. S.; Williams, J. A. G.; Woods, M. *J. Chem. Soc., Perkin Trans. 2* **1999**, 493.
- 41 The low-energy side of the ${}^4F_{3/2} \rightarrow {}^4I_{13/2}$ transition of Nd^{3+} at 1330 nm is distorted by absorption around 1400 nm, which is the first overtone of the 2950 cm^{-1} C-H vibration of the solvent (CH_3OD).
- 42 Ermolaev, V. L.; Sveshnikova, E. B. *Russ. Chem. Rev.* **1994**, 63, 905.
- 43 Beeby, A.; Faulkner, S. *Chem. Phys. Lett.* **1997**, 266, 116.
- 44 Slooff, L. H.; Polman, A.; Oude Wolbers, M. P.; van Veggel, F. C. J. M.; Reinhoudt, D. N.; Hofstraat, J. W. *J. Appl. Phys.* **1998**, 83, 497.
- 45 Klink, S. I.; Hebbink, G. A.; Grave, L.; van Veggel, F. C. J. M.; Reinhoudt, D. N.; Slooff, L. H.; Polman, A.; Hofstraat, J. W. *J. Appl. Phys.* **1999**, 86, 1181.
- 46 Weber, M. J. *Phys. Rev.* **1968**, 168, 283.

- 47 Polman, A. *Physica B* **2001**, *300*, 78.
- 48 The energy levels of the three dyes, the 0-0 transitions of the singlet and the triplet states, were determined from the spectra and are represented in Figure 1. The 0-0 transition of the singlet state are estimated as the crossing of the absorption and fluorescence spectra. The 0-0 of the triplet state was estimated from crossing of the singlet-triplet excitation spectrum and the phosphorescence spectrum of **1R₄Gd** at 77K. Although the singlet-triplet absorption is relative weak, the excitation spectrum could easily be distinguished from the singlet-singlet excitation of the phosphorescence (cf. ref 32 p. 54).
- 49 Delayed detection was accomplished by equipping the spectrofluorimeter with a rotating drum. Doing so a delay between excitation and emission of about 2 ms was accomplished. Compare ref. 64.
- 50 Tobita, S.; Arakawa, M.; Tanaka, I. *J. Phys. Chem.* **1984**, *88*, 2697; Tobita, S.; Arakawa, M.; Tanaka, I. *J. Phys. Chem.* **1985**, *89*, 5649.
- 51 Guldi, D. M.; Mody, T. D.; Gerasimchuk, N. N.; Magda, D.; Sessler, J. L. *J. Am. Chem. Soc.* **2000**, *122*, 8289.
- 52 The assumption here is that all other energy conversion processes are not temperature dependent. This is not strictly true but the effects are much smaller than the temperature dependence of the energy back-transfer rate (Turro, N. J. *Modern Molecular Photochemistry*, The Benjamin/Cummings Publishing Co., Inc., Menlo Park, 1978).
- 53 Payne, S. A.; Bibeau, C. *J. Luminesc.* **1998**, *79*, 143.
- 54 For the energy efficiency applies: $\eta_{ET} \approx k_{ET}/\Sigma k$, with $\Sigma k = k_{BT} + k_{ET} + \Sigma k_{others}$. The energy back-transfer depends on the temperature according: $k_{BT} \sim e^{-\Delta E/kT}$. Neglecting all other rates than k_{BT} , the intercept of a plot of $\ln(\eta_{ET})$ vs ΔE , at $\ln(\eta_{ET}) = 0$ ($\eta_{ET} = 1$) is an estimate of the energy gap necessary to prevent energy back transfer. As the other processes are neglected here, the found value for ΔE will be the lower limit.
- 55 Gonçalves e Silva, F. R.; Malta, O. L.; Reinhard, C.; Güdel, H. U.; Piguet, C.; Moser, J. E.; Bünzli, J. -C. G. *J. Phys. Chem. A* **2002**, *106*, 1670.
- 56 Blasse, G.; Grabmaier B.C. *Luminescent materials*, Springer-Verlag, Berlin, 1994.
- 57 The ${}^7H_{11/2}$ level of Nd^{3+} can be an acceptor level because of the selection rules. However, this level is higher in energy than the triplet states of the sensitizers and is therefore not taken into account.
- 58 Horrocks, W. DeW.; Bolender, J. P.; Smith, W. D.; Supkowski, R. M. *J. Am. Chem. Soc.* **1997**, *119*, 5972.
- 59 Rehm, D.; Weller, A. *Isr. J. Chem.* **1970**, *8*, 259.
- 60 $-\Delta G = -E(\text{dye}^{\bullet+}/\text{dye}) + E_{\text{dye}^*} + E(\text{Yb}^{3+}/\text{Yb}^{2+})$; $E(\text{dye}^{\bullet+}/\text{dye}) = 1.14$ V vs NHE (Jones III, G.; Qian, X. *J. Photochem. Photobiol. A-Chem.* **1998**, *113*, 125), $E(\text{Yb}^{2+}/\text{Yb}^{3+}) = 1.05$ V vs NHE (D. R. Lide (ed.) *Handbook of chemistry and physics*, 76th edition, CRC press, New York, 1996). The reduction

potential of Yb^{3+} is expected to be even higher as the triple charged ion is stabilized by the ligand. This leads to even lower values of the driving force.

⁶¹ $E(\text{Eu}^{3+}/\text{Eu}^{2+}) = -0.35 \text{ V (vs. NHE)}$, $E(\text{Yb}^{3+}/\text{Yb}^{2+}) = -1.05 \text{ V (vs. NHE)}$, D. R. Lide (ed.) *Handbook of chemistry and physics*, 76th edition, CRC press, New York, 1996.

⁶² Klink, S. I.; Hebbink, G. A.; Grave, L.; Peters, F. G. A.; van Veggel, F. C. J. M.; Reinhoudt, D. N.; Hofstraat, J. W. *Eur. J. Org. Chem.* **2000**, 192.

⁶³ van Houten, J.; Watts R. J. *J. Am. Chem. Soc.* **1976**, 98, 4853.

⁶⁴ Werts, M. H. V.; Verhoeven, J. W.; Hofstraat, J. W. *J. Chem. Soc., Perkin Trans. 2* **2000**, 433.

Chapter 5

*Inorganic nanoparticles doped with luminescent lanthanide(III) ions**

In this Chapter, the luminescence of lanthanide ions doped in inorganic nanoparticles is described. These redispersible LnPO_4 particles ($\text{Ln}^{3+} = \text{La}^{3+}, \text{Gd}^{3+}, \text{Lu}^{3+}, \text{or } \text{Y}^{3+}$) are small (5-7 nm), are crystalline, and are doped with the luminescent lanthanide ions $\text{Eu}^{3+}, \text{Pr}^{3+}, \text{Nd}^{3+}, \text{and } \text{Er}^{3+}$. The luminescence of the latter three ions cover the complete optical window from 1300 nm up to 1650 nm, which is of importance in telecommunication applications. In order to describe the luminescent decay of these particles, a model was made that takes into account the quenching of the ions by the solvent that surrounds the particles. With such a model, all decay curves could be fitted excellently, with lifetimes that are 10-1000 times higher than that of the corresponding ions in solution or in organic complexes.

* Part of the work described in this Chapter was published: Hebbink, G. A.; Stouwdam, J. W.; Reinhoudt, D. N.; van Veggel, F. C. J. M. *Adv. Mater.* **2002**, in press.

5.1 Introduction

Organic lanthanide ion complexes are potential materials for application in polymer-based optical components, because they form a homogeneous mixture with polymers and organic chromophores greatly enhance the absorption cross section of the complex.¹ Polymer-based optical devices and components have advantages in device fabrication and integration with other polymer-based optical components.² Devices can be made by spincoating the polymers from solution directly on the devices and integration can be achieved by standard lithographic clean-room techniques. However, a disadvantage of organic complexes is that the intrinsic quenching of near-infrared (NIR) emissive ions like Nd^{3+} and Er^{3+} by the organic ligand is very strong.³ Deuteration and fluorination⁴ reduces this quenching to some extent, but luminescent quantum yields remain low. Another disadvantage of organic complexes is the instability of the organic chromophores when applying the intense laser powers necessary to pump the lanthanide ions in order to achieve optical amplification.⁵ We have shown that the lissamine sensitizer of Nd^{3+} was bleached in about 1000 s by applying 1 W of laser power on a spot of 1 mm (by an Ar^+ ion laser operating at 515 nm). In general, inorganic glasses do not suffer to that extent from photobleaching⁶ and luminescent quantum yields close to unity have been reported, which would make them by far a better host for luminescent lanthanide ions.⁷

In order to blend inorganic materials with organic materials like polymers, these inorganic materials have to fulfill two requirements: solubility in the organic matrix and light scattering should be avoided, which of course are losses in optical devices. Compatibility of inorganic materials can be achieved by modifying the surface of inorganic nanoparticles with organic groups such that this organic surface is solubilized by the organic solvent.⁸ These nanoparticles form another phase than the solvent, and scatter is strongly dependent on the radius of the particles and the difference in refractive index between particle and the medium, according to Eq. 5.1.

$$\text{scattering} \sim \left(\frac{r}{\lambda}\right)^4 \left[\frac{\left(\frac{n_c}{n_m}\right)^2 - 1}{\left(\frac{n_c}{n_m}\right)^2 + 2} \right]^2 2\pi r^2 \quad \text{Eq. 5.1}$$

In Eq. 5.1 the relation between Rayleigh scattering and the particle radius r , wavelength of the light λ , the refractive indices of the particle, n_c , and the medium, n_m , is shown.⁹ For

comparison: a particle of 10 nm (radius) and the light wavelength of 1536 nm (emission line of Er^{3+}), and refractive indices of $n_c = 1.800$ and $n_m = 1.490$ ($\Delta n = 0.31$), the losses due to scattering are the same for a particle of 50 nm radius with an index of 1.492 in PMMA ($\Delta n = 0.002$). It was calculated⁹ that a scatter loss below 1 dB/cm is expected with particles smaller than 40 nm and a refractive index contrast of 1.48 for the matrix and 1.44 for the particles ($\Delta n = 0.04$).

The fabrication of inorganic glasses and particles doped with luminescent lanthanide ions is very common and applications are found in for instance lighting (TL tubes), television, and optical amplification (Erbium Doped Fiber Amplifiers, EDFAs).^{10,11} Numerous types of nanoparticles have been made by wet-chemical methods or bombardment techniques, followed by a heat-treatment, in general above 800 °C.^{7,12} Although these methods give excellently defined particles with good luminescent properties, they suffer from possibilities to process them further in polymers. Luminescent lanthanide ion doped particles that are processable are rather rare and in the available cases, only the visible emitting ions like Eu^{3+} and Tb^{3+} have been reported, while NIR emissive lanthanide ions have great potential use in optical telecommunication.

In a review, Tissue reported the use and preparation of nanoscale particles doped with lanthanide ions.⁸ The importance of embedding the particles in a matrix is pointed out in this paper. This embedding has mainly been focussed on inorganic materials and not on polymer-based materials, e.g. $\text{Y}_2\text{O}_3:\text{Eu}$ films and powders.^{13,14} Some redispersible semiconductor materials have been prepared, doped with lanthanide ions, although sensitized emission by the semiconductor particles was not proven. Recently, Bol *et al.* re-synthesized these nanoparticles with Eu^{3+} doping.¹⁵ However, upon excitation of the synthesized nanoparticles no Eu^{3+} emission was observed, the Eu^{3+} ions are probably not present in the semiconductor particles. Barium fluoride particles doped with Nd^{3+} ions were prepared by a reversed micro-emulsion technique, leading to particles with sizes in the micrometer range.¹⁶ Luminescence measured of the powders showed the 1052 nm Nd^{3+} emission (excitation at 488 nm), but luminescent lifetimes were in the microsecond region, the longest reported there was 11 μs , where 100-1000 μs was expected. A lanthanide ion based material that is formed in solution with surface capping by surfactant molecules is LaF_3 , however without luminescent doping.¹⁷ Although no luminescence from this type of nanoparticles in solution was reported, it could be an interesting material for NIR emissive ions, because of the low phonon energy in this material (300-400 cm^{-1}).¹⁸ The lower the phonon energy, the lower the quenching will be. Semi-conductor materials like mercury telluride emit in the NIR region as well.¹⁹ However, these type of NIR emissive materials are rather

unstable. Furthermore, laser action is difficult to achieve, and to date only one precedent of laser action by (visible emitting) semiconducting particles (CdSe) has been reported, by Bawendi *et al.*²⁰ Yttrium vanadate particles, doped with Eu^{3+} were reported with particle sizes between 15 and 30 nm.²¹ This colloidal material was stable in aqueous dispersion at various pH values, and luminescence of Eu^{3+} was reported with quantum yield values up to 38% with a Eu^{3+} concentration of 15% (versus Y^{3+}). By the group of Haase *et al.* yttrium vanadate particles are reported that are doped with luminescent lanthanide ions, i.e. Eu^{3+} and Tb^{3+} .^{22,23,24} In these complexes energy transfer from the vanadate groups to adjacent Eu^{3+} ions occurs, while energy transfer in between vanadate groups results in quenching of the vanadate excited states. The luminescence is quenched at the surface of the TOPO (tri-n-octylphosphine oxide) capped nanoparticles, giving a luminescence quantum yield of 15% for the Eu^{3+} emission.

Haase *et al.* reported redispersable lanthanide ion-doped nanoparticles that consist of lanthanum phosphate. These were doped with Eu^{3+} and Tb^{3+} ions as the luminescent ions. The nanocrystalline material doped with Eu^{3+} exhibited the same emission spectrum as the bulk material.²⁵ They showed that the wet chemical synthesis employed to make the colloidal particles does not change the symmetry (C_1) of the Eu^{3+} luminescent site as compared to the luminescence of the bulk material. The use of other luminescent dopants is illustrated with Ce^{3+} and the doping with Ce^{3+} and Tb^{3+} . In the first case the violet/blue luminescence of Ce^{3+} was observed, in the latter material, upon excitation of Ce^{3+} the green luminescence of Tb^{3+} was found. The luminescent lifetimes of the luminescent centers in $\text{LaPO}_4:\text{Eu}$ and $\text{CePO}_4:\text{Tb}$ were found not to be mono-exponential.²⁶ Fitting of the decay traces with correction for randomly distributed quenchers²⁶ yielded a good result with luminescent lifetimes in the absence of quenchers of 4.8 ms for $\text{LaPO}_4:\text{Eu}$ and 5.8 ms for $\text{CePO}_4:\text{Tb}$ with higher quenching factors in the case of Tb^{3+} . This fitting method considers only randomly distributed quenchers, whereas the authors reported a solvent effect on the luminescence. However, this solvent is not distributed randomly but at the surface of the particles, so this model needs refinement.²⁷

An important excitation pathway in Eu^{3+} doped inorganic materials is the charge transfer (CT) band. In this mechanism Eu^{3+} is reduced to Eu^{2+} and the coordinating anions in the crystal, e.g. phosphates or oxides, are oxidized upon absorption of a photon with sufficient energy. When the energy of this charge transfer band is not too low, deactivation of the CT band to the $^5\text{D}_j$ levels results in an excited Eu^{3+} ion, see Figure 5.1. This excitation pathway is strongly dependent on the host materials, because the crystal matrix is oxidized. Variations in the matrix will shift the CT band in the coordinate diagram in Figure 5.1 vertically and/or horizontally. Deactivation of the CT band to the $^7\text{F}_j$ states is the result when the energy level of the CT band is

too low or the offset from the center coordination center is too large in order to feed the 5D_J levels.²⁸ This mechanism is present in Yb^{3+} doped materials as well, because Yb^{3+} is also reduced relatively easily.²⁹

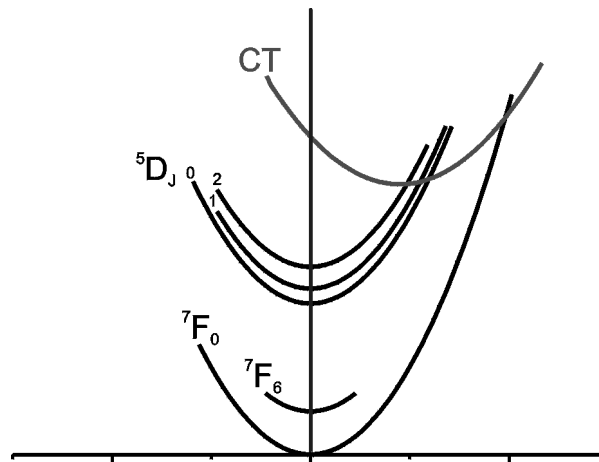


Figure 5.1 Coordinate diagram with the 7F_J groundstates ($J = 1-6$, levels with $J = 2-5$ are not shown), the 5D_J excited states ($J = 0-2$ are shown), and the charge transfer state of Eu^{3+} .²⁸

Luminescence from the CT band was observed in Yb^{3+} doped materials, i.e. the CT band deactivates (partly) radiatively.³⁰ In Eu^{3+} doped materials this luminescence is less likely, because the gap between the CT band and the 5D_J states is much smaller when compared with the gap of the CT band and the excited states of Yb^{3+} .

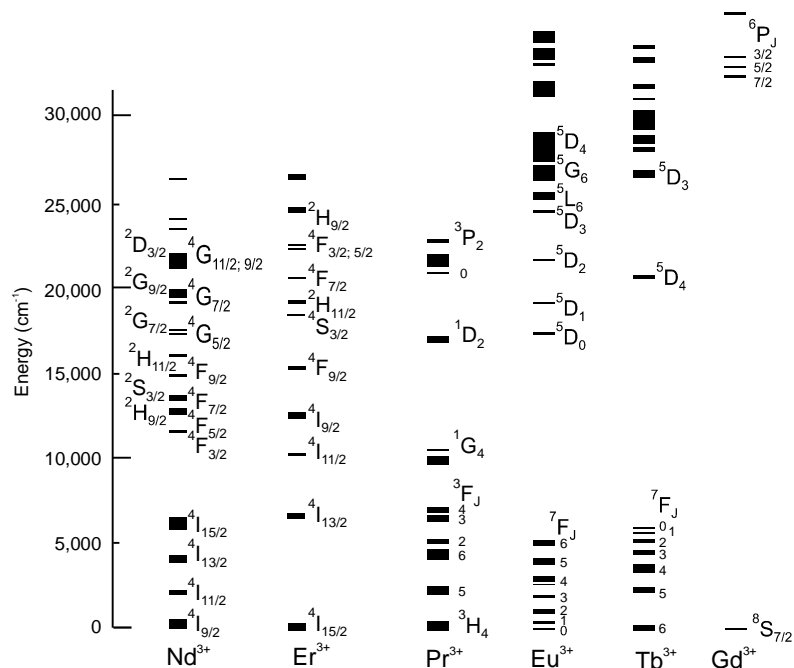


Figure 5.2 Energy level scheme of the Nd^{3+} , Er^{3+} , Pr^{3+} , Eu^{3+} , Tb^{3+} , and Gd^{3+} ions.³¹

An energy level scheme of the luminescent lanthanide ions that are reported in this Chapter, is depicted in Figure 5.2,³² with energy levels of the ions Nd^{3+} , Er^{3+} , Pr^{3+} , Eu^{3+} , and Gd^{3+} . Nd^{3+} , Er^{3+} , and Pr^{3+} are ions that emit in the NIR region (Pr^{3+} emits in the visible region as well), Eu^{3+} emits in the red region of the electromagnetic spectrum and is used to characterize the synthesized materials because the Eu^{3+} luminescence is well known and very sensitive to the environment. Gd^{3+} is used as a host material as well as La^{3+} , Lu^{3+} , and Y^{3+} . Although Gd^{3+} does have a partially filled 4f orbitals, the lowest 4f level of Gd^{3+} is located at $32,000\text{ cm}^{-1}$, much higher in energy than the emissive states of the luminescent dopings.

5.2 Results and discussion

5.2.1 Preparation and characterization of $\text{Ln}(1)\text{PO}_4:\text{Ln}(2)$ particles

The colloids doped with the NIR-emitting Eu^{3+} , Er^{3+} , Nd^{3+} , and Pr^{3+} ions were prepared according to a literature procedure.^{24,33} The particles were characterized with transmission electron microscopy (TEM), a typical photograph is shown of the $\text{LaPO}_4:\text{Pr}$ particles in Figure 5.3. The picture shows that the particles are not ideally spherical and that the average size of the particles is about 5-7 nm.³⁴ The inset shows a magnification of a particle to illustrate the high crystallinity. The particles seem to cluster on the TEM grid but in solution they are present as single particles. This has been measured before with small angle X-ray scattering.²⁷

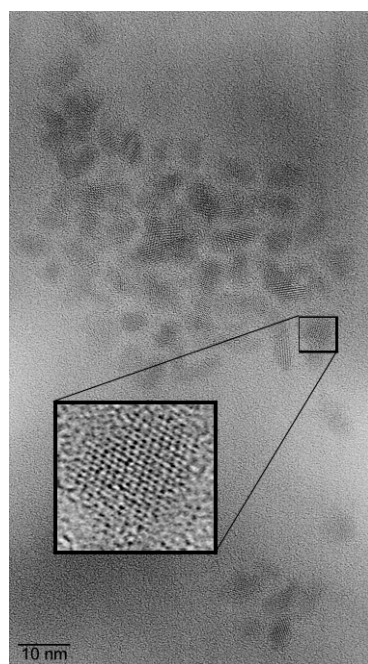


Figure 5.3 TEM image of $\text{LaPO}_4:\text{Pr}$ particles, deposited on a carbon grid. The inset shows a magnification of a particle that shows the high crystallinity of the particles.

The elemental composition of the colloidal powders was determined by elemental analyses and by X-ray fluorescence (XRF), the latter being an excellent technique to distinguish between the different lanthanide ions. The elemental composition obtained from elemental analyses and XRF are presented in Table 5.1.

Table 5.1 Elemental composition (Wt %) of $\text{LaPO}_4:\text{Ln}$ particles, stabilized with phosphate esters and tetramethyl ammonium salts.

	La ^a	Ln ^a	P ^a	C ^b	N ^b	H ^b
LaPO ₄ :Nd	41.97	2.42	12.19	6.33	1.01	2.16
LaPO ₄ :Er	41.80	2.36	12.56	5.57	1.20	2.63
LaPO ₄ :Pr	43.30	2.35	12.52	6.30	1.01	2.17

a XRF

b Elemental analysis

The molar ratio $\text{La}^{3+}:\text{Ln}^{3+}$ is in all cases about 19:1, as applied in the synthesis. Furthermore, the phosphor content is higher than stoichiometrically is needed for LnPO_4 , the excess in phosphor is present as phosphates and phosphate esters bound to the surface of the particles. The remaining 10% is organic material, mainly surface alkyl groups, tetramethylammonium salts, and traces of water. The presence of the organic groups was confirmed by ¹H NMR spectroscopy where broadened signals (3.3 ppm for NMe_4^+ and 1.2 and 0.9 ppm for surface bound ethylhexyl moieties) were found for these compounds. The line broadening is consistent with the surface binding of the organic groups to the particles.

The materials made are as follows: $\text{LnPO}_4:\text{Eu}$ with $\text{Ln}^{3+} = \text{La}^{3+}, \text{Gd}^{3+}, \text{Lu}^{3+},$ and Y^{3+} , and $\text{LaPO}_4:\text{Ln}$ with Ln^{3+} is (besides Eu^{3+}) $\text{Pr}^{3+}, \text{Nd}^{3+},$ and Er^{3+} . In all of these materials made, the amount of emissive lanthanide ion was 5% (molar ratio), relative to the host lanthanide ion.

5.2.2 VIS luminescence

The luminescence of Eu^{3+} is commonly used as a probe of the local environment, because this luminescence is very indicative of the environment of the europium ion and because the spectrum of Eu^{3+} is very well known. The host materials for the Eu^{3+} doped particles were chosen because the size of the ions varies from 0.8 Å for Lu^{3+} to 1.1 Å for La^{3+} and because they do not interact with the excited Eu^{3+} ion. The differences in ion size lead to significant differences in the bulk materials derived because the smaller lanthanide ions lead to a xenotime crystal structure and the larger ions to a monazite structure.³⁵ The synthesized materials were

dissolved in methanol and the absorption and luminescence spectra were taken. The absorption and excitation spectra of $\text{LaPO}_4:\text{Eu}$ in methanol are depicted in Figure 5.4.

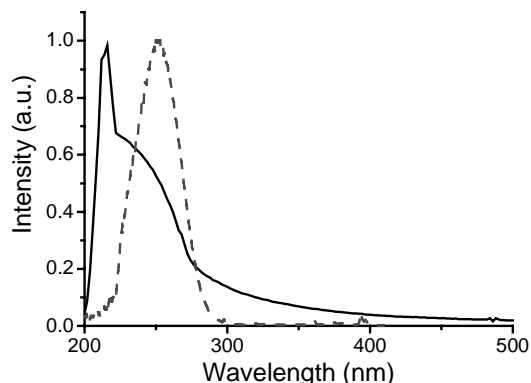


Figure 5.4 Absorption (solid line) and excitation spectrum (dashed line) of $\text{LaPO}_4:\text{Eu}$ in CH_3OH solution.

Upon comparing the absorption spectrum with the excitation spectrum, it is found that only part of the absorption spectrum leads to Eu^{3+} luminescence. The part that leads to luminescence is the charge transfer between host matrix and Eu^{3+} . Upon excitation, Eu^{3+} is reduced to Eu^{2+} , by oxidation of the phosphates. This charge transfer deactivates to form an excited Eu^{3+} . The other absorptions in the absorption spectrum that do not lead to Eu^{3+} emission are due to organic groups bound to the surface.

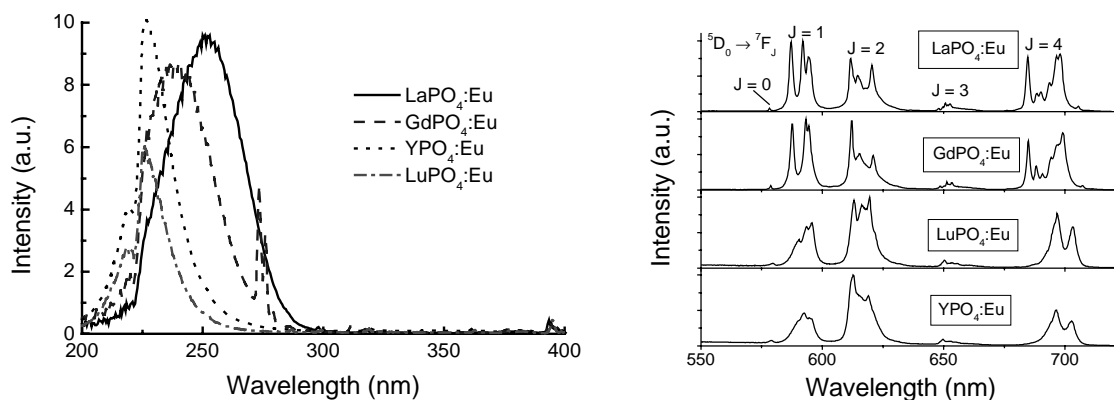


Figure 5.5 Excitation (left) and emission (right) spectra of $\text{LnPO}_4:\text{Eu}$ in MeOH solution. Excitation spectra: λ_{em} 612 nm and normalized on the 393 nm excitation peak. Normalized emission spectra: λ_{exc} 250 nm.

The excitation spectra of the $\text{LnPO}_4:\text{Eu}$ materials ($\text{Ln}^{3+} = \text{La}^{3+}, \text{Gd}^{3+}, \text{Lu}^{3+}, \text{and Y}^{3+}$) are depicted in Figure 5.5, all normalized on the 393 nm Eu^{3+} transition (${}^7\text{F}_0 \rightarrow {}^5\text{L}_6$). The intensities

of the charge transfer bands are about the same, but upon a decrease in host ion size, the excitation maximum is blue-shifted. The excitation spectra of YPO_4 and LuPO_4 exhibit a sharp cutoff around 220 nm, which is caused by the absorption of the excitation light by the solvent. The blue shift of the charge transfer band upon decreasing the host ion size can be explained by stronger binding of the phosphate groups to the smaller trivalent ions and by the smaller crystal site Eu^{3+} has in the YPO_4 and LuPO_4 lattices. This makes the phosphates more difficult to oxidize and the reduction of Eu^{3+} to Eu^{2+} less favorable. The sharp lines in the GdPO_4 host at 273, 276, and 278 nm and some smaller peaks around 310 nm are due to the excitation of Gd^{3+} ($^8\text{S}_{7/2} \rightarrow ^6\text{I}_J$, $^6\text{P}_J$, $J = 3/2, 5/2$, and $7/2$) and subsequent energy transfer to the Eu^{3+} excited states.

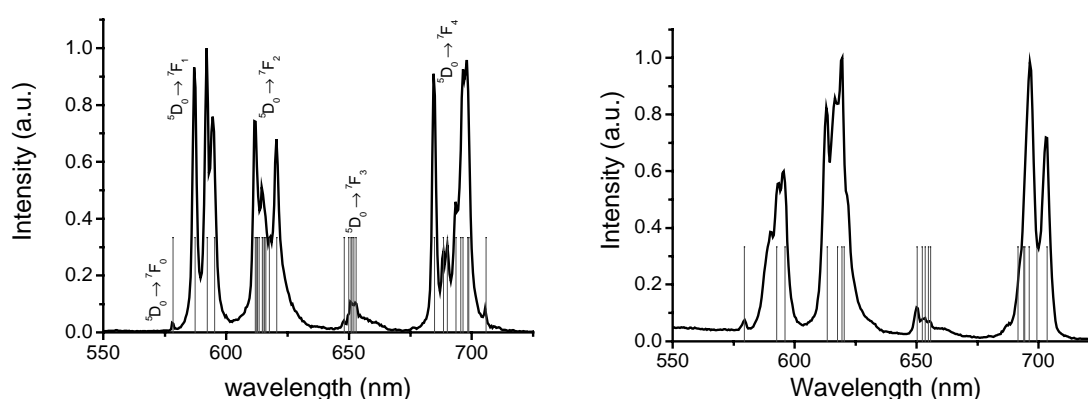


Figure 5.6 Left: $\text{LaPO}_4:\text{Eu}$ emission spectrum. Right: $\text{YPO}_4:\text{Eu}$ emission spectrum. Vertical lines in both spectra correspond to the reported data of the emission spectra of the bulk materials $\text{LaPO}_4:\text{Eu}$ and $\text{YPO}_4:\text{Eu}$.

The emission spectra of all four $\text{LnPO}_4:\text{Eu}$ materials exhibit the same characteristic Eu^{3+} emission lines for the $^5\text{D}_0 \rightarrow ^7\text{F}_J$ ($J = 0 - 4$) transitions. Emission from the $^5\text{D}_1$ excited state was observed as well (*vide infra*), only much weaker than the $^5\text{D}_0$ emission. All emission spectra have only one peak at about 579 nm for the $^5\text{D}_0 \rightarrow ^7\text{F}_0$ transition, indicative for the presence of only one Eu^{3+} emissive site. Some differences are observed in the emission spectra of the two larger host materials (La^{3+} and Gd^{3+}) as compared to the Eu^{3+} emission spectra of the smaller host materials (Y^{3+} , and Lu^{3+}). The relative intensities of the $^5\text{D}_0 \rightarrow ^7\text{F}_2$ transitions are different: 0.30, 0.30, 0.43, 0.50 for the doped LaPO_4 , GdPO_4 , LuPO_4 , and YPO_4 , respectively. Furthermore, a number of additional peaks are found in the $^5\text{D}_0 \rightarrow ^7\text{F}_4$ transition in the La^{3+} and Gd^{3+} material. These different emission spectra are due to a change in crystal structure of the material as for the bulk material a monazite structure is reported for LaPO_4 , while this is a xenotime structure in phosphate material of the smaller lanthanide ion. For the monazite

structure a C_1 symmetry was reported for the La^{3+} ions, the xenotime crystal structure has a higher symmetry (D_{2d}^{36}). In Figure 5.6 the emission spectra of the $\text{LaPO}_4:\text{Eu}$ and $\text{YPO}_4:\text{Eu}$ are shown, together with reported values for the europium transitions in the bulk materials ($\text{LaPO}_4:\text{Eu}^{37}$ and $\text{YPO}_4:\text{Eu}^{38}$). As can be seen, these emission spectra of the nanoparticles nicely match the luminescence spectra in the bulk materials.

The luminescent lifetimes of Eu^{3+} in the LaPO_4 matrix in methanol dispersion are reported in Table 5.2. In methanol the luminescent lifetimes could not be fitted with a single exponential decay, but bi-exponential fittings gave good results (Eq. 5.2). The values of the luminescence lifetimes in MeOH are: 7.1 ms (56%) and 3.9 ms (44%). Although there are some differences in the components at two different emission maxima, these differences fall within the experimental error. In fact, the weighted averages of the two components are the same at both wavelength (5.8 ms at 590 nm and 5.6 ms at 612 nm). In deuterated methanol the decay trace could be fitted with a single exponential with an averaged value of 6.3 ms. Methanol is a strong quencher of the Eu^{3+} luminescence, whereas deuterated methanol hardly quenches.³⁹ This leads to the conclusion that the solvent molecules at the surface of the nanoparticles play an important role in the quenching mechanisms and that this is the cause of the short component in the biexponential fit.

$$\frac{I_t}{I_0} = A_1 e^{-\frac{t}{\tau_1}} + A_2 e^{-\frac{t}{\tau_2}}; \quad A_1 + A_2 = 1 \quad \text{Eq. 5.2}$$

Table 5.2 Luminescent lifetime of $\text{LaPO}_4:\text{Eu}$ colloids.

Solvent	$\lambda_{\text{exc/em}}$ (nm)	τ_1 (ms) ^a	τ_2 (ms) ^a
CH ₃ OH	260/590	7.4 (52%)	4.1 (48%)
	260/612	6.8 (61%)	3.6 (39%)
CH ₃ OD	260/590	6.4	
	260/612	6.2	

^a Error values in the biexponential fits: ± 0.2 ms and $\pm 5\%$ in the pre-exponential factors

Due to the fact that there is only one sharp peak of the ${}^5\text{D}_0 \rightarrow {}^7\text{F}_0$ it was already concluded that only one luminescent Eu^{3+} is present in the materials. This observation is further corroborated by time-resolved spectroscopy where in various time domains after an excitation pulse the same total emission spectrum is detected (Figure 5.7). These emission spectra were taken shortly after the excitation pulse (0.2 ms) and at the end of the decay curve (29 ms). Although the intensity at the end of the decay is much lower, the shape of the spectrum is

essentially the same as in the early stages of the decay, thereby proving that only one kind of Eu^{3+} is present in the LaPO_4 host material.

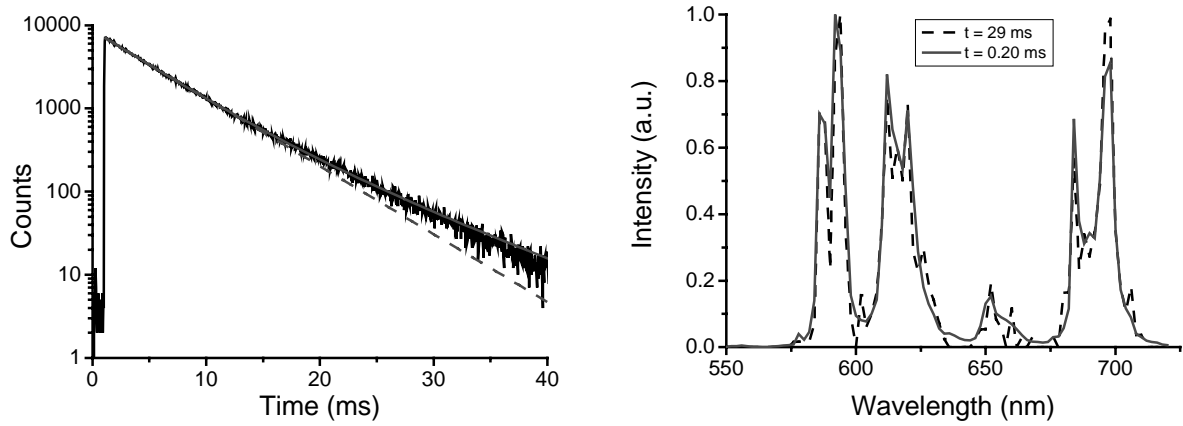


Figure 5.7 Left: decay trace of $\text{LaPO}_4:\text{Eu}$ in CH_3OH , solid line: decay curve with bi-exponential fit, dotted line: mono-exponential fit. Right: time-resolved spectra (normalized) with a delay of 0.2 ms and 29 ms after the excitation pulse, both spectra have a temporal resolution of $40 \mu\text{s}$ and a spectral resolution of 2 nm.

Although the decay curves could be fitted bi-exponentially, a fit that gives more insight in the physical meaning is needed. Strong quenchers are located outside the particles, i.e. the solvent. Going from the core to the edge along the axis of the spherical particle, the lifetime of the local Eu^{3+} luminescent centers will be decreased more strongly when closer to the edge. A particle consisting of a number of shells would be a good description. The (average) lifetime in each shell is related to the lifetime in other shells by the same radiative rate constant and a quenching constant that is dependent on the distance to the surface, see Eq. 5.3 with a model describing a particle consisting of 10 shells of equal volume. These shells with equal volume were chosen in order to give each emissive ion equal weight in the fit procedure.

$$I_t = I_0 \sum_{i=1}^{10} \frac{1}{10} e^{-k_i t}; \quad k_i = \frac{1}{\tau_i} = k_R + C \times f_q(r) \quad \text{Eq. 5.3}$$

In this equation: I_t the intensity at time t , I_0 the intensity at $t = 0$, $k_i = 1/\tau_i$ the rate constant in shell i , the reciprocal of the lifetime in shell i , t the time, k_R a rate constant in absence of quenching outside the particle (fit parameter), C a quenching constant (fit parameter), and $f_q(r)$ the quenching factor that takes into account the distance between a shell and surface and the distance dependence of the quenching ($1/r^6$), integrated over the volume outside a particle. For

more details on the fit procedure, see Appendix 5.A at the end of this chapter. Fitting the decay curves of LaPO₄:Eu in CH₃OH gives an excellent fit with $\tau_R = 6.3$ ms, $C = 1.2 \times 10^{-4} \text{ s}^{-1}$, and an averaged lifetime of 5.2 ms of the whole decay curve. It should be noted that the determined τ_R is a fit parameter and not necessarily the natural radiative lifetime of Eu³⁺. In principle, τ_R is the luminescent lifetime in absence of quenching groups outside the particle, quenching groups in the interior of the particle are included in this parameter. The other parameter C consists of various contributions like the strength of the quenching and the size and the size distribution of the particles, which are not monodisperse (Figure 5.3).

Werts *et al.* derived an equation (Eq. 5.4) that allows the evaluation of the natural radiative lifetime of Eu³⁺ from the emission spectrum⁴⁰ without the intervention of the Judd-Ofelt^{41,42} theory. The treatment by Werts *et al.* assumes that the energy and the oscillator strength of the magnetic dipole transition $^5D_0 \rightarrow ^7F_1$ are constant.

$$k_{\text{rad}} = \frac{1}{\tau_{\text{rad}}} = A_{\text{MD},0} n^3 \left(\frac{I_{\text{tot}}}{I_{\text{MD}}} \right) \quad \text{Eq. 5.4}$$

Here, the radiative rate k_{rad} or the radiative lifetime τ_{rad} is a function of the oscillator strength of the magnetic dipole transition $^5D_0 \rightarrow ^7F_1$ ($A_{\text{MD},0}$), the refractive index of the medium (n), 1.328 for methanol, and of the total emission area divided by the area of the magnetic dipole transition ($I_{\text{tot}}/I_{\text{MD}}$). The oscillator strength, $A_{\text{MD},0}$, of the $^5D_0 \rightarrow ^7F_1$ transition was determined to be 14.65 s^{-1} .⁴⁰ Applying this treatment to the emission spectrum of LaPO₄:Eu gives a radiative rate of 128 s^{-1} , which corresponds to a lifetime of 7.8 ms. Upon comparing this with the observed lifetimes the luminescent quantum yield is estimated to be 75% according the fit with Eq. 5.2, and 73% according the fit with Eq. 5.4.

The time evolution of the luminescence was observed in the early stages of the luminescence as well.⁴³ After the excitation pulse (microsecond pulses, instrumental response about 5 μs) the luminescence was monitored by reconstruction of a series of lifetime measurements at varying wavelengths. The luminescence in the first 200 μs resulted in the spectra depicted in Figure 5.8. Directly after the pulse green luminescence originating from the 5D_1 manifold was observed that decayed mono-exponentially with a time constant of about 23 μs . The rise-time of the 5D_0 luminescence was found to be 24 μs , which is similar to the decay of the 5D_1 luminescence. The fact that here a mono-exponential rise was found and not the bi-exponential behavior of the decay described before is probably due to the (slow) instrumental

response and the short rise-time. A careful examination of the 5D_0 emission rise reveals that the initial intensity at $t = 0$ is about 50% of the maximum intensity. The reason for this is that after the excitation pulse the charge transfer state depopulates fast to the excited 5D_J levels ($J = 0, 1, 2, 3$).¹⁴ This means that the 5D_0 is also directly populated from the charge transfer band in addition to population from the 5D_J ($J > 0$) levels. The excited states with $J = 1, 2, 3$ depopulate fast to the 5D_0 state, due to phonon coupling with the matrix and to coupling with transitions within the 7F levels of nearby Eu^{3+} centers. The latter mechanism was shown to be present in $\text{Y}_2\text{O}_3:\text{Eu}$ phosphors at high concentrations (above 1% Eu^{3+} versus Y^{3+}), similar to the concentration used here (5%).¹⁴ This coupling facilitates the deactivation of the 5D_1 to the 5D_0 emissive level and thereby exciting a Eu^{3+} (7F_0 , ground state) to higher 7F levels. Luminescence from higher excited states (5D_2 and 5D_3) was not observed, because of the very fast deactivation to the 5D_1 and 5D_0 states by the mechanisms outlined before.

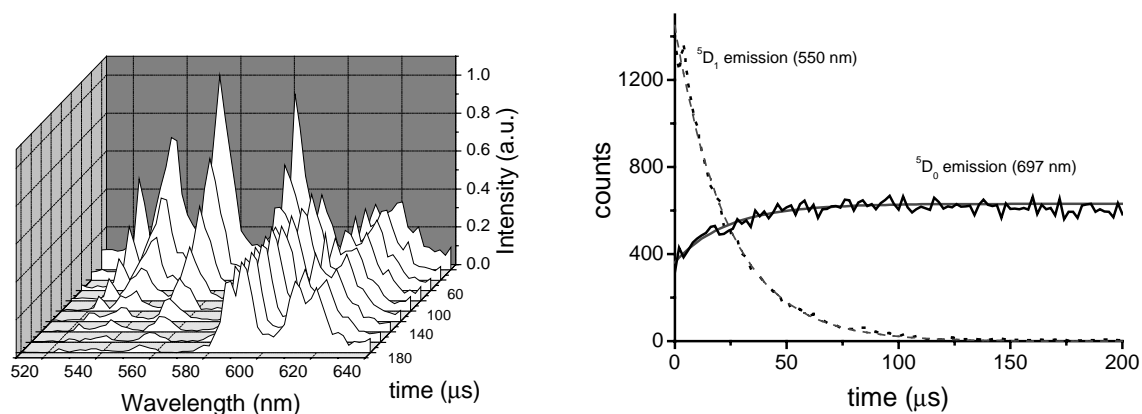


Figure 5.8 Time-resolved luminescence in the spectral domain (left), up to 200 μs after the excitation pulse. The time spacing between the individual spectra is 10 μs with a temporal resolution of 2 μs for each spectrum. Time-resolved luminescence in the time domain (right) at 550 nm (pure 5D_1 emission) and at 697 nm (pure 5D_0 emission), spectral resolution is 2 nm.

The emission and excitation spectra in the visible region of the Pr^{3+} -doped colloids are depicted in Figure 5.9. A number of excitation peaks are observed between 460 and 490 nm (measured by collecting the emission at 730 nm), attributed to the $^3H_4 \rightarrow ^3P_1$ ($J=2,1,0$) transitions. The emission spectrum in the visible was obtained by exciting the sample at 442 nm. The strongest emission peaks were observed around 490 nm, 530 nm, and 620 nm, attributed to the $^3P_0 \rightarrow ^3H_4$, $^3P_0 \rightarrow ^3H_5$ and $^1D_2 \rightarrow ^3H_4$ transitions, respectively.⁴⁴

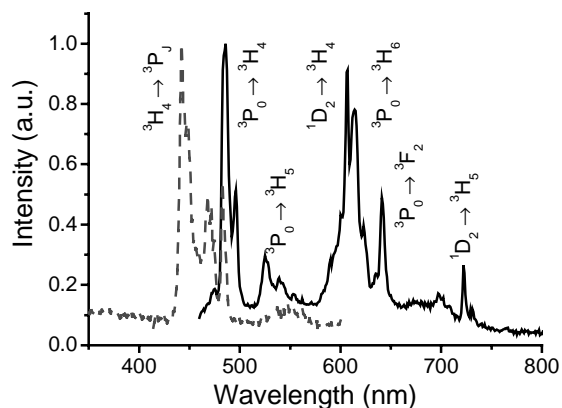


Figure 5.9 Excitation (dashed line) and VIS emission spectrum (solid line) of $\text{LaPO}_4:\text{Pr}$ in CD_3OD solution. Excitation spectrum: λ_{em} 620 nm, emission spectrum: λ_{exc} 442 nm.

5.2.3 NIR luminescence

Although the luminescence of the visible emitting doped particles is interesting because of the characterization of the material and possible applications like lighting and displays, the main interest in this thesis is NIR emission that is being used in telecommunication. In this section, the luminescence of redispersible nanoparticles in the NIR region is reported. For that reason, the particles were doped with Nd^{3+} , Er^{3+} , and Pr^{3+} ions.

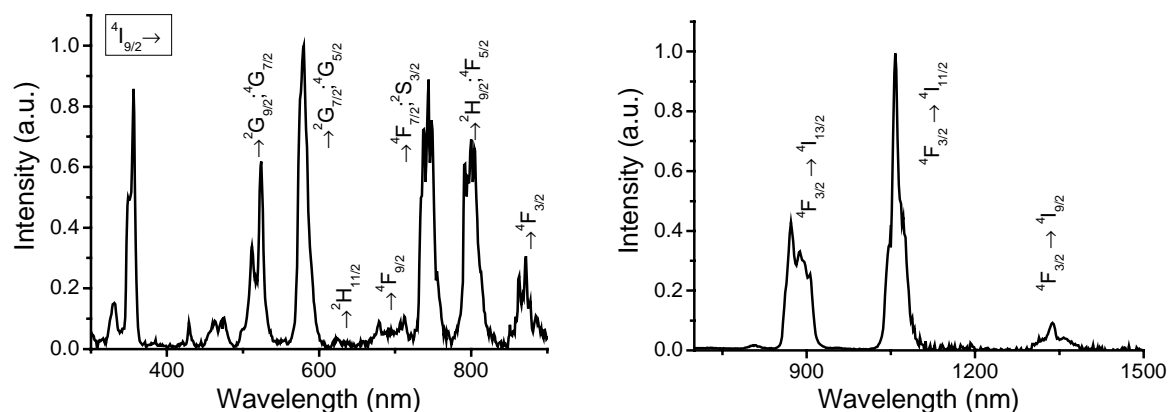


Figure 5.10 Excitation (left) and NIR emission spectra (right) of $\text{LaPO}_4:\text{Nd}$ in CD_3OD solution. Excitation spectrum: λ_{em} 1066 nm, emission spectrum: λ_{exc} 515 nm (Ar^+ ion laser).

The excitation and emission spectra of $\text{LaPO}_4:\text{Nd}$ are plotted in Figure 5.10. The excitation spectrum was recorded by exciting a sample with a Xe arc lamp and detecting the emission at 1066 nm with a Ge detector. The emission spectrum was measured by exciting a sample in CD_3OD with an Ar^+ ion laser operating at 515 nm, the $4\text{I}_{9/2} \rightarrow 2\text{G}_{7/2}$, $4\text{G}_{5/2}$ transition of Nd^{3+} . The

excitation spectrum of $\text{LaPO}_4:\text{Nd}$ in Figure 5.10 exhibits the typical lines of Nd^{3+} . The emission spectrum of $\text{LaPO}_4:\text{Nd}$ shows the Nd^{3+} transitions at 880, 1060, and 1330 nm (${}^4\text{F}_{3/2} \rightarrow {}^4\text{I}_{9/2}$, ${}^4\text{F}_{3/2} \rightarrow {}^4\text{I}_{11/2}$, and ${}^4\text{F}_{3/2} \rightarrow {}^4\text{I}_{13/2}$, respectively). The luminescence of $\text{LaPO}_4:\text{Er}$ is reported in Figure 5.11, the excitation spectrum was collected by measuring the Er^{3+} emission at 1536 nm, the emission spectrum by exciting Er^{3+} at 488 nm, the ${}^4\text{I}_{15/2} \rightarrow {}^4\text{F}_{7/2}$ transition.

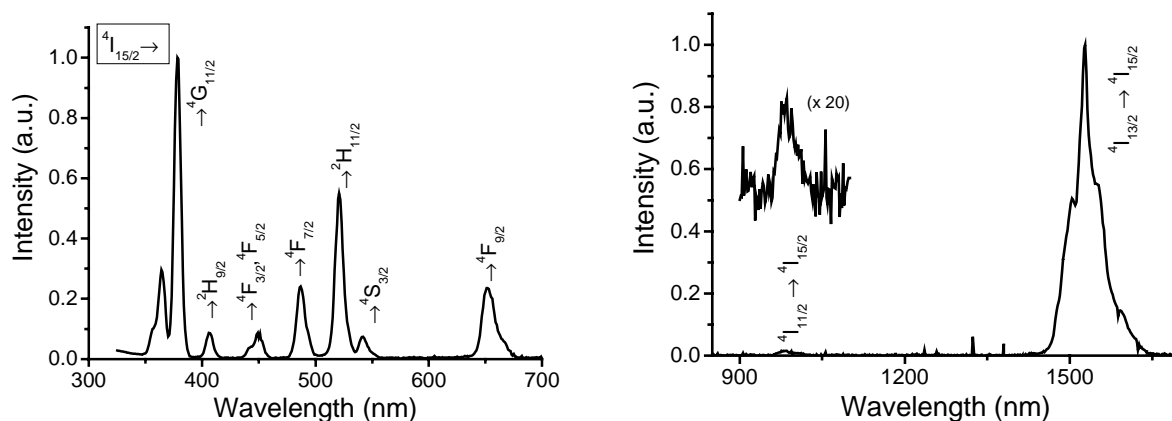


Figure 5.11 Excitation (left) and NIR emission spectra (right) of $\text{LaPO}_4:\text{Er}$ in CD_3OD solution. Excitation spectrum: λ_{em} 1536 nm, emission spectrum: λ_{exc} 488 nm (Ar^+ ion laser).

Upon excitation at 488 nm a luminescent peak at 1528 nm was observed (${}^4\text{I}_{13/2} \rightarrow {}^4\text{I}_{15/2}$) with shoulders at 1503, 1546, and 1590 nm. Another, much smaller emission peak was found at 981 nm, ascribed to the ${}^4\text{I}_{11/2} \rightarrow {}^4\text{I}_{15/2}$ transition of Er^{3+} .⁴⁵

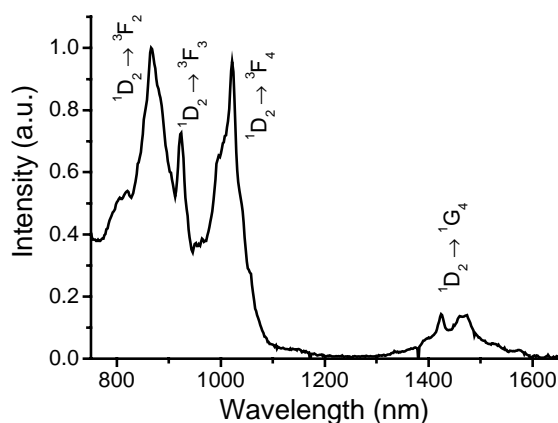


Figure 5.12 NIR emission spectrum of $\text{LaPO}_4:\text{Pr}$ in CD_3OD solution, λ_{exc} 476 nm (Ar^+ ion laser).

The emission spectrum of $\text{LaPO}_4:\text{Pr}$ in the NIR was obtained by exciting the sample with an Ar^+ ion laser at 476 nm and is depicted in Figure 5.12. The NIR spectrum of $\text{LaPO}_4:\text{Pr}$

exhibits a number of transitions between 800 and 1100 nm of the $^1D_2 \rightarrow ^3F_J$ ($J = 2, 3, 4$) transitions and a broad peak between 1400 nm and 1550 nm attributed to the $^1D_2 \rightarrow ^1G_4$ transition. With the lanthanide(III) ions Nd^{3+} , Er^{3+} , and Pr^{3+} the spectral region from 1300 nm to 1650 nm, which is of particular interest for telecommunication applications,⁴⁶ can thus be covered completely.

Luminescent lifetimes were determined by collecting the decay of the luminescence intensity of the strongest intensities of the luminescence spectra after excitation with the same Ar^+ ion laser lines as above, i.e. 515 nm for $LaPO_4:Nd$, 488 nm for $LaPO_4:Er$, and 476 nm for $LaPO_4:Pr$. The lifetimes of the Nd^{3+} doped particles were determined in solvents with varying deuteration grade: methanol, methanol- d_1 , and in methanol- d_4 , because the higher the deuteration grade, the lower the quenching will be.

Table 5.3 Luminescent lifetimes of $LaPO_4:Ln$, fitting according to Eq. 5.3.

Particle	Medium	$\lambda_{em}/\lambda_{exc}$ (nm)	Transition	τ_R (μs)	C (s^{-1})	τ_{ave} (μs)
$LaPO_4:Nd$	CH_3OH	514/880	$^4F_{3/2} \rightarrow ^4I_{9/2}$	84	2360	17
$LaPO_4:Nd$	CH_3OD	514/880	$^4F_{3/2} \rightarrow ^4I_{9/2}$	93	568	38
$LaPO_4:Nd$	CD_3OD	514/880	$^4F_{3/2} \rightarrow ^4I_{9/2}$	92	330	46
$LaPO_4:Er$	CD_3OD	488/1536	$^4I_{13/2} \rightarrow ^4I_{15/2}$	364	4.9	308
$LaPO_4:Pr$	CD_3OD	476/868	$^1D_2 \rightarrow ^3F_2$	11	8300	3.2

All decay traces measured could be fitted with the quenching model described for the Eu^{3+} luminescence in Appendix A, the results are summarized in Table 5.3. The decay curves of the Nd^{3+} doped particles in methanol with different deuteration grades gave excellent fits with a lifetime τ_R of about 90 μs for all particles and a quenching factor C that decreases with increasing deuteration grade: 2360 s^{-1} in methanol, 568 s^{-1} in methanol- d_1 , and 330 s^{-1} in methanol- d_4 . This is reflected in the averaged lifetimes over the whole particle: 17 μs , 38 μs , and 46 μs , respectively. All the luminescent lifetimes found are much higher, up to factors 100-1000, than those in solution or in organic complexes.⁴⁷ Other quenching mechanisms, such as the P-O vibration of the matrix, than solvent quenching may still be present and are incorporated in τ_R . The real radiative lifetimes of Nd^{3+} is reported to be in the order of 250-400 μs , that of Er^{3+} in the order of 8,000-20,000 μs . A simple calculation shows that the highest luminescent quantum yields ($\phi_{Ln} = \tau_{obs}/\tau_{rad}$) for the $LaPO_4:Ln$ particles are about 15% for both the Nd^{3+} - and the Er^{3+} -

doped particles. The luminescence lifetime of the Pr^{3+} -doped particles was much shorter. This was expected because the luminescence of Pr^{3+} is very sensitive to the environment because of various quenching mechanisms of the Pr^{3+} luminescence.⁴⁸

The luminescence of the Nd^{3+} -doped particles was compared with the luminescence of $\text{Nd}(\text{NO}_3)_3$ in methanol- d_4 and in DMSO- d_6 . Previously, Beeby and Faulkner reported the luminescent lifetime of that salt in solution.⁴⁹ These lifetimes and that of $\text{LaPO}_4:\text{Nd}$ and the relative luminescence intensities are reported in Table 5.4.

Table 5.4 Relative quantum yields of $\text{LaPO}_4:\text{Nd}$ in CD_3OD versus $\text{Nd}(\text{NO}_3)_3$ in DMSO- d_6 and CD_3OD .

Nd^{3+}	τ (μs)	$\tau_{\text{rel, CD3OD}}$	I/I_{CD3OD}	$\tau_{\text{rel, DMSO}}$	I/I_{DMSO}
CD_3OD	0.48	1	1	0.053	0.063
DMSO- d_6	9.02	19	16	1	1
$\text{LaPO}_4:\text{Nd}$	47	98	98	6.0	6.1

It can be seen that the (averaged) luminescent lifetime of $\text{LaPO}_4:\text{Nd}$ is enhanced to the same extent as the luminescence intensity. Comparing the luminescence of the nanoparticles in CD_3OD with that of the salt in CD_3OD , it is clear that the luminescence lifetime and quantum yield is enhanced by a factor of 100, proving that the ions are inside the particles and that the shielding by the particle to the solvent is very effective. Slight differences are due to variations in the radiative lifetime of Nd^{3+} in the three different environments.⁴¹

As an illustration of the processability, the $\text{LaPO}_4:\text{Nd}$ nanoparticles were incorporated in a polymer matrix on a quartz substrate. A solution of 0.9 g poly(methylmethacrylate) (PMMA) in 5 ml methylethylketone was mixed with a dispersion of 0.1 g of the dry nanoparticles (Nd^{3+} doped) in 5 ml methanol. Spincoating of this colloidal dispersion on the substrates gave transparent films of about 1 μm thickness (determined with DEK-TAK surface profiler). The neodymium ion concentration in this layer is about 10^{19} cm^{-3} . The only difference in the emission spectrum with that taken in CD_3OD solution is caused by absorption of part of the 1330 nm transition by C-H vibrations in the polymer matrix.

5.3 Conclusions

In conclusion, LnPO_4 particles that are small (5-7 nm) and redispersible in organic solution have been prepared. These particles were doped with lanthanide ions that emit visible (Eu^{3+} and

Pr³⁺) and near-infrared (Pr³⁺, Nd³⁺, and Er³⁺) light. The visible luminescence of Eu³⁺ was used to characterize the particles and it was found that the luminescent properties are similar to that in the bulk materials. Luminescent lifetimes of the emitting ions, both VIS and NIR, were found not to be mono-exponential. A procedure was developed that fits the decay traces with a model with the quenchers at the surface of a particle. This procedure gave good results, although different quenching modes than the solvent quenching at the surface may still be active. The luminescent lifetimes of the NIR-emitting lanthanide(III) ions are up to the millisecond region (Er³⁺), which is a 1000 fold higher than in organic complexes. The luminescent quantum yield and the luminescent lifetime of the Nd³⁺ doped particles were found to be a factor 100 higher than of Nd³⁺ ions in per-deuterated methanol solution. Furthermore, the particles have good processability and thus they possess the possibility to be incorporated in polymer-based devices, such as optical amplifiers and lasers.

5.4 Experimental

Photoluminescence in the visible region was measured with an Edinburgh Instruments FS900 instrument with a 450 W Xe arc lamp as excitation source and a red sensitive, Peltier element cooled Hamamatsu R955 PMT. Decay curves in the visible (Eu³⁺ luminescence) were measured with an Edinburgh Instruments FL900 by exciting the samples with a microsecond flashlamp (Xe flash lamp). Decay traces were fitted with the software installed on the instrument (Edinburgh Instruments F900, version 6.2.2). Excitation spectra of the NIR emission were detected with the FS900 instrument, fitted with a 600 lines/mm monochromator grating, an optical chopper operating at 87 Hz to mechanically modulate the emission signal, and a liquid nitrogen cooled ultra sensitive Edinburgh Analytical Instruments Ge detector, using standard lock-in techniques. Emission spectra and luminescence lifetimes in the NIR were measured by exciting the samples with a CW Ar⁺ ion laser operating at various wavelengths. The continuous light was modulated with an acousto-optic modulator and focused on the sample in 1×1×3.5 cm quartz cuvettes (Hellma, SQ series). The emitted signal was focussed with a 20 cm lens onto a monochromator and detected at the monochromator exit with a liquid nitrogen-cooled Ge detector (Northcoast) or a PMT for the spectral region between 700-1000 nm. All spectra were corrected for the instrument response. The NIR emission spectra were detected in two parts: up to 1100 nm with a red sensitive PMT (AgOCs), for higher wavelengths an ultra sensitive liquid nitrogen Ge detector was used. A total emission spectrum was reconstructed by scaling the two parts with the overlapping emission at 1066 nm.

5.5 References and notes

- ¹ Slooff, L. H.; Polman, A.; Klink, S. I.; Hebbink, G. A.; Grave, L.; van Veggel, F. C. J. M.; Reinhoudt, D. N.; Hofstraat, J. W. *Opt. Mater.* **2000**, *14*, 101.
- ² Booth, B. in *Polymers for lightwave and integrated optics*, Hornak, L. A. (Ed), Dekker, New York, 1992.
- ³ Hebbink, G. A.; Reinhoudt, D. N.; van Veggel, F. C. J. M. *Eur. J. Org. Chem.* **2001**, 4101.
- ⁴ Hasegawa, Y.; Ohkubo, T.; Sogabe, K.; Kwamura, Y.; Wada, Y.; Nakashima, N.; Yanagida, S. *Angew. Chem. Int. Ed.* **2000**, *39*, 357.
- ⁵ Slooff, L. H.; Polman, A.; Klink, S. I.; Grave, L.; van Veggel, F. C. J. M.; Hofstraat, J. W. *J. Opt. Soc. Am. B* **2001**, *18*, 1690.
- ⁶ Rambabu, U.; Buddhudu, S. *Opt. Mater.* **2001**, *17*, 401.
- ⁷ Slooff, L. H.; de Dood, M. J. A.; van Blaaderen, A.; Polman, A. *Appl. Phys. Lett.* **2000**, *76*, 3682.
- ⁸ Tissue, B. *Chem. Mater.* **1998**, *10*, 2837.
- ⁹ Slooff, L. H.; van Blaaderen, A.; Polman, A.; Hebbink, G. A.; Klink, S. I.; van Veggel, F. C. J. M.; Reinhoudt, D. N.; Hofstraat, J. W. *J. Appl. Phys.* **2002**, *91*, 3955.
- ¹⁰ Justel, T.; Nikol, H.; Ronda, C. *Angew. Chem. Int. Ed.* **1998**, *37*, 3085.
- ¹¹ a) Miniscalco, W. J. *J. Lightwave Tech.* **1991**, *9*, 234-250; b) Kik, P. G.; Polman, A. *M. R. S. Bull.* **1998**, *23*, 48.
- ¹² a) Kohls, M.; Schmidt, T.; Katschorek, H.; Spanhel, L.; Müller, G.; Mais, N.; Wolf, A.; Forchel, A. *Adv. Mater.* **1999**, *11*, 288; b) Bender, C. M.; Burlitch, J. M.; Barber, D.; Pollock, C. *Chem. Mater.* **2000**, *12*, 1969; c) St. John, J.; Coffey, J. L.; Chen, Y.; Pinizzotto, R. F. *J. Am. Chem. Soc.* **1999**, *121*, 1888.
- ¹³ Williams, D. K.; Bihari, B.; Tissue, B. M. *J. Phys. Chem. B* **1998**, *102*, 916.
- ¹⁴ Tallant, D. R.; Seager, C. H.; Simpson, R. L. *J. Appl. Phys.* **2002**, *91*, 4053.
- ¹⁵ Bol, A. A.; van Beek, R.; Meijerink, A. *Chem. Mater.* **2002**, *14*, 1121.
- ¹⁶ Bender, C. M.; Burlitch, J. M.; Barber, D.; Pollock, C. *Chem. Mater.* **2000**, *12*, 1969.
- ¹⁷ a) Krupke, W. F. *Phys. Rev.* **1966**, *145*, 325; b) Sarantopoulou, E.; Kollia, Z.; Cefalas, A. C. *Opt. Mater.* **2001**, *18*, 23.
- ¹⁸ Tanabe, S.; Hayashi, H.; Hanada, T.; Onodera, N. *Opt. Mater.* **2002**, *19*, 343.
- ¹⁹ Harrison, M. T.; Kershaw, S. V.; Burt, M. G.; Rogach, A. L.; Kornowski, A.; Eychmüller, A.; Weller, H. *Pure Appl. Chem.* **2000**, *72*, 295.
- ²⁰ V. I. Klimov, A. A. Mikhailovsky, S. Xu, A. Malko, J. A. Hollingsworth, C. A. Leatherdale, H. J. Eisler, M. G. Bawendi, *Science* **2000**, *290*, 314.
- ²¹ Huignard, A.; Gacoin, T.; Boilot, J. -P. *Chem. Mater.* **2000**, *12*, 1090.
- ²² Riwotzki, K.; Haase, M. *J. Phys. Chem. B* **2001**, *105*, 12709.
- ²³ Haase, M.; Riwotzki, K.; Meysammy, H.; Kornowski, A. *J. All. Compounds* **2000**, *303-304*, 191.

- ²⁴ Riwotzki, K.; Haase, M. *J. Phys. Chem. B* **1998**, *102*, 10129.
- ²⁵ Meyssamy, H.; Riwotzki, K.; Kornowski, A.; Naused, S.; Haase, M. *Adv. Mater.* **1999**, *11*, 840.
- ²⁶ Riwotzki, K.; Meyssamy, H.; Kornowski, A.; Haase, M. *J. Phys. Chem. B* **2000**, *104*, 2824.
- ²⁷ Riwotzki, K.; Meyssamy, H.; Schnablegger, H.; Kornowski, A.; Haase, M. *Angew. Chem. Int. Ed.* **2001**, *40*, 573.
- ²⁸ Blasse, G.; Grabmaier, B. C. *Luminescent materials* Springer Verlag, Berlin, 1994.
- ²⁹ Lide, D. R. (Ed.) *Handbook of chemistry and physics*, 76th edition, CRC press, New York, 1996.
- ³⁰ a) van Pieterse, L.; Meijerink, A. *J. Alloys Comp.* **2000**, *300-301*, 426; b) van Pieterse, L.; Heeroma, M.; de Heer, E.; Meijerink, A. *J. Lumin.* **2000**, *91*, 177.
- ³¹ Stein, G.; Würzberg, E. *J. Phys. Chem.* **1975**, *62*, 208.
- ³² Carnall, W. T.; Goodman, G. L.; Rajnak, K.; Rana, R. S. *J. Chem. Phys.* **1989**, *90*, 3443.
- ³³ Stouwdam, J. W.; van Veggel, F. C. J. M. *Nano Letters* **2002**, *in press*.
- ³⁴ Scattering of light by these kind of small particles will be minimal as illustrated by the fact that Rayleigh scattering is dependent on the particle radius versus the wavelength of the light to power four. With the particle radius below 5 nm and light wavelength above 1000 nm (the NIR region) scattering will be very low.
- ³⁵ *Gmelin's Handbuch der Anorganischen Chemie*, 8. Auflage, *Phosphor Teil A*, Verlag, Weinheim, 1965, p 251.
- ³⁶ Antic-Fidancev, E.; Hölsä, J.; Lemaitre-Blaise, M.; Porcher, P. *J. Phys. Condens. Matter* **1991**, *3*, 6829.
- ³⁷ Dexpert-Ghys, J.; Mauricot, R.; Faucher, M. D. *J. Lumin.* **1996**, *69*, 203.
- ³⁸ Morrison, C. A. and Leavitt R. P. in *Handbook on the physics and chemistry of rare earths*, volume 5, Gschneider, K. A.; Eyring, L. (ed.), North Holland Publishing company, Amsterdam, 1982.
- ³⁹ a) Oude Wolbers, M. P.; van Veggel, F. C. J. M.; Snellink-Ruël, B. H. M.; Hofstraat, J. W.; Geurts, F. A. J.; Reinhoudt, D. N. *J. Am. Chem. Soc.* **1997**, *119*, 138; b) Oude Wolbers, M. P.; van Veggel, F. C. J. M.; Snellink-Ruël, B. H. M.; Hofstraat, J. W.; Geurts, F. A. J.; Reinhoudt, D. N. *J. Chem. Soc. Perkin Trans. 2* **1998**, 2141.
- ⁴⁰ a) Werts, M. H. V.; Jukes, R. T. F.; Verhoeven, J. W. *Phys. Chem. Chem. Phys.* **2002**, *4*, 1542-1548; b) Werts, M. H. V. *Luminescent Lanthanide Complexes* PhD thesis, University of Amsterdam, 2000.
- ⁴¹ Judd, B. R. *Phys. Rev.* **1962**, *127*, 750.
- ⁴² Ofelt, G. S. *J. Chem. Phys.* **1962**, *37*, 511.
- ⁴³ Klink, S. I.; Hebbink, G. A.; Grave, L.; Oude Alink, P. G. B.; van Veggel, F. C. J. M.; Werts, M. H. V. *J. Phys. Chem. A* **2002**, *106*, 3681.
- ⁴⁴ Voloshin, A. I.; Shavaleev, N. M.; Kazakov, V. P. *J. Lumin.* **2001**, *93*, 199.

- ⁴⁵ Luminescence in the visible region of the emission spectrum was not observed, although this is in principle possible from higher excited states of Er^{3+} via internal conversion from the ${}^4\text{I}_{15/2} \rightarrow {}^4\text{F}_{7/2}$ level or via upconversion mechanisms.
- ⁴⁶ Amplification around 1.33 μm with Nd^{3+} (${}^4\text{F}_{3/2} \rightarrow {}^4\text{I}_{13/2}$ transition): Jaque, D.; Enguita, O.; García Solé, J.; Jiang, A. D.; Luo, Z. D. *Appl. Phys. Lett.* **2000**, *76*, 2176; and with Pr^{3+} (${}^1\text{G}_4 \rightarrow {}^3\text{H}_5$ transition): Nishida, Y.; Yamada, M.; Kanamori, T.; Kobayashi, K.; Temmyo, J.; Sudo, S.; Ohishi, Y. *IEEE J. Quantum Elec.* **1998**, *34*, 1332. Amplification around 1.4 μm with Pr^{3+} (${}^1\text{D}_2 \rightarrow {}^1\text{G}_4$ transition), emission in the S-band in telecommunication and amplification around 1.53 μm with Er^{3+} (${}^4\text{I}_{13/2} \rightarrow {}^4\text{I}_{15/2}$ transition): see ref 11 and Wilkinson, J. S.; Hempstead, M. *Curr. Opin. Solid State Mat. Sci.* **1997**, *2*, 194.
- ⁴⁷ Ermolaev, V. L.; Sveshnikov, E. B. *Russ. Chem. Rev.* **1994**, *63*, 905.
- ⁴⁸ Nishida, Y.; Yamada, M.; Kanamori, T.; Kobayashi, K.; Temmyo, J.; Sudo, S.; Ohishi, Y. *IEEE J. Quantum Elec.* **1998**, *34*, 1332.
- ⁴⁹ Beeby, A.; Faulkner, S. *Chem. Phys. Lett.* **1997**, *266*, 116.

Fitting of the luminescence decay curves with an ‘onion shell’ model

5.A.1 Model description

A model was developed in which a particle consists of a series of shells, such as an onion. A schematic presentation is depicted in Figure 5.A.1 with one subshell “i” gray.

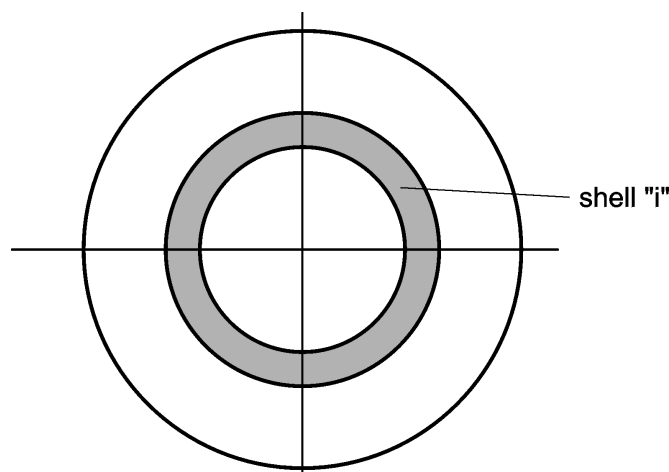


Figure 5.A.1 2D-representation of a particle with subshells.

The decay curves were fitted to the formula in Eq. 5.A.1. This model describes the particles as monodisperse particles, with each particle subdivided in 10 shells of equal volume. These shells have equal volume in order to give each luminescent ion equal weight in the fitting, with the assumption that the emissive ions are randomly distributed in the particles.

$$\frac{I_t}{I_0} = \sum_{i=1}^{10} \frac{1}{10} e^{-k_i t}; \quad k_i = \frac{1}{\tau_i} = k_R + C \times f_{q,i} \quad \text{Eq. 5.A.1}$$

According to Eq. 5.A.1, the normalized intensity (I_t/I_0) at time t is equal to the sum of the individual exponential decays of each shell. The rate constants (k_i or lifetime $\tau_i = 1/k_i$) in these exponentials are related to each other by the rate constant in absence of quenching (k_R) and the quenching factor $C \times f_{q,i}$ with quenchers located outside a particle. C is a fit parameter that is dependent on the individual ion, the size and size distribution of the particles, and on the strength of the quenching. The other parameter $f_{q,i}$ relates the quenching in each subshell to that in the other shells (*vide infra*).

5.A.2 Distance dependence of the quenching, the $f_{q,i}$ factor

The quenching of the ions inside the particle by quenchers outside a particle is regarded to take place via a dipole-dipole interaction type of mechanism, which results in quenching in a distance dependence to the power -6 .¹ The solvent molecules that are outside the particle cause the quenching. The total quenching should be integrated over the total volume outside the particles, according to Eq. 5.A.2. In this equation, $f_{q,i}$ is the quenching factor for a given shell, r the distance of that shell to a volume fraction dV . Integration over the total volume gives the total quenching factor $f_{q,i}$.

$$f_{q,i}(a) = \int_V r^{-6} dV \quad \text{Eq. 5.A.2}$$

This equation was solved for a particle shell i with luminescent center A by varying the radius r . Then three domains are found: first, a domain with every circle with radius r is inside the particle ($r < R-A$), second, a domain where only part of a circle with radius r is outside the particle ($R-A < r < R+A$, see Figure 5.A.2), and third, a domain with every circle with radius r outside the particle ($r > R+A$).

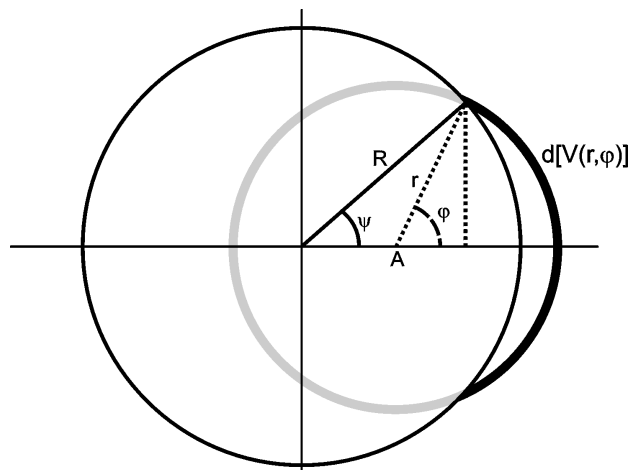


Figure 5.A.2 Definition of symbols used in the text in order to determine the quenching factor of a shell i at position A . In the model the quenching of the gray part of the shell is zero, i.e. this part is in the particle interior.

The fraction of a shell in the second domain that is outside the particle equals $2\pi r^2 (1 - \cos\phi)dr$. The volume fraction (dV) of a shell in the third domain is $4\pi r^2 dr$, multiplying this with r^{-6} and integrating this from $r = (R+A)$ to ∞ , results in $4/3\pi(R+A)^{-3}$ (Eq. 5.A.3). Dividing by the

particle radius R normalizes all these formulas. Therefore, the real particle radius will be present in the fit factor C .

$$f_{q,i}(A,\varphi) = \int_V r^{-6} dV = \int_{R-A}^{R+A} \frac{1}{r^6} 2\pi r^2 (1 - \cos\varphi) dr + \int_{R+A}^{\infty} \frac{1}{r^6} 4\pi r dr \quad \text{Eq. 5.A.3}$$

In Table 5.A.1 the quenching factor $f_{q,i}$ was calculated for ten subshells and with $a (=A/R)$ calculated as the center of each subshells, such that each shell contains 1/10 of the total volume of the particle.

Table 5.A.1 Quenching factor $f_{q,i}$ for all 10 subshells.

shell "i"	a(i)	$f_{q,i}$ (a)
1	0.08	4.3
2	0.38	6.7
3	0.50	9.9
4	0.59	15
5	0.67	25
6	0.74	46
7	0.81	99
8	0.87	2.8×10^2
9	0.92	1.3×10^3
10	0.98	4.0×10^4

5.A.3 Fitting of $\text{LaPO}_4:\text{Eu}$

In Figure 5.A.4 the decay of $\text{LaPO}_4:\text{Eu}$ is fitted with the onion shell model. This fit was obtained with $\tau_R = 1/k_R = 6.3$ ms and $C = 1.4 \times 10^{-4} \text{ ms}^{-1}$. This resulted in an averaged lifetime of 5.2 ms over the whole particle and a lifetime distribution over the particle as shown in Figure 5.A.4. From the lifetime distribution over the particle (Figure 5.A.3) it is found that there is only quenching close to the edge of the particle.

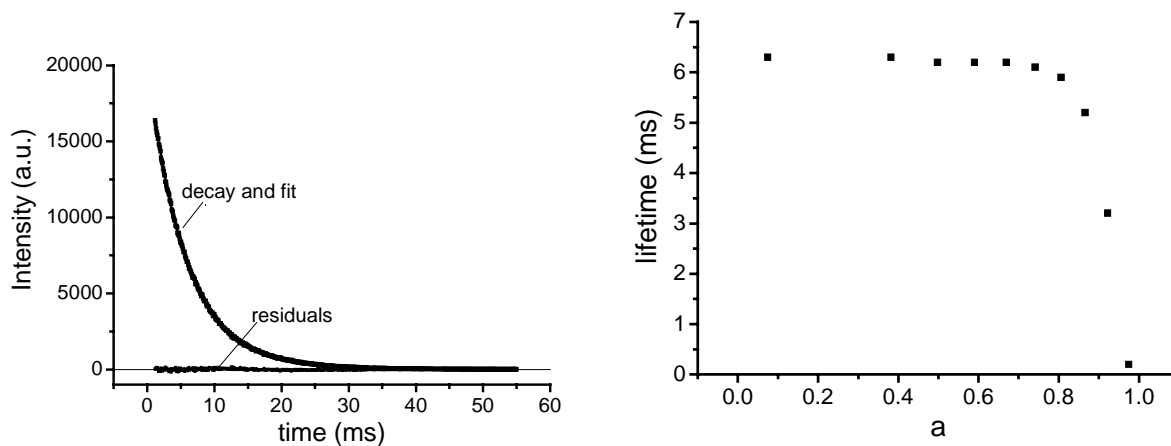


Figure 5.A.3 Left: decay of LaPO₄:Eu in CH₃OH, fitted with the model described in this Appendix. Right: lifetime distribution over the particle axis of LaPO₄:Eu.

5.A.4 Reference

- ¹ Ermolaev, V. L.; Sveshnikov, E. B. *Russ. Chem. Rev.* **1994**, *63*, 905.

Chapter 6

*Light-emitting diodes doped with lanthanide(III) ion complexes**

In this Chapter the synthesis, photo-luminescence, and electro-luminescence of some new near-infrared emitting lanthanide complexes is described. The sensitizers with carbonyl groups have excellent sensitization properties and the remaining fluorescence in these complexes is very low. Two complexes, that have a sensitizer that absorb light in the visible region, were doped in polymer light-emitting diodes. Upon applying a bias over the devices, Nd³⁺-based near-infrared light was detected.

* Part of the work described in this Chapter was published: Slooff, L. H.; Polman, A.; Cacialli, F.; Friend, R. H.; Hebbink, G. A.; van Veggel, F. C. J. M.; Reinhoudt, D. N. *Appl. Phys. Lett.* **2001**, 78, 2122-2124.

6.1 Introduction

Nowadays more and more research is being focussed on light-emitting diodes made of polymer materials.¹ These devices have great potential in commercial applications like lighting and displays. Recently, the first applications of organic light-emitting diodes became commercially available in car radios manufactured by Pioneer.² In general, a thin layer (typical < 100 nm) of organic material (polymers or low molecular weight organic molecules) is deposited onto an electrode. Subsequently, a counter-electrode is deposited on top of the organic material. Transparent indium tin oxide (ITO) on glass substrates is commonly used as the anode, because of the high work function, and a low work function metal like aluminum or calcium is usually employed as cathode. A schematic picture of such a device is depicted in Figure 6.1.

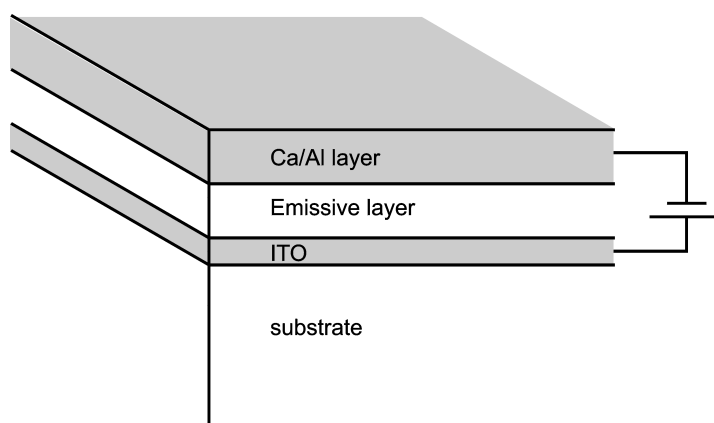


Figure 6.1 Schematic representation of a light-emitting diode.

Charges are injected into the organic material at the interfaces of the electrodes when a bias is applied.³ Holes, positive charges, are injected from the anode into the HOMO of the organic material and electrons are injected from the cathode into the LUMO. Upon migration of the charges, driven by the electrical field ($> 10^8$ V/m), by charge hopping from molecule to molecule or over polymer chains, they may recombine at some point into a bound hole-electron pair, also called an exciton, and an excited state is formed on the emissive material that can lead to luminescence. Both singlet and triplet states are formed in electro-luminescence (EL) operation because of the spin statistics of the charge carriers.⁴⁵ A lot of research effort is conducted in finding ways to exploit the triplet states formed,⁶ because triplet emission is in general very inefficient.⁷ A way to “harvest” these triplet states is the use of sensitizer functionalized lanthanide ion complexes. In general the triplet state of the sensitizer is the donating level of the excitation energy to the lanthanide ion.⁸ A Jablonski diagram of the (photo-luminescence) excitation of a lanthanide ion is depicted in Figure 6.2. Upon excitation of a

sensitizer and intersystem crossing the energy is transferred to the lanthanide ion. Also singlet state sensitization is a possibility,^{9,10} but this is not commonly observed because of a lower transfer probability.¹¹ Competing processes in the sensitization of lanthanide ions are singlet emission (fluorescence), triplet emission (phosphorescence), and non-radiative decay from both singlet and triplet states.

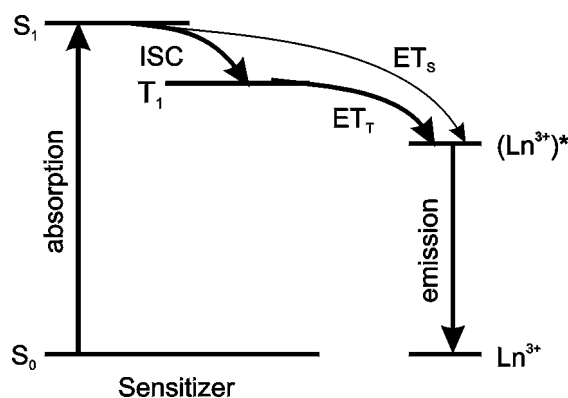


Figure 6.2 Jablonski diagram for the sensitization of lanthanide ions.

Gillin *et al.* reported near-infrared (NIR) emitting light-emitting diodes with the Er^{3+} or Nd^{3+} complexes of the anion of 8-hydroxyquinoline.¹² These complexes were evaporated onto ITO, with aluminum as the counter electrode. Yanagida *et al.* reported the fabrication of light-emitting diodes with β -diketonate complexes of Nd^{3+} , Er^{3+} , and Yb^{3+} sublimated on ITO substrates.¹³ Electro-luminescence in the NIR was observed in these OLEDs (organic light-emitting diodes) with relatively low external efficiencies in the order of 10^{-4} - 10^{-5} .

In this Chapter, the electro-luminescence (EL) of **1.Nd** and **3.Nd** is described of doped polymer light-emitting diodes (PLEDs). First the synthesis and the photo-luminescence (PL) properties in solution of the complexes **1.Ln**, **2.Ln**, and **3.Ln** is described. Subsequently, the electrochemical properties of **2.Ln** and **3.Ln** will be discussed in order to select the proper host material for the preparation of EL devices. Finally, the electro-luminescent properties of **1.Nd** and **3.Nd** will be dealt with. Complex **4.Nd** does not contain an additional sensitizer and was used as a reference material. The synthesis and PL in solution of **1.Nd** and **4.Nd** has been reported previously by our group.^{14,15} Complex **1.Nd** was chosen as sensitizer because it is a relatively efficient sensitizer of Nd^{3+} luminescence. Fluorenone (**2.Ln**) and naphthone (**3.Ln**) were used because of their high intrinsic intersystem crossing quantum yields which will give less remaining fluorescence in the visible region.

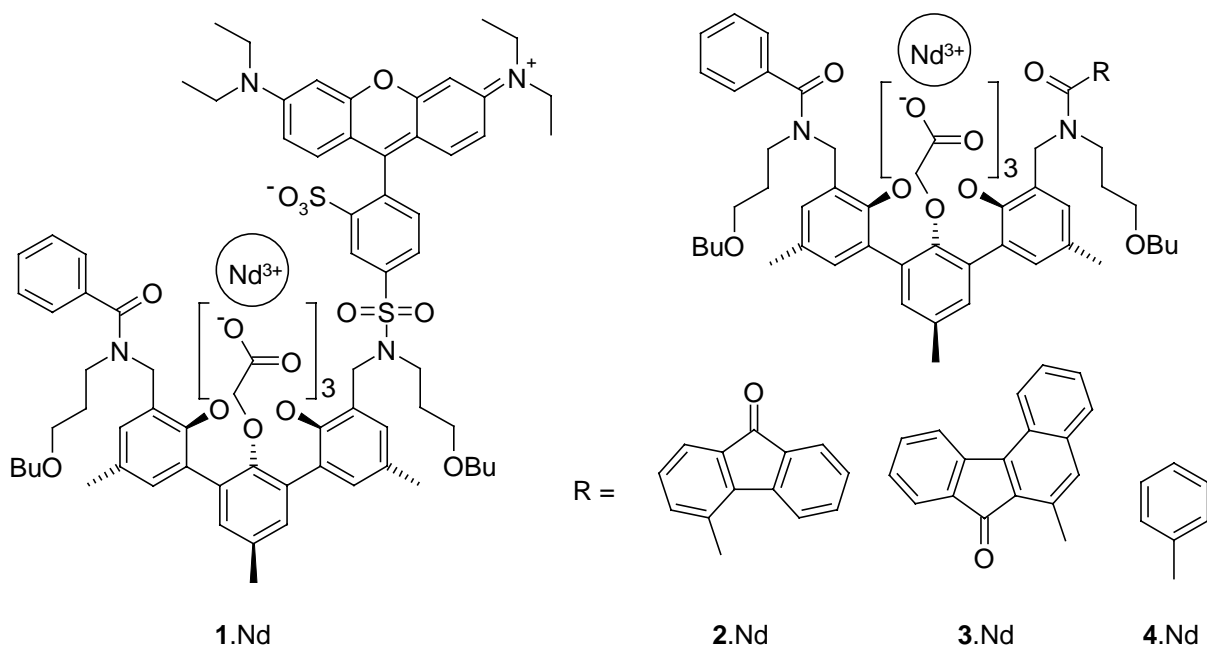
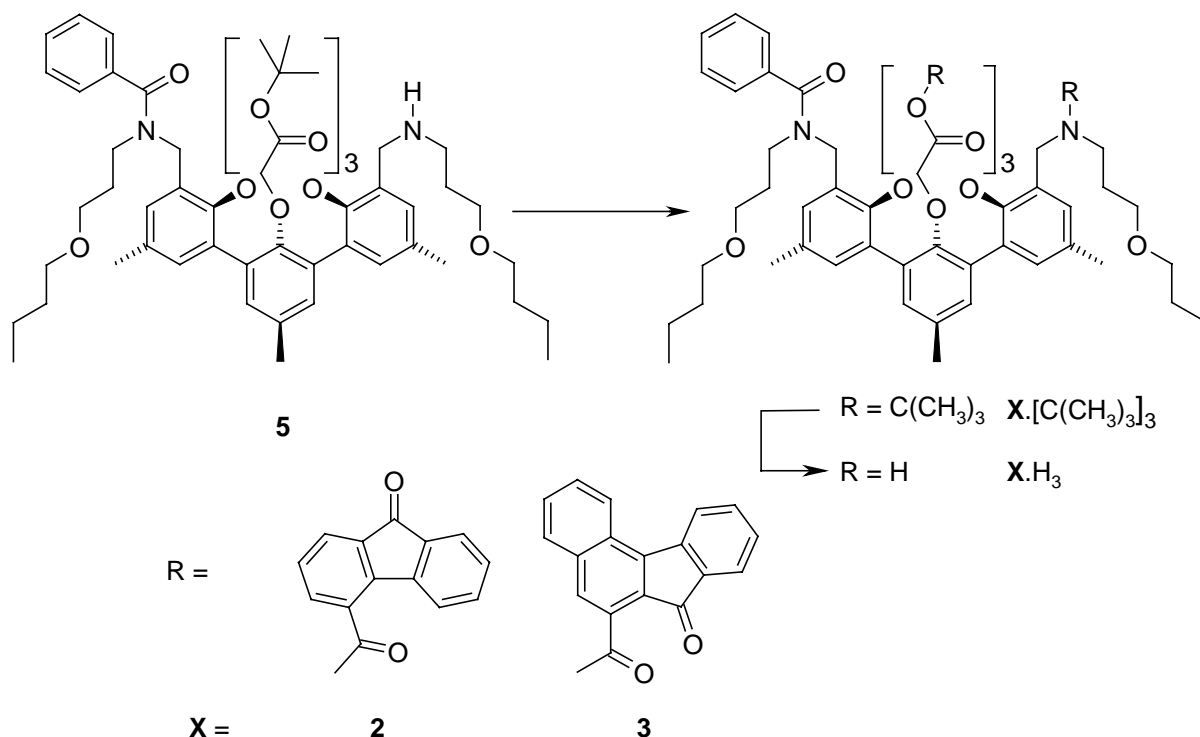


Figure 6.3

6.2 Results and discussion

6.2.1 Synthesis

The synthesis of complexes **2.Ln** and **3.Ln** is outlined in Scheme 6.1, the synthesis of **1.Nd** and **4.Nd** has been described previously. Compound **2**.[C(CH₃)₃]₃ was obtained by reacting monoamine **5** with 9-fluorenone-4-carbonyl chloride, in 75% yield. Hydrolysis of **2**.[C(CH₃)₃]₃ to **2**.H₃ was performed in pure TFA. Monoamine **5** was functionalized with naphthone acid,¹⁶ via a standard peptide coupling with HBTU and DIPEA, giving **3**.[C(CH₃)₃]₃ in 45% yield. The orange **3**.[C(CH₃)₃]₃ was hydrolyzed quantitatively to **3**.H₃ at room temperature by stirring it in pure TFA. The lanthanide ion complexes of **2**.H₃ and **3**.H₃ were prepared from the lanthanide nitrate salts (Er³⁺, Yb³⁺, Gd³⁺, and Nd³⁺). Since Gd³⁺ cannot accept energy from the sensitizers and does not emit in the NIR this ion is used as model in order to determine the luminescence properties in the presence of a lanthanide ion, but in absence of energy transfer. Complex formation was confirmed by mass spectrometry (FAB), from the mass and the isotope pattern corresponding to the complex. FT-IR spectroscopy showed a peak at 1,600 cm⁻¹ which indicates the presence of carboxylates (see Table 6.5 in the experimental section).



Scheme 6.1 Synthesis of the ligands, see the text for the synthetic details.

6.2.2 Luminescence in solution

Upon excitation of the lissamine sensitizer in **1.Nd** the characteristic Nd³⁺ luminescence was observed at 890 nm, 1066 nm, and 1330 nm with a luminescent lifetime of 1.1 μs in DMSO solution. The fluorescence of the lissamine sensitizer in the complex was significantly quenched to about 40% of that of the free ligand **1.H₃**.¹⁴

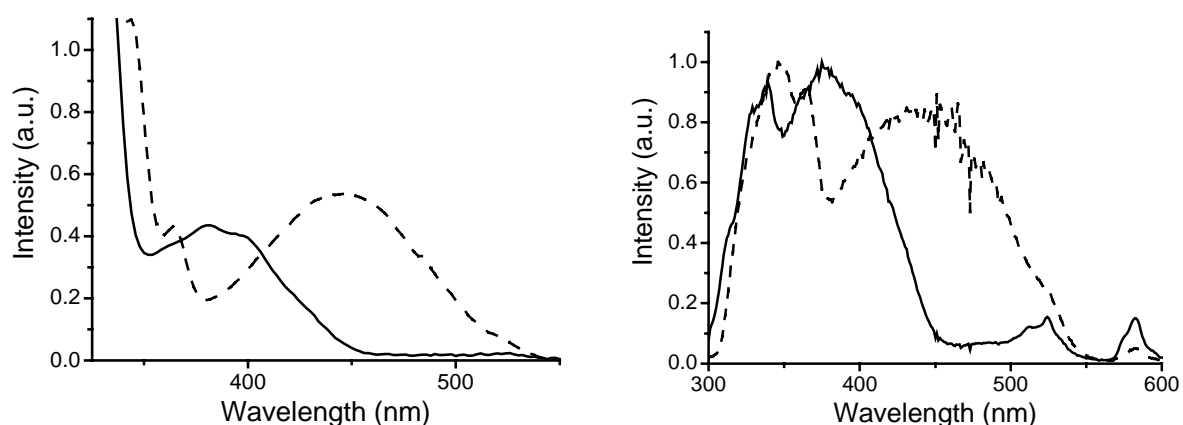


Figure 6.4 Left: absorption spectra of **2.Nd** (solid line), and **3.Nd** (dashed line). Right: excitation spectra of **2.Nd** (solid line) and **3.Nd** (dashed line), emission detected at 1066 nm.

The absorption and excitation spectra of **2.Nd** and of **3.Nd** depicted in Figure 6.4 have a maximum at 400 nm ($250 \text{ l}\times\text{mol}^{-1}\times\text{cm}^{-1}$) and at 450 nm ($1,000 \text{ l}\times\text{mol}^{-1}\times\text{cm}^{-1}$), respectively. The excitation spectra in Figure 6.4 were detected by measuring the Nd^{3+} luminescence intensity at 1066 nm. These spectra closely resemble the absorption spectra, proving the sensitized emission by both fluorenone and naphthone. Besides the broad excitation maxima of the chromophores, maxima at 520 nm and 580 nm are present, due to direct excitation of Nd^{3+} . The excitation, fluorescence, and emission spectra in the near-infrared (NIR) of **3.Nd** are depicted in Figure 6.5. In the visible region, the broad luminescence of the naphthone sensitizer has a significant tail in the NIR. The quantum yield of this fluorescence is about 0.03. The three transitions of Nd^{3+} at 890 nm, 1066, and 1330 nm (${}^4\text{F}_{3/2}\rightarrow{}^4\text{I}_{9/2}$, ${}^4\text{I}_{11/2}$, ${}^4\text{I}_{13/2}$, respectively) in the NIR are present.

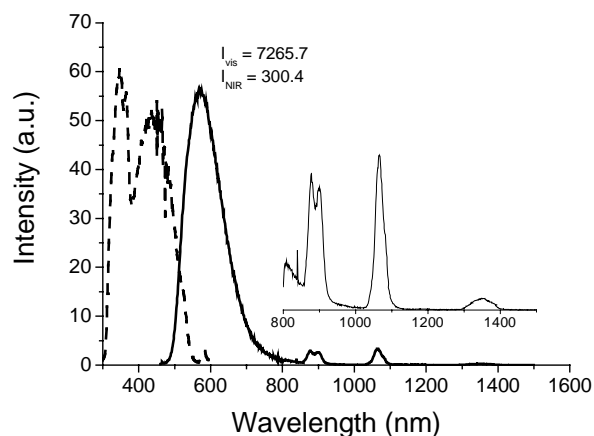


Figure 6.5 Excitation (dashed line) and emission (solid line) spectrum **3.Nd** in DMSO-d_6 . The inset shows a magnification (5 \times) of the NIR emission.

A number of properties of the luminescence of **3.Nd** in several solvents are summarized in Table 6.1, together with properties of the Gd^{3+} complex and of the free ligand. The solvents were chosen in order to find the effect of a range of different solvents. The fluorescence spectra of the Gd^{3+} complex and of the free ligand are similar to that of the Nd^{3+} complex, which proves that the lanthanide ions do not alter the sensitizers energetically. The fluorescence maximum of the sensitizer in **3.Nd** differed upon changing the solvent from toluene (570 nm) to DMSO (600 nm). There was also a difference in the fluorescence quantum yield in these solvents (1.8% in toluene and 0.2% in DMSO). The luminescence lifetimes in the visible are in the nanosecond regime (3.5 ns for **3.Nd** and 8.6 ns for **3.Gd**, in toluene). This reduction in fluorescence lifetime of the Nd^{3+} complex can be due to singlet energy transfer from the sensitizer to the lanthanide ion,

which is supported by the absence of oxygen quenching (*vide supra*) in **3.Nd**. However, the fluorescence observed is very weak, which makes it difficult to draw more definite conclusions.

Table 6.1 Luminescent properties of the **3.Ln**.

	solvent	$\phi_{\text{VIS}}^{\text{a}}$	τ_{VIS} (ns)	$\phi_{\text{NIR}}^{\text{c}}$	τ_{Nd} (μs)	$\phi_{\text{Nd}}^{\text{d}}$	$\eta_{\text{ET}} \times \phi_{\text{ISC}}^{\text{e}}$
3.Nd	toluene	1.8×10^{-2}	3.5	$\sim 1.2 \times 10^{-3}$	0.35	1.4×10^{-3}	0.86
3.Nd	CH_3OD	0.2×10^{-2}	5.6 ^b	$\sim 0.9 \times 10^{-3}$	0.67	2.8×10^{-3}	0.32
3.Nd	CH_2Cl_2	1.4×10^{-2}	nd	$\sim 0.5 \times 10^{-3}$	0.36	1.4×10^{-3}	0.36
3.Nd	$\text{DMSO-}d_6$	nd	nd	$\sim 0.7 \times 10^{-3}$	2.3	9.2×10^{-3}	0.76
3.Gd	toluene	3.8×10^{-2}	8.6	-	-	-	-
3.[(CH₃)₃]₃	toluene	3.7×10^{-2}	7.8	-	-	-	-

a Determined with $\text{Ru}(\text{bpy})_3$ in deoxygenated H_2O as a standard, which has $\phi = 0.042$ as quantum yield.¹⁷ Quantum

yield was calculated according: $\phi_{\text{u}} = \frac{n_{\text{u}}^2 A_{\text{Ru}} I_{\text{u}}}{n_{\text{Ru}}^2 A_{\text{u}} I_{\text{Ru}}} \phi_{\text{Ru}}$, with ϕ the quantum yield, n the refractive index of the

solution, A the absorption of the solution and, I the (integrated) intensity of the corrected emission spectra. The subscript 'u' stands for the unknown compound, 'Ru' for the standard (here $\text{Ru}(\text{bpy})_3$).

b Determined at 77 K in EtOH/MeOH 4:1 glass.

c Calculated by scaling the NIR intensity at 800 nm to the VIS intensity, versus the VIS luminescence quantum yield of the naphthone sensitizer (in toluene).

d $\phi_{\text{Nd}} = \tau_{\text{Nd}} / \tau_{\text{rad}}$; with τ_{rad} the (estimated) radiative lifetime of Nd^{3+} (in absence of quenchers).

e In case of triplet emission: $\eta_{\text{ET}} \times \phi_{\text{ISC}} = \phi_{\text{NIR}} / \phi_{\text{Nd}}$. In case of singlet energy transfer this column contains $\eta_{\text{ET}} = \phi_{\text{NIR}} / \phi_{\text{Nd}}$.

The quantum yields in the NIR were determined relative to the fluorescent quantum yields and are in the order of 0.1% and the highest in toluene. However, they are not very accurate because of the large difference between the emission of the Nd^{3+} and that of the reference. The luminescence lifetimes of the Nd^{3+} ions are in the microsecond region (0.35-2.3 μs), the highest in $\text{DMSO-}d_6$ because this solvent does not contain any quenching O-H, C-H, or O-D group. The luminescence efficiency of the lanthanide ions were calculated with a radiative lifetime of Nd^{3+} of 250 μs ¹⁸ ($\phi_{\text{Nd}} = \tau_{\text{Nd}} / \tau_{\text{rad}}$) and given in Table 6.1. The energy transfer efficiency ($\eta_{\text{ET}} = \phi_{\text{NIR}} / \phi_{\text{Nd}}$) is dependent on the solvent, as is the fluorescence of the sensitizer. The reason for the difference in the energy transfer efficiency could be due to structural variations in the complex. DMSO, which strongly coordinates to lanthanide ions, could "force" the sensitizer in such a

position that the distance between the sensitizer and the lanthanide ion is too large or the orientation such that there is a small orbital overlap of sensitizer and ion.

The emission spectra in the NIR part of the electromagnetic spectrum of **2.Nd** and of **3.Nd** are depicted in Figure 6.6. The Nd^{3+} spectra are identical, the main difference is the tail of the naphthone emission where there is hardly any fluorenone emission present in the NIR. This difference is explained by the fact that the fluorescence quantum yield of fluorenone is much lower than that of naphthone and that the fluorescence peak of fluorenone is not as broad as the naphthone fluorescence.

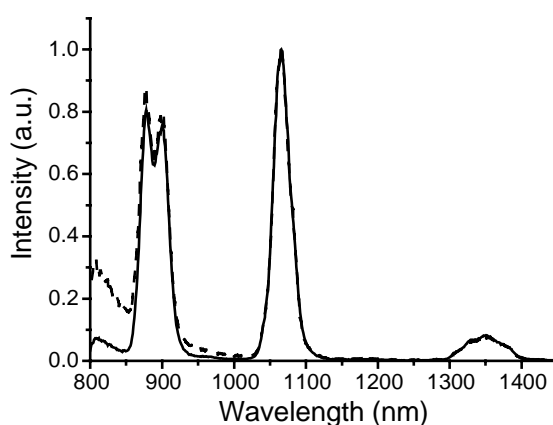


Figure 6.6 Emission spectra **2.Nd** (solid line, λ_{exc} 400 nm) and **3.Nd** (dashed line, λ_{exc} 450 nm) in DMSO-d_6 .

The luminescent lifetimes of the Nd^{3+} emission in various solvents are presented in Table 6.2.

Table 6.2 Luminescent lifetimes (of Nd^{3+} emission) of **2.Nd** in various solvents.

solvent	τ (μs)	$\Phi_{\text{Ln}}^{\text{a}}$	$\Phi_{\text{Ln, rel}}$
CHCl_3	0.39	1.6×10^{-3}	0.17
DMSO-d_6	2.3	9.2×10^{-3}	1.00
DMSO	1.5	6.0×10^{-3}	0.65
toluene	0.36	1.4×10^{-3}	0.15
CH_3OH	0.36	1.4×10^{-3}	0.15
CH_3OD	0.89	3.6×10^{-3}	0.39
CD_3OD	1.2	4.8×10^{-3}	0.52

a Determined according $\Phi_{\text{Ln}} = \tau_{\text{Nd}}/\tau_{\text{rad}}$, with $\tau_{\text{rad}} = 250 \mu\text{s}$.¹⁸

These are almost the same as of other *m*-terphenyl-based complexes. The longest lifetime, in DMSO-*d*₆ of 2.3 μs, corresponds to an estimated Nd³⁺ quantum yield of about 0.1%. The luminescent lifetime of **2.Nd** in solvents that do not coordinate to a lanthanide ion, i.e. chloroform and toluene, is the same as the lifetime in methanol (0.35 μs). From the luminescence properties of **4.Eu** it was found that in methanol the lanthanide ion is solvated by one methanol molecule.¹⁴ However, in solvents that do not coordinate, like chloroform and toluene, it is likely that the ion is hydrated, which explains the unexpected low lifetime in these solvents.

The luminescence intensities of **3.Nd** and **2.Nd** of the complexes in DMSO-*d*₆ and deoxygenated DMSO-*d*₆ are given in Table 6.3. The effect of oxygen provides information on the energy transfer rate, because molecular oxygen is a quencher of the triplet state of sensitizers. The oxygen quenching rate is in the order of 10⁷ s⁻¹ in a saturated DMSO solution.¹⁹

Table 6.3 Relative emission intensities of **3.Nd** and **2.Nd** in DMSO-*d*₆.

Complex	Rel. intensity ^a
3.Nd	1.00
3.Nd deoxygenated	1.00
2.Nd	0.84
2.Nd deoxygenated	1.32

a This value is determined from the surface under the ⁴F_{3/2}→⁴I_{11/2} emission peak around 1066 nm, relative versus the 1066 nm peak of **3.Nd** in DMSO solution and corrected for the absorbance of the solution.

There is no effect of oxygen on the emission intensity of **3.Nd**, which is indicative of relative fast energy transfer (> 10⁹ s⁻¹). The energy transfer from fluorenone to Nd³⁺ is much slower because there is a relative strong oxygen effect. The estimated energy transfer rate is about 4×10⁷ s⁻¹ in **2.Nd**.

Besides **3.Nd**, the luminescence of **3.Yb** and **3.Er** was measured as well. In Figure 6.7 the luminescence of **3.Yb** and **3.Er** are depicted with emission peaks at 980 nm (²F_{5/2}→²F_{7/2}) and 1536 nm (⁴I_{13/2}→⁴I_{15/2}), respectively. The luminescence of Yb³⁺ is superimposed on the tail of the naphthone fluorescence, which is indicative of an inefficient energy transfer from naphthone to Yb³⁺.

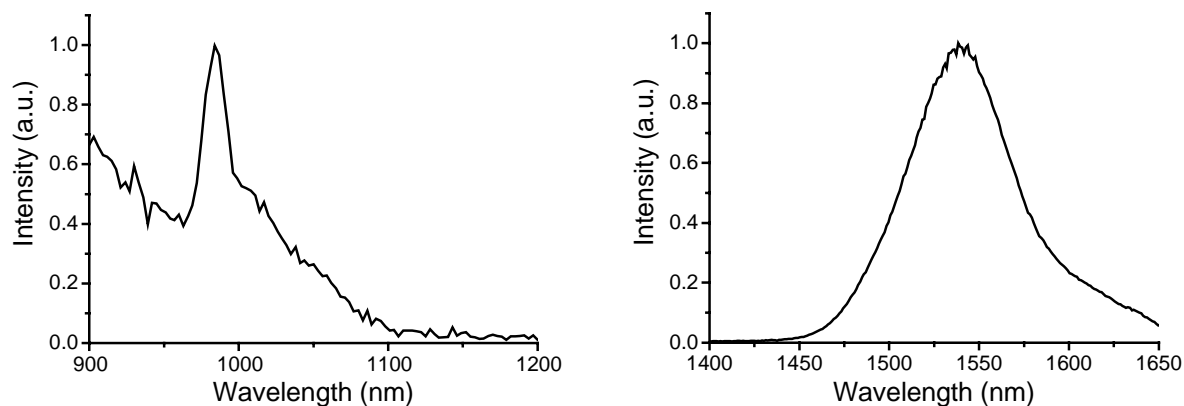


Figure 6.7 Left: Emission spectrum **3.Yb**. Right: emission spectrum **3.Er**. Both spectra were recorded in $DMSO-d_6$, λ_{exc} 450 nm.

6.2.3 Electro-chemistry

Electro-chemistry of the complexes was performed in order to determine the reduction potentials of complexes. These are necessary in order to determine which semiconducting polymer will be most appropriate as host for electro-luminescence studies.

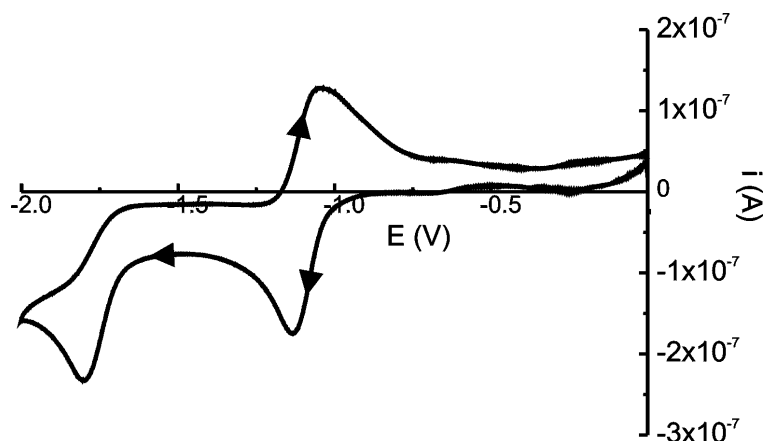


Figure 6.8 Cyclic voltammogram of **2.Nd** in $DMSO$ (Bu_4NClO_4 , vs. $Ag/AgCl$) obtained at a scan rate of 0.2 V/s.

The cyclic voltammogram (CV) of **2.Nd** presented in Figure 6.8 is representative for all other CVs of **2.Ln**. They all have a first reduction wave at about -1.1 V and a second reduction at -1.8 V (versus $Ag/AgCl$). In the oxidative sweep, there is only a distinct oxidation wave at -1.1 V. The reduction at -1.8 V is electrochemically irreversible, but chemically reversible since successive sweeps gave the same cyclic voltammograms. The reductive and oxidative waves at -1.1 V were also found when the maximum voltage in the sweep was -1.5 V. The CV data for the **2.Ln** and **3.Nd** complexes are summarized in Table 6.4. The average value of the cathodic and

the anodic potential peak of the first reduction and oxidation peaks, $E_{ave} = \frac{1}{2} (E_{pc} + E_{pa})$ is given. In all fluorenone complexes this averaged value is -1.1 V. For **3.Nd** this potential was less negative (-0.89 V). The second wave in **3.Nd** is located at -1.5 V, electrochemically irreversible, but chemically reversible because successive sweeps gave identical cyclic voltammograms.

Table 6.4 CV data of **2.Ln** and **3.Nd** in DMSO/ NBu_4ClO_4 vs. Ag/AgCl.

complex	E_{ave} (V) ^a
2.Nd	-1.08
2.Gd	-1.09
2.Yb	-1.10
2.Er	-1.08
3.Nd	-0.89

a The reported value is the average of the peak of the reductive wave (E_{pc}) and the peak of the oxidative wave (E_{pa}).

6.2.4 Electro-luminescence

Electro-luminescence (EL) of the Nd^{3+} complexes, which are depicted in Figure 6.3, was measured. The polymers, which were used in the polymer light-emitting diodes (PLED), are depicted in Figure 6.9. These EL devices were made by spincoating of a solution of the polymer in CH_2Cl_2 containing 10% (by weight, versus polymer) of the Nd^{3+} complex.

Materials

The EL of two blends will be described, first the EL of the blend of **1.Nd** with F8BT²⁰ (Figure 6.9) and then that of the blend of TFB²⁰ with **3.Nd**. These complexes were selected because they have relatively efficient sensitization properties of the Nd^{3+} luminescence and because they both absorb light in the visible region.

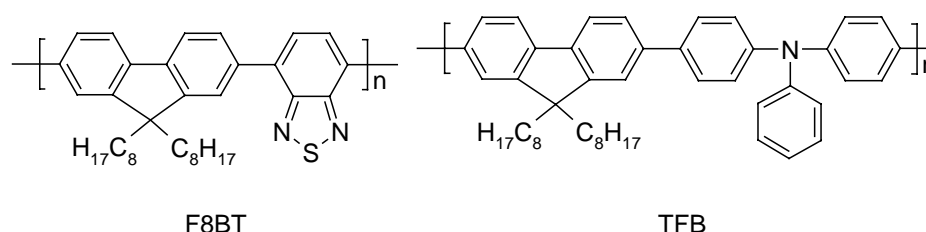


Figure 6.9 Semiconducting polymers used in the PLED devices.

The selection of antennas that absorb visible light was based on a low energy gap between excited and ground state and on the possibility of (singlet-singlet) energy transfer from the

semiconducting polymer to the sensitizer. An emission spectrum of F8BT and an absorption spectrum of **1.Nd** are depicted in Figure 6.10. It is clear that there is a large spectral overlap, which is excellent for energy transfer from F8BT to **1.Nd**.

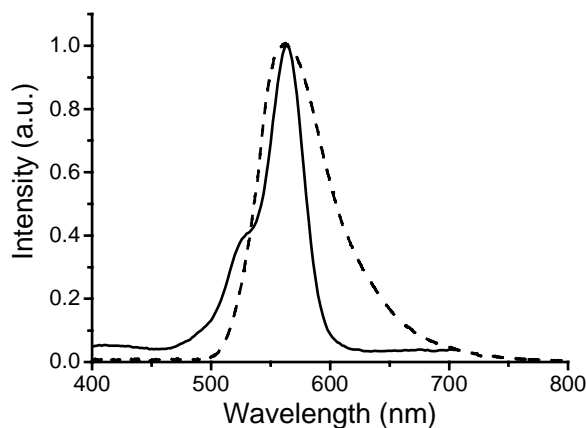


Figure 6.10 Emission of F8BT (dashed line) and absorption of **1.Nd** (solid line).

Another host material than F8BT was needed for **3.Nd**, because the singlet and triplet levels of this polymer are too low in energy for energy transfer to the naphthone group. TFB (Figure 6.9) is a good candidate because of the high spectral overlap of the TFB (singlet) emission with the absorption of the naphthone sensitizer (Figure 6.11). Furthermore, TFB has a low oxidation potential, which facilitates hole injection from the ITO/PEDOT anode.

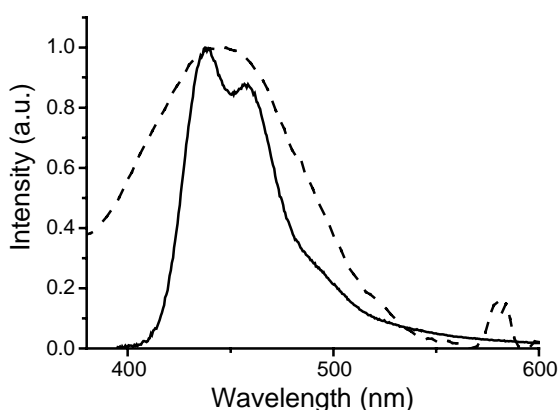


Figure 6.11 Emission spectrum of TFB (solid line) and absorption spectrum of **3.Nd** (dashed line).

The energy levels (ionization potentials and electron affinities) of ITO, TFB, **3.Nd**, and calcium, which was used as the anode material in the PLED devices, are depicted in Figure 6.12. The ionization potential and electron affinity of **3.Nd** were determined from the reduction

potential that was obtained in the CV measurement (-0.89 V vs. Ag/AgCl) and the position of the singlet energy level. This singlet level was obtained from the absorption and fluorescence spectrum of **3.Nd**: $19,500$ cm^{-1} (which is equal to 2.4 eV). These data give a LUMO level of 3.9 eV versus vacuum and a HOMO level of 6.3 eV for **3.Nd**.

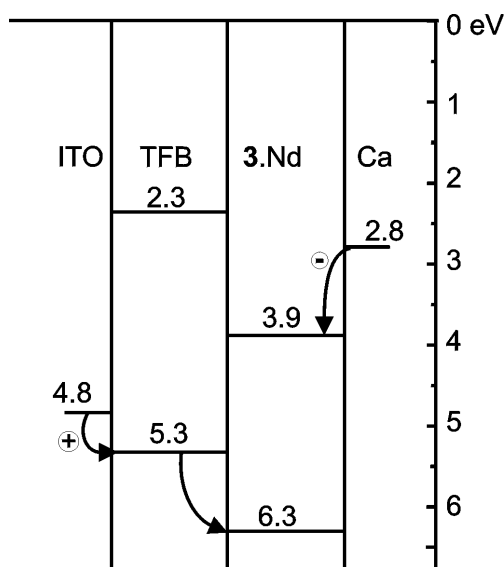


Figure 6.12 Scheme with energy levels (ionization potentials and electron affinities) in a PLED device with TFB and **3.Nd** sandwiched between ITO and calcium. The arrows indicate the injection of the charges (holes and electrons).

When a bias is applied over the devices, with the energy levels of Figure 6.12, it is expected that the holes are injected in the polymer material and that electrons will be injected in the **3.Nd** complex.

Preparation of the EL devices

A layer of PEDOT (a mixture of poly(3,4-ethylene dioxythiophene) and poly(styrenesulfonate)), was spincoated on an ITO (indium tin oxide) coated glass substrate, which was pre-treated with an oxygen plasma.²¹ Subsequently, a layer of about 80-100 nm of polymer containing 10% of Nd^{3+} complex was spincoated on top of the PEDOT. As counter electrode, calcium was evaporated on the polymer layer with a layer of aluminum on top of the calcium in order to protect the calcium from traces of water or oxygen. All samples were treated under vacuum or under N_2 atmosphere in order to protect the calcium layer. A schematic picture of the devices is shown in Figure 6.13.

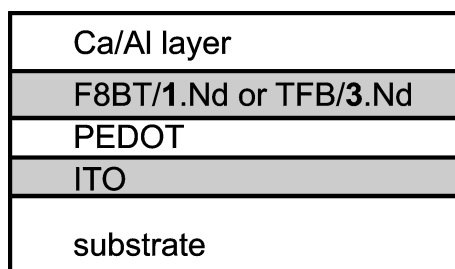


Figure 6.13 Schematic representation of the devices described in this Chapter.

Electro-luminescence of 1.Nd in F8BT

The electro-luminescence (EL) and the photo-luminescence (PL) of the devices made with the blend of F8BT and 1.Nd are depicted in Figure 6.14. This spectrum contains the lissamine-based fluorescence with a maximum at 600 nm, and Nd³⁺-based luminescence at 890 nm, due to the ${}^4F_{3/2} \rightarrow {}^4I_{9/2}$ transition. The other Nd³⁺ transitions could not be detected with the equipment used. However, there is no reason to assume that these are not present. The 1066 and 1330 nm transitions originate from the same excited state (${}^4F_{3/2}$) as the 890 nm emission and all these emission peaks have been observed in similar complexes.²²

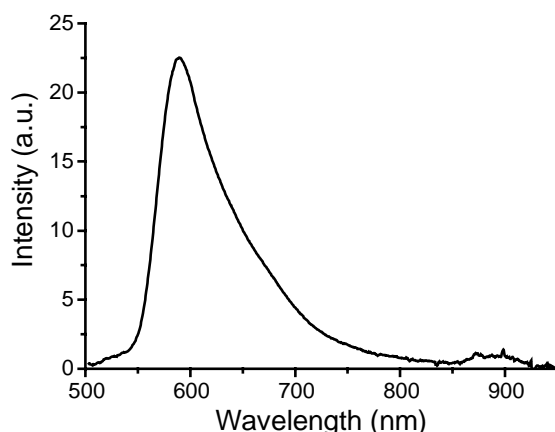


Figure 6.14 Electro-luminescence spectrum of the devices doped with 1.Nd obtained at a bias to the devices of 25 V.

No F8BT emission was detected, which can be due to two reasons, *viz.* complete energy transfer from the excited F8BT to the lissamine sensitizer or by charge trapping and recombination at the lissamine moiety, which prevents the excitation of F8BT. Energy transfer from F8BT to lissamine is probably an important pathway because there was also no F8BT emission in the PL experiment as well. However, this does not exclude charge trapping on the lissamine in the EL operation. The luminescence of different devices could be compared because

they were made in the same way with the same pixel sizes. Upon comparing, the EL intensity of a device with F8BT doped with **1.Nd** with the EL intensity of a device with only F8BT is was found that the emission intensity of the blend is much less intense. This is due to the quenching of F8BT by lissamine and quenching of lissamine by Nd^{3+} . The efficiency of Nd^{3+} in organic environment and in polymers is below 1%, due to quenching by vibrational modes of the organic molecules.²³ The relative Nd^{3+} emission in EL operation is about 4 times larger than in PL operation. This can be due to triplet state formation on lissamine directly or via triplet-triplet energy transfer from the polymer to lissamine.²⁴ The current-voltage (i-V) characteristics of the doped devices (Figure 6.15) show a characteristic diode behavior. The turn-on voltage of the devices (Figure 6.15, the voltage where the luminescence starts increasing) is about 15 V, whereas this is about 2.5 V for devices with undoped F8BT. The high turn-on voltage is probably due to charge-trapping by the lissamine moiety. The mobility of the charges on the lissamine is much lower than that on the polymer because the concentration of lissamine is much lower and because the only mechanism for charge migration over the lissamine moieties is by hopping, which is relatively inefficient.¹

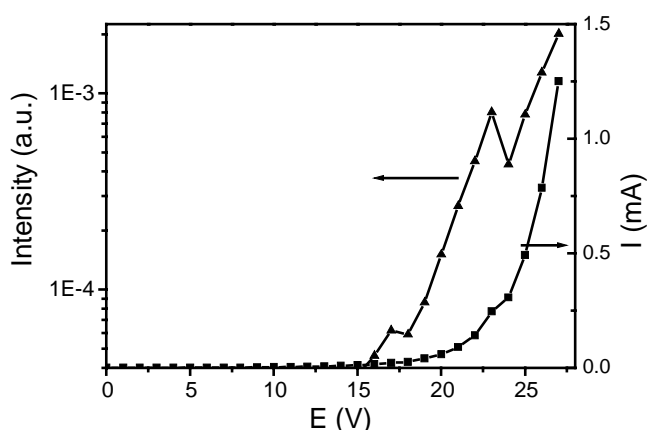


Figure 6.15 The intensity-voltage (left axis) and the current-voltage (right axis) characteristics of **1.Nd** doped in F8BT PLEDs.

*Electro-luminescence in **3.Nd** doped devices*

Devices with TFB doped with **3.Nd** were made in the same way as the devices with **1.Nd** in F8BT, thus on a layer of PEDOT (~ 40 nm) on ITO a layer (80-100 nm) of TFB doped with 10 wt% of **3.Nd** was spincoated. Calcium was evaporated on top of the devices as the cathode material. Upon applying a bias of 25 V the spectrum depicted in Figure 6.16 was obtained.

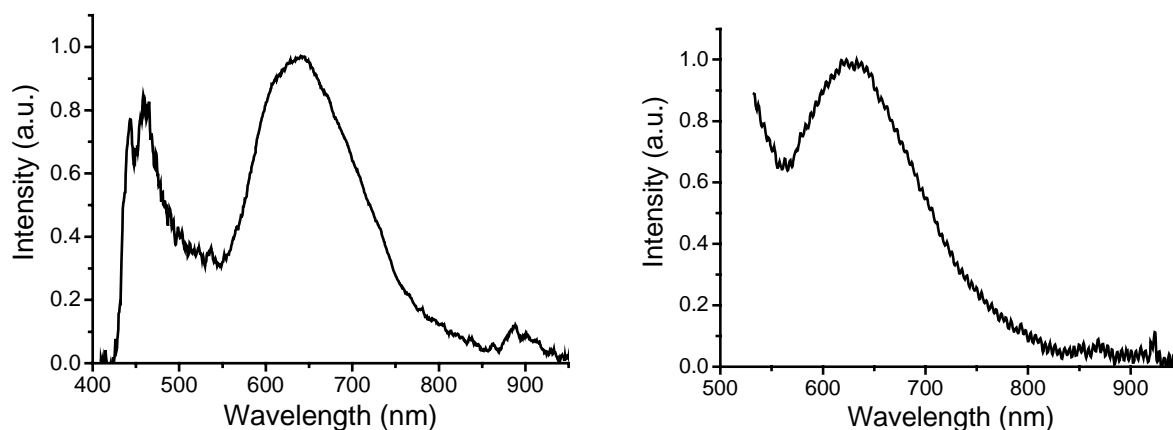


Figure 6.16 Left: electro-luminescence spectrum of **3.Nd** in TFB host with a bias of 25 V, right: EL spectrum of TFB alone.

Three distinct peaks are observed in this spectrum: at 450 nm the fluorescence of TFB, around 600 nm the naphthone fluorescence and TFB-based electro-luminescence, and at 890 nm the Nd^{3+} -based luminescence. The peak at 600 nm is due to the fluorescence of **3.Nd** and to TFB, because the EL spectrum of TFB alone exhibited a peak at 600 nm too. The reason for this emission is not clear, but it is probably phosphorescence from the TFB polymer. PL measurements on the devices (*vide infra*) substantiated this, because TFB-based luminescence around 600 nm was not observed in the PL measurements. More research is needed, like time-resolved electro-luminescence, to prove the TFB triplet emission. The current-voltage characteristics of these devices are presented in Figure 6.17, where a similar behavior of the diodes is found as in case of the **1.Nd** doped devices. Again there is a high turn-on voltage of about 18 V. The turn-on voltage of the devices with only TFB was much lower (4 V). The high turn-on voltage is caused by inefficient charge recombination as a result of charge trapping by **3.Nd**. A better match of the ionization potential and the electron affinity of polymer and sensitizer would be necessary in order to make more efficient devices. Upon increasing the voltage above 25-30 V the behavior of the device changed. Above 30 V the devices broke as can be seen in the i-V characteristics in Figure 6.17. However, when a voltage of 25 V is applied the electrical field generated is already very high ($> 2.5 \times 10^8$ V/m) and lowering the turn-on voltage of the devices would give more stable devices. In order to do so, a better match of the sensitizer with the host polymer is needed in terms of oxidation and reduction potential.

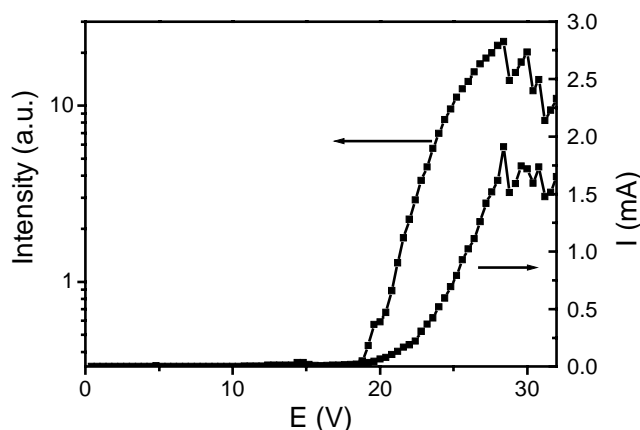


Figure 6.17 Intensity-voltage (right axis) and current-voltage (left axis) characteristics of **3.Nd** doped in the TFB light-emitting diode.

The photo-luminescence (PL) spectra of TFB and TFB doped with **3.Nd** are depicted in Figure 6.18. The naphthone emission is clearly visible as a shoulder of the TFB fluorescence at 600 nm. Nd^{3+} -based emission was only found in the doped device.

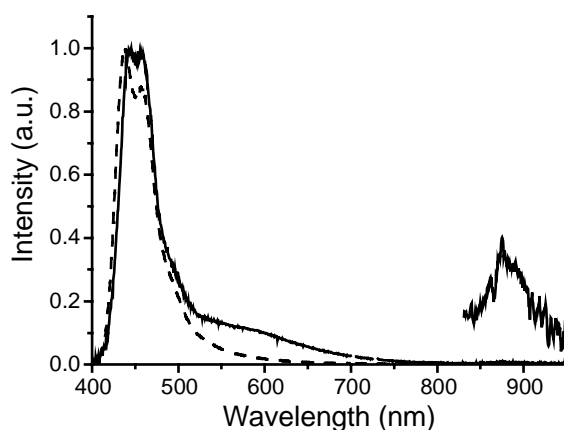


Figure 6.18 PL spectra of TFB (dashed) and TFB doped with 10% **3.Nd** (solid line), the inset is a magnification (25x) of the 890 nm Nd^{3+} emission in the doped TFB film.

These PL spectra prove that there is (singlet-singlet) energy transfer between the TFB host polymer and the naphthone sensitizer because there is naphthone fluorescence and Nd^{3+} luminescence in the doped devices. These emissions can be due to direct excitation of the naphthone. However, in the absence of energy transfer no **3.Nd** emission would be visible at all. The concentration, the absorption coefficient, and the fluorescence quantum yield of **3.Nd** are all about 10 times lower than these properties of TFB. Together, this would mean 1,000 times less

intense **3.Nd** emission than the TFB fluorescence. Although it is not completely clear from the spectra, due to the 600 nm emission of TFB, there is an indication that upon EL relative more Nd^{3+} luminescence is observed than in the PL experiment. This is based on the fact that the TFB emission at 600 nm does not show a shoulder or an enhancement when compared with the TFB fluorescence. The enhancement is due to the generation of triplet states on polymer and **3.Nd**. With the assumption that the emission at 600 nm in the TFB polymer under EL operation is phosphorescence (this needs further proof with for instance time-resolved electro-luminescence), it can be concluded that there is hardly any triplet energy transfer from polymer to the sensitizer and that both polymer and sensitizer are excited in the EL operation.

Although the sensitizers described did not give very efficient electro-luminescence, these sensitizers are essential because similar devices doped with **4.Nd** did not show any Nd^{3+} -based electro-luminescence. This complex **4.Nd** does not contain a sensitizer that is easily reduced or oxidized or that can accept energy from the polymers described. Therefore, this proves that sensitizers are needed and that no direct energy transfer from polymer to the lanthanide ion occurs.

6.3 Conclusions

In this Chapter, the preparation of lanthanide ion complexes is described with two new sensitizers: fluorenone and naphthone. Sensitized emission of Nd^{3+} , Yb^{3+} , and Er^{3+} was detected in solution. The naphthone complex of Nd^{3+} (**3.Nd**) and a lissamine functionalized Nd^{3+} (**1.Nd**) complex were incorporated in polymer light-emitting diodes and upon applying a voltage to these devices near-infrared Nd^{3+} -based luminescence was observed. Although this luminescence was not very efficient and high turn-on voltages ($> 15\text{V}$) were needed, the sensitizers are necessary for Nd^{3+} luminescence, because in devices doped with complexes without sensitizers no Nd^{3+} luminescence was observed.

6.4 Experimental

General

For the general details of the synthesis of the complexes see the experimental sections of Chapter 3 and Chapter 4. The naphthone acid was prepared according to a literature procedure.¹⁶

Synthesis

Compound 2.[$\text{C}(\text{CH}_3)_3$] To a solution of 1.3 g (1.2 mmol) **5** and 1.0 g (10 mmol) NEt_3 in 100 ml of CH_2Cl_2 a solution of 0.36 g (1.5 mmol) 9-fluorenone-4-carbonyl chloride in 50 ml of CH_2Cl_2 was added.

After stirring for one night at room temperature under argon atmosphere an additional amount of 100 ml CH_2Cl_2 was added. This solution was washed twice with 0.5 N HCl and twice with water. After drying over MgSO_4 and filtration, the organic solvent was removed under *vacuo*. Purification was performed by column chromatography with silica and EtOAc/hexane (2:3 v/v) as the eluent. Yield: 0.73 g (47 %) of a yellow oil. ^1H NMR (CDCl_3): δ 7.73-7.65 (m, 2H, Ar- H^{FL}), 7.54-7.25 (m, 10, Ar- H), 7.19-6.90 (m, 6H, Ar- H^{terph}), 5.16-4.75 (m, 4H, Ar CH_2N), 4.19-3.80 (m, 6H, OCH_2CO_2), 3.64-3.05 (m, 12H, $\text{CH}_2^{\text{tail}}$), 2.38-2.33 (m, 9H, Ar CH_3), 2.17-1.78 (m, 4H, $\text{CH}_2^{\text{tail}}$), 1.60-1.18 (m, 35H, $\text{C}(\text{CH}_3)_3$, $\text{CH}_2^{\text{tail}}$), 0.96-0.78 (m, 6H, $\text{CH}_3^{\text{tail}}$); ^{13}C NMR (CDCl_3): δ 192.5, 171.8, 169.4, 169.2, 167.5, 166.5, 152.0, 151.5, 150.5, 142.7, 140.3, 139.9, 136.3, 136.1, 134.4-126.1, 124.0, 123.9, 123.7, 81.1, 80.5, 70.3, 70.2, 69.8, 69.2, 68.9, 68.1, 67.0, 47.9, 47.8, 45.5, 42.6, 42.5, 41.9, 31.3, 31.1, 28.1, 27.5, 27.4, 27.3, 27.0, 20.5, 20.4, 20.1, 18.8, 18.7, 13.4, 13.3; MS (FAB, NBA): m/z 1259.7 [(M+H) $^+$, calcd for $\text{C}_{76}\text{H}_{95}\text{N}_2\text{O}_{14}$: 1259.7], 1281.7 [(M+Na) $^+$, calcd for $\text{C}_{76}\text{H}_{94}\text{N}_2\text{O}_{14}\text{Na}$: 1281.7]; IR: 1753.4 ($\text{C}=\text{O}^{\text{ester}}$), 1718.4 ($\text{C}=\text{O}^{\text{fluorenone}}$), 1637.6 ($\text{C}=\text{O}^{\text{amide}}$) cm^{-1} .

Compound 3. $[\text{C}(\text{CH}_3)_3]$ 50 mg (0.18 mmol) of naphthone acid¹⁶ was dissolved in 25 ml CH_2Cl_2 and 0.14 g (0.37 mmol) HBTU and 24 mg (0.19 mmol) DiPEA were added. After two hours 0.29 g (0.28 mmol) of **5** in 25 ml of CH_2Cl_2 was added and the solution was left stirring for 16 hours. After removal of CH_2Cl_2 under *vacuo* the crude mixture was purified using column chromatography with silica and EtOAc/hexane (2:3 v/v) and subsequent preparative TLC with the same eluent. Yield 53 % of a yellow solid, m.p. 65-68 $^\circ$ C. ^1H NMR (CDCl_3): δ 8.50-8.42 (m, 2 H, Ar- H^{NP}), 8.03-7.96 (m, 1H, Ar- H^{NP}), 7.86-7.43 (m, 7H, Ar- H^{NP}), 7.42-7.23 (m, 5H, Ar- H^{Bz}), 7.10-6.91 (m, 6H, Ar- H^{terph}), 5.16-4.60 (m, 4H, Ar $\text{CH}_2\text{-NCO}$), 4.08-2.88 (m, 16H, $\text{CH}_2^{\text{tail}}$), 2.40-2.18 (m, 9H, Ar CH_3), 1.95-0.76 (m, 41H, $(\text{CCH}_3)_3$, $\text{CH}_2^{\text{tail}}$), 0.85-0.48 (m, 6H, $\text{CH}_3^{\text{tail}}$); ^{13}C NMR (CDCl_3): δ 192.7, 192.6, 172.3, 169.7, 169.4, 168.1, 168.0, 167.9, 167.5, 167.2, 167.0, 152.1, 151.9, 151.8, 151.4, 151.2, 144.4, 143.6, 143.4, 137.4, 137.3, 134.3, 133.3, 131.8-126.6, 124.8, 124.7, 124.6, 124.1, 124.0, 123.4, 120.4, 108.5, 81.5, 81.3, 80.9, 80.8, 70.9, 70.6, 70.5, 70.3, 70.2, 69.6, 69.5, 68.7, 68.6, 67.6, 67.4, 48.4, 47.9, 46.3, 45.9, 43.1, 42.9, 42.3, 31.9, 31.8, 31.5, 29.7, 29.6, 29.3, 28.7, 28.1, 27.9, 27.8, 27.7, 27.6, 27.5, 27.1, 21.0, 20.9, 20.8, 20.7, 20.6, 19.3, 18.9, 14.1, 14.0, 13.9, 13.7; MS (FAB, NBA): m/z 1308.1 [(M-H) $^-$, calcd for $\text{C}_{80}\text{H}_{95}\text{N}_2\text{O}_{14}$: 1308.7]; EA: calcd C 73.37%, H 7.39% N 2.14%, found C 73.47%, H 7.08%, N 2.21%.

General procedure for the deprotection of the *tert*-butyl ester group The esters were stirred at room temperature under argon atmosphere in TFA. After 14 hours toluene was added and the solution was evaporated to dryness. Another amount of toluene was added and again the solvent was evaporated to dryness. The remaining solid was dissolved in CH_2Cl_2 and washed twice with 1 N HCl and twice with water. After drying over MgSO_4 and filtration the organic solvent was removed under *vacuo*.

Compound 2.H₃ The general procedure for *tert*-butyl deprotection was followed with 600 mg (0.47 mmol) of triester **2**. $[\text{C}(\text{CH}_3)_3]$. Yield 80% of a yellow solid, m.p. 92-94 $^\circ$ C, $\epsilon_{380 \text{ nm, methanol}} = 253 \text{ l}\times\text{mol}^{-1}\times\text{cm}^{-1}$. ^1H NMR (CD_3OD): δ 7.63-7.55 (m, 2H, Ar- H^{FL}), 7.51-7.23 (m, 10H, Ar- H), 7.15-6.77 (m, 6H, Ar- H^{terph}), 5.16-4.63 (m, 4H, Ar CH_2N), 4.19-3.63 (m, 4H, OCH_2CO_2), 3.51-3.25 (m, 8H, $\text{CH}_2^{\text{tail}}$), 3.18-

2.91 (m, 4H, CH_2^{tail}), 2.32-2.24 (m, 9H, Ar- CH_3), 2.03-1.68 (m, 4H, CH_2^{tail}), 1.54-0.92 (m, 8H, CH_2^{tail}), 0.87-0.65 (m, 6H, CH_3^{tail}); ^{13}C NMR (CD_3OD): δ 172.6, 170.4, 169.8, 169.7, 151.9, 151.1, 150.3, 142.2, 140.1, 139.5, 134.5-122.1 (ArC), 69.9, 69.7, 69.5, 69.3, 68.8, 68.7, 67.9, 67.8, 67.7, 66.7, 66.5, 43.0, 42.6, 42.0, 31.0, 30.9, 28.6, 27.5, 26.7, 26.6, 19.0, 18.8, 18.7, 18.5, 18.4, 18.2, 13.5, 12.3; MS (FAB, NBA): m/z 1091.3 [(M+H) $^+$, calcd for $C_{64}H_{71}N_2O_{14}$: 1091.5], 1113.2 [(M+Na) $^+$, calcd for $C_{64}H_{70}N_2O_{14}Na$: 1113.5] IR: 1784.7 (C=O $^{\text{acid}}$), 1717.2 (C=O $^{\text{fluorenone}}$), 1633 (C=O $^{\text{amide}}$), 1607.0 cm^{-1} EA: calcd C 70.44% H 6.47% N 2.57%, found C 69.59% H 6.44% N 2.79%.

Compound 3.H₃ This deprotection was performed according to the general procedure with 128 mg **3**.[C(CH₃)₃] in 25 ml TFA, the yield was quantitative. A yellow substance ($\epsilon_{438 \text{ nm, methanol}} = 1023 \text{ l}\times\text{mol}^{-1}\times\text{cm}^{-1}$), m.p. 102-104° C. 1H NMR (CD_3OD): δ 8.71-8.64 (m, 1H, Ar- H^{NP}), 8.28-8.21 (m, 1H, Ar- H^{NP}), 8.05-7.91 (m, 1H, Ar- H^{NP}), 7.84-7.60 (m, 7H, Ar- H^{NP}), 7.45-7.37 (m, 5H, Ar- H^{Bz}), 7.23-6.85 (m, 6H, Ar- H^{terph}), 5.18-4.51 (m, 4H, ArCH₂N), 4.27-82 (m, 6H, OCH₂CO₂), 3.76-2.91 (m, 12H, CH_2^{tail}), 2.48-2.18 (m, 9H, ArCH₃), 1.96-1.12 (m, 16H, CH_2^{tail}), 0.99-0.55 (m, 6H, CH_3^{tail}); ^{13}C NMR (CD_3OD): δ 194.3, 194.1, 174.2, 172.2, 172.0, 191.9, 153.7, 153.5, 153.3, 152.5, 152.3, 151.8, 146.0, 145.6, 145.1, 144.9, 144.1, 139.0, 138.8, 137.8, 136.2, 135.4, 134.8, 133.2-129.0, 127.7, 126.1, 125.2, 125.0, 124.9, 71.8, 71.5, 71.1, 70.8, 70.0, 69.8, 69.7, 68.7, 68.3, 45.2, 45.0, 44.8, 44.5, 44.0, 33.0, 32.9, 32.7, 32.6, 30.7, 29.2, 28.5, 23.6, 20.9, 20.7, 20.4, 20.3, 20.0, 14.3, 14.2, 14.1; MS (FAB, NBA): m/z 1141.6 [(M+H) $^+$, calcd for $C_{68}H_{73}N_2O_{14}$: 1141.5], 1163.7 [(M+Na) $^+$, calcd for $C_{68}H_{72}N_2O_{14}Na$: 1163.5]; IR: 1748.7 (C=O $^{\text{acid}}$), 1714.0 (C=O $^{\text{naphthone}}$), 1633.8 (C=O $^{\text{amide}}$), 1603.7 cm^{-1} ; EA: calcd C 71.56% H 6.36% N 2.45%, found C 71.22% H 6.26% N 2.26%.

General procedure for the preparation of the Ln³⁺ complexes In a typical experiment 100 mg of triacid was dissolved with three equivalents of Et₃N and a solution of the Ln(NO₃)₃.xH₂O (x = 5 or 6) in methanol was added. This mixture was left stirring under argon atmosphere at room temperature for one hour. Then the methanol was removed under *vacuo* and the residue was redissolved in 150 ml of CH₂Cl₂. This solution was washed three times with 200 ml water, dried over MgSO₄, and finally the organic solvent was evaporated to dryness. All the complexes were obtained in quantitative yield, the analytical data of the complexes are summarized in Table 6.5.

Table 6.5 Analysis of the complexes.

Complex	MS-FAB m/z^a	calc	IR (C=O $^{\text{amide}}$)	IR (C=O $^{\text{carb}}$)	IR (C=O $^{\text{sens}}$)
2.Nd	1232.6 (M+H) $^+$	1232.4	1636.9	1607.6	1718.6
2.Gd	1246.3 (M+H) $^+$	1245.4	1636.0	1607.8	1718.3
3.Gd	1296.5 (M+H) $^+$	1296.4	1635.6	1603.6	1713.8
3.Yb	1312.5 (M+H) $^+$	1312.4	1633.8	1602.2	1713.2
3.Nd	1280.4 (M+H) $^+$	1280.1	1634.1	1604.5	1714.9
3.Er	1306.2 (M+H) $^+$	1306.4	1635.7	1603.3	1713.8

a For all complexes the corresponding isotope pattern was found.

Luminescence

See for the experimental details of the luminescence in solution the experimental section of Chapter 4.

Electro-chemistry

Cyclic voltammetry was performed on a Metrohm 663 VA stand with a hanging mercury drop electrode as the working electrode and a glassy-carbon auxiliary electrode. As reference the Ag/AgCl/KCl electrode was used. Cyclic voltammograms were recorded with an Autolab (Ecochemie, Utrecht, the Netherlands) PGSTA10. The complexes were dissolved in DMSO (Uvasol, Merck) solutions with tetrabutylammonium perchlorate as the background electrolyte. Prior to the measurements the solutions were deoxygenated by purging them for 10 minutes with nitrogen. The cyclic voltammograms were recorded at a scan rate of 0.2 V/s.

Electro-luminescence

First ITO substrates were cleaned according to standard procedures, ending with an oxygen plasma treatment.²¹ Then a thin layer (~40 nm) of PEDOT/PSS was spincoated from aqueous solution. The substrates were annealed at 100° C for 1 hour under N₂ flow. Subsequently, a solution of 35 mg polymer (F8BT or TFB) with 4 mg 1.Nd or 3.Nd in 5 ml CH₂Cl₂ was spincoated at 1500 rpm on top of the substrates, resulting in a layer thickness of 80-100 nm (determined with DEKTAK surface profiling). Finally, Ca/Al counter electrodes were evaporated on top of the devices with an area of about 2 mm² with a background pressure of 5×10⁻⁶ mbar. After electrode evaporation all devices were kept under vacuum or under N₂ atmosphere. EL measurements were performed under vacuum. All EL measurements were performed at room-temperature. The voltage was supplied by a Keithley 230 voltage source and measured with digital Keithley 195A digital multimeter. The luminescence intensity was measured with a silicon photodiode, luminescence spectra were recorded with a CCD spectrometer (Oriel) with a spectral resolution better than 5 nm. PL measurements were performed on thin layers on quartz substrates, that were made by spincoating the same solution used to fabricate the EL devices. The excitation source was the UV lines of an Ar⁺ ion laser and spectra were recorded with the same CCD spectrometer.

6.5 References and notes

- ¹ Friend, R. H.; Gymer, R. W.; Holmes, A. B.; Burroughes, J. H.; Marks, R. N.; Taliani, C.; Bradley, D. D. C.; Dos Santos, D. A.; Bredas, J. L.; Logdlund, M.; Salaneck, W. R. *Nature* **1999**, 397, 121.
- ² See for instance the pioneer website <http://www.pioneerelectronics.com> in order to obtain more information on the car radios with OLED displays.
- ³ Forrest, S. *M.R.S. Bull.* **2001**, 26, 108.
- ⁴ Wohlgenannt, M.; Tandon, K.; Mazumdar, S.; Ramasesha, S.; Vardeny, Z. V. *Nature* **2001**, 409, 94.
- ⁵ Cao, Y.; Parker, I. D.; Yu, G.; Zhang, C.; Heeger, A. J. *Nature* **1999**, 397, 414.

- ⁶ a) Cleave, V.; Yahioğlu, G.; Le Barny, P.; Friend, R. H.; Tessler, N. *Adv. Mater.* **1999**, *11*, 285; b) Baldo, M. A.; O'Brien, D. F.; You, Y.; Shoustikov, A.; Sibley, S.; Thompson, M. E.; Forrest, S. R. *Nature* **1998**, *395*, 151.
- ⁷ Murov, S. L.; Carmichael, I.; Hug, G. L. *Handbook of photochemistry*, 2nd edition, Marcel Dekker, New York, 1993.
- ⁸ Parker, D.; Williams, J. A. G. *J. Chem. Soc., Dalton Trans.* **1996**, 3613.
- ⁹ Vögtle, F.; Gorka, M.; Vicinelli, V.; Ceroni, P.; Maestri, M.; Balzani, V. *Chem. Phys. Chem.* **2001**, 769.
- ¹⁰ de Sá, G. F.; Malta, O. L.; de Mello Donegá, C.; Simas, A. M.; Longo, R. L.; Santa-Cruz, P. A.; da Silva, E. F. *Coord. Chem. Rev.* **2000**, *196*, 165.
- ¹¹ See Chapter 4 of this thesis for more details on the energy transfer mechanisms and their probabilities.
- ¹² a) Khreis, O. M.; Curry, R. J.; Somerton, M.; Gillin, W. P. *J. Appl. Phys.* **2000**, *88*, 777; b) Curry, R. L.; Gillin, W. P.; Knights, A. P.; Gwilliam, R. *Opt. Mater.* **2001**, *17*, 161.
- ¹³ Kawamura, Y.; Wada, Y.; Hasegawa, Y.; Iwamuro, M.; Kitamura, T.; Yanagida, Y. *Appl. Phys. Lett.* **1999**, *74*, 3245.
- ¹⁴ Klink, S. I.; Hebbink, G. A.; Grave, L.; Peters, F. G. A.; van Veggel, F. C. J. M.; Reinhoudt, D. N.; Hofstraat, J. W. *Eur. J. Org. Chem.* **2000**, 1923.
- ¹⁵ Klink, S. I.; Oude Alink, P.; Grave, L.; Peters, F. G. A.; Hofstraat, J. W.; Geurts, F. A. J.; van Veggel, F. C. J. M. *J. Chem. Soc., Perkin Trans. 2* **2001**, 363.
- ¹⁶ Bunte, R.; Gundermann, K. -D.; Leitich, J.; Polansky, O. E.; Zander, M. *Chem. Ber.* **1986**, *119*, 3251.
- ¹⁷ Eaton, D. F. *J. Photochem. Photobiol. B* **1988**, *2*, 523.
- ¹⁸ Klink, S. I.; Hebbink, G. A.; Grave, L.; van Veggel, F. C. J. M.; Reinhoudt, D. N.; Slooff, L. H.; Polman, A.; Hofstraat, J. W. *J. Appl. Phys.* **1999**, *86*, 1181.
- ¹⁹ The rate of diffusion-controlled molecular oxygen quenching of the triplet state is the product of the diffusion controlled quenching rate (k_{diff}) and the oxygen concentration ($[\text{O}_2]$) in MeOH (Murov, S. L.; Carmichael, I.; Hug, G. L. *Handbook of photochemistry*, 2nd edition, Marcel Dekker, New York, 1993). From this follows: $k_{\text{ox}} = k_{\text{diff}} \times [\text{O}_2] = 10^{10} \text{ M}^{-1} \text{ s}^{-1} \times 2.1 \times 10^{-3} \text{ M} = 2 \times 10^7 \text{ s}^{-1}$.
- ²⁰ Bernius, M. T.; Inbasekaran, M.; O'Brien, J.; Wu, W. *Adv. Mater.* **2000**, *12*, 1737.
- ²¹ Cacialli, F.; Kim, J. S.; Brown, T. M.; Morgado, J.; Granström, M.; Friend, R. H.; Gigli, G.; Cingolani, R.; Favaretto, L.; Barbarella, G.; Daik, R.; Feast, W. J. *Synth. Metals* **2000**, *109*, 7.
- ²² Slooff, L. H.; Polman, A.; Klink, S. I.; Hebbink, G. A.; Grave, L.; van Veggel, F. C. J. M.; Reinhoudt, D. N.; Hofstraat, J. W. *Opt. Mater.* **2000**, *14*, 101.
- ²³ See Chapter 3 of this thesis for a more details on the efficiency of NIR emissive lanthanide ions in organic environment.

- ²⁴ Recently, experiments showed that in **1.Nd** upon photo-excitation (in solution) the main pathway of the sensitization process of Nd^{3+} occurs mainly via the singlet state of lissamine. However, this does not mean that in EL the triplet state of lissamine is not capable of sensitizing Nd^{3+} . Hebbink, G. A.; Klink, S. I.; Grave, L.; Oude Alink, P. G. B.; van Veggel, F. C. J. M. *Submitted to Chem. Phys. Chem.*

Chapter 7

Polymer waveguides doped with lanthanide ions

In this Chapter the luminescence of lanthanide ions in polymer matrices is described with the aim to construct a polymer-based optical amplifier. It is shown that the luminescence of the Nd^{3+} complexes is virtually identical to that of the complexes in solution. Polymer waveguides were designed based on waveguide cross sections calculated for the micrometer region in order to obtain single- or bimodal waveguiding at the 1320 nm telecommunication wavelength. Simulations were performed to investigate the feasibility to obtain optical gain with Nd^{3+} - and Er^{3+} -doped polymer waveguides. It was found that this should be possible with the lanthanide complexes, but only at relatively high power and therefore it is not a practical approach. The achievement of optical gain in waveguides doped with the nanoparticles (Chapter 5) is predicted to occur at pump powers in the tens to hundreds of milliwatts, which is achievable in practice. This dramatic effect is mainly due to the difference in luminescent lifetimes of the organic complexes and the doped nanoparticles.

7.1 Introduction

A disadvantage of inorganic fibers doped with lanthanide ions^{1,2} is that they are relatively inflexible and difficult to integrate with optical components that are based on polymers. Furthermore, low dopant concentrations are needed in order to prevent clustering of lanthanide ions. The clustering leads to significant losses because of energy-transfer processes between the lanthanide ions like cross relaxation. As is stated in Chapter 1, the ultimate goal of the research described in this thesis is to obtain optical amplification in polymer-based waveguides. With polymers, various waveguide structures can be made because the deposition and patterning of polymers is relatively easy, e.g. by spincoating and (standard) lithographic techniques.³ Active waveguides are for instance made by doping of polymers with lanthanide ion complexes. Previously, the luminescence of a lissamine-functionalized Nd³⁺ complex (see Chapter 6) in polymers was detected.⁴ It was found that the luminescence in the polymer matrix was comparable with that in solution, however, upon excitation for longer time (minutes) and at relatively high powers (40 mW), the lissamine moiety was not stable. Koeppen *et al.* calculated the feasibility of optical amplification of polymers doped with the visible emitting Sm³⁺ ions.⁵ They calculated that a gain of 20 dB⁶ should be achieved in a 60 cm long fiber doped with 10²⁰ Sm³⁺ ions per cubic centimeter. Chen *et al.* reported an optical gain of 8 dB in a 5 cm long polymeric waveguide at 1066 nm, doped with 10²⁰ Nd³⁺ ions per cm³.⁷ So far, no optical amplification was reported in polymeric waveguides at telecommunication wavelengths like 1.33 μm and 1.55 μm .

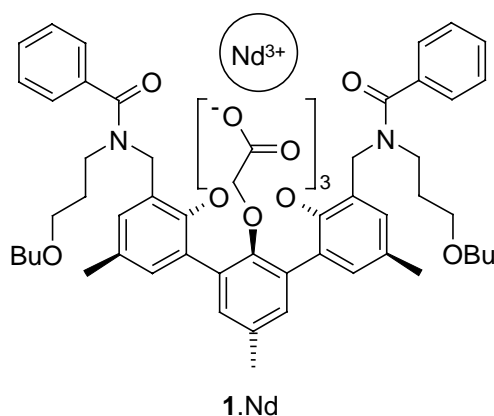


Figure 7.1 Molecular structure of 1.Nd.

In this Chapter, the use of the lanthanide ions in complexes and nanoparticles in polymer-based amplifiers is investigated. These complexes and particles are described in other Chapters of this thesis. First the luminescence of Nd³⁺ ion complexes (1.Nd,⁸ Figure 7.1) in polymers like

PS, PMMA, and PC (Figure 7.2) is dealt with. Subsequently, the design and characterization of polymer waveguides that were doped with the lanthanide complexes is described. Finally, a calculation is presented in order to estimate the optical gain at telecommunication wavelengths (1320 nm (Nd^{3+}), 1536 nm (Er^{3+})) with the designed waveguides.

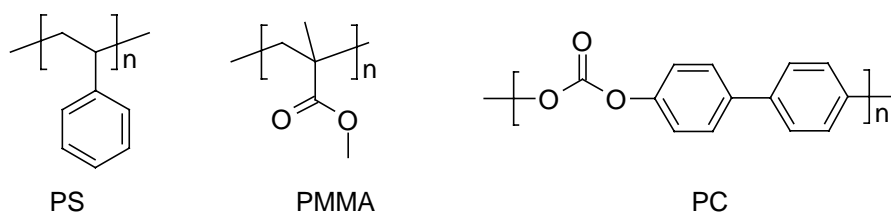


Figure 7.2 Molecular structures of the polymers PS (poly(styrene)), PMMA (poly(methylmethacrylate)), and PC (poly(carbonate)).

7.2 Results and discussion

7.2.1 Luminescence of 1.Nd in polymer matrices on quartz substrates.

Thin layers (1-2 μm) of polymers doped with 1.Nd were prepared on solid substrates, either silicon wafers (oxidized wafers with a buffer layer of 3.2 μm layer of SiO_2 between the polymer and the silicon) or quartz substrates. The polymer layers were deposited by spincoating of a solution of 0.1 g solid material (polymer with 10% 1.Nd) in 1 ml CHCl_3 . The layer thickness was determined with DEKTAK surface profiling.

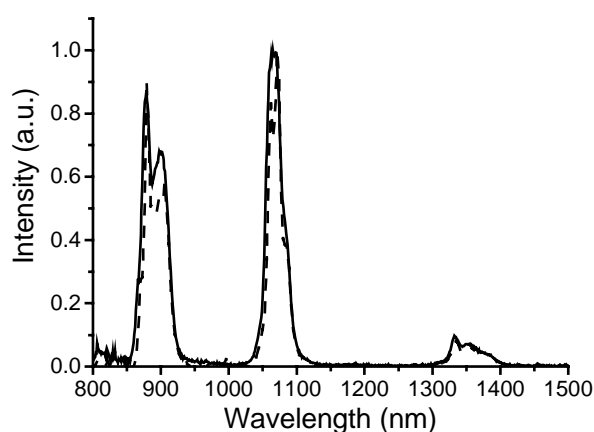


Figure 7.3 Luminescence spectra of 1.Nd in CHCl_3 solution (solid line) and in a thin layer of PS spincoated on a quartz substrate (dashed).

The near-infrared (NIR) emission spectra of 1.Nd in solution (CHCl_3) and in a polymer matrix (poly(styrene), PS) are depicted in Figure 7.3. These two spectra are virtually identical

and have the typical emission lines at 890 nm (${}^4F_{3/2} \rightarrow {}^4I_{9/2}$), 1066 nm (${}^4F_{3/2} \rightarrow {}^4I_{11/2}$), and 1330 nm (${}^4F_{3/2} \rightarrow {}^4I_{13/2}$). The fact that these two spectra are identical is important, because it proves that the medium does not significantly change the emission spectrum. The reason for this is that the crystal field of Nd^{3+} is not changed because of the organic cage that encapsulates the ion. The luminescent lifetimes of the layers containing **1.Nd** and of solutions of **1.Nd** were measured and these are summarized in Table 7.1.

Table 7.1 Luminescent lifetimes of **1.Nd** in polymer matrix (PS) on a quartz substrate, and in CHCl_3 and DMSO solution.

	τ_{PS} (μs)	τ_{CHCl_3} (μs)	τ_{DMSO} (μs)
1.Nd	0.78	0.43	1.5

The higher lifetime in DMSO is attributed to the fact that no water, which is a strong quencher of Nd^{3+} luminescence, is coordinated to the ion because of the substitution by DMSO. Surprisingly, the lifetime in the polymer matrix is substantially higher than in chloroform. It is expected that water is still coordinated to the lanthanide ion in chloroform (compare Chapter 6). After spincoating, the quenching is reduced, which is most likely due to a reduction of the number of coordinated water molecules.⁹ It was already pointed out that the luminescence of Nd^{3+} doped nanoparticles ($\text{LaPO}_4:\text{Nd}$, Chapter 5) in a PMMA matrix was similar to the emission luminescence in methanol.

7.2.2 Design of polymer waveguides, their fabrication and characterization

Several waveguide designs were calculated in order to determine the propagation mode of the optical wave.¹⁰ The calculations were started with a basic design of straight $1 \times 1 \mu\text{m}$ channels of PMMA (refractive index, $n = 1.49$) on silicon wafers with a $3.2 \mu\text{m}$ layer of SiO_2 ($n = 1.45$), with air ($n = 1$) as the top cladding. In such a design only the zeroth order mode is guided of 1320 nm light. Waveguides were made by spincoating of solutions of PMMA in chloroform containing 10% of **1.Nd** on the oxidized silicon substrates. A loss spectrum of these layers is depicted in Figure 7.4 with strong absorption peaks at 1150 nm (third overtone of the C-H vibration) and at 1400 nm (combination of stretch and bend vibrations of C-H groups). Clearly visible are the optical windows around 1300 nm and below 1100 nm. The small absorption maximum around 900 nm is due to the optical transition of Nd^{3+} (${}^4F_{3/2} \rightarrow {}^4I_{9/2}$).

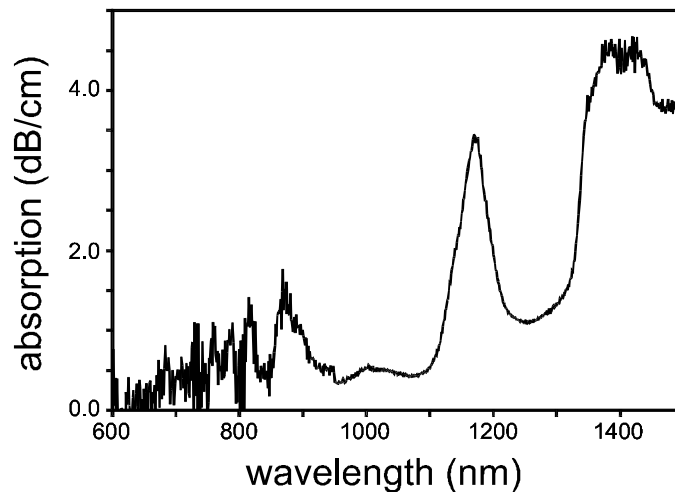


Figure 7.4 Optical loss spectrum determined on a 1.Nd doped PMMA layer of 1 μm thickness on a silicon wafer with a 3.2 μm SiO_2 layer.

Channels of varying width (2- 5 μm) were made by reactive ion etching techniques (Figure 7.5). The inset in this Figure shows that most of the intensity was guided as one optical mode in a 2×1 μm channel waveguide at a wavelength of 1320 nm. However, waveguide losses were very high, more than 6 dB/cm. These losses should be substantially lowered (< 1 dB/cm) in order to obtain a proof of principle of optical amplification.

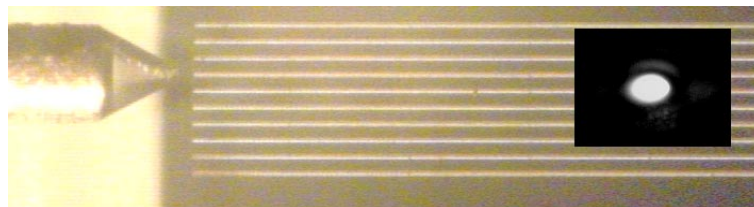


Figure 7.5 Overview of substrate with PMMA channel waveguides. On the left part of the photograph the tip of the optical fiber is visible, the width of the channels is 2-5 μm . The inset shows the optical mode of a 2×1 μm waveguide, at 1320 nm.

An important reason for the high losses in these channel waveguides is the relatively large surface area of the channels and the high refractive index contrast between the channels (PMMA) and the air cladding. Therefore, small imperfections, mainly caused by the polymer etching procedure in the sidewalls of the channels, are a source of the large waveguide losses. These can be suppressed by decreasing the surface area and the refractive index contrast between core and cladding. Ridge waveguides (Figure 7.6) are a way to decrease the surface area, because their sidewalls are smaller and thus less critical. A possible ridge waveguide consist of

PS or PC ($n = 1.58$) embedded between cladding layers of PMMA ($n = 1.49$) or sandwiched between SiO_2 ($n = 1.46$) and PMMA. This lead to calculated dimensions of a layer height of $1.5 \mu\text{m}$ with a ridge height of $0.2 \mu\text{m}$ (i.e. a slab thickness of $1.5 - 0.2 = 1.3 \mu\text{m}$ and a width of $2 \mu\text{m}$). An alternative structure is the ‘reversed’ structure, with trenches in the bottom cladding of PMMA or SiO_2 . Both designs gave a bimodal profile of the propagation mode at 1320 nm .¹¹

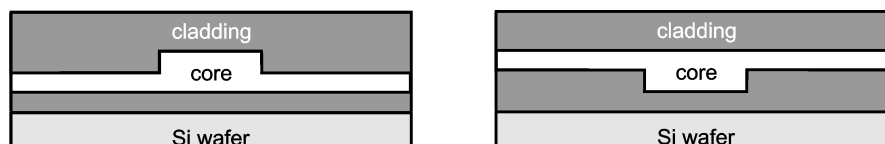


Figure 7.6 Ridge waveguide design, with the ridges in the top cladding (left) or reversed, in the bottom cladding (right).

Trenches in SiO_2 are relatively easily made by reactive ion etching with a CHF_3 plasma. The advantage of these trenches is that SiO_2 is not soluble in any of the solvents and side effects like solvation of the bottom cladding do no play a role. Layers of $1.5 \mu\text{m}$ PC were spun on top of $3 \mu\text{m}$ thick PMMA layers that were deposited on oxidized ($3.2 \mu\text{m}$ SiO_2) silicon wafers. Ridges in the polymer layer were etched by reactive ion etching with oxygen plasma and a protecting aluminum mask. The ridge waveguides were obtained after a wet-chemical removal of the aluminum mask. Two microscope pictures of the ridges are found in Figure 7.7, which show that these ridges are straight and smooth. The deposition of a layer of (doped) PC on a flat layer of PMMA was simple. However, the subsequent deposition of another layer of PMMA on top of the ridges resulted in a destruction of the PC ridges. Even the use of a non-solvent for PC (like THF) resulted in partial destruction of the polymer ridges.¹² This problem might be solved by the use of polymers that are cross-linked prior to the deposition of the top layer.



Figure 7.7 Two microscope photographs that show a part of the ridge waveguides with different thickness.

7.2.3 Calculation of optical gain in waveguides doped with Nd^{3+} and Er^{3+} .

The achievable optical gain in Nd^{3+} -doped polymer waveguides was estimated. The optical gain was calculated at 1320 nm, with optical pumping at 579 nm (a Nd^{3+} absorption line with a relatively high absorption cross section $\epsilon = 15 \text{ l}\cdot\text{mol}^{-1}\cdot\text{cm}^{-1}$, $\sigma_a = 2.5 \times 10^{-20} \text{ cm}^2$). An energy level scheme of the four-level Nd^{3+} system is depicted in Figure 7.8. The levels 1-4 are the Nd^{3+} ground state ($^4\text{I}_{9/2}$), the lower level of the laser transition ($^4\text{I}_{13/2}$), the metastable lasing level $^4\text{F}_{3/2}$, and the excited state $^4\text{G}_{5/2;7/2}$, respectively. It is assumed that the transitions from the level 4 to 3 and the transition from the level 2 to 1 are much faster than the absorption transition $1 \rightarrow 4$ and the emission transition $3 \rightarrow 2$, which results in empty levels 4 and 2.

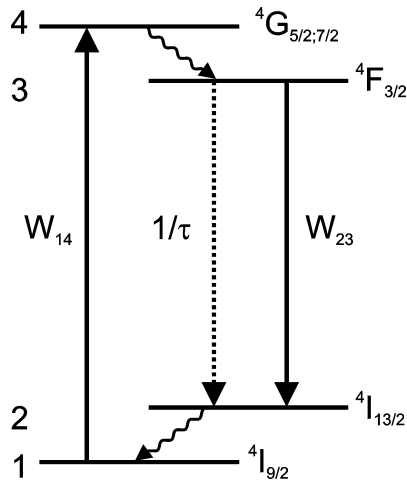


Figure 7.8 The 4-level system of Nd^{3+} , excitation/absorption from level 1 to level 4 (rate is W_{14}) at 579 nm, spontaneous decay (radiative and non-radiative, rate $1/\tau$) and stimulated emission (rate W_{32}) at 1320 nm. In the model, it is assumed that the decays from level 4 to 3 and from level 2 to 1 are much faster than the transitions between 1 and 4 and 2 and 3. Therefore $N_4 = N_2 = 0$ and $N_1 + N_3 = N_{\text{tot}}$.

Using this approximation, in the steady state situation the populations of N_1 and N_3 are given by Eq. 7.1. The rate equations are both equal to zero and therefore they are identical, but with $N_1 + N_3 = N_{\text{tot}}$ it is a determined set of equations.

$$\begin{aligned} \frac{dN_1}{dt} &= 0 = -W_{14}N_1 + \left(\frac{1}{\tau} + W_{32} \right) N_3 \\ \frac{dN_3}{dt} &= 0 = +W_{14}N_1 - \left(\frac{1}{\tau} + W_{32} \right) N_3 \\ N_1 + N_3 &= N_{\text{tot}} \end{aligned} \quad \text{Eq. 7.1}$$

N_1 , N_3 , and N_{tot} are the populations of the ground state (1), excited state (3), and the total population, respectively. Furthermore, W_{14} is the absorption rate, τ is the lifetime of level N_3 (spontaneous emission), and W_{32} is the rate of the stimulated emission. The rate for absorption (W_{14}) and the rate of stimulated emission (W_{32}) were calculated according to Eq. 7.2.

$$\begin{aligned} W_{14} &= \sigma_a I_p; & W_{32} &= \sigma_e I_s \\ I_p &= \frac{P_p}{h\nu_p A}; & I_s &= \frac{P_s}{h\nu_s A} \end{aligned} \quad \text{Eq. 7.2}$$

In these equations, I_p and I_s are the photon densities of the pump and the signal source, respectively, σ_a is the absorption cross section at the pump wavelength and σ_e is the stimulated emission cross section. P_p and P_s are the power of pump and signal, ν_p and ν_s are the light frequencies of pump and signal, respectively, h is Planck's constant, and A is the cross section of the waveguide. The assumption is made that both the pump and the signal are uniformly distributed in the waveguide, with an overlap of the intensities that is unity. In practice, both pump and signal will have their own propagation modes, which are not uniformly distributed. Therefore, the calculated gain will be an overestimation of the experimental value. The pump and signal power along a waveguide are given by Eq. 7.3, in which z is the position along the waveguide.

$$\begin{aligned} dI_p &= W_{14} N_1 dz \\ dI_s &= W_{32} N_3 dz \end{aligned} \quad \text{Eq. 7.3}$$

These equations were numerically solved with the values for the different parameters as shown in Table 7.2 and with step values for dz of 0.02 cm.¹³ These parameters were obtained from several sources. The absorption cross-section at 579 nm was derived from an absorption spectrum. The lifetimes of spontaneous emission were those of 1.Nd in polymer layers (~0.8 μ s) or the averaged value of the LaPO₄:Nd particles that were reported in Chapter 5 (~50 μ s). The emission cross section at 1320 nm was reported by Dai *et al.* ($\sigma_e = 3 \times 10^{-21}$ cm²).¹⁴ This corresponds very well with the estimated emission cross section at 1066 nm (5×10^{-20} cm², reported by Slooff *et al.*¹⁹) and the fact that the emission strength of the 1320 nm is about 5-10 times smaller than at 1066 nm.¹⁵ The concentration of Nd³⁺ of 10^{20} cm⁻³ corresponds to a concentration of 1.Nd in a polymer of 10 % (by weight).

Table 7.2 The parameters that were used in the optical gain calculations of Nd^{3+} .

Parameter	Value	Units
P_p	0.1-1	W
σ_a	2.5×10^{-20}	cm^2
σ_e	3×10^{-21}	cm^2
λ_p	579	nm
λ_s	1320	nm
τ	0.8-80	μs
N_{tot}	1×10^{20}	cm^{-3}
length	4	cm
height	1.5	μm
width	2	μm

The calculated optical gain was 1.7 dB over a 4 cm long waveguide at a pump power of 1 W and a luminescent lifetime of 0.8 μs (1.Nd). The same waveguide, doped with the nanoparticles that have a luminescent lifetime of 50 μs , gives an optical gain of 8.6 dB. This is an enhancement of 7.2 of the initial intensity. The relation between the optical gain and the lifetime of spontaneous emission according to this model is shown in Figure 7.9.

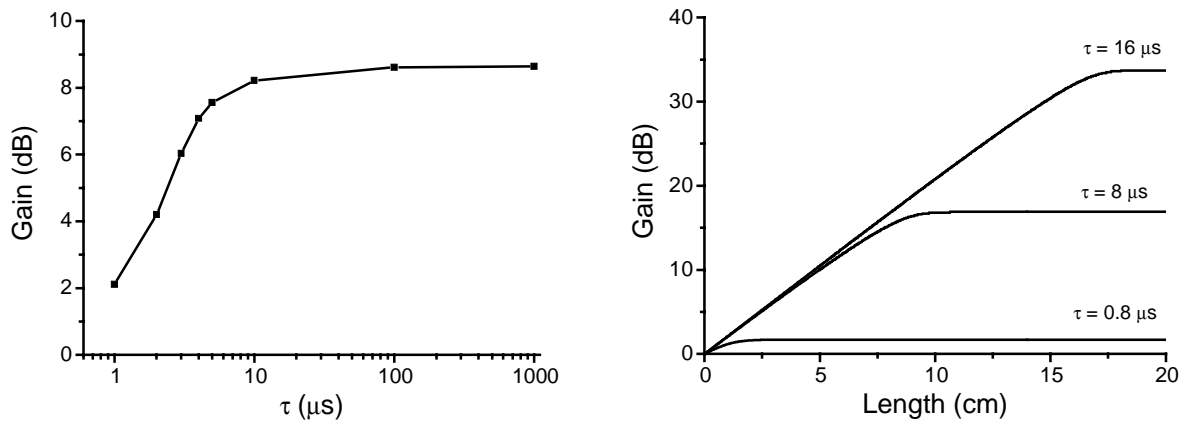


Figure 7.9 Right: relation between the optical gain in a 4 cm long waveguide and the spontaneous emission lifetime, calculated according to the model described in the text. Left: optical gain as a function of length for different lifetimes.

Figure 7.9 shows that relative small increases in the luminescent lifetime of 0.8 to 8 μs already give a dramatic increase in optical gain. The ‘flattening’ of the gain curve above a

lifetime of 8 μs is due to the saturation of the N_3 level at the applied high pump power. The population of the N_3 level can of course never be larger than the total concentration N_{tot} and at higher lifetimes or higher pump powers the population of N_3 comes close to N_{tot} . Therefore, there is a maximum in the initial differential gain (about 2 dB/cm). At higher lifetimes this gain per units of waveguide length is maintained over a longer waveguide segment (see Figure 7.9). A luminescent lifetime of 8 μs or higher is relatively easily obtained with the doped nanoparticles (see Chapter 5). In these calculations, effects of optical losses in the waveguides were not taken into account. However, significant losses are expected with the small waveguide dimensions in the design ($1.5 \times 2 \mu\text{m}$). Therefore, waveguide losses of 1 dB/cm were taken into account both for the pump and the signal wavelength.¹⁶ The results of these calculations on a 4 cm long waveguide with varying pump power are depicted in Figure 7.10.

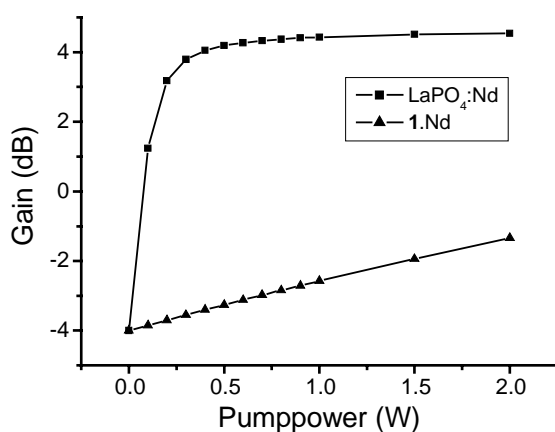


Figure 7.10 Dependence of optical gain to the pump power in 4 cm long waveguides taking waveguide losses into account of 1 dB/cm for both the pump and the signal wavelength.

Even with a low pump power (0.1 W) the waveguides doped with nanoparticles have a net optical gain. The estimated threshold power for net gain is 30 mW. The waveguides doped with 1.Nd do show a reduction in the waveguide losses, but net gain is achievable in these waveguides only with pump powers above 3.2 W. This is of course not a practical value. The reason that so far no optical gain at 1320 nm in polymer waveguides doped with Nd^{3+} was measured is most likely due to the low luminescent lifetime of Nd^{3+} in the polymers and to the low emission cross section at that wavelength. At a signal wavelength of 1066 nm ($\sigma_e = 3 \times 10^{-20} \text{ cm}^2$)¹⁴ the threshold for optical gain in waveguides doped with 1.Nd at 4 cm decreased to 0.45 W, the maximum gain at 1.5 cm of 2.5 dB. In a waveguide doped with the nanoparticles, the threshold decreases to 5 mW in a 4 cm long waveguide with a 1 dB/cm loss at pump and signal

wavelength. Figure 7.11 shows the optical gain in the doped waveguides as a function of the waveguide length and the waveguide loss. In the waveguides doped with $1.Nd$, after 4 cm no more gain can be achieved, because the pump light (with a power of 0.1-1 W) is almost completely consumed. With a longer lifetime of level 3, the maximum is reached much further in the waveguide. This difference is due to the fact that the absorption of light is directly proportional to the population of level 1 (N_1), which population is higher at a shorter lifetime of level 3. The optical gain reaches a maximum where the excitation source is almost completely diminished by absorption and waveguide losses.

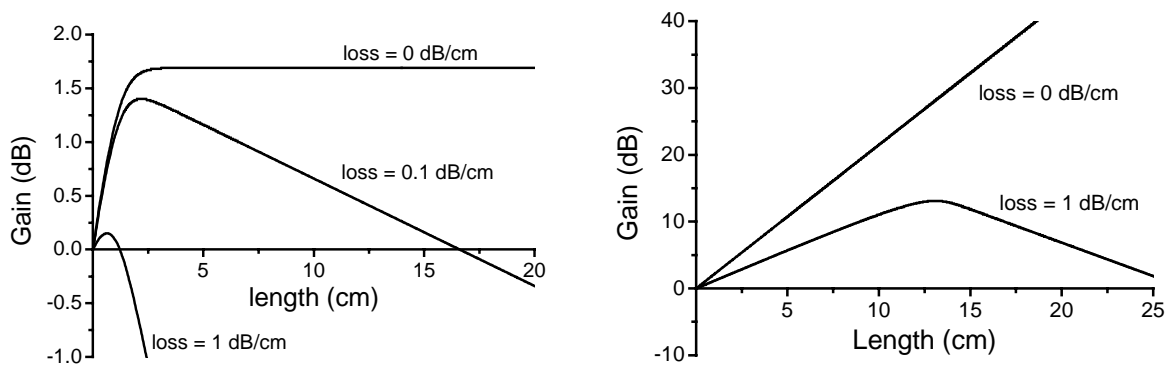


Figure 7.11 Optical gain is a function of the waveguide length. Left: waveguides doped with $1.Nd$ with a lifetime of $0.8 \mu s$, right: waveguides doped with the $LaPO_4:Nd$ nanoparticles, lifetime is $50 \mu s$.

Enhancing the absorption cross section of the organic complexes with sensitizers like lissamine¹⁷ (see Chapter 6) can increase the optical gain. For this experiment, another way of pumping would be needed, because all pump light would be absorbed in the first few micrometers of the waveguide if butt coupling (coupling at the beginning of a waveguide) is used. Pumping could be performed with an elliptical lens that focuses the pump light over an area of $2 \mu m$ by $4 cm$ on top of the waveguide. In a waveguide of $1.5 \mu m$ thickness with an absorption cross section of $10^{-16} cm^2$ (and $10^{20} cm^{-3}$ ions) almost all the light will be absorbed ($\approx 95\%$).⁴ It was estimated that an optical gain of 3.5 dB at 4 cm can be achieved with this doping. However, this way of pumping is very demanding on the sensitizer. The lissamine sensitizer photo-bleached very rapidly at a pump power of $1 W/mm$.⁴ Inorganic sensitizers could be an alternative, like for instance ruthenium complexes¹⁸ or inorganic semiconductors.

In the case of Er^{3+} , a similar model can be used to calculate the optical gain. However, Er^{3+} is a three-level system and absorption of the signal laser needs to be taken into account. This leads to a model as presented in Figure 7.12.

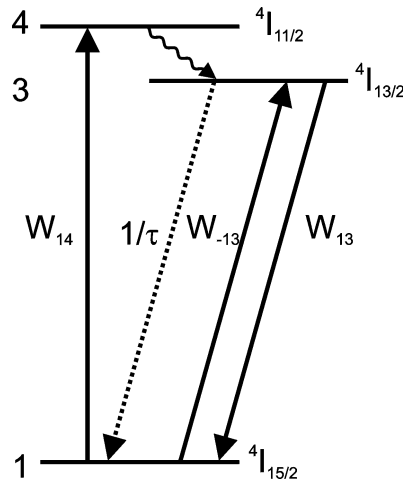


Figure 7.12 The three-level system of Er^{3+} , with the same assumptions as the four-level system of Nd^{3+} described above.

In the steady state situation, the N_3 and N_1 populations are calculated according to Eq. 7.4.

$$\begin{aligned} \frac{dN_1}{dt} = 0 &= -(W_{14} + W_{-13})N_1 + \left(\frac{1}{\tau} + W_{13} \right) N_3 \\ \frac{dN_3}{dt} = 0 &= +(W_{14} + W_{-13})N_1 - \left(\frac{1}{\tau} + W_{13} \right) N_3 \\ N_1 + N_3 &= N_{\text{tot}} \end{aligned} \quad \text{Eq. 7.4}$$

Furthermore, the pump-power and the signal power are calculated according to Eq. 7.5.

$$\begin{aligned} dI_p &= W_{14} N_1 dz \\ dI_s &= W_{13} N_3 dz - W_{-13} N_1 dz \end{aligned} \quad \text{Eq. 7.5}$$

The same waveguide dimensions were taken as for the Nd^{3+} -doped system discussed above, the other parameters are summarized in Table 7.3.^{19,20} The absorption cross section at the signal wavelength is taken the same as the stimulated emission cross section σ_e , which results in $W_{-13} = W_{13}$. The effect of the lifetime is even more dramatic than in the case of the organic Nd^{3+} complexes. With a luminescent lifetime of $1 \mu\text{s}$ a threshold power of 4.4 W would be needed in a 4 cm long waveguide. With a luminescent lifetime of $44 \mu\text{s}$ the threshold power is calculated to

be 0.1 W. With the 308 μs lifetime of the Er^{3+} -doped nanoparticles ($\text{LaPO}_4\text{:Er}$, see Chapter 5) a gain of 6.6 dB can be achieved.

Table 7.3 Values for parameters used in the model describing the Er^{3+} optical gain.

parameter	value	units
σ_a	1×10^{-21}	cm^2
σ_e	5×10^{-21}	cm^2
λ_p	1480	nm
λ_s	1536	nm
N_{tot}	1×10^{20}	cm^{-3}
τ	1-308 ^a	μs

a The lifetime of an organic Er^{3+} complex (1 μs) or the lifetime of the inorganic $\text{LaPO}_4\text{:Er}$ (308 μs) particles.

These calculations significantly change when waveguide losses of 1 dB/cm for pump and signal wavelength are introduced. In the 4 cm long $\text{LaPO}_4\text{:Er}$ -doped waveguides the gain is 1.6 dB by pumping at 0.1 W. Since important side effects like up-conversion and excited state absorption are not taken into account, the calculated gain should be regarded with care. The threshold for gain at 4 cm is 60 mW. However, it should be noted that initially a positive gain is achieved in these $\text{LaPO}_4\text{:Er}$ -doped waveguides with a maximum at 2 cm (Figure 7.13). In waveguides with 1.Er a pump power of 18 W is needed in order to achieve the same gain profile! Nevertheless, it can be concluded that Er^{3+} -doped nanoparticles are promising as dopants in polymer amplifiers.

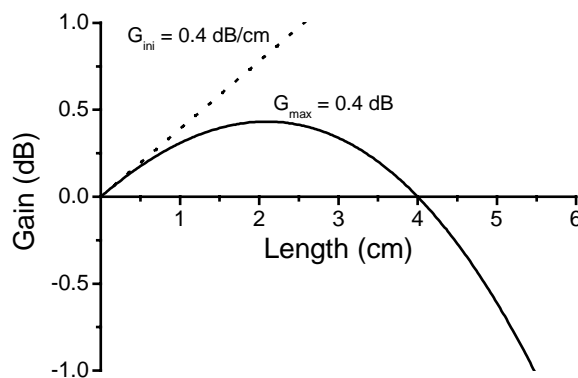


Figure 7.13 Gain profile of a waveguide doped with $\text{LaPO}_4\text{:Er}$ ($\tau = 308 \mu\text{s}$). The pump power is 60 mW and waveguide losses for both pump and signal power are 1 dB/cm.

7.3 Conclusions

Optical gain in polymer waveguides is possible with the Nd^{3+} complexes but will in practice be difficult to achieve because of the high pump powers required. The nanoparticles doped with Nd^{3+} in polymer waveguides are promising because they have high luminescent lifetimes that are of key importance in achieving optical gain. Even at low pump powers and with waveguide losses taken into account optical gain seems possible. The use of sensitizers enhances optical gain in Nd^{3+} doped waveguides, but very stable sensitizers are a requisite. Optical gain in polymers doped with Er^{3+} complexes will be impossible because the luminescent lifetime of Er^{3+} is too low. However, the enhancement of the Er^{3+} lifetime by incorporation in the nanoparticles will be sufficient for optical gain at 1536 nm. For optical gain in polymers, lanthanide complexes or doped nanoparticles should have lifetimes in the range of 50 μs for Nd^{3+} and 300 μs for Er^{3+} . It will be impossible to achieve such high luminescent lifetimes with organic complexes, and in practice, optical amplification in polymers will be limited to the use of nanoparticles.

7.4 Experimental

Luminescence measurements in solution were performed as described in Chapter 4. For measurement on quartz substrates, the sample chamber of the FLS900 or the LP900 Edinburgh Analytical Instruments was fitted with a solid sample holder, which enables to modify the angle of substrate and excitation beam (Xe arc lamp or N_2 laser). The transmittance measurements were performed with a sliding prism method.²¹ Spincoating of the polymers was performed in standard clean room conditions with polymer solutions of 0.1 g/ml on oxidized wafers (3.2 μm SiO_2 layer, deposited on 3" Si wafers with PECVD (Plasma Enhanced Chemical Vapor Deposition)). After annealing of the polymer layers at temperatures below 100 $^\circ\text{C}$, 40 nm aluminum was evaporated (Balzers BAK600) as resist for the reactive ion etching (RIE). Patterns in the aluminum layer were created by photolithography with 1.2 μm photoresist (Arch, 907/12, 4000 RPM for 20 s and a prebake of 95 $^\circ\text{C}$, at higher prebake temperatures the aluminum layer was found to crack). After UV exposure (4.3 s) the photoresist was developed in standard OPD developer for 48-50 s. Subsequently, the aluminum was etched for 2 minute with aluminum etch. In all steps the quality of the polymer layers and of the photoresist and aluminum layers and ridges were checked with DEKTAK and with optical microscopy. After the aluminum etch the polymer layers were etched with reactive ion etching for 1 minute with an O_2 plasma (Elektrotech PF340). A power of 20 W and at a pressure of 10 mTorr were applied, the temperature of the wafer was kept at 10 $^\circ\text{C}$. Ridges in the polymer of 100 nm were thus obtained. Remaining photoresist was removed by UV exposure and development. Aluminum was removed with standard aluminum etch.

7.5 References and notes

- ¹ Weber, J. K. R.; Felten, J. J.; Cho, B.; Nordine, P. C. *Nature* **1998**, *393*, 769.
- ² Wilkinson, J. S.; Hempstead, M. *Curr. Opin. Solid St. M.* **1997**, *2*, 194.
- ³ Booth, B. L. *J. Lightw. Techn.* **1989**, *7*, 1445.
- ⁴ Slooff, L. H.; Polman, A.; Klink, S. I.; Hebbink, G. A.; Grave, L.; van Veggel, F. C. J. M.; Reinhoudt, D. N.; Hofstraat, J. W. *Opt. Mater.* **2000**, *14*, 101.
- ⁵ Koeppen, C.; Yamada, S.; Garito, A. F.; Dalton, L. R. *J. Opt. Soc. Am. B.* **1997**, *14*, 155.
- ⁶ The expression of (optical) gain in decibels is calculated according to: $\text{Gain (dB)} = 10 \times \log(I/I_0)$. Therefore, a gain of 20 dB corresponds to a 100 times enhancement in signal intensity.
- ⁷ a) Chen, R. T.; Lee, M.; Natarajan, S.; Lin, C.; Ho, Z. Z.; Robinson, D. *IEEE Photon. Techn. Lett.* **1993**, *5*, 1328; b) Karve, G.; Bihari, B.; Chen, R. T. *Appl. Phys. Lett.* **2000**, *77*, 1253.
- ⁸ Klink, S. I.; Hebbink, G. A.; Grave, L.; Peters, F. G. A.; van Veggel, F. C. J. M.; Reinhoudt, D. N.; Hofstraat, J. W. *Eur. J. Org. Chem.* **2000**, 1923.
- ⁹ van Veggel, F. C. J. M.; Oude Wolbers, M. P.; Reinhoudt, D. N. *J. Phys. Chem. A* **1998**, *102*, 3060.
- ¹⁰ The propagation mode was calculated with the commercial program TempSelene of Alcatel.
- ¹¹ With air instead of PMMA as the top cladding with these dimensions, the propagation is single mode.
- ¹² After spincoating of the (top) PMMA cladding layer, the ridges in the PC were not straight anymore, as if they had been 'floating' in the PMMA solution.
- ¹³ With one step $dz = 0.02$ less than 1% of the excitation light is consumed in all simulations that are discussed, furthermore, no differences were found with step sizes that were 1,000 times smaller.
- ¹⁴ Dai, H.; Stafsuud, O.M.; Dunn, B. *Appl. Opt.* **1991**, *30*, 4330.
- ¹⁵ Slooff, L. H.; Polman, A.; Cacialli, F.; Friend, R. H.; Hebbink, G. A.; van Veggel, F. C. J. M., Reinhoudt, D. N. *Appl. Phys. Lett.* **2001**, *78*, 2122.
- ¹⁶ These losses can have several sources like scatter, absorption by impurities, or cross relaxation of the excited lanthanide ions. Furthermore, noise caused by amplified spontaneous emission is not taken into account as well.
- ¹⁷ Klink, S. I.; Oude Alink, P.; Grave, L.; Peters, F. G. A.; Hofstraat, J. W.; Geurts, F. A. J.; van Veggel, F. C. J. M. *J. Chem. Soc., Perkin Trans. 2* **2001**, 363.
- ¹⁸ Klink, S. I.; Keizer, H.; van Veggel, F. C. J. M. *Angew. Chem. Int. Ed.* **2000**, *39*, 4319.
- ¹⁹ Slooff, L. H.; van Blaaderen, A.; Polman, A.; Hebbink, G. A.; Klink, S. I.; van Veggel, F. C. J. M.; Reinhoudt, D. N.; Hofstraat, J. W. *J. Appl. Phys.* **2002**, *91*, 3955.
- ²⁰ Strohhöfer, C.; Polman, A. *J. Appl. Phys.* **2001**, *90*, 4314.
- ²¹ Weber, M. J.; Dunn, F. A.; Leibolt, W. N. *Appl. Opt.* **1973**, *12*, 755.

In this thesis the synthesis, characterization, and photophysical properties of lanthanide ion complexes have been described with the aim to incorporate them in applications like light-emitting diodes and optical amplifiers. For efficient applications, the luminescence properties of the (near-infrared emissive) lanthanide ions should be understood better.

In Chapter 1 the goal of the research has been described, i.e. to study the properties of near-infrared (wavelength between 750 and 3000 nm) emitting lanthanide(III) ion complexes and to incorporate these ions in polymer-based devices, like light-emitting diodes and optical amplifiers.

In Chapter 2, the recent literature concerned with near-infrared emissive lanthanide ions in polymer waveguides and in light-emitting diodes has been described. Furthermore, a number of basic properties of the emission of lanthanide ions have been treated with the emphasis on the near-infrared emitting ions. Polymers doped with lanthanide ions have been discussed. Most of the literature deals with dopings of visible emitting complexes based on Eu^{3+} and Tb^{3+} . Near-infrared (NIR) emission in polymers has been described with Nd^{3+} -, Yb^{3+} -, and Er^{3+} -based luminescence. In the case of Nd^{3+} , optical amplification at 1066 nm has been described. Only a few near-infrared emissive light-emitting diodes (NIR-LEDs) with lanthanide ions as the emitters have been reported. The final part of Chapter 2 has been devoted to the more general emission of lanthanide ions. The most important issue is non-radiative deactivation of the excited state of ions that emit NIR light. This quenching renders that these ions emit rather inefficiently in organic media. After the physics of emission and excitation, sensitizers for the (NIR) lanthanide(III) luminescence have been described. A sensitizer is a compound that donates its excited state energy to an energy acceptor, here a lanthanide ion. Although various sensitizers have been reported not all pathways are understood yet.

In Chapter 3 the effect of deuteration of organic ligands on the lifetime of a number of NIR emissive lanthanide ions (Nd^{3+} , Yb^{3+} , and Er^{3+}) has been studied. Deuteration is a well-known strategy in order to reduce luminescence quenching. Long luminescent lifetimes and/or high quantum yields are necessary for applications like optical amplification and light-emitting diodes. A new synthesis route has been established that makes the use of commercially available deuterated reagents possible. The lifetime of the deuterated complexes has been enhanced 2-3 times when compared with the normal, undeuterated complexes. Although this increase is significant, it is still not even close to the radiative lifetime of the ions.

Sensitized emission is the process in which an energy donor (the sensitizer) is excited and subsequently transfers its energy to an energy acceptor (here the emitter). Sensitized emission of Nd^{3+} , Yb^{3+} , and Er^{3+} by three structurally related dyes, i.e. fluorescein, eosin, and erythrosin, has been the goal in Chapter 4. Complexes have been prepared with the sensitizing moiety in close proximity of the lanthanide ion; this would facilitate the energy transfer step. It was expected that the intrinsic differences in intersystem crossing quantum yield of the three dyes would result in energy transfer differences, because energy is transferred from the triplet state of a sensitizer to a lanthanide ion. However, the paramagnetic and heavy lanthanide ions induce an external heavy atom effect that diminishes the intrinsic differences. Therefore, the energy transfer in the complexes is governed by the energy transfer mechanism. This results in a higher luminescence efficiency of the fluorescein-functionalized complexes than in the others. The $^4\text{F}_{9/2}$ excited state of Nd^{3+} could be identified as the accepting level of Nd^{3+} in these complexes, because of the selection rules for energy transfer and because of the energy difference between donor (triplet state of the sensitizer) and acceptor level.

Another method to enhance the luminescence lifetimes that still gives the possibility to dope the ions in polymer waveguides has been described in Chapter 5. The ions were incorporated in inorganic nanoparticles stabilized with an organic surfactant. This monolayer makes the particles processible in organic solvents and polymers. The luminescence of the LaPO_4 nanoparticles, with sizes between 5-8 nm, has been described for particles doped with Eu^{3+} (visible emission), Pr^{3+} (visible and NIR), and Nd^{3+} and Er^{3+} (both NIR). It was found that the emission spectrum of the Eu^{3+} -doped particles is similar to that of the bulk LaPO_4 materials, proving that the ions are inside the particles. The luminescence decay curves could be fitted with an 'onion-shell' model (see Appendix 5.A) that treats the particles consisting of a number of shells with quenching groups outside the particles. In the NIR, the lifetimes are enhanced 100-1000 times when compared with the luminescence lifetimes in organic materials, which is an important step towards applications like optical amplification.

In Chapter 6 a number of NIR emissive complexes have been described which have been incorporated in light-emitting diodes. First, the synthesis and luminescence of lanthanide complexes with new sensitizers have been described. These sensitizers, with a carbonyl moiety, show little remaining fluorescence due to the high intersystem crossing and thus potentially excellent Ln^{3+} sensitizers. NIR-LED devices were made of Nd^{3+} complexes functionalized with one of the carbonyl sensitizers and a complex functionalized with lissamine, a highly fluorescent sensitizer. NIR electro-luminescence was detected at operating voltages above 15 V. The ratio of dye fluorescence and NIR emission was decreased upon comparing photo-luminescence with

electro-luminescence. This is attributed to the direct formation of triplet states in electro-luminescence operation.

The incorporation of lanthanide ion complexes in polymer waveguides has been described in Chapter 7. First the luminescence of an organic complex in PMMA layers has been presented, which is not significantly different than in solution. Calculations of optical gain of Nd^{3+} - and Er^{3+} -doped waveguides have shown that this is possible with organic complexes, but high pump powers will be required in order to achieve significant gain (i.e. > 1 dB/cm). The use of the nanoparticles, such as described in Chapter 5, makes the realization of optical gain realistic. The luminescent lifetime of both Nd^{3+} and Er^{3+} in these particles is long enough to make amplification possible, even in the presence of relatively high waveguide losses (1 dB/cm). Sensitized emission enhances the gain as well, however this method is very demanding on the sensitizer, which should be very stable under strong excitation powers in order to prevent destruction by for instance photobleaching. In conclusion, in order to achieve optical amplification in polymer-based waveguides with the aid of near-infrared emitting lanthanide ions, they should possess a very stable sensitizer or the luminescent lifetimes should be in the order of 50 μs or higher for Nd^{3+} and 100 μs or higher for Er^{3+} . These lifetimes are easily obtained with doped nanoparticles.

Samenvatting

In dit proefschrift worden de synthese, karakterisering en de fotofysische eigenschappen van lanthanide-complexen beschreven waarbij het doel is om ze in lichtgevende diodes en optische versterkers in te bouwen. Voor deze toepassingen is het van belang om de eigenschappen van deze complexen goed te begrijpen om deze vervolgens zo te ontwerpen dat ze zo efficiënt mogelijk licht geven.

In hoofdstuk 1 is het doel van het onderzoek nader toegelicht. Dit doel is om de eigenschappen van lanthanide-complexen die nabij-infrarood licht (licht met een golflengte tussen 750 en 3000 nm) geven beter te begrijpen en om deze complexen op te nemen in toepassingen gebaseerd op polymeren. In dit geval zijn die organische lichtgevende diodes en polymere golfgeleiders voor optische versterking.

In hoofdstuk 2 worden lanthanide-ionen in lichtgevende diodes en polymere golfgeleiders besproken aan de hand van recente literatuur die verschenen is. Na deze toepassingen zijn hier ook de eigenschappen van de lanthanide-luminescentie beschreven met een nadruk op de lanthanide-ionen die nabij-infrarood licht geven. Het grootste deel van de literatuur over de genoemde toepassingen gaat over complexen die zichtbaar licht geven, zoals complexen van Eu^{3+} (rood licht) of Tb^{3+} (groen licht). Het nabij-infrarode licht van Nd^{3+} , Yb^{3+} en Er^{3+} in deze toepassingen is zeldzamer. Met Nd^{3+} is optische versterking bij 1066 nm gerapporteerd en lichtgevende diodes met complexen van Nd^{3+} , Yb^{3+} en Er^{3+} zijn ook beschreven. Het grootste probleem van deze nabij-infrarode emissie is de sterke stralingsloze deactivering van de aangeslagen toestand van deze ionen door de directe omgeving van het ion. Dit zorgt er voor dat de emissie erg inefficiënt is. Het laatste deel van dit hoofdstuk gaat over ‘*gesensitizeerde*’ emissie. Dit is het proces waarbij een antenne (de ‘*sensitizer*’) in de aangeslagen toestand wordt gebracht en daarna zijn energie overbrengt naar een acceptor (hier het lanthanide-ion) dat daarbij in de aangeslagen toestand komt.

In hoofdstuk 3 is een nieuwe syntheseroute beschreven waarbij lanthanide-complexen werden gedeutereerd. Dit deutereren is een methode om stralingsloze deactivering van de aangeslagen toestand van lanthanides door de omgeving te verminderen. Afname van deze deactivering in de complexen is erg belangrijk aangezien hoge levensduren en/of hoge kwantumopbrengsten belangrijk zijn voor de beoogde toepassingen. Voor de nabij-infrarood stralende complexen (Nd^{3+} , Yb^{3+} en Er^{3+}) is de luminescentie-levensduur met een factor 2-3 verhoogd door het deutereren. Dit is een significant verschil maar stralingsloze effecten blijven toch nog erg hoog.

Gesensitizeerde emissie is het onderwerp van hoofdstuk 4. Dit is het proces waarbij een geëxciteerde donor zijn energie overdraagt aan een acceptor. In dit hoofdstuk zijn als donor drie kleurstoffen van hetzelfde type (fluoresceïne, eosine en erythrosine) gebruikt en als acceptor de ionen Nd^{3+} , Yb^{3+} en Er^{3+} . De complexen werden zo ontworpen dat het lanthanide-ion zich dichtbij de kleurstof bevindt om zo een efficiënte energieoverdracht te bewerkstelligen. De drie kleurstoffen hebben wat betreft structuur veel overeenkomsten, maar toch zijn er verschillen die van belang zouden kunnen zijn voor energieoverdracht naar een lanthanide-ion. Deze intrinsieke verschillen in de kleurstoffen worden echter tenietgedaan door de nabijheid van de zware en paramagnetische lanthanide-ionen. Een klein verschil in de energieniveaus van de aangeslagen toestanden bleek hierdoor toch zeer belangrijk en hierdoor werd het mogelijk om het $^4\text{F}_{9/2}$ -niveau van Nd^{3+} als het accepterende niveau te bepalen. Deze selectie was mogelijk op grond van het energieverval (tussen donor- en acceptorniveaus), de selectieregels voor energieoverdracht en de aanwezigheid van een mechanisme waarbij energie teruggaat van Nd^{3+} naar de kleurstof.

Een andere methode om de levensduren en kwantumopbrengsten te verhogen is het onderwerp van hoofdstuk 5. De lanthanide-ionen werden opgenomen in anorganische nanodeeltjes (met een grootte van 5-8 nm) die gestabiliseerd worden door organische groepen. Hierdoor bevindt het ion zich in een omgeving met weinig groepen die de aangeslagen toestand deactiveren (namelijk LaPO_4), én het blijft mogelijk om ze op te nemen in een organisch polymeer. De deeltjes werden gedoteerd met Eu^{3+} , waarbij uit de luminescentie van Eu^{3+} bleek dat de ionen zich in een LaPO_4 matrix bevonden. De levensduur van de emissie kon bepaald worden met een 'uenschil'-model waarbij deactivering plaatsvindt door groepen buiten het deeltje. Op deze manier kon een goede beschrijving gegeven worden van de gemeten luminescentie-afname. Voor het nabij-infrarode licht van Pr^{3+} , Nd^{3+} en Er^{3+} werden zelfs levensduren gevonden die 100-1000 maal groter waren dan in organische complexen in dezelfde oplosmiddelen! Dit is een erg belangrijke stap in de richting van toepassingen gebaseerd op lanthanide-ionen die nabij-infrarood licht geven, zoals optische versterking.

In hoofdstuk 6 zijn een aantal complexen met enkele nieuwe *sensitizers* beschreven die nabij-infrarood licht geven. Deze werden uiteindelijk gedoteerd in lichtgevende diodes. De nieuwe *sensitizers* hebben een carbonyl groep in hun structuur die bevorderlijk is voor de *sensitizing* van lanthanide-ionen, aangezien fluorescentie wordt onderdrukt (minder storend licht van de sensitizer op de achtergrond) en de donerende triplettoestand sterker wordt gevoed. De Nd^{3+} -complexen al of niet gefunctionaliseerd met lissamine (een sterk fluorescente *sensitizer*) werden in lichtgevende diodes aangebracht. Bij voltages boven 15 V werd luminescentie van Nd^{3+} waargenomen. De verhouding van fluorescentie tot Nd^{3+} -emissie was

gunstiger voor Nd^{3+} bij elektroluminescentie dan bij fotoluminescentie. Waarschijnlijk komt dit door de directe vorming van de aangeslagen triplet toestand bij elektroluminescentie.

In hoofdstuk 7 worden polymere golfgeleiders, gedoteerd met lanthanidecomplexen beschreven. De luminescentie van de Nd^{3+} -complexen in dunne lagen PMMA week slechts weinig af van de luminescentie in oplossing. Berekeningen aan golfgeleiders met organische Nd^{3+} - en Er^{3+} -complexen laten zien dat optische versterking mogelijk is, maar dat de benodigde vermogens niet realistisch zullen zijn. Het gebruik van de nanodeeltjes zal een sterke verbetering geven en optische versterking wordt hiermee haalbaar. Zelfs bij verliezen in de golfgeleiders zelf (1 dB/cm) is versterking nog steeds goed haalbaar. *Gesensitizeerde* emissie is ook een oplossing voor het verkrijgen van meer versterking, maar dit zal veel vragen van de gebruikte *sensitizers*, omdat die namelijk fotostabiel zullen moeten zijn. Het verkrijgen van optische versterking in polymere golfgeleiders is zeker realistisch als de levensduren van de organische verbindingen hoog genoeg zijn, namelijk boven de 50 μs voor Nd^{3+} en boven de 100 μs voor Er^{3+} . Met anorganische nanodeeltjes zijn deze waarden haalbaar.

Dankwoord

Nu alles bijna achter de rug is, is het tijd om een dankwoord te schrijven. Zonder de hulp en steun van een hele groep mensen was dit onderzoek namelijk niet mogelijk geweest.

In de eerste plaats wil ik David bedanken waarvan ik na mijn afstuderen het vertrouwen en de mogelijkheid kreeg om te promoveren in zijn groep. David, ik heb het zeer gewaardeerd hoe jij deze groep leidt, waarin iedereen veel vrijheid heeft om onderzoek te doen en waarbij het ook mogelijk is om binnen (of buiten) de groep alle metingen en experimenten te doen die nodig zijn.

Frank van Veggel is in de afgelopen vier jaar mijn dagelijks begeleider geweest en ik heb veel van hem geleerd over onderzoek doen en over het opschrijven van die resultaten. Frank, bedankt voor je betrokken begeleiding en je onmisbare hulp bij het schrijven van artikelen en het proefschrift.

Het project is uitgevoerd met geldelijke steun van CW-STW. De gebruikerscommissie wil ik bedanken voor hun inbreng in het project. Ik had het voorrecht dat er ‘technische ondersteuning’ bij mijn project was. Deze ondersteuning werd achtereenvolgens ingevuld door Lennart Grave, Patrick Oude Alink en Léon Woldering. Ik wil jullie alledrie bedanken voor jullie bijdrage aan het onderzoek en jullie gezelligheid. Werk dat jullie hebben gedaan is op vele plaatsen in dit proefschrift terug te vinden, maar ook in een aantal publicaties dat niet of slechts zijdelings in het proefschrift zijn opgenomen. Steve Klink was in veel opzichten mijn voorganger. Ik heb veel van hem geleerd over lanthanides en luminescentie en we hebben ook veel kunnen samenwerken wat heeft geleid tot een hele serie gezamenlijke publicaties. Steve, bedankt hiervoor en ook bedankt voor het doornemen van mijn concept.

Zeker in de eerste paar jaar van mijn onderzoek toen we onze eigen ‘Edinburgh’ nog niet hadden, was ik voor luminescentiemetingen afhankelijk van Akzo-Nobel waar wel de nodige apparatuur stond. Ik wil Teun de Bruin, Monique Ramsamoedj en Esther van der Linden bedanken voor de gastvrijheid en de hulp die ze mij in Arnhem altijd gaven. Jurriaan Zwier wil ik bedanken voor de gastvrijheid en hulp bij mijn metingen in Amsterdam, waar de apparatuur later opgesteld stond. Hans Hofstraat was in eerste instantie verantwoordelijk voor die apparatuur en toen het naar Amsterdam was verhuisd gaf hij mij de gelegenheid om daar verder te kunnen meten. Hans, bedankt voor de samenwerking en voor de ideeën en suggesties die je altijd paraat had.

De samenwerking met Albert Polman en Lenneke Slooff van het Amolf instituut in Amsterdam heb ik altijd als erg stimulerend ervaren. Dit kwam vooral door de combinatie van jullie fysische kennis en onze chemische kennis. Michiel de Dood wil ik bedanken voor de hulp

bij de metingen die ik bij het Amolf mocht doen. Sami Musa en Alfred Driessen wil ik bedanken voor het meedenken en de hulp bij het ontwerpen van polymere golfgeleiders. Hoewel het tot dusver nog niet heeft geleid tot optische versterking hoop ik dat de samenwerking in de nabije toekomst tot optische versterking zal leiden. Chapter 6 would not have been possible without the cooperation with Franco Cacialli, Anna Köhler, and Clare Boothby from the group of prof. Richard Friend in Cambridge (UK). Thank you very much for the cooperation and for the possibility to spend some time in Cambridge. Wiljan Stouwdam wil ik bedanken voor de samenwerking die heeft geleid tot hoofdstuk 5. Ook wil ik je bedanken voor het kritische doornemen van mijn concept-proefschrift. Roel Fokkens wil ik hiervoor ook bedanken, en voor het meten van de ESI en MALDI spectra die op het laatste moment nog nodig waren.

Voor de toe- en afvoer van chemicaliën en andere benodigdheden was de hulp van Joop Toevank, Irene Wolbers, Mark Brouwer en Marcel de Bruine onontbeerlijk. De bestelde chemicaliën waren steeds snel aanwezig en we konden altijd op jullie rekenen als er iets geregeld moest worden. Carla Weber-van der Ploeg wil ik bedanken voor de hulp bij het afhandelen van de administratieve zaken. Voor de analyse en karakterisering van mijn verbindingen wil ik Tieme Stevens (Massa), Hannie Visser (NMR), Annemarie Montanaro (EA) en Louise Vrielink (XRF) bedanken.

De collegae van SMCT wil ik bedanken voor de gezelligheid binnen en buiten het lab. Naast de mensen die ik al genoemd heb, wil ik nog een aantal bij naam noemen (in willekeurige volgorde natuurlijk): Jasper Michels, Menno de Jong, Wiljan Stouwdam, Léon Woldering, Lennart Grave, Patrick Oude Alink, Steve Klink, Jurriaan Huskens, Jessica Kerckhoffs, Francesca Corbellini, Marta Reinoso, Xue-Mei Li, Tommaso Auletta en het SMCT-voetbalteam (Campiono!!). Wiljan Stouwdam en Léon Woldering, bedankt dat jullie paranimf willen zijn, het zwarte pinguïn pak zal jullie best wel staan! Huisgenoot Léon Segeren wil ik bedanken voor de gezelligheid de afgelopen jaren, eerst in Deppenbroek en later aan de Sterrenstraat.

Mijn vader en moeder ben ik dankbaar voor de steun en voor de belangstelling die ze altijd hebben getoond in mijn onderzoek.

Mirjam, bedankt voor je liefde, geduld en steun, vooral de laatste tijd als ik weer eens aan het schrijven was.

Gerald

Publications based on this thesis:

- *Chapter 3*: Increased Luminescent Lifetimes of Ln³⁺ Complexes Emitting in the Near-Infrared as a Result of Deuteration, Hebbink, G. A.; Reinhoudt, D. N.; van Veggel, F. C. J. M.; *Eur. J. Org. Chem.* **2001**, 4101-4106.
- *Chapter 4*: The Unexpected Sensitization Efficiency of the Near-Infrared Nd³⁺, Er³⁺, and Yb³⁺ Emission by Fluorescein Compared to Eosin and Erythrosin, Hebbink, G. A.; Grave, L.; Woldering, L. A.; Reinhoudt, D. N.; van Veggel, F. C. J. M. *submitted to J. Phys. Chem. A*.
- *Chapter 5*: Lanthanide(III)-Doped Nanoparticles that Emit in the Near-Infrared, Hebbink, G. A.; Stouwdam, J. W.; Reinhoudt, D. N.; van Veggel, F. C. J. M. *Adv. Mater.* **2002**, *in press*.
- *Chapter 6*: Near-Infrared Electroluminescence of Polymer Light-Emitting Diodes Doped with a Lissamine-Sensitized Nd³⁺ Complex, Slooff L. H.; Polman A.; Cacialli F.; Friend R. H.; Hebbink G. A.; van Veggel F. C. J. M.; Reinhoudt D. N. *Appl. Phys. Lett.* **2001**, 78, 2122-2124.

Publications related to this thesis:

- Singlet Energy Transfer as the Main Pathway in the Sensitization of Near-Infrared Nd³⁺ Luminescence by Dansyl and Lissamine Dyes, Hebbink, G. A.; Klink, S. I.; Grave, L.; Oude Alink, P. G. B.; van Veggel, F. C. J. M. *Chem. Phys. Chem.* **2002**, *in press*.
- Rare-earth doped polymers for planar optical amplifiers, Slooff, L. H.; van Blaaderen, A.; Polman, A.; Hebbink, G. A.; Klink, S. I.; van Veggel, F. C. J. M.; Reinhoudt, D. N.; Hofstraat, J. W. *J. Appl. Phys.* **2002**, 91, 3955-3980.
- Synergistic Complexation of Eu³⁺ by a Polydentate Ligand and a Bidentate Antenna to Obtain Ternary Complexes with High Luminescence Quantum Yields, Klink, S. I.; Hebbink, G. A.; Grave, L.; Oude Alink, P. G. B.; van Veggel, F. C. J. M. *J. Phys. Chem. A* **2002**, 106, 3681-3689.
- Visible and Near-Infrared Light Emitting Calix[4]arene-Based Ternary Lanthanide Complexes, Hebbink, G. A.; Klink, S. I.; Oude Alink, P. G. B.; van Veggel, F. C. J. M. *Inorg. Chim. Acta* **2001**, 317, 114-120; *Inorg. Chim. Acta* **2001**, 323, 171.
- Near-Infrared and Visible Luminescence from Terphenyl-Based Lanthanide(III) Complexes Bearing Amido and Sulfonamido Pendant Arms, Klink, S. I.; Hebbink, G. A.; Peters, F. G. A.; Grave, L.; Van Veggel, F. C. J. M.; Reinhoudt, D. N.; Hofstraat, J. W. *Eur. J. Org. Chem.* **2000**, 10, 1923-1931.
- Optical Properties of Lissamine Functionalised Nd³⁺ Complexes in Polymer Waveguides and Solution, Slooff, L. H.; Polman, A.; Klink, S. I.; Hebbink, G. A.; Grave, L.; Van Veggel, F. C. J. M.; Reinhoudt, D. N.; Hofstraat, J. W. *Opt. Mat.* **2000**, 14, 101-107.
- Sensitized Near-Infrared Luminescence from Polydentate Triphenylene-Functionalised Nd³⁺, Yb³⁺, and Er³⁺ Complexes, Klink, S. I.; Hebbink, G. A.; Grave, L.; Van Veggel, F. C. J. M.; Reinhoudt, D. N.; Slooff, L. H.; Polman, A.; Hofstraat, J. W. *J. Appl. Phys.* **1999**, 86, 1181-1183.

Curriculum vitae

Gerald Hebbink werd geboren op 9 oktober 1973 te Wisch. Na het VWO aan het Ulenhof College in Doetinchem begon hij in 1992 aan de studie Chemische Technologie aan de Universiteit Twente te Enschede. Tijdens zijn studie deed hij een vier maanden durende stage bij Akzo-Nobel Central Research in Deventer waar hij werkte aan de stabiliteit van rubber vulkanisatie-versnellers. In 1997 werkte hij aan zijn afstudeerproject in de groep van prof. dr. ir. D. N. Reinhoudt. Dit onderzoek had tot doel de synthese en karakterisering van lanthanide-complexen. Na zijn afstuderen verbleef hij drie maanden in Parma (Italië) onder leiding van dr. A. Casnati en prof. R. Ungaro als een Erasmus/Socrates student. Hier werd gewerkt aan de synthese van calix[4]areen verbindingen. Na terugkeer in Nederland begon hij in april 1998 aan zijn promotie-onderzoek binnen de vakgroep Supramoleculaire Chemie en Technologie onder leiding van prof. dr. ir. D. N. Reinhoudt en dr. ir. F. C. J. M. van Veggel. Dit STW project had als doel het ontwikkelen van optische versterkers op basis van organische lanthanide-complexen. De resultaten van dit onderzoek staan beschreven in dit proefschrift.